SPECIATION OF Fe IN AMBIENT AEROSOL AND CLOUDWATER

Thesis by

Ronald Lyn Siefert

Thesis Advisor

Michael R. Hoffmann

In Partial Fulfillment of the Requirements

for the Degree of

Doctor of Philosophy

California Institute of Technology

Pasadena, CA

1997

(Submitted August 15, 1996)

Acknowledgments

This thesis (as most) is actually a collective work, with contributions from many people both directly and indirectly. I first want to thank my family for all of their support and love. My wife, Julie, has been a wonderful part of my life, ever since I first played soccer against her over 15 years ago at Chester Park in Duluth. I especially want to thank her for her patience and understanding during all of the field studies which have taken me to the other side of the world. It is always difficult to explain to people that these field studies to mountains, tropical islands and exotic ports is work, but she always understood. I also want to thank her for giving me two beautiful children, Jacob and Tara, who have enlightened our lives more then we probably know. It is always a great feeling to come home after a long day in the lab (or a long month at sea), and have your children give you a big hug and smile. I also want to thank my parents and sister who were also always there for me and supportive in all my decisions.

My advisor, Prof. Mike Hoffmann, gave me the independence to pursue my own ideas, and was always available to discuss science when I needed guidance. I also want to thank Prof. Morgan, whose door was always open when I had a question, and all of the faculty that I have had the opportunity to meet at Caltech. Their enthusiasm for discovery was very contagious.

I also want to thank all of the friends I have made at Caltech. My fellow students were always willing to either help me with a problem, or escape from it for a little while (or a long while). Mike Hannigan, Clo Butcher, Matt Fraser, Anne Johansen, Sam Webb, Jeremy Semrau, Simo Pehkonen, Peter Green, Janet Kesselman, Nicole Peill, Russ Mau, etc., truly made life at Caltech an enjoyable experience. I'll never forget the crossword breaks, mountain biking, softball games (followed by Super A's), barbecues, camping and countless other activities which filled in all that extra time I had. Playing and helping coach hockey with Bob Lane, Pavel Svitek, Dale Laird, etc., was certainly a great escape for me

at Caltech. I highly recommend stapling a few people (especially from USC or UCLA) to the boards every now and then to relieve some of that graduate school stress. Of course I shouldn't forget to thank my orthopedic surgeons, physical therapists, USC Medical Center, Huntington Memorial Hospital, the paramedics/ambulance crew in Newport Beach, and of course my health insurance for making it all possible (15 years of injury free hockey in the land of 10,000 frozen lakes, and I get hurt my rookie season in L.A., how humiliating). I also would have been lost without the help of: Joe Fontana and Rich Eastvedt for actually constructing my sampling equipment; Rayma Harrison and Susan Leising for showing me the way through the maze of literature; and Linda Scott, Fran Matzen, Carmen Lopez and Jennifer Packman for knowing how to actually get things done.

ABSTRACT

Atmospheric iron (Fe) is thought to play an important role in cloudwater chemistry (e.g., S(IV) oxidation, oxidant production, etc.), and is also an important source of Fe to certain regions of the worlds oceans where Fe is believed to be a rate-limiting nutrient for primary productivity. This thesis focuses on understanding the chemistry, speciation and abundance of Fe in cloudwater and aerosol in the troposphere, through observations of Fe speciation in the cloudwater and aerosol samples collected over the continental United States and the Arabian Sea. Different chemical species of atmospheric Fe were measured in aerosol and cloudwater samples to help assess the role of Fe in cloudwater chemistry. Chapter 2 presents a set of experiments which used ambient aerosol samples suspended in aqueous solution and then irradiated with uv-light to simulate cloudwater conditions. These experiments found Fe to be a critical component for the production of H_2O_2. Chapter 3 discusses the development and application of a novel photochemical extraction method for the determination of photochemically-available Fe in ambient aerosol samples. Photochemically-available Fe ranged from < 4 ng m^{-3} to 308 ng m^{-3}, and accounted for 2.8% to 100% of the total Fe in aerosol samples collected in California and New York. Calculations based on the results of these experiments predicted that redox reactions of Fe in cloudwater could be an important in situ source of oxidants ($^{\bullet}OH$, $HO_2^{\bullet}/O_2^{\bullet-}$). Chapter 4 presents results of several field studies which measured the redox states of Fe and other transition metals (Mn, Cu and Cr) in cloudwater. These measurements were then used in thermodynamic models which predicted Fe(III) to be either as Fe(III)-hydroxy species or Fe(III)-oxalate species. However, an un-identified strong chelating ligand with Fe(III) was also suggested by the thermodynamic model results. Chapter 5 presents results of a field study conducted on the Arabian Sea. Total atmospheric labile-Fe(II) ranged between < 0.09 ng m^{-3} to 7.5 ng m^{-3} during the inter-monsoon period, and was consistently below the

detection limit during the southwest-monsoon period. The labile-Fe(II) measured during the inter-monsoon period was predominantly found in the fine fraction of the aerosol. Principal component analysis revealed a significant source of Fe and Mn which was not associated with the main aeolian dust component.

TABLE OF CONTENTS

LIST OF FIGURES

Chapter 2:

Chapter 2:

Chapter 3:

Chapter 4:

Chapter 5:

LIST OF TABLES

Chapter 2:

Chapter 3:

Chapter 4:

Chapter 5:

Chapter 1:

Introduction and Overview

PREFACE

This thesis, "Chemical Characterization of Iron in Atmospheric Cloudwater and Aerosols," consists of four papers. I was first author on all four of these papers. The first paper (Chapter 2) was published in *Geochimica et Cosmochimica Acta*, the second paper (Chapter 3) was published *in The Journal of Geophysical Research*, the third paper (Chapter 4) is ready for submission *to The Journal of Air and Waste Management,* and the fourth paper (Chapter 5) is ready for submission *to The Journal of Geophysical Research.* Much of this thesis centers around the analysis of aerosol and cloudwater samples collected over the continental United States and the Arabian Sea. I was involved in every component of this research. These components included: 1) aerosol collector design and construction, 2) field preparation, 3) coordination of field studies with other scientists, ship masters, etc., 4) sample collection, 5) sample analysis, 6) thermodynamic and kinetic modeling, 7) statistical analysis, and 8) manuscript writing. Due to the location and duration of the numerous field studies included in this thesis, other people also helped significantly in the collection and chemical analysis of samples. These people included: Anne M. Johansen, Simo O. Pehkonen and Samuel M. Webb. While working on this thesis I also contributed to several other papers and projects related to this thesis, but not included. I was second-author on two papers which involved laboratory studies which were relevant to the atmospheric chemistry of Fe. These papers were titled: "Photoreduction of iron oxyhydroxides and photooxidation of halogenated acetic acids: Implications for tropospheric chemistry" [*Pehkonen et al.*, 1995], and "Photoreduction of iron oxyhydroxides in the presence of important atmospheric organic compounds" [*Pehkonen et al.*, 1993]. Both of these papers were published in *Environmental Science and Technology*.

INTRODUCTION

Cloudwater and aerosol chemistry is a poorly understood component of atmospheric chemistry compared to gas-phase atmospheric chemistry. Recent discoveries of sulfur oxidation in clouds ("acid rain") and the role of polar stratospheric clouds (PSCs) in stratospheric ozone chemistry have revealed the importance of cloudwater and aerosol chemistry in the troposphere and stratosphere. Atmospheric Fe is thought to play an important role in cloudwater chemistry (including sulfur oxidation, organic acid production and destruction, and oxidant production and destruction), and is also an important source of Fe to certain regions of the worlds oceans where Fe is a rate-limiting nutrient for primary productivity. This thesis focuses on the understanding the chemistry and abundance of Fe in cloudwater and aerosol in the troposphere, through observations of Fe speciation in the cloudwater and aerosol samples collected over the continental United States and the Arabian Sea.

Background

In order to understand the chemistry occurring in clouds and aerosols, the detailed chemical speciation of transition metals (e.g., Fe, Mn, Cu, and Cr) must be understood. A knowledge of the transition metal chemical species (for all oxidation states) as a function of variables such as pH, organic ligands, and inorganic ligands is critical to the assessment of atmospheric reaction pathways involving S(IV), O_2, RHCO, NO_x, ROOH and H_2O_2 in heterogeneous phases. In addition, a knowledge of the detailed chemical speciation of Fe is also important to the assessment of the ability of marine biota to utilize atmospherically-derived trace elements as micronutrients.

Iron (Fe) is the fourth most abundant element in the earth's crust and the most abundant first-row transition element. Because of it's abundance in the earth's crust, Fe is

also the most abundant first-row transition element in atmospheric aerosols since, on a global scale, aeolian dust is a major source of refractory elements to the atmosphere. The next three abundant first-row transition elements in the atmosphere are Mn, Cu and Cr. Several studies have investigated the particle size distribution and source identification of these transition metals in the atmosphere [*Galloway et al.*, 1982; *Lantzy and Mackenzie*, 1979; *Nriagu*, 1989; *Nriagu and Davidson*, 1986; *Puxbaum*, 1991]. But only a few studies have looked at the speciation or reactivity of trace metals in the fogwater or cloudwater [*Behra and Sigg*, 1990; *Erel et al.*, 1993; *Kotronarou and Sigg*, 1993; *Xue et al.*, 1991] or in ambient aerosol [*Kopcewicz and Kopcewicz*, 1991; *Kopcewicz and Kopcewicz*, 1992; *Siefert et al.*, 1994; *Spokes et al.*, 1994; *Zhu et al.*, 1993; *Zhuang et al.*, 1992].

Iron is predominantly found as either ferric iron (Fe(III)), or ferrous iron (Fe(II)) in the earth's crust, lakes and oceans. Mn, Cu and Cr can also be found in several oxidation states in natural waters: 1) Mn as Mn(II), Mn(III) and Mn(IV), 2) Cu as Cu(I) and Cu(II), and 3) Cr as Cr(III) and Cr(VI). These metals are known to participate in a variety of redox reactions in natural waters involving S(IV), organic compounds, oxidants and metal ions [*Conklin and Hoffmann*, 1988; *Faust and Hoffmann*, 1986; *Graedel et al.*, 1986; *Weschler et al.*, 1986; *Wiersma and Davidson*, 1986]. Fe and Mn are also found as particulate oxides and hydrous oxides in natural waters, which can also participate in a variety of redox reactions on the surface of these particles which are similar to those of dissolved Fe and Mn [*Faust and Hoffmann*, 1986; *Kieber and Helz*, 1992; *Regazzoni and Blesa*, 1991; *Siffert and Sulzberger*, 1991; *Stone*, 1986].

Figure 1 shows an overview of Fe in the atmosphere. Sources of Fe and other transition elements to the atmosphere include: aeolian dust, volcanic activity and anthropogenic sources [*Nriagu*, 1989; *Nriagu and Davidson*, 1986; *Puxbaum*, 1991]. Meteoritic Fe is also a detectable source of Fe to the atmosphere [*Kopcewicz and Kopcewicz*, 1992]. Once in the atmosphere Fe can be cycled between "dry" aerosol

particles (hereafter referred to as aerosol particles) and cloudwater droplets. "Dry" refers to atmospheric conditions where the relative humidity is not high enough (i.e., supersaturation conditions) for the aerosol particles to grow to cloud-size drops. These "dry" aerosol particles can be incorporated into cloud droplets by either the aerosol particle serving as a nucleus for a cloud drop, or an interstitial aerosol particle impacting on pre-existing cloud drop. Overall, aerosol particles undergo an estimated of 10 nucleation/evaporation cycles before they are removed from the atmosphere by wet or dry deposition [*Junge*, 1964]. Once in a cloud droplet, Fe can be involved in S(IV) oxidation, organic acid production/destruction, and oxidant (e.g., $^{\bullet}OH$, HO_2) production/destruction [*Graedel et al.*, 1986; *Faust, 1994* ; *Jacob et al.*, 1989]. This chemistry can also potentially change the speciation or mineral form of Fe present in the atmosphere, effectively "weathering" the Fe as it is advected. Finally, the Fe is removed from the atmosphere through either wet or dry deposition. This deposition is critical to certain regions of the oceans where Fe is a rate-limiting nutrient to phytoplankton growth and therefore determines the primary productivity of these regions of the oceans [*Ditullio et al.*, 1993; *Kolber et al.*, 1994; *Martin et al.*, 1994; *Martin and Gordon*, 1988; *Price et al.*, 1994]. The metal speciation is critical to the ability of the marine biota to utilize atmospherically-derived trace elements as micronutrients [*Hudson and Morel*, 1990; *Hudson and Morel*, 1993; *Morel et al.*, 1991; *Wells et al.*, 1994; *Wells et al.*, 1995]. The primary source of Fe to these regions of the oceans is through atmospheric deposition .

Thesis Work

The goal of this thesis was to characterize atmospheric Fe, along with various other species relevant to the chemistry of Fe, in cloudwater and aerosol to help understand the role of Fe in heterogeneous atmospheric chemistry, and also its role as a nutrient source to surface ocean waters. This goal was achieved by the development and application of several collection and analytical methods. These methods were used in a multitude of field

studies to investigate Fe speciation in aerosol and cloudwater. Figure 2 outlines the different measurements conducted for Fe in ambient aerosol samples. Figre 3 outlines the different measurements conducted for Fe in cloudwater samples.

The second chapter discusses experiments using atmospheric aerosol samples collected from Whiteface Mtn. (NY), Pasadena (CA), and Sequoia National Park (CA). The aerosol samples were suspended in aqueous solutions ("simulated cloudwater"), followed by addition of various organic acids (oxalic, formic and acetic acids), which are commonly observed in cloudwater. The solution was then irradiated with ultraviolet light (similar intensity to ambient sunlight) and various species were measured (i.e., H_2O_2, $Fe(II)_{aq}$ and pH). These experiments found Fe to be a critical component for the production of H_2O_2 in the simulated cloudwater experiments.

The third chapter discusses the development and application of a novel photochemical extraction method for the determination of photochemically-available Fe. This method was used to characterize Fe in aerosol samples collected from Whiteface Mtn. (NY), Pasadena (CA), San Nicholas Island (CA) and Yosemite National Park (CA). Several aerosol samples were collected during biomass burning episodes. Photochemically-available Fe ranged from < 4 ng m^{-3} to 308 ng m^{-3}, and accounted for 2.8% to 100% of the total Fe in the sample. Calculations based on the results of these experiments predicts that redox reactions of Fe in cloudwater could be an important in situ source of oxidants ($^{\bullet}OH$, $HO_2^{\bullet}/O_2^{\bullet-}$).

The fourth chapter discusses results of several field studies which measured the redox states of Fe and other transition metals (Mn, Cu and Cr) in cloudwater. Other measurements, relevant to the speciation and redox chemistry of these metals, included: pH, total elemental concentrations, organic anions, inorganic anions, cations, peroxides, and formaldehyde. Several cloud events were sampled at Whiteface Mtn (NY), San Pedro Hill (CA) and Bakersfield (CA). The results of the measurements were then used in thermodynamic models to calculate the speciation of the metals in the cloudwater samples.

Fe(III) was found to occur either as Fe(III)-hydroxy species or Fe(III)-oxalate species. However, an un-identified strong chelating ligand with Fe(III) was also suggested by the data. A kinetic model was also used to investigate the metal redox chemistry.

The fifth chapter discusses results of a field study conducted aboard the research vessel Meteor on the Arabian Sea. Aerosol samples were collected and immediately analyzed for labile-Fe(II) fractions (along with other important species) during two separate cruises in 1995. The first cruise occurred during the inter-monsoon period and the second occurred during the southwest-monsoon. A high volume dichotomous virtual impactor (HVDVI) was used to collect aerosol in the fine and coarse fractions. Total atmospheric labile-Fe(II) ranged between < 0.09 ng m^{-3} and 7.5 ng m^{-3} during the inter-monsoon period, and was consistently below the detection limit during the southwest-monsoon period. The labile-Fe(II) measured during the inter-monsoon period was found predominantly in the fine fraction of the aerosol. Principal component analysis revealed a significant source of Fe and Mn which was not associated with the main aeolian dust component.

Overall, this thesis has provided further insight into cloudwater and aerosol chemistry in the atmosphere. However, more sensitive analytical methods, better collection techniques, and laboratory experiments will certainly bring new discoveries regarding these complicated dynamic systems.

FIGURE CAPTIONS

FIGURE 1 Overview of atmospheric iron.

FIGURE 2 The different measurements conducted for Fe in ambient aerosol samples.

FIGURE 3 The different measurements conducted for Fe in cloudwater samples.

REFERENCES

Behra, P., and L. Sigg, Evidence for redox cycling of iron in atmospheric water droplets, *Nature*, *344* (6265), 419-421, 1990.

Conklin, M.H., and M.R. Hoffmann, Metal ion-sulfur(IV) chemistry. 2. Kinetic studies of the redox chemistry of copper(II)-sulfur(IV) complexes, *Environ. Sci. Technol.*, *22*, 891-898, 1988.

Ditullio, G.R., D.A. Hutchins, and K.W. Bruland, Interaction of iron and major nutrients controls phytoplankton growth and species composition in the tropical North Pacific Ocean, *Limnol. & Ocean.*, *38* (3), 495-508, 1993.

Erel, Y., S.O. Pehkonen, and M.R. Hoffmann, Redox chemistry of iron in fog and stratus clouds, *J. Geophys. Res. A.*, *98* (D10), 18423-18434, 1993.

Faust, B.C., Photochemistry of clouds, fogs and aerosols, *Environ. Sci. Technol.*, *28* (5), 217A-222A, 1994.

Faust, B.C., and M.R. Hoffmann, Photoinduced reductive dissolution of alpha-Fe2O3 by bisulfite, *Environ. Sci. Technol.*, *20*, 943-948, 1986.

Galloway, J.N., J.D. Thornton, S.A. Norton, H.L. Volchok, and R.A.N. Mclean, Trace-metals in atmospheric deposition - A review and assessment, *Atmos. Environ.*, *16*, 1677-1700, 1982.

Graedel, T.E., M.L. Mandich, and C.J. Weschler, Kinetic model studies of atmospheric droplet chemistry, 2. Homogenous transition metal chemistry in raindrops, *J. Geophys. Res.*, *91*, 5205-5221, 1986.

Hudson, R.J.M., and F.M.M. Morel, Iron transport in marine phytoplankton: Kinetics of cellular and medium coordination reactions, *Limnol. Ocean.*, *35* (5), 1002-1020, 1990.

Hudson, R.J.M., and F.M.M. Morel, Trace-metal transport by marine microorganisms: Implications of metal coordination kinetics, *Deep Sea Res.*, *40*, 129-150, 1993.

Jacob, D.J., E.W. Gottlieb, and M.J. Prather, Chemistry of the polluted boundary layer, *J. Geophys. Res.*, *94*, 12975-13002, 1989.

Junge, C.E., The modification of aerosol size distribution in the atmosphere, US Army, 1964.

Kieber, R.J., and G.R. Helz, Indirect photoreduction of aqueous chromium(VI), *Environ. Sci. Technol.*, *26*, 307-312, 1992.

Kolber, Z.S., R.T. Barber, K.H. Coale, S.E. Fitzwater, R.M. Greene, K.S. Johnson, S. Lindley, and P.G. Falkowski, Iron limitation of phytoplankton photosynthesis in the equatorial Pacific Ocean, *Nature*, *371* (6493), 145-149, 1994.

Kopcewicz, B., and M. Kopcewicz, Mossbauer study of iron-containing atmospheric aerosols, *Struct. Chem.*, *2* (3-4), 303-312, 1991.

Kopcewicz, B., and M. Kopcewicz, Seasonal variations of iron concentration in atmospheric aerosols, *Hyperfine Interactions*, *71* (1-4), 1457-1460, 1992.

Kotronarou, A., and L. Sigg, SO2 Oxidation in atmospheric water: role of Fe(II) and effect of ligands, *Environ. Sci. & Technol.*, *27* (13), 2725-2735, 1993.

Lantzy, R.J., and F.T. Mackenzie, Atmospheric trace metals: Global cycles and assessment of Man's impact, *Geochim. et Cosmochim. Acta*, *43*, 511-523, 1979.

Martin, J.H., K.H. Coale, K.S. Johnson, S.E. Fitzwater, R.M. Gordon, S.J. Tanner, C.N. Hunter, V.A. Elrod, J.L. Nowicki, and e. al., Testing the iron hypothesis in ecosystems of the equatorial Pacific Ocean, *Nature*, *371* (6493), 123-129, 1994.

Martin, J.H., and R.M. Gordon, Northeast Pacific iron distributions in relation to phytoplankton productivity, *Deep Sea Res. A.*, *35* (2), 177-196, 1988.

Morel, F.M.M., R.J.M. Hudson, and N.M. Price, Limitation of productivity by trace-metals in the sea, *Limnol. Oceanogr.*, *36* (8), 1742-17455, 1991.

Nriagu, J.O., A global assessment of natural sources of atmospheric trace metals, *Nature*, *338*, 47-49, 1989.

Nriagu, J.O., and C.I. Davidson, Toxic metals in the atmosphere, in *Advances in environmental science and technology*, Wiley, New York, 1986.

Pehkonen, S.O., R.L. Siefert, Y. Erel, S. Webb, and M.R. Hoffmann, Photoreduction of iron oxyhydroxides in the presence of important atmospheric organic compounds, *Environ. Sci. Technol.*, *27* (10), 2056-2062, 1993.

Pehkonen, S.O., R.L. Siefert, and M.R. Hoffmann, Photoreduction of iron oxyhydroxides and the photooxidation of halogenated acetic acids, *Environ. Sci. Technol.*, *29*, 1215-1222, 1995.

Price, N.M., B.A. Ahner, and F.M.M. Morel, The equatorial Pacific Ocean - grazer controlled phytoplankton populations in an iron limited ecosystem, *Limnol. & Ocean.*, *39* (3), 520-534, 1994.

Puxbaum, H., Metal compounds in the atmosphere, in *Metals and their compounds in the environment*, edited by E. Merian, pp. 257-286, VCH Publishers, 1991.

Regazzoni, A.E., and M.A. Blesa, Reactivity of surface Fe(III)-thiocyanate complexes characterized by the dissolution of hematite in acidic thiocyanate solutions, *Langmuir*, *7*, 473-478, 1991.

Siefert, R.L., S.O. Pehkonen, Y. Erel, and M.R. Hoffmann, Iron photochemistry of aqueous suspensions of ambient aerosol with added organic acids, *Geochim. et Cosmochim. Acta*, *58* (15), 3271-3279, 1994.

Siffert, C., and B. Sulzberger, Light-induced dissolution of hematite in the presence of oxalate: a case study, *Langmuir*, *7*, 1627-1634, 1991.

Spokes, L.J., T.D. Jickells, and B. Lim, Solubilisation of aerosol trace metals by cloud processing: A laboratory study, *Geochim. et Cosmochim. Acta*, *58* (15), 3281-3287, 1994.

Stone, A.T., Adsorption of organic reductants and subsequent electron transfer on metal oxide surfaces, in *Geochemical Processes at Mineral Surfaces*, edited by J.A. Davis, and K.F. Hayes, American Chem. Soc., 1986.

Wells, M.L., N.M. Price, and K.W. Bruland, Iron limitation and the cyanobacterium synechococcus in equatorial pacific waters, *Limnol. Ocean.*, *39* (6), 1481-1486, 1994.

Wells, M.L., N.M. Price, and K.W. Bruland, Iron chemistry in seawater and its relationship to phytoplankton: a workshop report, *Marine Chem.*, *48*, 157-182, 1995.

Weschler, C.J., M.L. Mandich, and T.E. Graedel, Speciation, photosensitivity, and reactions of transition metal ions in atmospheric droplets, *J. Geophys. Res.*, *91*, 5189-5204, 1986.

Wiersma, G.B., and C.I. Davidson, Trace metals in the atmosphere of remote areas, in *Toxic trace metals in the atmosphere*, edited by J.O. Nriagu, and C.I. Davidson, pp. 201-266, Wiley, New York, 1986.

Xue, H.B., M.D.S. Goncalves, M. Reutlinger, L. Sigg, and W. Stumm, Copper(I) in fogwater: determination and interactions with sulfite, *Environ. Sci. & Technol.*, *25* (10), 1716-1722, 1991.

Zhu, X.R., J.M. Prospero, D.L. Savoie, F.J. Millero, R.G. Zika, and E.S. Saltzman, Photoreduction of iron(III) in marine mineral aerosol solutions, *J. Geophys. Res. A.*, *98* (ND5), 9039-9046, 1993.

Zhuang, G., Z. Yi, R.A. Duce, and P.R. Brown, Link between iron and sulfur cycles suggested by detection of Fe(II) in remote marine aerosols, *Nature*, *355* (6360), 537-539, 1992.

Figure 1

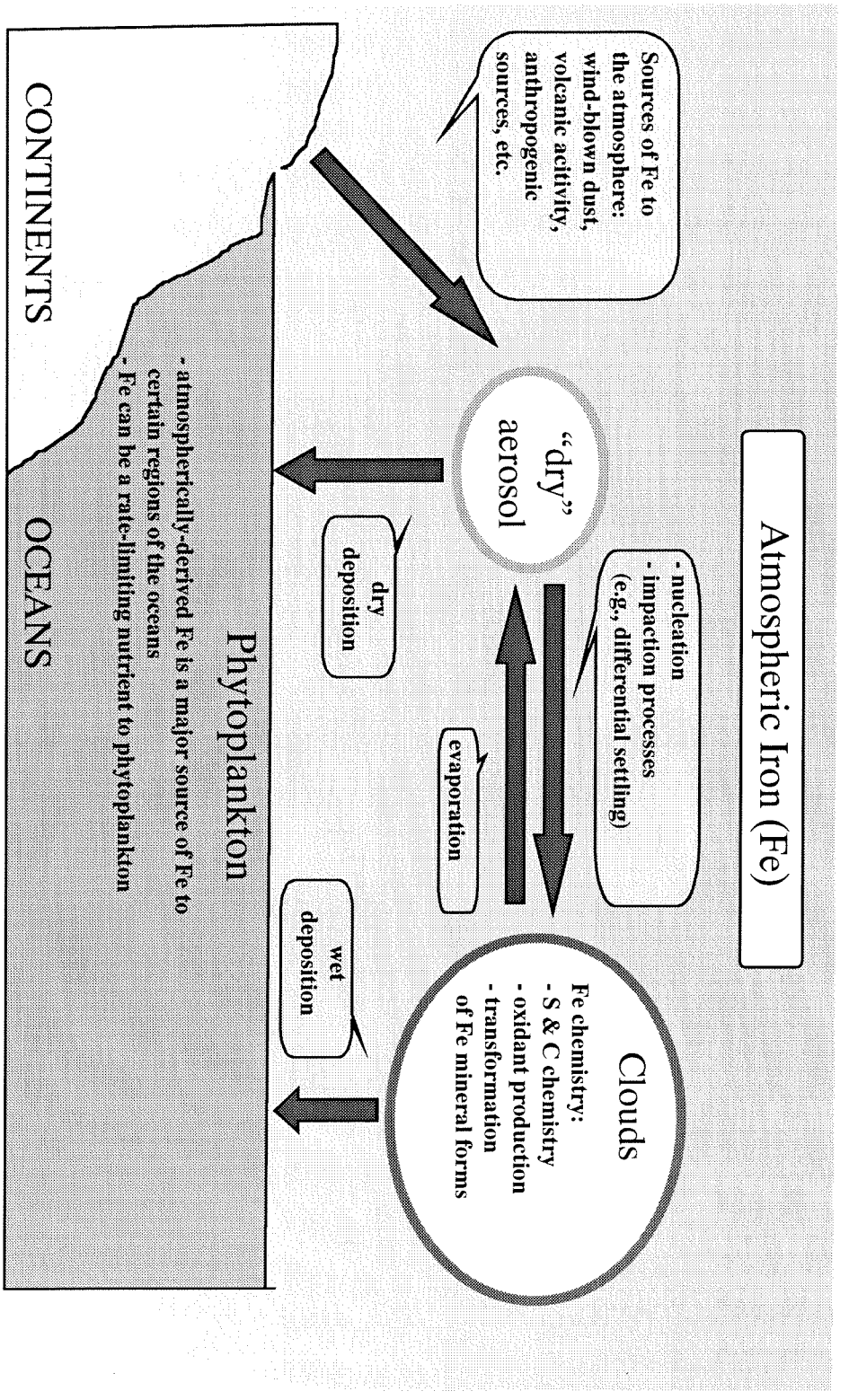
Atmospheric Iron (Fe)
Sources of Fe to the atmosphere: wind-blown dust, volcanic acitivity, anthropogenic sources, etc.
"dry" aerosol
- nucleation
- impaction processes
(e.g., differential settling)
evaporation
dry deposition
Clouds
Fe chemistry:
- S & C chemistry
- oxidant production
- transformation of Fe mineral forms
wet deposition
Phytoplankton
- atmospherically-derived Fe is a major source of Fe to certain regions of the oceans
- Fe can be a rate-limiting nutrient to phytoplankton
CONTINENTS
OCEANS

Figure 2

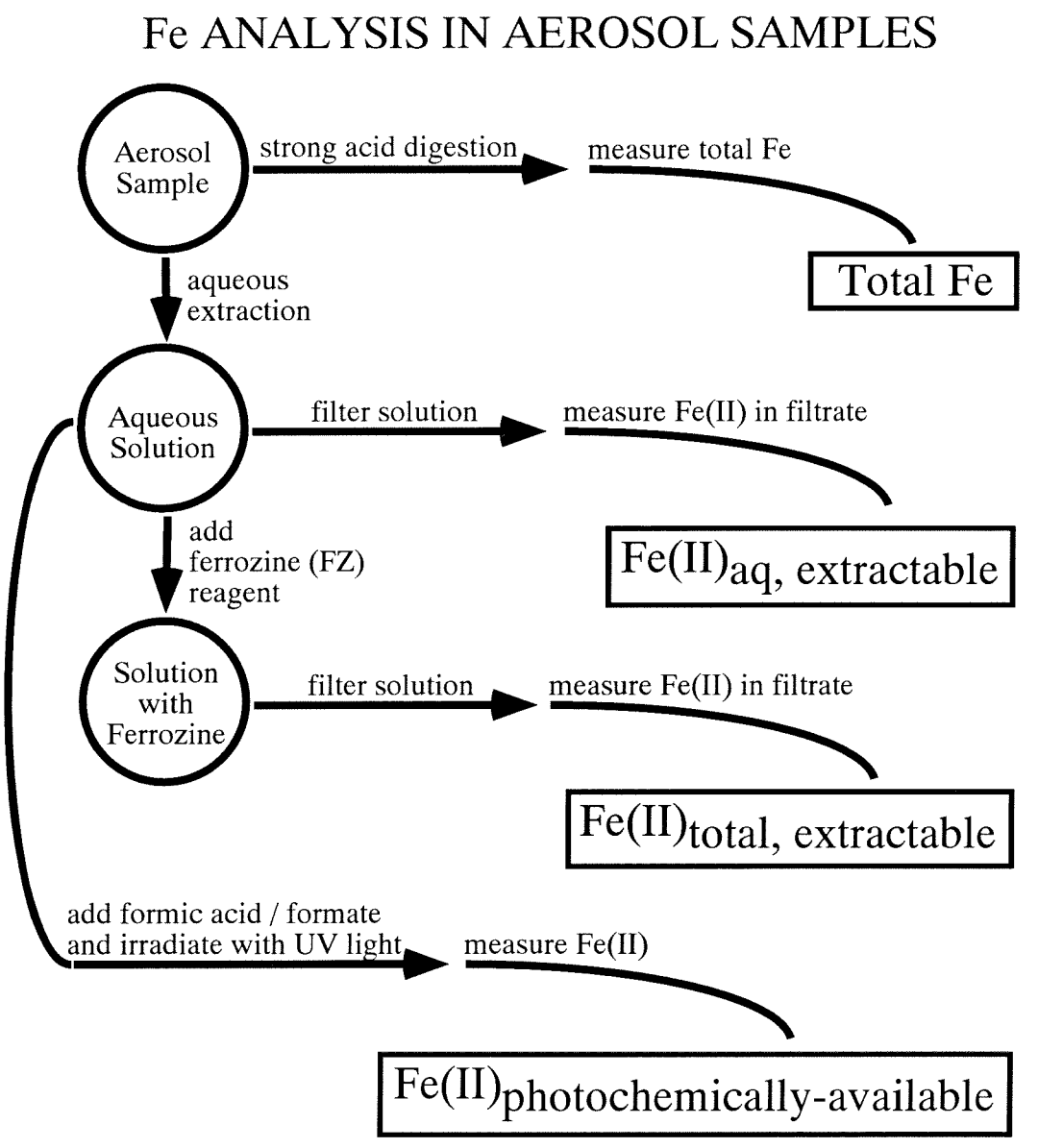
Fe ANALYSIS IN AEROSOL SAMPLES
Aerosol Sample
strong acid digestion
measure total Fe
Total Fe
aqueous extraction
Aqueous Solution
filter solution
measure Fe(II) in filtrate
Fe(II)aq, extractable
add ferrozine (FZ) reagent
Solution with Ferrozine
filter solution
measure Fe(II) in filtrate
Fe(II)total, extractable
add formic acid / formate and irradiate with UV light
measure Fe(II)
Fe(II)photochemically-available

Figure 3

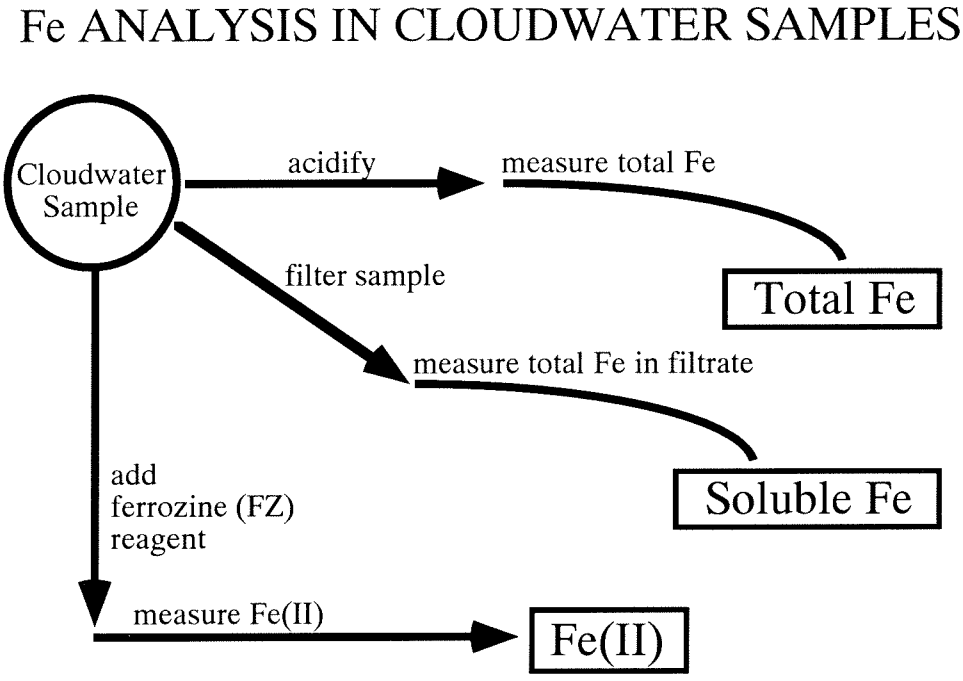
Fe ANALYSIS IN CLOUDWATER SAMPLES
Cloudwater Sample
acidify
measure total Fe
Total Fe
filter sample
measure total Fe in filtrate
Soluble Fe
add ferrozine (FZ) reagent
measure Fe(II)
Fe(II)

Chapter 2:

Iron Photochemistry of Aqueous Suspensions of Ambient Aerosol with Added Organic Acids

[Ronald L. Siefert, Simo O. Pehkonen, Yigal Erel, and Michael R. Hoffmann, *Geochimica et Cosmochimica Acta*, 58, 3271-3279, 1994]

ABSTRACT

Experiments to simulate cloudwater conditions were carried out by using ambient aerosol samples suspended in an aqueous solution. Electron-donors known to exist in atmospheric cloudwater (oxalate, formate or acetate) were then added to the simulated cloudwater, and the solution irradiated with ultraviolet light while important species were measured (i.e., H_2O_2, Fe_{total}, $Fe(II)_{aq}$ and pH). A total of four different ambient aerosol samples were used in the simulated cloudwater experiments; they were collected from Whiteface Mountain, NY (1), Pasadena, CA (2) and Sequoia National Park, CA (1). Hydrogen peroxide (H_2O_2) photoproduction was observed in the simulated cloudwater experiments with added oxalate. $Fe(II)_{aq}$ photoproduction was observed in the simulated cloudwater experiments with and without added acetate or added formate using ambient aerosol collected simultaneously with the ambient aerosol used in the added oxalate experiments. The production of $Fe(II)_{aq}$ showed that Fe from the ambient aerosol was available for photochemical redox reactions. In all cases, the production rates for $Fe(II)_{aq}$ and H_2O_2 in the light were greater than production rates in non-irradiated control experiments. The simulated cloudwater experiments (with 4 different aerosol samples) showed similar behavior to previous experiments carried out with synthetic Fe-oxyhydroxy polymorphs in the presence of oxalate, formate or acetate. The Fe present in the ambient aerosol appears to be a critical component for the production of H_2O_2 in the simulated cloudwater experiments.

INTRODUCTION

Iron (Fe) is a common element found in cloudwater and fogwater with total Fe concentrations ranging from 0.4 μM to 424 μM [Behra and Sigg, 1990; Waldman *et al.*, 1982; Munger *et al.*, 1983; Fuzzi *et al.*, 1988; Jacob *et al.*, 1985]. Ambient aerosol is the source of Fe and other transition metals to cloudwater. Fe is introduced into the atmosphere through soil dust, fly ash from fossil fuel power plants, industrial emissions and from the exhaust of internal combustion engines [Seinfeld, 1986]. Meteoric aerosol is also believed to be a source of Fe to the atmosphere [Kopcewicz and Kopcewicz, 1991]. Concentrations of Fe in tropospheric aerosols range from: 0.6 to 4160 ng/m^3 in remote areas, 55 to 14500 ng/m^3 in rural areas and 21 to 32820 ng/m^3 in urban areas [Schroeder *et al.*, 1987]. Aerosol particles are incorporated into cloudwater as condensation nuclei or are captured by cloudwater through impaction or differential settling. These processes result in a suspension of particles and dissolved species in cloudwater derived from atmospheric aerosol particles. A fraction of the Fe present in the particles can dissolve into solution [Zhu *et al.*, 1992] along with other water soluble species. However, the nature of the Fe containing phase is extremely important in determining the rate and extent of Fe dissolution (e.g. is the Fe present as an amorphous Fe-oxyhydroxide, hematite, in an alumino-silicate matrix, as a salt, etc.). The Fe phase is also important for the *in situ* photoreactivity of Fe [Pehkonen *et. al.*, 1993].

Fe(III)-carboxylate complexes in aqueous solution have been shown to undergo photochemical redox reactions where the Fe(III) is reduced to Fe(II) and the complexed organic anion is oxidized [Pehkonen *et al.*, 1993; Faust and Zepp, 1993; Zuo and Hoigné, 1992]. The Fe(III) in these complexes can either be in solution or a surface species associated with an Fe-oxyhydroxy polymorph [Pehkonen *et al.*, 1993]. The three most abundant measured carboxylate species in atmospheric water are formate, acetate and oxalate [Erel *et al.*, 1993; Kawamura and Kaplan, 1991; Zuo and Hoigné, 1992; Munger

et al., 1989]. Hydrogen peroxide (H_2O_2) is an important product in the photochemistry of the Fe(III)-oxalate complex in the presence of dissolved oxygen [Zuo and Hoigné, 1992]. Aqueous solutions of Fe-oxyhydroxy polymorphs in the presence of oxalate also produce H_2O_2 photochemically [Pehkonen *et al.*, 1993]. These aqueous-phase photochemical reactions of Fe(III)-oxalate complexes have been proposed to be a source of H_2O_2 in cloudwater [Zuo and Hoigné, 1992]. Previously, it has been thought that the primary source of atmospheric H_2O_2 was controlled by gas-phase reactions [Gunz and Hoffmann, 1990; Sakugawa *et al.*, 1990; Thompson, 1992]. H_2O_2 is efficiently scavenged by clouds in the atmosphere due to its high Henry's Law constant [Seinfeld, 1986]. However, there is more evidence that in cloud production of H_2O_2 could be an important source of H_2O_2 to clouds. Recent experiments have shown the production of H_2O_2 in irradiated authentic fogwater and cloudwater [Faust *et al.*, 1993; Zuo and Hoigné, 1993]. Irradiations of authentic fogwater and cloudwater have also produced peroxy radicals ($RO_2^{\bullet}$ and $HO_2^{\bullet}$) which can further react to form peroxides [Faust and Allen, 1992].

H_2O_2 is an important atmospheric species for both gas-phase reactions and aqueous-phase reactions [Gunz and Hoffmann, 1990; Sakugawa *et al.*, 1990; Thompson, 1992]. Cloudwater H_2O_2 is the principal oxidant of S(IV) to S(VI) in the atmosphere [Jacob and Hoffmann, 1983; Hoffmann and Boyce, 1983; Hoffmann and Jacob, 1984], however, this reaction is limited by the availability of H_2O_2 [Jacob and Hoffmann, 1983; Pandis and Seinfeld, 1989]. H_2O_2 can also be important as a source of hydroxyl radical ($OH^{\bullet}$) in the atmospheric oxidation of dimethyl sulfide (DMS) to non-sea-salt sulfate ($NSS\text{-}SO_4^{2-}$) aerosol (H_2O_2 can photolyse and produce two $OH^{\bullet}$). Charlson *et al.* [1987] have proposed a climate feedback mechanism involving phytoplankton, atmospheric sulfur and cloud albedo where the oxidation of DMS to $NSS\text{-}SO_4^{2-}$ is a critical step. H_2O_2 is also considered to be a plant phytotoxin [Gaffney *et al.*, 1987; Möller, 1989].

Overall, understanding the sources of H_2O_2 in the atmosphere is critical to understanding many important chemical mechanisms.

Previous studies in cloudwater/fogwater photochemistry have centered around the use of authentic fogwater or cloudwater in experiments [Faust *et al.*, 1993; Zuo and Hoigné, 1993; Faust and Allen, 1992]. In this paper, experiments were carried out to understand the role of ambient aerosol in cloudwater chemistry, since ambient aerosol is the source of Fe and many other cloudwater species. Ambient aerosol samples were suspended in aqueous solution and irradiated with light to simulate cloudwater. In most experiments, important atmospheric electron donors (formate, acetate and oxalate), which are known to complex Fe and undergo photochemical redox reactions, were added to the aqueous suspensions. Our principle experimental objectives were to determine if the Fe present in the ambient aerosol particulate samples could be involved in photochemical redox reactions, and to compare these results to previous studies of Fe-oxyhydroxide systems using the same electron donors [Pehkonen *et al.*, 1993].

METHODS

Ambient Aerosol Collection

Ambient aerosol was collected on 47 mm Gelman Zefluor PTFE filters with a pore size of 1 μm. Collection sites were located at Whiteface Mountain, NY (WMNY), Sequoia National Park, CA (SNPCA), and Pasadena, CA (PCA). A volumetric flow rate of approximately 10 L min^{-1} through each filter was maintained with a critical orifice. Filters, polycarbonate filter holders and labware were cleaned rigorously before use [Patterson and Settle, 1976]. The filter cleaning procedure consisted of a 10% HF bath for 24 hours and a 10% HNO_3 bath for 24 hours with several water rinses between each step and after the final bath (ultra-pure acids from Seastar Chemicals, Sidney, B.C., Canada, and 18.2 MΩ-cm Milli-Q water were used for all steps). Filter holders were cleaned in two warm HNO_3 baths with several water rinses between baths and also after the second bath. The first bath consisted of a 5% reagent grade HNO_3 solution and lasted for 24 hours, while the second bath consisted of a 1% Seastar HNO_3 in 18.2 MΩ-cm Milli-Q water also lasted for 24 hours. After collection the filters were stored at 21°C and a relative humidity of 50% for several days and then weighed. After weighing the samples were stored in the dark at 4°C, for periods ranging from 1 to 12 weeks prior to use in photochemical experiments.

Simulated Cloudwater Experimental Procedure

The filter, used to collect the ambient aerosol, was placed in a photochemical reactor vessel (borosilicate glass) with approximately 100 ml of 18.2 MΩ-cm Milli-Q water and sonicated for 1.5 hours in the dark to suspend the ambient aerosol particles into solution (Branson 5200 Sonicator). After sonication, the filter was removed and stored at 21°C and 50% relative humidity for several days and then weighed to determine the total dissolved solids in the simulated cloudwater solution. After removal of the filter, the

organic acid was added (except in the case of no added electron donor experiments) and the pH was adjusted using perchloric acid and sodium hydroxide (a Teflon coated magnetic stir bar continually mixed the solution). After the solution was allowed to equilibrate for about ten minutes, initial measurements were taken (e.g. pH, Fe(II), total metals, H_2O_2, etc.). An 11 ml aliquot of the solution was removed and kept in the dark as a non-irradiated control.

A 450 Watt Xenon lamp (PRA) with a 320 to 390 nm bandpass filter (Kopp GS7-60-1) was used as the light source. This bandpass filter was chosen since it has been previously shown that most of the Fe redox photochemistry occurs with wavelengths less than 400 nm [Siffert and Sulzberger, 1991; Pehkonen *et al.*, 1993]. The photon flux between 320 and 390 nm was measured using a chemical actinometer, Aberchrome 540 [Heller and Langan, 1981]. The photon flux for all the experiments was close to natural sunlight over the same wavelength range (i.e. $\approx 1.3 \times 10^{16}$ photons sec^{-1} cm^{-2} at sea level with a solar zenith angle of 30°) [Demerjian *et al.*, 1980]. The reactor vessel had a flat window with an area of 8.5 cm^2. The temperature of the reactor vessel was kept at ambient temperature via fan-driven air cooling.

All aliquots were filtered through a 0.2 μm cellulose acetate syringe filter before chemical analysis except the aliquots for total metal concentrations. H_2O_2 was measured fluorometrically [Kok *et al.*, 1986], while $Fe(II)_{aq}$ was measured colorimetrically [Stookey, 1970; Carter, 1971]. Initial rates of H_2O_2 photoproduction were determined by a linear least-squares fit of the linear data points at the beginning of the experiments. Oxalate concentrations were measured using ion chromatography (Dionex BIOLC ion chromatograph with PAX-500 anion column and a NaOH eluent). A strong mineral-acid digestion procedure (using ultra-pure HF, HNO_3 and HCl acids from Seastar Chemicals) was used to dissolve particulates for total metal concentration measurements. The procedure consisted of: evaporation of the aliquot to dryness; digestion of the residue with 1 g concentrated HF and 1 g concentrated HNO_3; shaking of the solution overnight;

evaporation of the solution to dryness; and finally re-digestion of the residue in 10 g of 10% HCl. Cr_{tot}, Mn_{tot}, Fe_{tot} and Cu_{tot} concentrations were measured using ICP-MS (Perkin Elmer - SCIEX Elan 5000). Aliquots for total metal analysis were removed at the end of each experiment. An aliquot to determine the amount of Fe adsorbed to the walls of the reactor vessel was also taken at the end of the experiment. The sample for adsorbed Fe was obtained by acidifying the remaining solution in the reactor vessel to pH 0.5 (using HCl Seastar acid), waiting 30 minutes and then removing an aliquot for total metals analysis as described above.

The initial oxalate/oxalic acid, formate/formic acid, and acetate/acetic acid concentrations for the experiments with added organic acids was 5.4 mM (except where noted). For brevity, the acid and anion form of the carboxylic acids will only be referred to by their anion name (e.g. oxalate/oxalic acid will be referred to as oxalate). The initial pH was between 3.15 and 3.22 for the added oxalate experiments; and between 4.20 and 4.25 for the added formate, added acetate and "no electron donor" experiments.

RESULTS AND DISCUSSION

Ambient Aerosol and Simulated Cloudwater

Table 1 summarizes the collection period, total suspended particulate matter and transition metal concentrations (Cr, Mn, Fe, Cu) for the four different ambient aerosol collections. The Fe concentrations for the three collections were within the ranges given by Schroeder *et al.* [1987].

The total dissolved solids concentrations for all the simulated cloudwater experiments were between 30 and 47 mg/l. Total solids concentrations in typical fogwater and cloudwater were calculated by summing the average concentrations of cations, anions, metals and total organic carbon (i.e. K^+, Na^+, Mg^{2+}, Ca^{2+}, NH_4^+, Cl^-, SO_3^{2-}, SO_4^{2-}, NO_3^-, HCO_2^-, $CH_3CO_2^-$, $C_2O_4^{2-}$, Al_{tot}, Si_{tot}, Mn_{tot}, Fe_{tot}, and total organic carbon) [Erel *et al.*, 1993]. The average total solids concentration of fogwater and cloudwater samples was found to be 170 mg/l [Erel *et al.*, 1993]. Total dissolved concentrations in the simulated cloudwater were in reasonable agreement with actual cloudwater and fogwater concentrations.

The sonication procedure was used to dislodge the non-soluble fraction of ambient aerosol particles from the filters and also dis-aggregate these particles. This procedure may cause an increase in surface area compared to cloud processes. However, there may be a decrease in surface area compared to cloud processes if the procedure does not completely dis-aggregate the particles. The simulated cloudwater experiments all followed identical sonication procedures allowing for the comparison of experiments.

Differences in Fe_{tot} for experiments containing ambient aerosol collected during the same period were found. The differences may be caused by: different [Total Dissolved/Suspended Solids from Filter] concentrations, and/or, Fe adsorbing to the walls of the reactor vessel. Fe_{tot} concentrations in the formate and acetate experiments were greater than the Fe_{tot} concentrations in the oxalate experiments for both PCA and SPCA

aerosol samples. This may be due to the formation of Fe(II) in the formate and acetate experiments, which would increase the overall solubility of Fe in solution. The procedure to determine the Fe adsorbed to the walls of the reactor vessel indicated that between 0% and 35% of the total Fe in the simulated cloudwater solutions was adsorbed to the walls by the end of the experiments. These differences in adsorbed iron are probably due to the different redox chemistry during the course of the experiments.

Oxalate concentrations in fogwater and cloudwater have been found to be between 0 to 13 μM [Erel *et. al.*, 1993], formate concentrations between 12 and 43 μM, and acetate concentrations between 6 and 31 μM [Munger *et al.*, 1989]. The higher concentrations of oxalate (100 - 5400 μM), formate (100 - 5560 μM) and acetate (5560 μM) in these experiments were used to increase the buffer capacity of the solution, to keep the ionic strength constant, and to allow comparison of the data to other experiments carried out with synthetic Fe-oxyhydroxide polymorphs [Pehkonen *et al.*, 1993]. Erel *et al.* [1993] have also shown, by thermodynamic speciation calculations, that greater than 98% of $Fe(III)_{aq}$ was complexed with oxalate in cloudwater. The species included in the calculation were: [Fe(III)] = 1.2 μM; [Fe(II)] = 1.8 μM; $[SO_4^{2-}]$ = 260 μM; [(acetate + formate)] = 77 μM; [oxalate] = 13 μM; $[H_2O_2]$ = 41 μM; [formaldehyde] = 10 μM and pH = 3.4. Zuo and Hoigné [1992] also concluded that Fe(III)-oxalato complexes are often the predominant species. The reason Fe(III) is predominantly complexed with oxalate is due to the extremely high stability constants of oxalate with Fe(III) compared to the stability constants of other species present. The calculated $Fe(III)_{aq}$ speciation in these experiments is similar to ambient cloudwater. Fe(III) on the surface of the Fe-oxyhydroxide is also predicted to be complexed by oxalate, since Fe(III) on the surface of Fe-oxyhydroxides behaves similarly to $Fe(III)_{aq}$ [Stumm and Morgan, 1981].

Simulated Cloudwater with Added Oxalate

Experiments using aerosol collected at each location resulted in significant H_2O_2 production. Figure 1 shows the production of H_2O_2 using aerosol collected at Whiteface Mountain, NY (WMNY); Sequoia National Park, CA (SNPCA); and Pasadena, CA (PCA). In each case, an aliquot of solution was removed prior to irradiation and stored in the dark (labeled as "In-Dark" in Fig. 1). The dark controls showed no significant production of H_2O_2. $Fe(II)_{aq}$ was always found to exist below detection limit in the oxalate experiments where H_2O_2 is produced. The method for determining H_2O_2 is also sensitive to other organic peroxides [Kok *et al.*, 1986]. Low-levels of peroxides were measured during experiments where no electron-donors were added to the ambient aerosol suspension (see *Simulated Cloudwater with Formate, Acetate or No Electron-Donor* sub-section). It was only during the experiments where oxalate was added to the suspension that peroxide production was significant. Experiments by Zuo Y. and Hoigné J. [1992] showed that Fe(III)-oxalate complexes produce H_2O_2 and not organic peroxides. Therefore, H_2O_2 was the peroxide being produced in the added oxalate experiments in Fig. 1 and Fig. 2.

Figure 1 also shows the production of H_2O_2 with no ambient aerosol sample suspended in solution. Pehkonen *et al.* [1993] also found that aqueous oxalate can photolyze and produce H_2O_2. However, the initial H_2O_2 production rate in each of the simulated cloudwater experiments with added oxalate was greater than the production rate of H_2O_2 from the photolysis of oxalate alone. Initial rates of H_2O_2 production are shown in Table 2.

The production of H_2O_2 in each experiment also resulted in an increase of pH, which is in agreement with the following mechanism [Zuo and Hoigné, 1992]:

$$Fe(III)(H_2O)_6^{3+} + C_2O_4^{2-} \quad \Leftrightarrow \quad Fe(III)(H_2O)_4(C_2O_4^{2-})^{+} + 2H_2O \qquad (1)$$

$$Fe(III)(H_2O)_4(C_2O_4^{2-})^+ \xrightarrow{h\upsilon} Fe(II)(H_2O)_4(C_2O_4^{\bullet-})^+ \quad (2)$$

$$Fe(II)(H_2O)_4(C_2O_4^{\bullet-})^+ + O_2 \xrightarrow{2H_2O} Fe(II)(H_2O)_6 + O_2^{\bullet-} + 2CO_2 \quad (3)$$

$$O_2^{\bullet-} + H^+ \Leftrightarrow HO_2^{\bullet} \quad (4)$$

$$H^+ + HO_2^{\bullet} + Fe(II) \rightarrow H_2O_2 + Fe(III) \quad (5)$$

$$2HO_2^{\bullet} \rightarrow H_2O_2 + O_2 \quad (6)$$

This mechanism for homogenous reactions is similar to proposed heterogeneous chemistry on the surface of Fe(III)-oxyhydroxides [Pehkonen *et al.*, 1993; Zuo and Hoigné, 1992]. A proton is consumed in steps 4 and 5, resulting in the observed increase of pH during the course of the experiments. PCA aerosol resulted in the most rapid pH rise; this is likely due to the greater availability of photoactive Fe in the PCA ambient aerosol compared to other aerosol samples.

An alternative pathway involving the semiconductor properties of iron oxide polymorphs [Faust *et al.*, 1989; Kormann *et al.*, 1988] can also lead to the formation of H_2O_2 as follows:

$$Fe_xO_y \xrightarrow{h\upsilon} h^+_{vb} + e^-_{cb} \quad (7)$$

$$e^-_{cb} + O_2 \rightarrow O_2^{\bullet-} \quad (8)$$

$$h^+_{vb} + C_2O_4^{2-} \rightarrow C_2O_4^{\bullet-} \quad (9)$$

$$C_2O_4^{\bullet-} + O_2 \rightarrow O_2^{\bullet-} + 2CO_2 \quad (10)$$

where h_{vb}^+ is a surface-trapped valence band hole, and e_{cb}^- is a surface-trapped conduction band electron in the photoexcited semiconductor.

During steady state photolysis, there is also a loss of H_2O_2 due to its reactions with $Fe(II)_{aq}$, $Fe(III)_{aq}$ [Zepp *et al.*, 1992; Zuo and Hoigné, 1992] or semiconducting Fe-oxyhydroxy polymorphs [Kormann *et al.*, 1988] as follows:

$$Fe(II) + H_2O_2 \rightarrow Fe(III) + OH^{\bullet} + OH^- \quad (11)$$

$$Fe(III) + H_2O_2 \rightarrow Fe(II) + HO_2^{\bullet} + H^+ \quad (12)$$

$$2h_{vb}^+ + H_2O_2 \rightarrow O_2 + 2H^+ \quad (13)$$

$$2e_{cb}^- + H_2O_2 \rightarrow 2OH^- \quad (14)$$

The dynamic behavior of H_2O_2 in Fig. 1 can be explained by the combination of reactions 1 through 14. Pehkonen *et al.* [1993] measured oxalate concentrations during the course of photoexperiments carried out with synthetic Fe oxyhydroxides and found that in experiments where H_2O_2 concentrations sharply decreased, the oxalate concentration had also decreased, but was still above 1 mM (where $[oxalate]_{initial}$ = 6.0 mM). This seems to indicate that the destruction rate of H_2O_2 is the primary reason for sharp decreases in H_2O_2 concentration, and that after an induction period, the destruction rate increases rapidly resulting in the lower H_2O_2 concentrations. The PCA experiment shows this behavior, and the WMNY experiment also shows a similar trend. The SNPCA experiment shows a slower initial rate in comparison to the PCA and WMNY experiments. Results of photochemical reactions of oxalate with different synthetic Fe(III) oxyhydroxides and soluble Fe(III) showed that the initial production rate of H_2O_2

was dependent on the form of Fe present in solution [Pehkonen *et al.*, 1993]. The different initial H_2O_2 production rates normalized to $[Fe]_{tot}$ in Fig. 1 is likely due to different forms of Fe present in the simulated cloudwater.

Figure 2a shows an experiment which used ambient aerosol collected simultaneously with the filter used for the SNPCA experiment shown in Fig. 1. In this experiment only 100 μM oxalate was added to the suspension, and the pH was kept constant at 3.22 by the addition of perchloric acid. This concentration was closer to measured oxalate concentrations in fogwater and cloudwater [Erel *et. al.*, 1993]. The H_2O_2 concentration profile is very similar to the higher oxalate concentration experiment shown in Fig. 1. The decrease in the concentration of H_2O_2 toward the end of the experiment, with 100 μM oxalate, is probably due to the depletion of the oxalate. Another experiment using PCA ambient aerosol shows this behavior. Figure 2b is an experiment with 100 μM oxalate added to the suspension of ambient aerosol. In this experiment, the oxalate concentration was measured three times during the experiment and is also plotted along with the H_2O_2 concentration. Figure 2c is another experiment which used ambient aerosol collected simultaneously with the ambient aerosol used in Fig. 2b, however measurements were taken more frequently. These results show the destruction of oxalate accompanied by an increase in H_2O_2 concentration. It is clear (Fig. 2b) that when the oxalate is depleted, the H_2O_2 concentration decreases.

It is important to observe that even though the initial oxalate concentration for the SNPCA simulated cloudwater experiment (Fig. 2a) was only 100μM compared to 5.4 mM in the experiment shown in Fig. 1b, the initial H_2O_2 production rate normalized to actinic flux only decreased by 53% (See Table 2). This can be explained by assuming that the Fe(III) speciation did not change substantially when the oxalate concentration changed, since oxalate has a relatively high complexing constant with Fe(III).

Calculations based on the simulated cloudwater experiments with added oxalate were carried out to determine the impact that clouds could have on H_2O_2 concentrations

in the atmosphere. H_2O_2 production rates of 14 μM hr^{-1} in clouds (this is the initial non-normalized H_2O_2 production rate for the PCA experiment) correspond to gas-phase production rates of 0.36 ppb hr^{-1} (assuming the liquid water content (LWC) = 10^{-6}). The aqueous-phase fraction of H_2O_2 in clouds with LWC = 10^{-6} is 63 %; therefore the aqueous-phase production of H_2O_2 would increase the gas-phase H_2O_2 concentration by a rate of 0.13 ppb hr^{-1} assuming H_2O_2 is in equilibrium between the gas phase and liquid phase. H_2O_2 formed in cloudwater can also be transferred to the gas phase when the cloudwater droplets evaporate. However, the production of H_2O_2 in actual cloudwater would be dependent on the amount of oxalate present. This oxalate can be produced via reactions with organic compounds present in the cloudwater, or transferred from the gas phase.

Simulated Cloudwater with Added Formate, Added Acetate or No Added Electron-Donor

Figure 3 shows additional experiments that were carried out using ambient aerosol collected simultaneously with the ambient aerosol used for the experiments shown in Fig. 1. Formate or acetate was added to these simulated cloudwater experiments (except Fig. 3a where no electron-donor was added). A previous study has shown that both formate and acetate photoreductively dissolve Fe-oxyhydroxides producing $Fe(II)_{aq}$ and also photochemically reduce $Fe(III)_{aq}$ to $Fe(II)_{aq}$ [Pehkonen *et al.*, 1993]. The experiments shown in Fig. 3 were performed to determine the Fe available for photochemical redox reactions in the ambient aerosol samples by measuring the production of $Fe(II)_{aq}$.

The first experiment contained ambient aerosol collected at PCA with no added electron donor. The pH was kept constant at 4.2 by adding perchloric acid. H_2O_2 concentrations were measured to be between 1 and 2 μM (with no clear production or destruction trend). There was an increase in $Fe(II)_{aq}$ from 0.4 μM at the beginning of the

experiment to 2.0 μM after 24 hours with most of the increase occurring during the beginning of the experiment. The increase in $Fe(II)_{aq}$ was probably due to the photoreduction of $Fe(III)_{aq}$ or surficial Fe(III) in the presence of electron donors already present in the ambient aerosol. The second experiment contained ambient aerosol collected at PCA with an added initial formate concentration of 5.56 mM. The formate acted as the electron donor and buffer (the pH remained constant at 4.2). H_2O_2 was assumed to be negligible in light of the results in the "no-electron donor" experiment and thus was not measured. $Fe(II)_{aq}$ increased from 0.5 μM at the beginning of the experiment to 2.4 μM after 24 hours with most of the increase occurring during the beginning of the experiment.. The third experiment used ambient aerosol collected at PCA with an initial acetate concentration of 5.56 mM. The acetate acted as the electron donor and buffer (the pH remained constant at 4.2). $Fe(II)_{aq}$ increased from 0.5 μM at the beginning of the experiment to 2.0 μM after 24 hours with most of the increase occurring during the beginning of the experiment. The fourth experiment used ambient aerosol collected simultaneously with the ambient aerosol used for the SNPCA experiment shown in Fig. 1. The solution had an initial formate concentration of 5.56 mM. $Fe(II)_{aq}$ increased from 0.2 μM to 1.6 μM. The fifth experiment also used ambient aerosol collected simultaneously with the ambient aerosol used for the SNPCA experiment shown in Fig. 1. The solution had an initial acetate concentration of 5.56 mM. However, in this experiment, $Fe(II)_{aq}$ only increased from 0.2 μM to 0.4 μM. The sixth experiment used ambient aerosol collected simultaneously with the ambient aerosol used for the experiment shown in Fig. 2b and Fig. 2c. The solution had an initial acetate concentration of 100 μM. In this experiment, $Fe(II)_{aq}$ increased from 0.1 μM to 1.4 μM. There was not enough WMNY ambient aerosol samples to carry out experiments with added formate or acetate.

Formate and acetate are known to photoreductively dissolve Fe oxyhydroxides [Pehkonen *et al.*, 1993], and this photoreduction along with the homogenous reduction of

$Fe(III)_{aq}$ results in the $Fe(II)_{aq}$ concentrations shown in Fig. 3. Pehkonen *et al.* [1993] showed that formate is a more effective photoreductant of Fe(III) oxyhydroxides than acetate, and the formate experiments in Fig. 3 show the highest concentration of $Fe(II)_{aq}$ at the end of the experiments. Pehkonen *et al.* [1993] also showed that different Fe oxyhydroxides have different photoreductive dissolution rates and this behavior is also seen in comparing the PCA and SNPCA experiments in Fig. 3. The added formate and added acetate PCA experiments show a similar behavior, but the added formate SNPCA experiment shows a greater rate of $Fe(II)_{aq}$ production then in the added formate SNPCA experiment. These results may be due to different forms of Fe present in the PCA and SNPCA ambient aerosol. Figure 3 shows that Fe present in the ambient aerosol for PCA and SNPCA is photoactive (i.e. available for photochemical redox reactions). However, the amount of photoactive Fe in the SNPCA simulated cloudwater experiments is less than the amount of photoactive Fe in the PCA simulated cloudwater experiments (this is seen by comparing both the added formate and added acetate experiments). These results are also consistent with the slower initial H_2O_2 production rates shown in Table 2 for SNPCA ambient aerosol compared to PCA ambient aerosol.

CONCLUSIONS

Simulated cloudwater experiments were carried out by suspending ambient aerosol samples into an aqueous solution and then irradiating the solution with light. The photoproduction of H_2O_2 in these simulated cloudwater experiments, with added oxalate, supports previous studies which propose fogwater and cloudwater as important sources of H_2O_2 in the atmosphere. The different initial H_2O_2 production rates normalized to Fe_{total} for these experiments also appears to be due to different forms of iron present in the different ambient aerosol samples. Simulated cloudwater experiments with and without added formate and acetate also showed that Fe from ambient aerosol samples was available for photochemical redox reactions. The aqueous photoproduction of H_2O_2 is observed with aqueous suspensions of four different ambient aerosol samples collected from a variety of locations [Whiteface Mountain, NY(1); Sequoia National Park, CA(1); and Pasadena, CA(2)]. In all cases, the production rates for $Fe(II)_{aq}$ and H_2O_2 in the light were greater than production rates in non-irradiated control experiments. These simulated cloudwater experiments provide a new tool for studying fogwater and cloudwater chemistry.

Acknowledgments: We thank the staff of ASRC at Whiteface Mountain, especially Anne Foster and Richard MacDonald, and also the staff at Sequoia National Park, especially Diane Ewell and Annie Esperanza, for their help. We also thank Prof. Andy Friedland at Dartmouth College. We also thank Prof. J. Morgan for helpful discussions, and Mike Wong for his help in the laboratory. We also thank the reviewers for there contributions to the paper. Support for this research has been provided by a grant from the National Science Foundation, Division of Atmospheric Sciences, Atmospheric Chemistry Section (ATM 9015775; ATM 9303024). This research was also sponsored by the U.S. Department of Energy, Office of Energy Research, Environmental Sciences Division, Office of Health and Environmental Research, under appointment to the Graduate Fellowships for Global Change administered by Oak Ridge Institute for Science and Education.

REFERENCES

Behra P. and Sigg L. (1990) Evidence for redox cycling of iron in atmospheric water droplets. *Nature* **344**, 419-421.

Carter P. (1971) Spectrophotometric determination of serum iron at the submicrogram level with a new reagent (ferrozine). *Anal. Biochem.* **40,** 450-458.

Charlson R. J., Lovelock J. E., Andreae M. O. and Warren S. G. (1987) Oceanic phytoplankton, atmospheric sulphur, cloud albedo and climate. *Nature* **326,** 655-661.

Demerjian K. L., Schere K. L. and Peterson J. T. (1980) Theoretical estimates of actinic (spherically integrated) flux and photolytic rate constants of atmospheric species in the lower troposphere. *Adv. Environ. Sci. Technol.* **10,** 369.

Erel Y., Pehkonen S. O. and Hoffmann M. R. (1993) Redox chemistry of Iron in fog and stratus clouds. *J. Geophys. Res.* **98,** 18423-18434.

Faust B. C. and Allen J. M. (1992) Aqueous-phase photochemical sources of peroxyl radicals and singlet molecular oxygen in clouds and fog. *J. Geophys. Res.* **97,** 12913-12926.

Faust B. C., Anastasio C., Allen J. M. and Arakaki T. (1993) Aqueous phase photochemical formation of peroxides in authentic cloud and fog waters. *Science* **260**, 73-75.

Faust B. C. and Zepp R. G. (1993) Photochemistry of aqueous iron(III)-polycarboxylate complexes: roles in the chemistry of atmospheric and surface waters. *Envir. Sci. Technol.* **27,** 2517 - 2522.

Faust B. C., Hoffmann M. R. and Bahnemann D. W. (1989) Photocatalytic oxidation of sulfur-dioxide in aqueous suspensions of alpha-Fe_2O_3. *J. Phys. Chem.* **93**, 6371-6381.

Fuzzi S., Orsi G. Nardini G., Facchini M. C., McLaren E. and Mariotti M. (1988) Heterogeneous processes in the Po Valley radiation fog. *J. of Geophys. Res.* **93,** 11141-11151.

Gaffney J. S., Streit G. E., Spall W. D. and Hall J. H. (1987) Beyond acid rain. *Envir. Sci. Technol.* **21,** 519 - 524.

Gunz D. W. and Hoffmann M. R. (1990) Atmospheric chemistry of peroxides: a review. *Atmos. Envir.* **24A,** 1601 - 1633.

Heller H. G. and Langan J. R. (1981) A new reusable chemical actinometer. *J. C. S. Perkin I* 341.

Hoffmann M. R. and Boyce S. D. (1983) Catalytic autooxidation of aqueous sulfur dioxide in relationship to atmospheric systems. In *Trace Atmospheric Constituents: Properties, Transformations, and Fates* (ed. S. E. Schwartz), pp. 147-172. Wiley.

Hoffmann M. R. and Jacob D. J. (1984) Kinetics and mechanism of the catalytic oxidation of dissolved SO_2 in atmospheric droplets: free radical, polar and

photoassisted pathways. In *SO_2, NO, NO_2 Oxidation Mechanisms: Atmospheric Considerations*, (ed. J. G. Calvert), Vol. III, pp. 101-172. Butterworth Publishers.

Jacob D. J. and Hoffmann M. R. (1983) A dynamic model for the production of H^+, NO_3^-, and SO_4^{2-} in urban fog. *J. Geophys. Res.* **88,** 6611-6621.

Jacob D. J., Waldman J. M., Munger J. W. and Hoffmann M. R. (1985) Chemical composition of fogwater collected along the California coast. *Envir. Sci. Technol.* **19,** 730 -735.

Kawamura K. and Kaplan I. R. In *Organic Compounds in Rainwater* (eds. Hansen L. D. *et al.*), 233-284, CRC Press.

Kok G. L., Thompson K. and Lazrus A. L. (1986) Derivatization technique for the determination of peroxides in precipitation. *Anal. Chem.* **58,** 1192-1194.

Kopcewicz B. and Kopcewicz M. (1991) Mössbauer study of iron-containing atmospheric aerosols. *Struct. Chem.* **2**, 303-312.

Kormann C., Bahnemann D. W. and Hoffmann M. R. (1988) Photocatalytic production of H_2O_2 and organic peroxides in aqueous suspensions of TiO_2, ZnO, and desert sand. *Envir. Sci. & Tech.* 22, 798-806.

Möller D. (1989) The possible role of H_2O_2 in new-type forest decline. *Atmos. Environ.* **23,** 1625-1627.

Munger J. W., Waldman J. M., Jacob D. J. and Hoffmann M. R. (1983) Fogwater chemistry in an urban atmosphere. *J. of Geophys. Res.* **88,** 5109-5132.

Munger J. W., Collett Jr J., Daube Jr B. and Hoffmann M. R. (1989) Chemical composition of coastal stratus clouds: dependence on droplet size and distance from the coast. *Atmos. Environ.* **23,** 2305-2320.

Pandis S. N. and Seinfeld J. H. (1989) Sensitivity analysis of a chemical mechanism for aqueous-phase chemistry. *J. Geophys. Res.* **94,** 1105-1126.

Patterson C. C. and Settle D. M. (1976) The reduction of orders of magnitude errors in lead analyses of biological materials and natural waters by evaluating and controlling the extent and sources of industrial lead contamination introduced during sample collecting, handling, and analysis. *NBS Spec. Publ. (U.S.)* no. 422, 321-351.

Pehkonen S. O., Siefert R. L., Erel Y., Webb S. and Hoffmann M. R. (1993) Photoreduction of iron oxyhydroxides in the presence of important atmospheric organic compounds. *Envir. Sci. & Tech.* **27**, 2056-2062.

Sakugawa H., Kaplan I. R., Tsai W. and Cohen Y. (1990) Atmospheric hydrogen peroxide. *Envir. Sci. & Tech.* **24,** 1452-1461.

Schroeder W. H., Dobson M., Kane D. M. and Johnson N. D. (1987) Toxic trace elements associated with airborne particulate matter: a review. *J. Air Pollut. Control Assoc.* **37,** 1267-1285.

Seinfeld J. H. (1986) *Atmospheric Chemistry of Air Pollution*. Wiley-Interscience, New York.

Siffert C. and Sulzberger B. (1991) Light-induced dissolution of hematite in the presence of oxalate: a case study. *Langmuir* **7**, 1627-1634.

Stookey L. L. (1970) Ferrozine- a new spectrophotometric reagent for iron. *Anal. Chem.* **42,** 119-781.

Stumm W. and Morgan J. J. (1981) *Aquatic Chemistry*. Wiley-Interscience, New York.

Thompson A. M. (1992) The oxidizing capacity of the Earth's atmosphere: probable past and future changes. *Science* **256,** 1157-1165.

Waldman J. M., Munger J. W., Jacob D. J., Flagan R. C., Morgan J. J. and Hoffmann M. R. (1982) The chemical composition of acid fog. *Science* **218**, 677-680.

Zepp R. G., Faust B. C. and Hoigné J. (1992) Hydroxyl radical formation in aqueous reactions (ph 3-8) of iron(II) with hydrogen-peroxide - The photo-fenton reaction. *Environ. Sci. Technol.* **26,** 313-319.

Zhu X., Prospero J. M., Millero F. J., Savoie D. L. and Brass G. W. (1992) The solubility of ferric ion in marine mineral aerosol solutions at ambient relative humidities. *Marine Chemistry* **38**, 91-107.

Zuo Y. and Hoigné J. (1992) Formation of hydrogen peroxide and depletion of oxalic acid in atmospheric water by photolysis of iron(III)-oxalato compounds. *Environ. Sci. Technol.* **26,** 1014-1022.

Zuo Y. and Hoigné J. (1993) Evidence for photochemical formation of H_2O_2 and oxidation of SO_2 in authentic fog water. *Science* **260**, 71-73.

FIGURE CAPTIONS

FIGURE 1 H_2O_2 photoproduction in aqueous solutions of added oxalate and suspended ambient aerosol collected at: ***a***, Whiteface Mountain, NY from 9/10/92 to 9/22/92; ***b***, Sequoia National Park, CA from 10/5/92 to 10/13/92; and ***c***, Pasadena, CA from 9/1/92 to 9/10/92. ***d*** is a control experiment without any ambient aerosol. $[Oxalate]_{initial}$ = 5.4 mM, I_o = 7.3 x 10^{15} photons sec^{-1} cm^{-2} (320 to 390 nm). [Total Dissolved/Suspended Solids from Filter] = 29.9 mg/l, 36.3 mg/l, and 43.4 mg/l, and $[Fe]_{total}$ = 1.1 μM, 2.4 μM, and 4.8 μM, for Whiteface Mtn., NY; Sequoia National Park, CA; and Pasadena, CA; respectively.

FIGURE 2 H_2O_2 photoproduction in aqueous solutions of added oxalate and suspended ambient aerosol collected at: ***a***, Sequoia National Park, CA from 10/5/92 to 10/13/92; ***b*** and ***c***, Pasadena, CA from 11/3/92 to 11/9/92. $[Oxalate]_{initial}$ = 100 μM. I_o = 5.3 x 10^{15} photons sec^{-1} cm^{-2} (320 to 390 nm) for ***a***, and I_o = 4.5 x 10^{15} photons sec^{-1} cm^{-2} (320 to 390 nm) for ***b*** and I_o = 2.0 x 10^{15} photons sec^{-1} cm^{-2} (320 to 390 nm) for ***c***. [Total Dissolved/Suspended Solids from Filter] = 32.9 mg/l, 29.4 mg/l and 26.3 mg/l for ***a, b*** and ***c***; respectively. $[Fe]_{total}$ = 1.8 μM, 2.0μM and 3.4 μM for ***a, b*** and ***c***; respectively.

FIGURE 3 $Fe(II)_{aq}$ photoproduction in aqueous solutions of suspended ambient aerosol collected at: ***a***, Pasadena, CA from 9/1/92 to 9/10/92 with no added electron donor; ***b***, Pasadena, CA from 9/1/92 to 9/10/92 with added formate; ***c***, Pasadena, CA from 9/1/92 with added acetate; ***e***, Sequoia National Park, CA from 10/5/92 to 10/13/92 with added acetate; and ***f***, Pasadena, CA from 11/3/92 to 11/9/92 with added formate. $[Electron\ donor]_{initial}$ = 5.56 mM in ***b***, ***c***, ***d*** and ***e***. $[Formate]_{initial}$ = 100 μM for ***f***. I_o = 5.3 x 10^{15} photons sec^{-1} cm^{-2} (320 to 390 nm) for ***a***, ***b***, ***c***, ***d*** and ***e***. I_o = 2.0 x 10^{15} photons sec^{-1} cm^{-2} (320 to 390 nm) for ***e***. [Total Dissolved/Suspended Solids from Filter] = 45.7 mg/l,

46.3 mg/l, 36.5 mg/l, 32.9 mg/l, 36.5 mg/l and 29.6 mg/l for ***a, b, c, d, e*** and ***f***; respectively. $[Fe]_{total}$ = 8.4 μM, 11 μM, 12 μM, 4.0 μM, 2.7 μM and 2.3 μM for ***a, b, c, d, e,*** and ***f***; respectively.

TABLE 1. Collection site, site elevation, collection period, total suspended particulate (TSP) and metal concentrations (Fe, Mn, Cu, Cr) for the ambient aerosol collections.

Collection Site	Elev. (m)	Collection Period (Dates)	TSP ($\mu g\ m^{-3}$)	Fe ($ng\ m^{-3}$)	Mn ($ng\ m^{-3}$)	Cu ($ng\ m^{-3}$)	Cr ($ng\ m^{-3}$)
Whiteface Mtn., NY	700	09/10/92 to 09/22/92	20	37	1.2	< 0.4	< 0.1
Sequoia NP, CA	800	10/05/92 to 10/13/92	78	1100	43	4.5	1.9
Pasadena, CA	230	09/01/92 to 09/10/92	52	910	18	17	2.8
Pasadena, CA	230	11/03/92 to 11/09/92	60	1710	41	35	6.6

TABLE 2. Initial H_2O_2 production rates for experiments shown in Figure 1 and Figure 2.

Collection Site	Figure	Linear period used for calculation	$d[H_2O_2]/dt$ ($\mu M\ hr^{-1}$)	$d[H_2O_2]/dt$ normalized to $[Fe]_{total}$ ($\mu M\ \mu M^{-1}\ hr^{-1}$)	$d[H_2O_2]/dt$ normalized to actinic flux ($\mu M\ J^{-1}\ hr^{-1}$)*
Whiteface Mt., NY	1a	0 to 3.25 hr	10.3	9.36	1.41
Sequoia NP, CA	1b	0 to 11.5 hr	2.95	1.23	0.40
Pasadena, CA	1c	0 to 2.25 hr	14.4	3.00	1.97
not applicable	1d	0 to 24 hr	1.40	not applicable	0.19
Sequoia NP, CA	2a	5 to 15 hr	1.12	0.62	0.21
not applicable	2a	5 to 23 hr	0.54	not applicable	0.10
Pasadena, CA	2b	0 to 3.5 hr	3.22	1.61	0.77
Pasadena, CA	2c	0 to 4 hr	1.67	0.49	0.84

* $J = 10^{15}$ photons sec^{-1} cm^{-2} (320-390 nm)

FIGURE 1

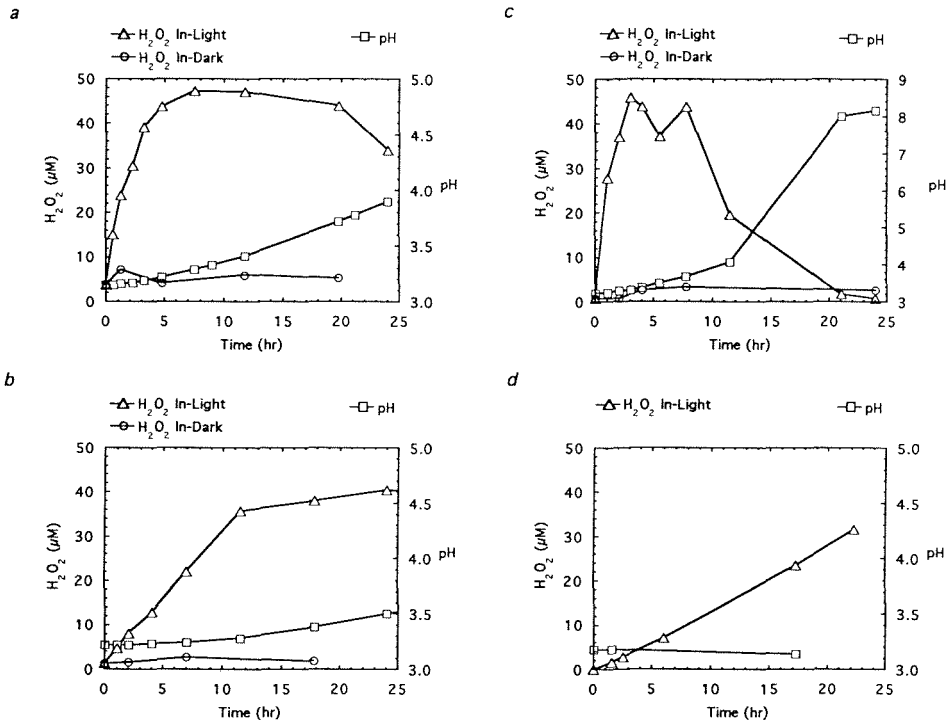

FIGURE 2

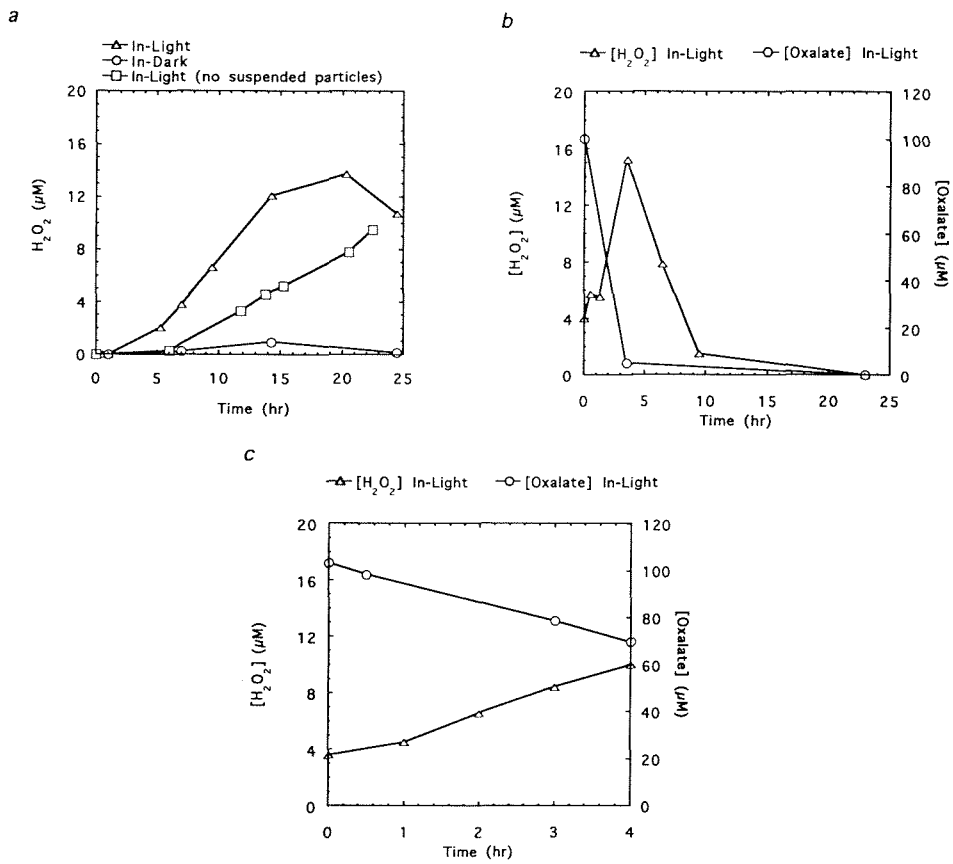
a
In-Light
In-Dark
In-Light (no suspended particles)
H2O2 (μM)
Time (hr)
b
[H2O2] In-Light
[Oxalate] In-Light
[H2O2] (μM)
[Oxalate] (μM)
Time (hr)
c
[H2O2] In-Light
[Oxalate] In-Light
[H2O2] (μM)
[Oxalate] (μM)
Time (hr)

FIGURE 3

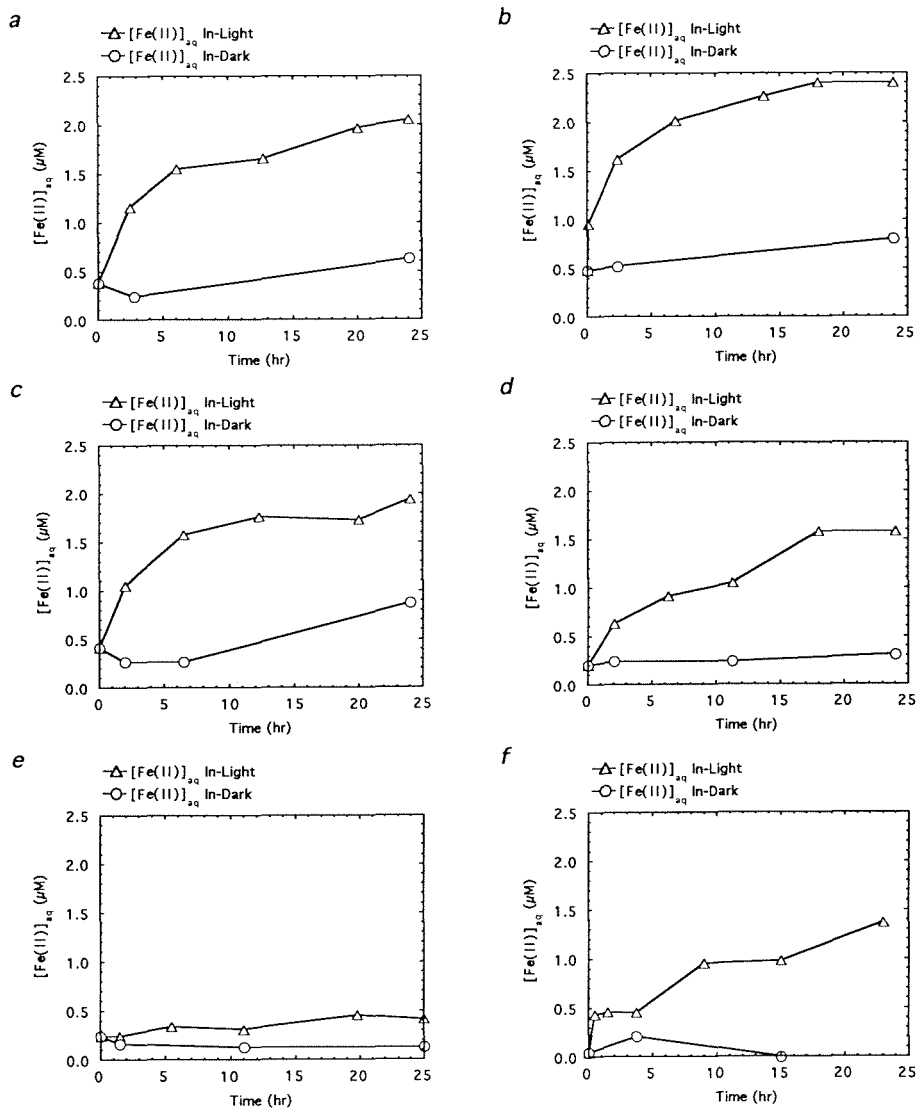
a
b
c
d
e
f
[Fe(II)]aq In-Light
[Fe(II)]aq In-Dark
[Fe(II)]aq (μM)
Time (hr)
0.0
0.5
1.0
1.5
2.0
2.5
0
5
10
15
20
25

Chapter 3:

Determination of Photochemically Available Iron in Ambient Aerosols

[Ronald L.Siefert, Samuel M. Webb, and Michael R. Hoffmann, *Journal of Geophysical Research,* 101, 14441-14449, 1996]

ABSTRACT

Experiments to determine the concentration of photochemically-available Fe in ambient aerosol samples were carried out using a novel photochemical extraction procedure. Ambient aerosol samples, which were collected on Teflon filters, were suspended in an aqueous solution within a photochemical reactor and irradiated. Under these conditions the relative amount of $Fe(II)_{aq}$ to Fe_{total} was shown to increase. This process, referred to as "photochemical weathering", is due to the reduction of $Fe(III)_{aq}$ species and the reductive dissolution of Fe(III)-oxyhydroxides minerals present in the aerosol sample. The extent and rate of $Fe(II)_{aq}$ photo-production was used to characterize the Fe in aerosol samples collected from Whiteface Mountain, NY, Pasadena, CA, San Nicholas Island, CA, and Yosemite National Park, CA. Photochemically-available Fe concentrations found ranged from < 4 ng/m^3 [0.07 nmoles/m^3] to 308 ng/m^3 [5.52 nmoles/m^3], Fe_{total} concentrations ranged from 10 ng/m^3 [0.18 nmoles/m^3] to 3400 ng/m^3 [61 nmoles/m^3], and the percentage of photochemically-available Fe to Fe_{total} ranged from 2.8% to 100%. Aerosol samples were also collected during biomass burning events in Southern California; these samples showed insignificant changes in the photochemically-available Fe (compared to non-biomass burning samples) in conjunction with large increases of Fe_{total}. Calculations based on these experiments predicts that Fe redox chemistry in cloudwater could be an important *in situ* source of oxidants ($^{\bullet}OH$, $HO_2^{\bullet}/O_2^{-}$). The estimated oxidant production rate in cloudwater based on these experiments is between 0 and 60 nM s^{-1}, with an average value of 16 nM s^{-1}. This estimated *in situ* oxidant production rate due to Fe chemistry is approximately equal to previous estimates of the oxidant flux to cloudwater from the gas-phase.

INTRODUCTION

Iron (Fe), which is one of the most abundant elements in the earth's crust, is present primarily as Fe(II) and Fe(III) forms [*Taylor and McLennan*, 1985]. Particulate Fe is transferred to the atmosphere by wind, volcanic activity, and through anthropogenic sources [*Cass and McRae*, 1983; *Seinfeld*, 1986; *Gomes and Gillette*, 1993]. Total Fe concentrations in tropospheric aerosols range from: 0.6 to 4160 ng/m^3 in remote areas, 55 to 14500 ng/m^3 in rural areas and 21 to 32820 ng/m^3 in urban areas [*Schroeder, et al.*, 1987], and cloudwater concentrations range from 0.4 μM to 424 μM [*Waldman, et al.*, 1982; *Munger, et al.*, 1983; *Jacob, et al.*, 1985; *Fuzzi, et al.*, 1988; *Behra and Sigg*, 1990].

Atmospheric particulates are the source of Fe and other transition metals to cloudwater. Ambient aerosol particles are incorporated into cloudwater as condensation nuclei or are dynamically captured by impaction or differential settling. These processes result in a suspension of particles and dissolved species in cloudwater derived from aerosol particles. A fraction of the total Fe present in aerosol can dissolve into solution [*Zhu, et al.*, 1992; *Zhuang, et al.*, 1992; *Zhu, et al.*, 1993] along with other water soluble species. Once in the droplet, Fe can participate in a variety of homogeneous and heterogeneous electron-transfer reactions. The specific mineral form of the particulate Fe is important to both the dissolution rate and the photoreactivity of the particles [*Pehkonen, et al.*, 1993; *Pehkonen, et al.*, 1995].

Fe(III)/Fe(II) redox couples are important mediators of charge-transfer reactions in natural waters [*Schwarzenbach, et al.*, 1993]. Fe(III)-carboxylate complexes have been shown to undergo photo-assisted redox reactions where the Fe(III) is reduced to Fe(II) and the complexed organic anion is oxidized [*Zuo and Hoigné*, 1992; *Faust and Zepp*, 1993; *Pehkonen, et al.*, 1993; *Pehkonen, et al.*, 1995]. The Fe(III) species can either be aqueous Fe(III) complexes or surficial Fe(III) complexes associated with an Fe-oxyhydroxy

polymorph (e.g., goethite, hematite, amorphous Fe-oxyhydroxide) [*Pehkonen, et al.*, 1993]. *Pehkonen et al.* [1993] have shown that Fe(III)-carboxylate photochemistry, can be an important pathway for the degradation of carboxylic acids in the atmosphere. The degradation products include lower chain carboxylic acids and hydrogen peroxide (H_2O_2) [*Zuo and Hoigné*, 1992; *Pehkonen, et al.*, 1993; *Siefert, et al.*, 1994]. In previous studies, it has been assumed that the primary source of atmospheric H_2O_2 was controlled by gas-phase reactions [*Gunz and Hoffmann*, 1990; *Sakugawa, et al.*, 1990; *Thompson*, 1992]. However, *Zuo and Hoigné* [1992] have shown that the photolysis of Fe(III)-oxalate complexes may be an important source of H_2O_2 in cloudwater. In addition, this pathway for the heterogeneous production of H_2O_2 may be an important factor in regulation of the oxidation capacity of the atmosphere.

The availability of Fe also affects S(IV)/S(VI) chemistry. Aqueous SO_3^{2-} can react with $Fe(III)_{aq}$ in oxic waters to yield $Fe(II)_{aq}$, SO_4^{2-}, HSO_5^- and H_2O_2 via the formation of $SO_3^{-\bullet}$, $SO_4^{-\bullet}$, $SO_5^{-\bullet}$ and $HO_2^\bullet$ [*Jacob, et al.*, 1986; *Breytenbach, et al.*, 1994]. Iron can also indirectly oxidize S(IV), through the production of H_2O_2 by the photolysis of the Fe(III)-oxalate complex and the subsequent oxidation of S(IV) by H_2O_2 [*Hoffmann and Edwards*, 1975; *McArdle and Hoffmann*, 1983]. This indirect S(IV) mechanism may be very important since H_2O_2 is the principal oxidant of S(IV) to S(VI) in the atmosphere from pH 2 to 4 [*Hoffmann and Boyce*, 1983; *Jacob and Hoffmann*, 1983; *Hoffmann and Jacob*, 1984]. Iron is also a limiting nutrient to primary phytoplankton growth in certain regions of the open ocean [*Martin and Gordon*, 1988; *Ditullio, et al.*, 1993; *Kolber, et al.*, 1994; *Martin, et al.*, 1994; *Price, et al.*, 1994]; and the speciation of Fe is critical to the rate of Fe uptake by phytoplankton.

Investigation of cloudwater photochemistry has been centered around the use of ambient fogwater or cloudwater [*Faust and Allen*, 1992; *Zuo and Hoigné*, 1992; *Faust, et al.*, 1993], or synthetic Fe oxide particles [*Pehkonen, et al.*, 1993; *Pehkonen, et al.*, 1995] in laboratory experiments. Several investigators have examined the speciation of Fe in

ambient aerosols by determining: 1) the concentration of Fe(II) [*Zhuang, et al.*, 1992; *Zhu, et al.*, 1993], 2) the concentration of soluble Fe [*Zhu, et al.*, 1993; *Spokes, et al.*, 1994], and 3) the mineral form of the Fe through Mossbauer spectroscopy [*Kopcewicz and Kopcewicz*, 1991; *Kopcewicz and Kopcewicz*, 1992]. These procedures measured the concentration of Fe in specific phases, but did not directly address the dynamic time-dependent reactivity of the Fe.

Similar studies have focused on the photoreactivity of suspended ambient aerosol samples in aqueous solution [*Zhu, et al.*, 1993; *Siefert, et al.*, 1994]. For example, *Zhu et al.* [1993] explored the photolysis of aqueous Fe solutions, that were leached from marine aerosol samples. They chose their experimental conditions to simulate haze aerosol solutions with an ionic strength = 0.1 M and a pH = 1. Their experiments showed a high-level of photoreactivity of the Fe leached from marine aerosol samples in the presence of various inorganic anions. However, the filters leached by *Zhu et al.* [1993] may have contained a significant amount of photochemically-available Fe. For example, *Pehkonen et al.* [1993] showed that the photoreduction of Fe also occurs with particulate Fe(III), thus the experimental methods used by *Zhu et al.* [1993] may not represent the total photoreactivity of Fe in aerosol samples.

Quantification of the amount of photochemically-available Fe in aerosol samples is important, since it should account for all of the species of Fe that may take part in Fe-induced photochemistry in the atmosphere. In this paper, we describe a series of experiments that were carried out to determine the amount of photochemically-available Fe ($Fe_{PA,total}$), soluble Fe(II) ($Fe(II)_{soluble}$) and total Fe (Fe_{total}) present in a variety of ambient aerosol samples.

METHODS

Ambient Aerosol Collection

Ambient aerosol was collected on 47 mm Gelman Zefluor PTFE filters with a pore size of 1 μm. Collection sites were located at Whiteface Mountain, NY (WMNY), Yosemite National Park, CA (YNPCA), San Nicholas Island, CA, (SNICA) and Pasadena, CA (PCA) (Figure 1). These locations were chosen to provide several diverse sampling regions. The sites at YNPCA and WMNY provided two continental environments with varying weather patterns. PCA provided a polluted, urban atmosphere and SNICA provided a coastal, island environment. A volumetric flow rate of 10 L min^{-1} through each filter was maintained with a critical orifice. A set of 2 to 9 filters were used for each collection. Filters, polycarbonate filter holders and labware were cleaned rigorously before use by following similar procedures as outlined by *Patterson and Settle* [1976]. The Gelman Zefluor filters were placed in a warm 10% HF bath for 24 hours followed by a warm 10% HNO_3 bath, also for 24 hours. The filters were rinsed with water between the baths and after the final bath (ultra-pure acids from Seastar Chemicals, Sidney, B.C., Canada, and 18.2 MΩ-cm Milli-Q UV water were used for all steps). The filter holders were placed in a warm 5% HNO_3 bath (reagent grade HNO_3) for 24 hours followed by a warm 1% HNO_3 (Seastar Chemicals, ultra-pure HNO_3) bath. The filter holders were rinsed with water between the baths, and also after the second bath. After collection of aerosol samples, the filters were stored in the dark at 21°C and a relative humidity of 50% for 24 hours and then weighed (these were the same conditions used to pre-weigh the filters). This weighing technique is similar to the one followed by *Ligocki et al.* [1993]. After weighing the samples were stored in the dark at 4°C, for periods ranging from 2 months to 2 years prior to use in photochemical experiments.

Simulated Cloudwater: Experimental Procedures

The 47 mm diameter filter used to collect the ambient aerosol sample was securely placed in an all Teflon™ photochemical reactor vessel (Figure 2). The vessel was designed in order to allow the entire filter surface to be irradiated during the experiments. The reactor vessel was then placed in a box designed to minimize the irradiation of the reactor vessel from ambient light. An aqueous solution of 500 μM formate/formic acid (for simplicity, formate, the anion name of the acid will be used) at a pH of 4.25 ± 0.05 was then added to the vessel. The pH of the formate solution was measured using a combination electrode (FUTURA Plus combination electrode, Beckman Instruments, Inc.) with a portable pH meter (PHM 80, Radiometer America, Inc.), and using a two point calibration (with pH 4 and pH 7 buffer solutions). Even though the pH values in cloudwater vary over a wide range depending on meteorological conditions, anthropogenic sources, liquid water content and other parameters, a pH of 4.25 was chosen as a representative cloudwater pH for these experiments. At a pH of 4.25, the oxidation of $Fe(II)_{aq}$ by oxygen is relatively slow with a calculated half-life of $Fe(II)_{aq}$ of 113 hr assuming P_{O_2} = 0.21 atm [*Wehrli*, 1990]. Formate was chosen as the buffer since it is commonly the most abundant carboxylate species found in cloudwater [*Munger*, 1989; *Munger, et al.*, 1989; *Kawamura and Kaplan*, 1991; *Zuo and Hoigné*, 1992; *Erel, et al.*, 1993]. Formate concentrations in fogwater and cloudwater have been found to vary between 12 and 75.6 μM [*Munger*, 1989; *Munger, et al.*, 1989; *Erel, et al.*, 1993]. The higher concentrations of formate (500 μM) in these experiments was used to increase the buffering capacity of the solution and to maintain a constant ionic strength (I = 310 μM). Overall, the experiments were designed to be have conditions similar to observed cloudwater conditions.

Rigorous procedures were employed to minimize Fe contamination. The reactor vessel was cleaned in a warm 5% HNO_3 bath for several hours and rinsed with 18.2 MΩ-cm Milli-Q water before use. Control experiments were carried out periodically with a

clean filter to determine the level of Fe contamination. In all cases, no detectable Fe(II) was produced. A quartz window was placed on top of the vessel to prevent evaporation. Before the vessel was irradiated, a 2 mL aliquot was taken to record the initial pH and initial $Fe(II)_{aq}$ concentration. A 450 Watt Xenon lamp (Oriel) with a 320 nm cutoff filter and an IR filter was used as the light source. The photon flux between 320 and 390 nm, which was measured using a chemical actinometer, Aberchrome 540 [*Heller and Langan*, 1981], was $I_0 = 1.5 \times 10^{15}$ photons cm^{-2} sec^{-1} in all experiments (except where noted). This photon flux is about an order of magnitude lower then natural sunlight over the same wavelength range. For example, natural sunlight with a zenith angle of 30° has a photon flux between 320 and 390 nm of 1.3×10^{16} photons cm^{-2} sec^{-1} [*Demerjian, et al.*, 1980]. The reactor vessel had a vertical window with an area of 13.4 cm^2. The reactor vessel was kept at a temperature of 28 °C, via fan-driven air cooling. $Fe(II)_{aq}$ was measured colorimetrically with ferrozine [*Stookey*, 1970; *Carter*, 1971]. All aliquots were filtered through a 0.2 μM cellulose acetate syringe filter before analysis Aliquots taken for total metal analysis were not filtered.

At the end of the photochemical experiment, when $Fe(II)_{aq}$ concentrations had reached a steady-state, HCl was added to the remaining solution in the reactor vessel until a pH of 1 was reached. The solution was then stirred overnight to extract any remaining Fe from the filter. An aliquot of this solution was removed and analyzed for total metals. The filter was then removed from the reactor vessel and weighed (after equilibrating to 21°C and a relative humidity of 50%) to determine the mass of particulates suspended or dissolved into solution during irradiation. A strong mineral-acid digestion procedure (using ultra-pure HF, HNO_3 and HCl acids from Seastar Chemicals) was used to dissolve the remaining particulates on the filter for total metal measurements. The procedure involved using a ceramic knife and a polycarbonate cutting board to take a $\approx$ 1/4 slice from the filter. The filter slice was then weighed and compared to the total filter mass to determine the filter slice fraction, which was used later to calculate the total concentration on the filter. The

filter slice was then placed in 2 g of concentrated HF and 2 g of concentrated HNO_3. This was followed by vigorous shaking of the solution and filter slice overnight. After the extraction the filter slice was removed and the solution was evaporated to dryness. The resulting residue was then digested in 10 g of 10% HCl. Concentrations of iron were measured using ICP-MS (Perkin Elmer - SCIEX Elan 5000). These concentrations (along with the volume of solution in the digestion and the volume of air sampled) were then used to calculate the atmospheric concentrations of Fe_{total}.

Pseudo First-Order Kinetic Analysis

The production of $Fe(II)_{aq}$ in the experiments was assumed to be a pseudo first-order process as follows:

$$Fe(III)_{PA} \xrightarrow{k'} Fe(II)_{aq} \qquad (1)$$

where $Fe(III)_{PA}$ ≡ photochemically available Fe(III)

and k' ≡ psuedo first-order rate constant

the corresponding rate law is given by

$$\frac{d[Fe(III)_{PA}]}{dt} = -k' [Fe(III)_{PA}] \qquad (2)$$

integration yields

$$[Fe(III)_{PA}] = [Fe(III)_{PA}]_0 \, e^{-k' t} \qquad (3)$$

The mass (mole) balance on $[Fe(II)_{aq}]$ is given by

$$[Fe(II)_{aq}] = [Fe(II)_{aq}]_0 + ([Fe(III)_{PA}]_0 - [Fe(III)_{PA}]) \qquad (4)$$

Combining eqs 3 and 4 yields eq 5

$$[Fe(II)_{aq}] = [Fe(II)_{aq}]_0 + [Fe(III)_{PA}]_0 (1 - e^{-k' t}) \quad (5)$$

Values for $[Fe(II)_{aq}]_0$, $[Fe(III)_{PA}]_0$ and k' were determined by fitting the experimental data to eq 5. Total photochemically-available Fe ($Fe_{PA,total}$) was then defined as

$$[Fe_{PA,total}] = [Fe(II)_{aq}]_0 + [Fe(III)_{PA}]_0 \quad (6)$$

$Fe_{PA,total}$ represented all the Fe in the aerosol sample which was already present as Fe(II), or could be reduced to Fe(II) by photochemical reactions.

These fitted parameters (along with the volume of solution in the experiment and the volume of air sampled) were then used to calculate the atmospheric concentrations of $Fe(II)_{soluble}$ (using $[Fe(II)_{aq}]_0$) and $Fe_{PA,total}$ (using $[Fe_{PA,total}]$).

Computational Determination of Chemical Speciation

Chemical speciation calculations were performed using the program MINEQL [*Westall, et al.*, 1976] which uses the equilibrium constant approach (defined by a system of mass action equations) to solve a chemical equilibrium problem.

RESULTS AND DISCUSSION

A typical kinetic profile for $Fe(II)_{aq}$ released photochemically from an aerosol sample is shown in Figure 3. At t = 0 minutes, the shutter is opened, allowing the solution and sample filter to be irradiated. $[Fe(II)_{aq}]$ increased until a steady-state was reached (in

some experiments there was no measured increase in $[Fe(II)_{aq}]$, in which case the pseudo first-order rate constant was not measurable). The total Fe in the solution and on the filter was analyzed at the end of the experiment. The observed $[Fe(II)_{aq}]$ vs. time curve was fitted according to eq 5 to yield $[Fe(II)]_0$, $[Fe(III)_{PA}]_0$ and k'. These concentrations were then used to determine the atmospheric concentrations of soluble Fe(II) ($Fe(II)_{soluble}$), and total photochemically-available Fe ($Fe_{PA,total}$).

Experiments were not conducted to determine Fe(II) production in the dark, since previous studies showed no (or extremely slow) Fe(II) production in the absence of light compared to irradiated solutions [*Zhu, et al.*, 1993; *Siefert, et al.*, 1994]. *Zhu et al.* [1993] found that Fe(II) concentrations, in extracted aerosol filter sample solutions, increased rapidly when the solutions were exposed to sunlight.

The total dissolved solids (TDS) concentrations due to the dissolution and suspension of the aerosol sample on the filter (excluding the TDS associated with the formate buffer solution) were between 3.1 mg l^{-1} and 48.3 mg l^{-1} for all the experiments. Using data from *Erel et al.* [1993], TDS concentrations for fogwater and cloudwater samples were calculated by summing the concentrations cations, anions, metals, and total organic anions for the different samples. The TDS for these fogwater and cloudwater samples and ranged from 21 mg l^{-1} to 355 mg l^{-1}. The TDS concentrations in the experiments were in the lower range of these observed TDS concentrations for fogwater and cloudwater.

Effect of Formate Concentration and Light Intensity

Experiments were performed on ambient aerosol samples collected in Pasadena where the formate concentration ($[HCO_2^-]_T$) was varied to determine its effect on the $Fe(II)_{aq}$ production rate (where $[HCO_2^-]_T = [HCO_2H] + [HCO_2^-]$). Formate concentrations of 0 mM, 0.5 mM and 6.0 mM were used. The pH of the 0 mM added formate system was adjusted using perchloric acid. Over this concentration range, only a small change in

$Fe(II)_{aq}$ production rates or final $[Fe(II)_{aq}]$ levels were observed (Figure 4). These results show that sufficient electron donors were present in the ambient aerosol for the photoreduction of $Fe(III)_{aq}$ and $Fe(III)_{surficial}$. Overall, no correlation was observed between $d[Fe(II)_{aq}]/dt$ and $[HCO_2^-]_T$, or between final $[Fe(II)_{aq}]$ and $[HCO_2^-]_T$.

Several experiments were also performed to determine if the reduction rate constant(s) were significantly greater than the oxidation rate constant(s) after $[Fe(II)_{aq}]$ had reached a steady-state at the end of the experiments. The absolute rates of $Fe(II)_{aq}$ oxidation and $Fe(III)_{aq}$ reduction are equal at the steady-state, but the concentrations of $Fe(II)_{aq}$ and $Fe(III)_{aq}$ change to meet this steady-state condition depending on the redox kinetics as the following equations illustrate:

$$Fe(III)_{aq} \xrightarrow{k_{reduction}} Fe(II)_{aq} \tag{7}$$

$$Fe(II)_{aq} \xrightarrow{k_{oxidation}} Fe(III)_{aq} \tag{8}$$

It should be noted that $k_{reduction}$ in this analysis is not necessarily the same as the pseudo first-order rate constant (k') in equation 1. For example, the initial Fe could be a solid Fe oxyhydroxide which follows dissolution kinetics (k' in equation 1); and after the Fe is in solution, it would follow the faster homogeneous kinetics of eqs 7 and 8. The overall process is described kinetically as follows:

$$\frac{d[Fe(II)_{aq}]}{dt} = k_{oxidation}\,[Fe(II)_{aq}] - k_{reduction}\,[Fe(III)_{aq}] \tag{9}$$

where

$$[Fe_{PA,total}] = [Fe(II)_{aq}] + [Fe(III)_{aq}] \quad (10)$$

At steady state,

$$\frac{d[Fe(II)_{aq}]}{dt} = 0 \quad (11)$$

therefore combining equations (9), (10) and (11) and rearranging gives

$$\frac{[Fe(II)_{aq}]}{[Fe_{PA,total}]} = \frac{1}{\frac{k_{oxidation}}{k_{reduction}} + 1} \quad (12)$$

In order for eq 5 to be valid, the ratio $\frac{k_{oxidation}}{k_{reduction}}$ must be << 1. This condition was tested after $[Fe(II)_{aq}]$ reached a steady-state by increasing I_0 by a factor of 3 or 10. This increase in incident light intensity was assumed to increase $k_{reduction}$, however, $k_{oxidation}$ might also be expected to increase since many oxidants have photochemical origins. In either case, $k_{reduction}$ and $k_{oxidation}$ are unlikely to change in such a way that $\frac{k_{oxidation}}{k_{reduction}}$ remains exactly the same after increasing the light intensity. Therefore by changing the light intensity and by measuring $[Fe(II)_{aq}]$, the condition of $\frac{k_{oxidation}}{k_{reduction}} << 1$ was verified. In each case, $[Fe(II)_{aq}]$ did not change after an increase in I_0. These results showed that increasing the incident light intensity by a factor of 3 or 10 after the steady-state condition was reached, did not influence the final steady-state amount of $Fe(II)_{aq}$ produced in the experiment. Thus, we

assumed that the other experiments also conformed to the condition $\frac{k_{oxidation}}{k_{reduction}} << 1$. Therefore, the steady-state $[Fe(II)_{aq}]$ at the end of these experiments was used to calculate the total photochemically-available Fe ($Fe_{PA,total}$) in the experiments.

Atmospheric Concentrations of $Fe(II)_{soluble}$, $Fe_{PA,total}$ and Fe_{total}

Table 1 provides a summary of locations, collection times, total suspended particulate concentrations (TSP) and meteorological conditions for the ambient aerosol samples. A summary of results of the photochemical experiments is given in Table 2. These results include the atmospheric concentrations of Fe_{total}, $Fe(II)_{soluble}$, and $Fe_{PA,total}$. The pseudo first-order rate constant for the photoreduction of $Fe(III)_{PA}$ to $Fe(II)_{aq}$ and the initial production rate of $Fe(II)_{aq}$ are also tabulated. All of the experiments were performed at pH of 4.25 ± 0.05.

The urban sampling site in Pasadena (CA) is located near Los Angeles (LA). This site had the largest concentrations of Fe_{total} and $Fe_{PA,total}$, with average concentrations of 660 and 120 ng/m^3 respectively. Assuming a cloud liquid water content (LWC) of 10^{-6} (1.0 cm^3 H_2O per m^3 of air) and incorporation of all of the ambient aerosol particulate matter into the cloudwater; the average aqueous concentrations of Fe_{total} and $Fe_{PA,total}$ would have been 12 μM and 2 μM, respectively. Under conditions in which easterly winds prevailed with high levels of precipitation, the $Fe_{PA,total}$ concentration were reduced by over 50%, and Fe_{total} was also reduced by about 40%. The elevated Fe concentrations in Pasadena, which is influenced by onshore breezes, are probably due to the anthropogenic loading as air parcels are advected across the LA basin.

Aerosol samples, collected in Pasadena during the Altadena hillside fires of late October and early November of 1993 (a city bordering the northern edge of Pasadena), contained large amounts of ash and had a total suspended particulate concentration (TSP) of 182 ± 10 μg/m^3. Fe concentrations in these fire-related samples were 7 times greater for

Fe_{total}, but only 1.5 times greater for $Fe_{PA,total}$ then other aerosol samples collected from the same site when there were no fires. From the data in Table 2, it is clear that the differences for Fe_{total}, $Fe(II)_{soluble}$, and $Fe_{PA,total}$ between repeated experiments are unusually high for ambient aerosol collected during the Altadena fires. This variability in samples collected during the same event may be the result of the variable composition of ash collected among filters. The high Fe and TSP concentrations in this case are the direct result of the fires, probably due to the combustion of biomass and the suspension of dust and soil particles. The pseudo first-order rate constant calculated for these experiments was significantly smaller than the k's calculated for the other aerosol samples (except for the SNICA 2 sample which was also collected downwind of a fire). The average half-life of $Fe(III)_{PA}$ for the PCA 3 sample is approximately 360 minutes. For comparison, the average half-life of $Fe(III)_{PA}$ is approximately 17 minutes for all the other calculated rate constants in Table 2 (not including the SNICA 2 sample). The Altadena fire resulted in increases in Fe_{total} atmospheric concentrations, but did not increase $Fe_{PA,total}$ concentrations significantly. However, the $Fe_{PA,total}$ that was produced during the fire storm was the least reactive (based on k') compared to the other samples.

Aerosol samples from San Nicholas Island, CA (100 km offshore from LA) contained substantially less Fe_{total} and $Fe_{PA,total}$, than the Pasadena samples. The aerosol collected on San Nicholas Island is primarily of marine origin, although some anthropogenic input can occur due to offshore air flow from the LA Basin. Aerosol sources from the LA basin have been detected, when an air parcel oscillates between San Nicholas Island and LA, due to the alternating onshore and offshore breezes [*Rosenthal, et al.*, 1979]. In addition, anthropogenic input to San Nicholas Island from the Point Conception and Morro Bay areas has been documented [*Rosenthal, et al.*, 1979]. Aerosol samples were also collected on San Nicholas Island during the 1993 Malibu, California fire. Strong Santa Ana wind conditions spread the smoke plume from these fires directly over the island (Figure 5). However, since the site is over 100 km from the source of the

plume, large pieces of ash were absent. The aerosol samples collected over this period showed a 4 fold increase in $Fe_{PA,total}$ and 3 fold increase in Fe_{total} compared to the San Nicholas Island, CA sample (SNICA 2) which was of marine origin. This increase was clearly due to airborne particulates created by the Malibu fire conditions.

The sampling site at Whiteface Mountain, NY, was subjected to the highest amount of precipitation. In the sampling period from September through December, 1992, precipitation was measured on more than 60 days. The general air flow in this region, although highly variable, was dominated by wind from the northern Great Lakes region and southern Canada. At Whiteface Mt., the $Fe_{PA,total}$ and Fe_{total} concentrations appeared to decrease as the seasons changed from fall to winter. The ratio of $Fe_{PA,total}$ to Fe_{total} concentrations remained relatively constant throughout, and was higher than at any other site. A high ratio of $Fe_{PA,total}$ to Fe_{total} concentrations (on average 85%) suggests a "photochemical weathering" of Fe aerosol particles [*Duce and Tindale*, 1991; *Zhuang, et al.*, 1992; *Zhuang, et al.*, 1992]. Since the air masses arriving at Whiteface Mt. had a high water content, Fe in the aerosol may have been more readily available because of the greater possibility of active cloudwater photochemistry than in aerosol samples collected from drier air masses. Before a cloud condensation nucleus (CCN) is deposited by precipitation, it often goes through a number of hydration and evaporation cycles. *Junge* [1964] estimated that a single CCN may undergo 10 hydration/evaporation cycles before precipitation. The high frequency of precipitation at Whiteface Mountain as compared to Pasadena and the other west coast sites may explain the higher observed ratios of $Fe_{PA,total}$ to Fe_{total} concentrations.

Ambient aerosol collected at Yosemite National Park, CA also showed a seasonal trend in the ratios of $Fe_{PA,total}$ to Fe_{total} concentrations. A pronounced decrease in the ratio of $Fe_{PA,total}$ to Fe_{total} concentrations occurs during the months of November and December compared to July. The air parcels during the winter originated primarily from the coastal region, while during the summer air parcels originated from continental areas. This

directional difference in the air masses may explain the change in the ratios of $Fe_{PA,total}$ to Fe_{total} concentrations in the associated aerosol. Furthermore, the moist marine air may have induced more chemical weathering of the aerosol particles leading to higher ratios of $Fe_{PA,total}$ to Fe_{total} concentrations.

Comparison of Experimental Fe(II) Photoproduction Rates to Known Fe Oxidation/Reduction Rates

Iron oxidation and reduction rates in the photochemically-available iron experiments were calculated and compared to the observed photo-production of $Fe(II)_{aq}$. The Fe oxidation and reduction rates were calculated using rate constants available in the literature. The following reactions were used in the calculation:

$$Fe^{2+} + H_2O_2 \rightarrow Fe^{3+} + \bullet OH + OH^- \quad (13)$$

$$Fe(OH)^+ + H_2O_2 \rightarrow Fe(OH)^{2+} + \bullet OH + OH^- \quad (14)$$

$$Fe(OH)^{2+} + h\upsilon \rightarrow Fe^{2+} + \bullet OH \quad (15)$$

$$Fe(OOCCOOH)^{2+} + h\upsilon \rightarrow Fe^{2+} + 2CO_2 + \bullet HO_2 \quad (16)$$

The oxidation of Fe(II) by O_2 is extremely slow under these conditions [*Wehrli*, 1990] and therefore was not included. Other reactions are also possible (including heterogeneous reactions), however, the above reactions were chosen since they are representative of the likely range of reactions possible. Table 3 shows the concentrations used in the reaction rates calculations. A range of concentrations existed for each species in Table 3, and the

concentrations in Table 3 are a representative set of values for the experiments shown in Table 2. Table 4 shows the rate constants and calculated reaction rates. The results in Table 4 show that the $Fe(III)_{aq}$ reduction rates are greater than $Fe(II)_{aq}$ oxidation rates. This calculation is in agreement with the experiments shown in Table 2, since $Fe(II)_{aq}$ was never observed to decrease in these experiments. The observed initial $Fe(II)_{aq}$ production rates in the experiments were between 0 and 60 nM s^{-1} (See Table 2), with an average value of 16 nM s^{-1}. These observed rates are within, or greater, than calculated rates shown in Table 4. Overall, these observed rates are in reasonable agreement with the calculated rates, since the calculated rates use average concentrations for Fe, organic ligands, etc.

Using the observed initial $Fe(II)_{aq}$ production rates we can also estimate the production of oxidants ($OH^{\bullet}$, and $HO_2^{\bullet}$) in the experiments due to Fe chemistry. Equations 15 and 16 show that the rate of $Fe(II)_{aq}$ production is equal to the oxidant production rate (actually the rate of $Fe(II)_{aq}$ production is equal to the minimum oxidant production rate since cycling of Fe(II)/Fe(III) is possible). Therefore, the estimated oxidant production rate is between 0 and 60 nM s^{-1}, with an average value of 16 nM s^{-1}. These values can be used as estimates of the oxidant production rate in the atmosphere by assuming a LWC of $\approx 10^{-6}$ and that the aerosol sampling duration was $\approx$ 7 days. These assumptions would mean that $\approx$ 100 ml of water would be collected during this sampling duration if the LWC was always 10^{-6}. And since the experiments use 80 ml of solution, it is reasonable to relate the estimated oxidant production in the experiments to aqueous-phase atmospheric chemistry. Therefore, the estimated cloudwater oxidant production rate in the atmosphere based on these experiments is between 0 and 60 nM s^{-1}, with an average value of 16 nM s^{-1}. *Chameides and Davis* [1982] estimated the flux of oxidants to the aqueous phase from the gas-phase in the atmosphere to be between 0.3 and 30 nM s^{-1}. Therefore, the estimated *in situ* oxidant production rate due to Fe chemistry is roughly equal to the estimated oxidant flux from the gas-phase.

CONCLUSIONS

Photolysis of aqueous solutions containing ambient aerosol samples was performed in order to quantify the photochemically labile Fe available for aqueous photochemical reactions. Photochemically-available Fe concentrations found ranged from < 4 ng/m^3 to 308 ng/m^3, Fe_{total} concentrations ranged from 10 ng/m^3 to 3400 ng/m^3, and the percentage of photochemically-available Fe to Fe_{total} ranged from 2.8% to 100% for aerosol samples collected in marine, coastal and mountainous regions. Passage of air masses through climatic and anthropogenic regions have a demonstrable effect on the ratio of $Fe_{PA,total}$ to Fe_{total} concentrations. Wet conditions, in which the aerosol particles may undergo chemical weathering in clouds, appears to increase the relative amount of $Fe_{PA,total}$ compared to Fe_{total}. The urban Los Angeles basin has higher atmospheric levels of Fe_{total}, but the ratio of $Fe_{PA,total}$ to Fe_{total} concentrations remained relatively constant. $Fe_{PA,total}$ concentrations in the southern California region were not affected by extensive biomass burning during the fall of 1993, even though Fe_{total} increased significantly. Overall, the Fe added to the atmosphere during these fires was not readily available for photochemical reactions. The observed $Fe(II)_{aq}$ production rates in the experiments were in agreement with the calculated $Fe(II)_{aq}$ production rates using rate constants from the literature.

The estimated cloudwater oxidant production rate in the atmosphere based on these experiments is between 0 and 60 nM s^{-1}, with an average value of 16 nM s^{-1}. *Chameides and Davis* [1982] estimated the flux of oxidants to the aqueous phase from the gas phase in the atmosphere to be between 0.3 and 30 nM s^{-1}. Therefore, the estimated *in situ* cloudwater oxidant production rate due to Fe chemistry is approximately equal to the estimated oxidant flux from the gas-phase.

Acknowledgments: Special thanks are extended to Anne Foster and Richard MacDonald of the ASRC at Whiteface Mountain, Prof. Andy Friedland at Dartmouth College, Diane Ewell and Annie Esperanza of Sequoia National Park and Dr. Jan van Wagtendonk at Yosemite National Park for their help. We also thank Prof. J. J. Morgan of Caltech for helpful discussions. Support for this research has been provided by a grant from the National Science Foundation, Division of Atmospheric Sciences, Atmospheric Chemistry Section (ATM 9015775; ATM 9303024). This research was also sponsored by the U.S. Department of Energy, Office of Energy Research, Environmental Sciences Division, Office of Health and Environmental Research, under appointment to the Graduate Fellowships for Global Change administered by Oak Ridge Institute for Science and Education.

REFERENCES

Behra, P. and L. Sigg, Evidence for redox cycling of iron in atmospheric water droplets, *Nature, 344*, 419-421, 1990.

Breytenbach, L., W. Vanpareen, J. J. Pienaar and R. van Eldik, The influence of organic acids and metal ions on the kinetics of the oxidation of sulfur(IV) by hydrogen peroxide, *Atmos. Environ., 28*, 2451-2459, 1994.

Carter, P., Spectrophotometric determination of serum iron at the submicrogram level with a new reagent (ferrozine), *Anal. Biochem., 40*, 450-458, 1971.

Cass, G. R. and G. J. McRae, Source-receptor reconciliation of routine air monitoring data for trace metals: An emission inventory assisted approach, *Environ. Sci. Technol., 17*, 129-139, 1983.

Chameides, W. L. and D. D. Davis, The free radical chemistry of cloud droplets and its impact upon the composition of rain, *J. Geophys. Res., 87*, 4863-4877, 1982.

Demerjian, K. L., K. L. Schere and J. T. Peterson, Theoretical estimates of actinic (spherically integrated) flux and photolytic rate constants of atmospheric species in the lower troposphere, *Adv. Environ. Sci. Technol., 10*, 369, 1980.

Ditullio, G. R., D. A. Hutchins and K. W. Bruland, Interaction of iron and major nutrients controls phytoplankton growth and species composition in the tropical North Pacific Ocean, *Limnol. & Ocean., 38*, 495-508, 1993.

Duce, R. A. and N. W. Tindale, Atmospheric transport of iron and its deposition in the ocean, *Limnol. & Ocean., 36*, 1715-1726, 1991.

Erel, Y., S. O. Pehkonen and M. R. Hoffmann, Redox chemistry of iron in fog and stratus clouds, *J. Geophys. Res. A., 98*, 18423-18434, 1993.

Faust, B. C. and J. M. Allen, Aqueous phase photochemical sources of peroxyl radicals and singlet molecular oxygen in clouds and fogs, *J. Geophys. Res. A., 97*, 12913-12926, 1992.

Faust, B. C., C. Anastasio, J. M. Allen and T. Arakaki, Aqueous phase photochemical formation of peroxides in authentic cloud and fogwaters, *Science, 260*, 73-75, 1993.

Faust, B. C. and J. Hoigné, Photolysis of Fe(III)-hydroxy complexes as sources of OH radicals in clouds, fog and rain, *Atmos. Environ., 24A*, 79-89, 1990.

Faust, B. C. and R. G. Zepp, Photochemistry of aqueous iron(III)-polycarboxylate complexes: Roles in the chemistry of atmospheric and surface waters, *Environ. Sci. Technol., 27*, 2517-2522, 1993.

Fuzzi, S., G. Orsi, G. Nardini, M. C. Facchini, E. McLaren and M. Mariotti, Heterogeneous processes in the Po Valley radiation fog, *J. Geophys. Res. A., 93*, 11141-11151, 1988.

Gomes, L. and D. A. Gillette, A comparison of characteristics of aerosol from dust storms in central Asia with soil derived dust from other regions, *Atmos. Environ., 27*, 2539-2544, 1993.

Gunz, D. W. and M. R. Hoffmann, Atmospheric chemistry of peroxides: A review, *Atmos. Environ. A, 24*, 1601 - 1633, 1990.

Hartwick, T. J., The rate constant of the reaction between ferrous ions and hydrogen peroxide in acid solution, *Can. J. Chem., 35*, 428-436, 1957.

Heller, H. G. and J. R. Langan, A new reusable chemical actinometer, *J. C. S. Perkin I,* 341, 1981.

Hoffmann, M. R. and S. D. Boyce, Catalytic autooxidation of aqueous sulfur dioxide in relationship to atmospheric systems, in *Trace Atmospheric Constituents: Properties, Transformations, and Fates*, edited by S. E. Schwartz, 147-172, Wiley, New York, 1983.

Hoffmann, M. R. and J. O. Edwards, Kinetics of the oxidation of sulfite by hydrogen peroxide in acidic solution, *J. Phys. Chem., 79*, 2096-2098, 1975.

Hoffmann, M. R. and D. J. Jacob, Kinetics and mechanism of the catalytic oxidation of dissolved SO_2 in atmospheric droplets: Free radical, polar and photoassisted pathways, in

SO_2, NO, NO_2 Oxidation Mechanisms: Atmospheric Considerations, edited by J. G. Calvert, 101-172, Butterworth Publishers, Boston, 1984.

Jacob, D. J. and M. R. Hoffmann, A dynamic model for the production of H^+, NO_3^-, and SO_4^{2-} in urban fog, *J. Geophys. Res., 88*, 6611-6621, 1983.

Jacob, D. J., J. M. Waldman, J. W. Munger and M. R. Hoffmann, Chemical composition of fogwater collected along the California coast, *Environ. Sci. Technol., 19*, 730-736, 1985.

Jacob, D. J., J. M. Waldman, J. W. Munger and M. R. Hoffmann, The H_2SO_4-HNO_3-NH_3 system at high humidities and in fogs. 2. Comparison of field data with thermodynamic calculations, *J. Geophys. Res. A., 91*, 1089-1096, 1986.

Junge, C. E., The modification of aerosol size distribution in the atmosphere, *Contract-Da 91-591-EVC 2979*, US Army, 1964.

Kawamura, K. and I. R. Kaplan, Organic compounds in rainwater, in *Organic Chemistry of the Atmosphere*, edited by L. D. Hansen and D. J. Eatough, 233-284, CRC Press, Boston, 1991.

Kolber, Z. S., R. T. Barber, K. H. Coale, S. E. Fitzwater, R. M. Greene, K. S. Johnson, S. Lindley and P. G. Falkowski, Iron limitation of phytoplankton photosynthesis in the equatorial Pacific Ocean, *Nature, 371*, 145-149, 1994.

Kopcewicz, B. and M. Kopcewicz, Mossbauer study of iron-containing atmospheric aerosols, *Struct. Chem., 2*, 303-312, 1991.

Kopcewicz, B. and M. Kopcewicz, Seasonal variations of iron concentration in atmospheric aerosols, *Hyperfine Interactions, 71*, 1457-1460, 1992.

Lacroix, S., Étude de quelques complexes et composés peu soluble des ions: Al^{3+}, Ga^{3+}, In^{3+}, *Ann. de Chim., 4*, 5-27, 1949.

Ligocki, M. P., L. G. Salmon, T. Fall, M. C. Jone, W. W. Nazaroff and G. R. Cass, Characteristics of airborne particles inside southern California museums., *Atmos. Environ., 27(5)*, 697-711, 1993.

Martin, J. H., K. H. Coale, K. S. Johnson, S. E. Fitzwater, R. M. Gordon, S. J. Tanner, C. N. Hunter, V. A. Elrod and J. L. Nowicki, Testing the iron hypothesis in ecosystems of the equatorial Pacific Ocean, *Nature, 371*, 123-129, 1994.

Martin, J. H. and R. M. Gordon, Northeast Pacific iron distributions in relation to phytoplankton productivity, *Deep Sea Res. A., 35*, 177-196, 1988.

McArdle, J. V. and M. R. Hoffmann, Kinetics and mechanism of the oxidation of aquated sulfur dioxide by hydrogen peroxide at low pH, *J. Phys. Chem., 87*, 5425-5429, 1983.

Millero, F. J. and S. Sotolongo, The oxidation of Fe(II) with H_2O_2 in seawater, *Geochim. Cosmochim. Acta, 53*, 1867-1873, 1989.

Munger, J. W., The Chemical Composition of Fogs and Clouds in Southern California, Ph. D. thesis, California Institute of Technology, 1989.

Munger, J. W., J. J. Collett, B. J. Daube and M. R. Hoffmann, Chemical composition of coastal stratus clouds: Dependence on droplet size and distance from the coast, *Atmos. Environ., 23*, 2305-2320, 1989.

Munger, J. W., J. M. Waldman, D. J. Jacob and M. R. Hoffmann, Fogwater chemistry in an urban atmosphere, *J. Geophys. Res., 88*, 5109-5121, 1983.

Patterson, C. C. and D. M. Settle, The reduction of orders of magnitude errors in lead analysis of biological materials and natural waters by evaluating and controlling the extent and sources of industrial lead contamination introduced during sampling, collecting, handling and analysis, *National Bureau of Standards, Special Publication, 422*, 321-351, 1976.

Pehkonen, S. O., R. L. Siefert, Y. Erel, S. Webb and M. R. Hoffmann, Photoreduction of iron oxyhydroxides in the presence of important atmospheric organic compounds, *Environ. Sci. Technol., 27*, 2056-2062, 1993.

Pehkonen, S. O., R. L. Siefert and M. R. Hoffmann, Photoreduction of iron oxyhydroxides and the photooxidation of halogenated acetic acids, *Environ. Sci. Technol., 29*, 1215-1222, 1995.

Price, N. M., B. A. Ahner and F. M. M. Morel, The equatorial Pacific Ocean - grazer controlled phytoplankton populations in an iron limited ecosystem, *Limnol. & Ocean., 39*, 520-534, 1994.

Rosenthal, J., T. E. Battalino, H. Hendon and V. R. Noonkester, Marine/continental history of aerosols at San Nicholas Island, Pacific Missile Test Center, Point Mugu, CA, 1979.

Sakugawa, H., I. R. Kaplan, W. Tsai and Y. Cohen, Atmospheric hydrogen peroxide, *Environ. Sci. Technol., 24*, 1452-1462, 1990.

Schroeder, W. H., M. Dobson, D. M. Kane and N. D. Johnson, Toxic trace elements associated with airborne particulate matter: A review, *J. Air Pollut. Control Assoc., 37*, 1267-1285, 1987.

Schwarzenbach, R. P., P. M. Gschwend and D. M. Imboden, *Environmental Organic Chemistry*, J. Wiley, 1993.

Seinfeld, J. H., *Atmospheric Chemistry and Physics of Air Pollution*, 738, Wiley, 1986.

Siefert, R. L., S. O. Pehkonen, Y. Erel and M. R. Hoffmann, Iron photochemistry of aqueous suspensions of ambient aerosol with added organic acids, *Geochim. et Cosmochim. Acta, 58*, 3271-3279, 1994.

Smith, R. M. and A. E. Martell, *Critical Stability Constants*, Plenum Press, 1974.

Spokes, L. J., T. D. Jickells and B. Lim, Solubilisation of aerosol trace metals by cloud processing: A laboratory study, *Geochim. et Cosmochim. Acta, 58*, 3281-3287, 1994.

Stookey, L. L., Ferrozine- a new spectrophotometric reagent for iron, *Anal. Chem., 42*, 119-781, 1970.

Taylor, S. R. and S. M. McLennan, *The continental crust: its composition and evolution*, 9-52, Blackwell Scientific Publications, 1985.

Thompson, A. M., The oxidizing capacity of the Earth's atmosphere: probable past and future changes, *Science, 256*, 1157-1165, 1992.

Waldman, J. M., J. W. Munger, D. J. Jacob, R. C. Flagan, J. J. Morgan and M. R. Hoffmann, The chemical composition of acid fog, *Science, 218*, 677-680, 1982.

Wehrli, B., Redox reactions of metal ions at mineral surfaces, in *Aquatic Chemical Kinetics*, edited by W. Stumm, 311-336, Wiley-Interscience, New York, 1990.

Westall, J. C., J. L. Zachary and F. M. M. Morel, MINEQL, a computer program for the calculation of chemical equilibrium composition of aqueous solutions, *Tech. Note 18*, Dept. of Civil Engineering, Massachusetts Institute of Technology, 1976.

Zhu, X. R., J. M. Prospero, F. J. Millero, D. L. Savoie and G. W. Brass, The solubility of ferric iron in marine mineral aerosol solutions at ambient relative humidities, *Marine Chem., 38*, 91-107, 1992.

Zhu, X. R., J. M. Prospero, D. L. Savoie, F. J. Millero, R. G. Zika and E. S. Saltzman, Photoreduction of iron(III) in marine mineral aerosol solutions, *J. Geophys. Res. A., 98*, 9039-9046, 1993.

Zhuang, G., Z. Yi, R. A. Duce and P. R. Brown, The chemistry of iron in marine aerosols, *Global Biogeochem. Cycles, 7*, 711, 1992.

Zhuang, G., Z. Yi, R. A. Duce and P. R. Brown, Link between iron and sulfur cycles suggested by detection of Fe(II) in remote marine aerosols, *Nature, 355*, 537-539, 1992.

Zuo, Y. and J. Hoigné, Formation of hydrogen peroxide and depletion of oxalic acid in atmospheric water by photolysis of iron(III)-oxalato compounds, *Environ. Sci. Technol., 26*, 1014-1022, 1992.

FIGURE CAPTIONS

FIGURE 1 Ambient aerosol collection sites: Whiteface Mountain, NY (WMNY); Yosemite National Park, CA (YNPCA); San Nicholas Island, CA (SNICA); Pasadena, CA (PCA).

FIGURE 2 Reactor vessel used in photochemically-available Fe experiments.

FIGURE 3 $Fe(II)_{aq}$ production curve in a typical photochemically-available Fe experiment ($[HCO_2^-]_T$ = 0.5 mM, pH = 4.25, and $I_0 = 1.5 \times 10^{15}$ photons (between 320 and 390 nm) $cm^{-2}\ sec^{-1}$). The ambient aerosol sample used for this experiment was collected at Yosemite National Park, CA from July 29 to August 9, 1993.

FIGURE 4 Effect of varying formic concentration on $Fe(II)_{aq}$ production.

FIGURE 5 Satellite image of the smoke plume from the 1993 Malibu, California fires.

TABLE 1. Summary of ambient aerosol collection locations, collection times, total suspended particulate and meteorological conditions.

Label	Location[a]	Collection Time	TSP[b] $\mu g/m^3$	Meteorologic Conditions[c]
WMNY 1	WMNY	92/09/22 11:00 to 92/10/06 12:15	11.2 ± 6.0	high precipitation
WMNY 2	WMNY	92/10/06 13:10 to 92/10/20 13:05	6.2 ± 0.3	high precipitation
WMNY 3	WMNY	92/10/20 13:05 to 92/11/03 12:52	5.4 ± 0.3	high precipitation
WMNY 4	WMNY	92/11/03 13:00 to 92/11/18 11:30	4.1 ± 0.2	high precipitation
WMNY 5	WMNY	92/11/18 11:33 to 92/12/01 10:06	3.9 ± 0.2	high precipitation
WMNY 6	WMNY	93/05/12 08:42 to 93/05/26 10:05	11.1 ± 0.6	high precipitation
PCA 1	PCA	93/02/21 16:00 to 93/03/01 16:00	24.7 ± 0.2	E source, rain
PCA 2	PCA	93/08/27 14:30 to 93/09/04 14:30	41.2 ± 2.1	W source (marine/anthropogenic)
PCA 3	PCA	93/10/27 10:00 to 93/10/29 12:00	182 ± 9.9	Santa Ana winds, Altadena fires
YNPCA 1	YNPCA	92/11/09 15:30 to 92/11/17 14:00	4.6 ± 0.2	W to NW source (marine/S.F.)
YNPCA 2	YNPCA	92/11/30 13:00 to 92/12/13 12:00	4.3 ± 0.2	precipitation
YNPCA 3	YNPCA	93/07/22 13:30 to 93/07/29 13:30	17.2 ± 0.1	E source (continental), dry
YNPCA 4	YNPCA	93/07/29 13:30 to 93/08/09 09:00	20.1 ± 1.0	E source (continental), dry
YNPCA 5	YNPCA	93/10/05 12:00 to 93/10/17 07:30	9.4 ± 0.2	W source (marine)
SNICA 1	SNICA	93/11/02 12:00 to 93/11/07 00:30	52.1 ± 2.6	Santa Ana winds, Malibu fires
SNICA 2	SNICA	93/11/17 11:30 to 93/12/01 08:40	17.9 ± 2.8	W source (marine)

[a] Whiteface Mountain, NY (WMNY), Pasadena, CA (PCA), Yosemite National Park, CA (YNPCA) and San Nicholas Island, CA (SNICA).

[b] total suspended particulate (TSP).

[c] using NOAA Daily Weather Maps, Climate Analysis Center.

TABLE 2. Atmospheric concentrations of total Fe (Fe_{total}), soluble ferrous Fe ($Fe(II)_{soluble}$), and total photochemically-available Fe ($Fe_{PA,total}$). Also the psuedo first-order rate constant (k') for the photoreduction of $Fe(III)_{PA}$ to $Fe(II)_{aq}$ and the initial production rate of $Fe(II)_{aq}$.

Label	Fe_{total} ng/m^3	$Fe(II)_{soluble}$ ng/m^3	$Fe_{PA,total}$ ng/m^3	$Fe(II)_{soluble}/Fe_{total}$ %	$Fe_{PA,total}/Fe_{total}$ %	k min^{-1}	d[Fe(II)]/dt nM sec^{-1}
WMNY 1	32 ± 3	23 ± 4	32 ± 6	70.2 ± 15.4	99.5 ± 20.9	NM[a]	NM
WMNY 1	29 ± 2	15 ± 1	21 ± 2	53.3 ± 6.3	71.5 ± 8.4	0.0596 ± 0.0341	14.1 ± 8.6
WMNY 2	24 ± 2	19 ± 3	26 ± 4	77.1 ± 15.5	108.6 ± 20.4	0.0262 ± 0.0231	9.0 ± 8.5
WMNY 3	18 ± 2	< 4	17 ± 8	< 22	94.4 ± 47.2	NM	NM
WMNY 4	12 ± 1	5 ± 1	11 ± 1	45.2 ± 10.8	87.3 ± 14.5	0.0094 ± 0.0035	2.3 ± 0.9
WMNY 5	10 ± 1	< 5	< 7	< 50	< 70	NM	NM
WMNY 6	72 ± 6	35 ± 2	40 ± 3	48.4 ± 4.9	55.9 ± 6.0	0.0409 ± 0.0338	10.0 ± 9.0
PCA 1	222 ± 18	42 ± 3	65 ± 4	18.7 ± 2.0	29.2 ± 2.9	0.0303 ± 0.0070	18.1 ± 4.6
PCA 1	197 ± 16	43 ± 4	73 ± 5	21.9 ± 2.7	37.2 ± 4.0	0.0091 ± 0.0025	7.1 ± 2.1
PCA 2	283 ± 23	32 ± 14	131 ± 18	11.2 ± 5.1	46.2 ± 7.5	0.0136 ± 0.0042	34.7 ± 11.5
PCA 2	304 ± 24	34 ± 11	121 ± 15	11.1 ± 3.8	39.9 ± 5.7	0.0115 ± 0.0041	25.9 ± 9.7
PCA 2	343 ± 28	43 ± 8	103 ± 10	12.5 ± 2.5	30.0 ± 3.9	0.0348 ± 0.0088	53.9 ± 15.0
PCA 2	305 ± 27	54 ± 14	130 ± 17	17.7 ± 4.8	42.7 ± 6.9	0.0114 ± 0.0044	22.3 ± 9.1
PCA 2	217 ± 18	41 ± 4	96 ± 6	19.0 ± 2.6	44.0 ± 4.6	0.0357 ± 0.0065	50.1 ± 9.8
PCA 3	3367 ± 297	41 ± 9	308 ± 11	1.2 ± 0.3	9.2 ± 0.9	0.0022 ± 0.0002	4.0 ± 0.4
PCA 3	1764 ± 132	65 ± 14	219 ± 17	3.7 ± 0.8	12.4 ± 1.3	0.0017 ± 0.0003	1.8 ± 0.4
PCA 3	2105 ± 160	55 ± 7	59 ± 10	2.6 ± 0.4	2.8 ± 0.5	NM	NM
PCA 3	3180 ± 280	49 ± 18	107 ± 23	1.6 ± 0.6	3.4 ± 0.8	0.0019 ± 0.0015	0.7 ± 0.6
YNPCA 1	23 ± 2	16 ± 4	18 ± 4	67.8 ± 16.3	76.6 ± 19.3	NM	NM
YNPCA 2	31 ± 2	20 ± 2	26 ± 2	64.9 ± 7.6	83.3 ± 10.0	0.0400 ± 0.0278	9.6 ± 7.2
YNPCA 3	84 ± 7	< 9	25 ± 5	< 11	30.2 ± 6.2	0.0375 ± 0.0181	13.9 ± 7.2
YNPCA 3	93 ± 8	11 ± 2	32 ± 3	11.4 ± 2.7	34.9 ± 4.5	0.0190 ± 0.0046	9.4 ± 2.4
YNPCA 4	158 ± 11	34 ± 1	49 ± 2	21.2 ± 1.7	31.0 ± 2.4	0.0582 ± 0.0079	25.5 ± 3.8
YNPCA 5	53 ± 1	< 5	11 ± 3	< 9	20.5 ± 4.8	0.0205 ± 0.0082	7.9 ± 3.4
YNPCA 5	59 ± 2	< 5	11 ± 1	< 9	17.9 ± 1.9	0.1673 ± 0.1043	60.8 ± 38.1
YNPCA 5	74 ± 3	< 5	10 ± 1	< 7	13.9 ± 0.6	0.1459 ± 0.0115	51.4 ± 4.2
YNPCA 5	109 ± 1	< 5	11 ± 1	< 5	10.3 ± 0.4	0.0887 ± 0.0081	27.1 ± 2.6
SNICA 1	316 ± 23	70 ± 8	85 ± 11	22.1 ± 3.1	27.0 ± 3.9	NM	NM
SNICA 2	159 ± 5	< 7	10 ± 2	< 70	6.6 ± 1.4	0.0081 ± 0.0046	2.8 ± 1.7
SNICA 2	195 ± 6	< 7	16 ± 7	< 44	8.1 ± 3.8	0.0051 ± 0.0041	3.1 ± 2.6
SNICA 2	117 ± 9	20 ± 2	26 ± 2	17.5 ± 2.0	22.4 ± 2.5	0.0014 ± 0.0006	0.4 ± 0.2

[a] not measureable.

TABLE 3. Thermodynamic calculation for Fe(II) and Fe(III) speciation.

Components & Species	$\log\beta_t$[a]	Reference[b]	Concentration[c]
pH			4.25
$acetate_{total}$			1.0×10^{-5} M
$formate_{total}$			5.0×10^{-4} M
$oxalate_{total}$			1.0×10^{-6} M
$Fe(II)_{total}$			1.0×10^{-6} M
$Fe(III)_{total}$			1.0×10^{-6} M
Fe^{2+}			1.0×10^{-6} M
$FeOH^{+}$	4.5	1	4.5×10^{-12} M
Fe^{3+}			8.2×10^{-9} M
$FeOH^{2+}$	11.4	2	3.9×10^{-7} M
$Fe(OH)_2^{+}$	20.1	2	3.3×10^{-8} M
$Fe(oxalate)^{+}$	9.40	3	4.9×10^{-7} M
$Fe(oxalate)_2^{-}$	16.2	3	7.4×10^{-8} M
$Fe(oxalate)_3^{3-}$	20.8	3	7.0×10^{-11} M

[a] β_t is cumulative equilibrium constant.

[b] References: (1) *Smith and Martell* [1974]; (2) *Faust and Hoigné* [1990]; (3) *Lacroix* [1949].

[c] species concentrations were calculated using MINEQL [*Westall*, 1976]

TABLE 4. Rate constants for the $Fe(II)_{aq}$ oxidation and $Fe(III)_{aq}$ reduction reactions and the calculated Fe oxidation and reduction rates using the information in Table 3 and assuming $[H_2O_2] = 1 \times 10^{-6}$ M.

Reaction	Rate Constant	Reference[a]	d[Fe(II)]/dt[b] nM s^{-1}
(13)	6.3×10^{1} M^{-1} s^{-1}	1	-0.06
(14)	5.9×10^{6} M^{-1} s^{-1}	2	-0.03
(15)[c]	1.5×10^{-7} s^{-1}	3	-0.00015
(16)[d]	6.3×10^{-4} s^{-1}	4	0.25
(17)[d]	5.8×10^{-2} s^{-1}	5	4.3

[a] References: (1) Hartwick [1957]; (2) *Millero and Sotolongo* [1989]; (3) *Wehrli* [1990]; (4) *Faust and Hoigné* [1990]; (5) *Zuo & Hoigné* [1993].

[b] minus sign indicates -d[Fe(II)]/dt and plus sign indicates +d[Fe(II)]/dt.

[c] psuedo first order with respect to $[Fe(II)]_{total}$ assuming $P_{oxygen} = 0.21$ atm and pH = 4.25.

[d] for clear sky photolysis (solar noon, 30 June)

FIGURE 1

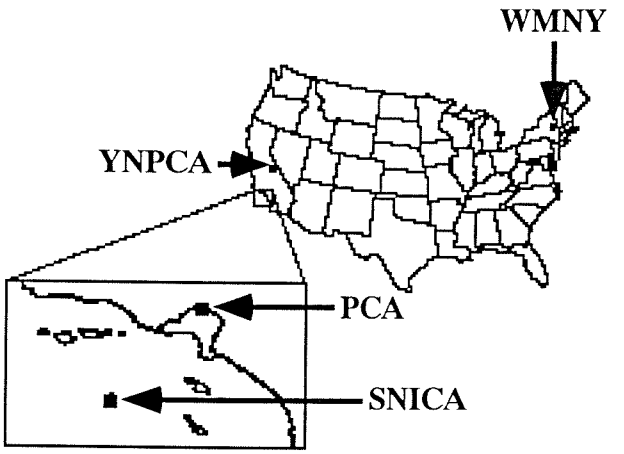

FIGURE 2

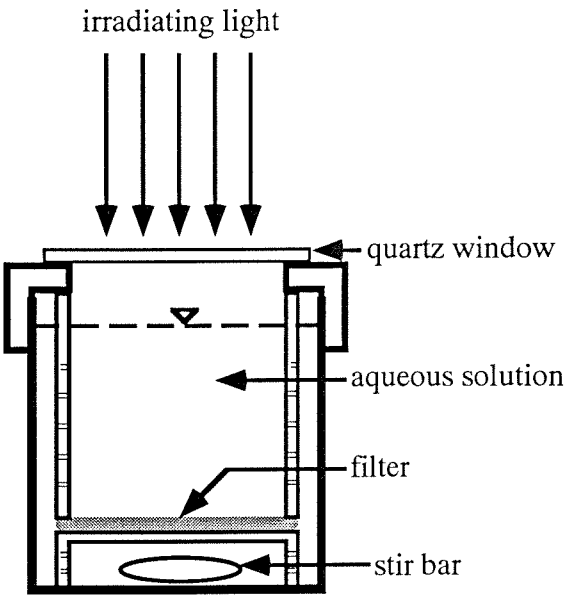
irradiating light
quartz window
aqueous solution
filter
stir bar

FIGURE 3

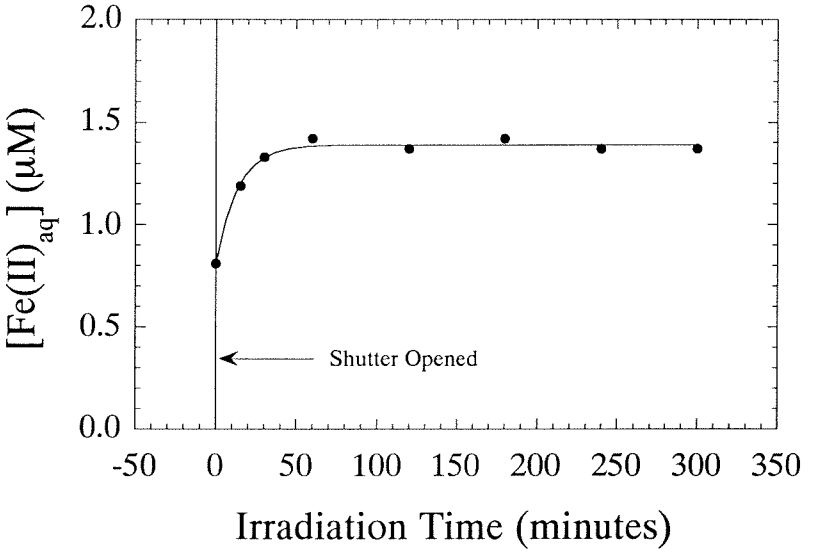
2.0
1.5
1.0
0.5
0.0
[Fe(II)aq] (μM)
Shutter Opened
-50
0
50
100
150
200
250
300
350
Irradiation Time (minutes)

FIGURE 4

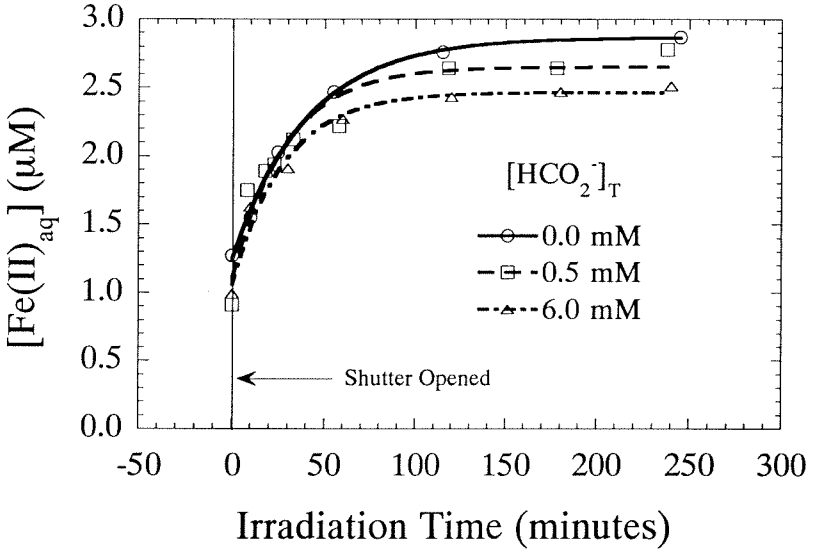
3.0
2.5
2.0
1.5
1.0
0.5
0.0
[Fe(II)aq] (μM)
-50
0
50
100
150
200
250
300
Irradiation Time (minutes)
[HCO2-]T
0.0 mM
0.5 mM
6.0 mM
Shutter Opened

FIGURE 5

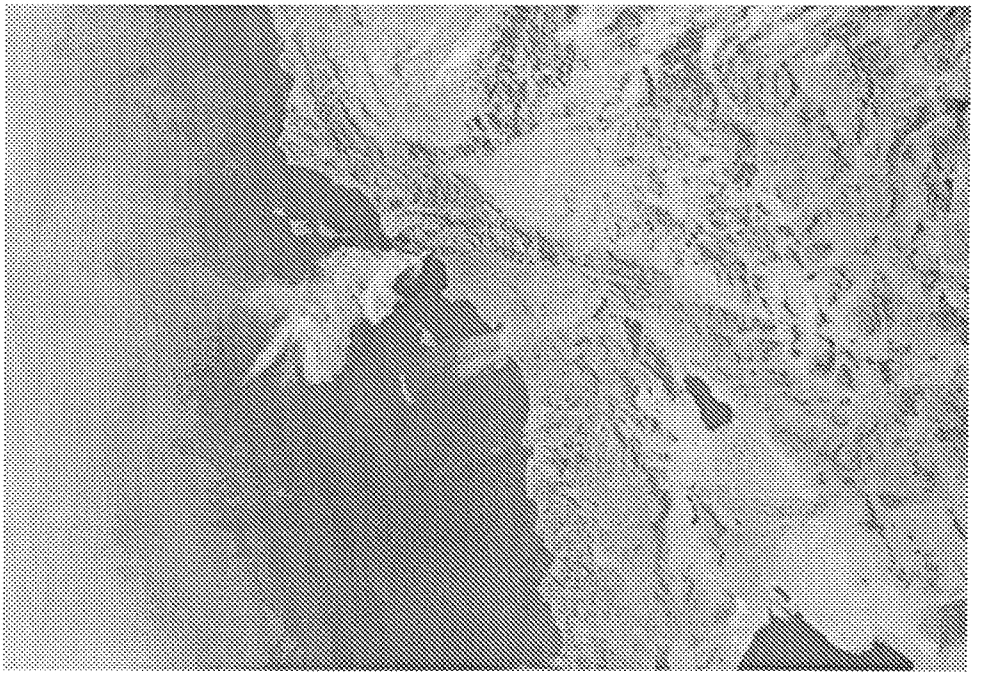

Chapter 4:

Measurements of Trace Metal (Fe, Cu, Mn & Cr) Oxidation States in Fog and Stratus Clouds

[Ronald L. Siefert, Anne M. Johansen, Simo O. Pehkonen, and Michael R. Hoffmann
submitted to *The Journal of Air and Waste Management*]

ABSTRACT

The oxidation state of four transition metals (Fe, Mn, Cu & Cr) in cloudwater has been investigated during several cloud events at Whiteface Mountain (NY), one cloud event at San Pedro Hill (CA) and one fog event at Bakersfield (CA). Samples were collected and immediately analyzed for the oxidation states of four transition metals: 1) Fe(II) [44 measurements], 2) Cu(I) [30 measurements], 3) Mn(IV) [27 measurements], and 4) Cr(III) [3 measurements]. Extreme care was taken to minimize contamination and interferences when measuring these oxidation states. Particulate and dissolved concentrations of these metals were also determined. Other measurements performed, relevant to the redox chemistry of these metals, included pH, total elemental concentrations (Fe, Cu, Mn, Cr, Al, K, Ca, Na and Mg), organic anions (formate, acetate, glycolate, oxalate), inorganic anions (chloride, sulfate, nitrate, sulfite), cations (sodium, calcium, magnesium, potassium), peroxides, and formaldehyde. These measurements were then used in thermodynamic speciation models to understand the speciation of ambient fog and cloudwater. From this analysis, two different cases were found for $Fe(III)_{soluble}$ speciation. Fe(III) was found to exist either as $Fe(OH)_2^+$ or $Fe(Oxalate)_2^-$. However, an un-identified strong chelating ligand with Fe(III) was also suggested by the data. Cu(I) and Cu(II) were calculated to be predominantly Cu^+ and Cu^{2+} (with less than 10% as Cu(II)-oxalate complexes). A chemical kinetic model was also used to investigate the transition metal chemistry. The model results indicate Fe(II) should be the predominant chemical form of Fe during daylight conditions. This prediction is in agreement with the field measurements in which the highest ratios of $Fe(II)/Fe_{total}$ were found in samples collected during the day. The model results also indicated Fe(III) should be the predominant form of Fe during nighttime conditions, this is also in agreement with the field measurements. In the model, Cu(II) and Mn(II) were the predominant oxidation states during daylight and nighttime conditions, with Cu(I) and Mn(III) increasing during daylight conditions. Mn(III)

concentrations were never high enough to influence the redox chemistry of Cr. Overall, Cr(VI) in cloudwater is predicted to be reduced to Cr(III).

INTRODUCTION

In order to understand the dynamical chemical changes occurring in cloud, fog, and haze aerosols, the detailed chemical speciation of transition metals must be resolved. A knowledge of the chemical speciation of all oxidation states for the transition metals present as a function of variables such as pH, organic ligands, and inorganic ligands is critical to the computational assessment of *in situ* atmospheric reaction pathways involving S(IV), O_2, RHCO, NO_X, ROOH, and H_2O_2 in heterogeneous phases. In addition, a knowledge of the detailed chemical speciation of metals in atmospheric deposition is important to understanding the speciation of these metals in sea water. In addition, this speciation of metals in sea water is critical to assessing the ability of marine biota to utilize atmospherically-derived trace elements as micro-nutrients [*Hudson and Morel*, 1990; *Hudson and Morel*, 1993; *Morel et al.*, 1991; *Wells et al.*, 1994; *Wells et al.*, 1995]. Several studies have found Fe to be a rate-limiting nutrient to primary phytoplankton growth in certain regions of the open ocean [*Ditullio et al.*, 1993; *Kolber et al.*, 1994; *Martin et al.*, 1994; *Martin and Gordon*, 1988; *Price et al.*, 1994]; and the speciation of Fe is critical to the rate of Fe uptake by phytoplankton. Overall, a knowledge of the speciation of trace metals in atmospheric deposition and the subsequent speciation changes upon introduction to marine waters is important to the assessment of the ability of marine biota to utilize atmospherically-derived elements for nutritional needs.

Several first-row transition metals are thought to play a major role in the redox cycle of sulfur and organic compounds in the troposphere, as well as controlling free radical production in clouds [*Conklin and Hoffmann*, 1988a; *Conklin and Hoffmann*, 1988b; *Faust and Hoffmann*, 1986; *Graedel et al.*, 1986; *Hoffmann and Jacob*, 1984; *Jacob et al.*, 1989; *Jacob and Hoffmann*, 1983; *Kotronarou and Sigg*, 1993; *Martin and Hill*, 1987; *Siefert et al.*, 1994; *Weschler et al.*, 1986; *Xue et al.*, 1991b; *Zhuang et al.*, 1992; *Zuo and*

Hoigné, 1992]. Both Mn and Fe can catalyze the oxidation of S(IV) by oxygen, and together they have a synergistic effect [*Berglund and Elding*, 1995; *Berglund et al.*, 1993; *Conklin and Hoffmann*, 1988b; *Faust and Allen*, 1994; *Kraft and Van Eldik*, 1989a; *Kraft and Van Eldik*, 1989b; *Martin and Good*, 1991; *Martin et al.*, 1991]. Sedlak and Hoigné [*Sedlak and Hoigné*, 1993; *Sedlak and Hoigné*, 1994] have investigated the redox cycling of Fe and Cu in the presence of oxalate, and its implications for S(IV) oxidation. The photochemistry of Fe(III)-hydroxy and Fe(III)-oxalato complexes and the subsequent production of Fe(II) and oxidants ($OH^{\bullet}$, $HO_2^{\bullet}/O_2^{\bullet-}$) has also been studied [*Faust and Hoigné*, 1990; *Zuo and Hoigné*, 1992]. Modeling studies have also looked at transition metal redox chemistry in cloudwater [*Jacob et al.*, 1989; *Matthijsen et al.*, 1995; *Sedlak and Hoigné*, 1993; *Seigneur and Constantinou*, 1995]. Jacob *et al.* [*Jacob et al.*, 1989] concluded that the major source of S(VI) is the reaction S(IV) + Fe(III), provided a non-radical mechanism in which Fe(III) is not reduced is operative. Zuo *et al.* [*Zuo and Hoigné*, 1994] have also looked at the photochemical decomposition of oxalic, glyoxalic and pyruvic-acid catalyzed by iron in atmospheric waters. Overall, transition metal complexes play an important role in aqueous-phase atmospheric chemistry.

Iron (Fe), manganese (Mn), copper (Cu) and chromium (Cr) are the most abundant transition metals in the atmosphere, and were the focus of these field studies. Iron (Fe), is the most abundant transition metal in the earth's crust, and is present primarily as Fe(II) and Fe(III) forms [*Taylor and McLennan*, 1985]. These transition metals are known to participate in a variety of redox reactions in natural waters [*Balistrieri et al.*, 1992; *Conklin and Hoffmann*, 1988a; *Conklin and Hoffmann*, 1988b; *Faust and Hoffmann*, 1986; *Graedel et al.*, 1986; *Johnson et al.*, 1992; *Seigneur and Constantinou*, 1995; *Weschler et al.*, 1986; *Wiersma and Davidson*, 1986]. Fe and Mn are also found in the form of oxides and hydrous oxides in natural waters which can catalyze redox reactions involving sulfur. Chromium (Cr) in the hexavalent form (Cr(VI)) is believed to be carcinogenic and can be absorbed by ingestion, through the skin and by inhalation; whereas trivalent chromium

(Cr(III)) is not considered to be carcinogenic [*EPA*, 1984; *EPA*, 1994]. Therefore, an understanding of the atmospheric speciation of Cr (which will depend on the cloud chemistry) is important in the assessment of potential health risks associated with the atmospheric deposition of Cr [*Seigneur and Constantinou*, 1995].

Previous field studies have determined the occurrence, particle-size distribution and sources of transition metals in the atmosphere [*Galloway et al.*, 1982; *Lantzy and Mackenzie*, 1979; *Nriagu*, 1989; 1986; *Puxbaum*, 1991]. But only a few studies have looked at the speciation or reactivity of trace metals in the fog or cloud water [*Behra and Sigg*, 1990; *Erel et al.*, 1993; *Kotronarou and Sigg*, 1993; *Xue et al.*, 1991b] or in ambient aerosols[*Kopcewicz and Kopcewicz*, 1991; *Kopcewicz and Kopcewicz*, 1992; *Siefert et al.*, 1994; *Spokes et al.*, 1994; *Zhu et al.*, 1993; *Zhuang et al.*, 1992]. In this study, measurements of Fe, Cu, Mn and Cr oxidation states in ambient samples have been combined with thermodynamic and kinetic models to assess the role of transition metal chemistry in aqueous-phase atmospheric chemistry.

METHODS

Cloudwater and Fogwater Collection

Fogwater and cloudwater samples were collected at three sites: Whiteface Mountain, NY (hereafter referred to as "WM"); San Pedro Hill, CA (hereafter referred to as "SP"); and Bakersfield, CA (hereafter referred to as "BK"). Clouds associated with frontal systems were sampled at Whiteface Mountain (NY) which is a high-elevation site (elev. 1512 m a.s.l.) located in rural northeastern United States. Coastal stratus clouds were sampled at San Pedro Hill (CA) which is located 2.5 km inland of the Pacific Ocean (elev. 450 m a.s.l.) located on the easternmost hill of the Palos Verde Peninsula. Los Angeles Harbor is located 6 km east of San Pedro Hill (CA). Radiation fogs were sampled at Bakersfield (CA) which is in the Southern San Joaquin Valley.

Fog and cloudwater samples were collected using two collector designs: 1) a Caltech active strand cloudwater collector (CASCC) [*Daube et al.*, 1987] and 2) a passive cloudwater collector (PCC) [*Collett*, 1989]. Both of these collectors were constructed out of materials to minimize trace metal contamination. The CASCC was constructed primarily out of polypropylene, and used Teflon strands as the impaction surfaces for the cloud droplet collection. The PCC was constructed out of Teflon coated anodized aluminum, and also used Teflon strands as the impaction surfaces for the cloud droplet collection. The CASCC was used at the San Pedro (CA) and Bakersfield (CA) sites, while the PCC was used at the Whiteface Mountain (NY) site. The cloudwater collectors were acid-cleaned before use by following similar procedures as outlined by *Patterson and Settle* [*Patterson and Settle*, 1976]. Acid-cleaned low-density polyethylene (LDPE) bottles and Teflon labware were used to collect cloudwater samples, and also used in the wet-chemistry methods used for determining trace metal oxidation states and total concentrations. All bottles were acid-cleaned before use following similar procedures outlined by *Patterson and*

Settle [*Patterson and Settle*, 1976]. Ultra-pure acids from Seastar Chemicals (Sidney, B.C., Canada), and 18.2 MΩ-cm Milli-Q UV water were used in the cleaning protocols.

Overview of Analytical Procedures

Measurements of reactive species were measured immediately after collection ("on site") in order to minimize the possible changes in speciation due to reactions occurring during sample storage. Trace metal oxidation states, pH, formaldehyde and sulfite were all measured "on site". Hydrogen peroxide (H_2O_2) was measured by reacting H_2O_2 in the cloudwater sample with p-hydroxyphenylacetic acid (POPHA), which forms a fluorescent dimer of POPHA [*Kok et al.*, 1986; *Lazrus et al.*, 1985]. The solution with the fluorescent dimer was then measured within 48 hours. Other species were stabilized immediately after collection and measured later in the laboratory.

Analytical Procedures Performed on Site

The cloudwater pH was measured within 10 minutes of collection using a combination electrode (FUTURA Plus combination electrode, Beckman Instruments, Inc.) with a portable pH meter (PHM 80, Radiometer America, Inc.). A two point calibration (with pH 4 and pH 7 buffer solutions) was also performed in the field.

Analytical methods for trace metal oxidation states were all started within 10 minutes of sample collection. A portable spectrophotometer (Shimadzu UV-1201) was used for all colorimetric measurements made in the field. Spectrophotometric cells with various geometry's were used in order to minimize sample aliquots while keeping the detection limits as low as possible.

Ferrous iron (Fe(II)) was measured colorimetrically by complexation with ferrozine [*Carter*, 1971; *Stookey*, 1970]. A 0.1 ml aliquot of an ammonium acetate buffer solution (10%) was added to a 2 ml aliquot of the cloudwater sample, followed by 0.2 ml of the ferrozine reagent solution (75 mg ferrozine in 25 ml of H_2O with 1 drop HCl). The

absorbance was then measured at 562 nm. The absorbance of the cloudwater sample was also measured at 562 nm and used as the "blank" absorbance. The increase in absorbance at 562 nm was attributed to $Fe(II)_{soluble}$ in the cloudwater sample.

Oxidized manganese (Mn(IV)) was measured using a modification to the leuco-crystal violet (LCV) method [*Kessick et al.*, 1972; *Murray et al.*, 1984; *Spratt et al.*, 1994]. This method utilizes the oxidation of the leuco base of the dye crystal violet by Mn oxides. A 1.25 ml aliquot of an acetate buffer (0.6 M, pH 4.0) was added to a 25 ml aliquot of the cloudwater sample, followed by 0.5 ml of LCV reagent solution (10 mg LCV in 9 ml of H_2O and 1 ml of 1 M HCl). The dye was then concentrated using an organic extraction step. A 5 ml aliquot of isobutanol/toluene (1:1 by volume) was added to the solution and vigorously mixed for 1 minute. The organic layer was then allowed to separate and was extracted. The absorbance of the extracted organic layer was measured at 591 nm using a 5 cm spectrophotometeric cell. Other oxidants (e.g., Mn(III), Cl(I), Cr(III), Fe(III)) can also oxidize LCV, however they oxidize LCV at rates much slower then the oxidation rate due to Mn(IV) [*Spratt et al.*, 1994]. Therefore the LCV technique was selective to Mn(IV).

Cu(I) was determined spectrophotometrically by use of bathocuproine (2,9-dimethyl-4,7-diphenyl-1,10-phenanthroline) and an extraction technique [*Diehl and Smith*, 1958; *Smith and Wilkins*, 1953]. Organic extraction of Cu(I) is necessary due to the reagent's low solubility in water, but it also serves as a pre-concentration step and it may reduce interfering matrix effects. Others [*Moffett et al.*, 1985; *Xue et al.*, 1991a] have used the sulphonated and water soluble version of bathocuproine to simplify the analysis. However, the low concentrations of Cu(I) encountered in our samples required a pre-concentration step for detection. In the field, 50 ml of the collected fog sample were extracted with 5 ml of freshly prepared bathocuproine in isoamyl alcohol (1 g/L, 2.8 mM) by shaking for 5 minutes and letting the phases separate for 2 minutes. The organic phase was then transferred into a low volume 5 cm cuvette to determine the absorbance at 482 nm. Due to the nature of this technique, a true blank, performed by extracting the sample

with the organic phase before adding the dye, could not be carried out. However, with a few exceptions, matrix effects could be neglected. The fact that many of our samples exhibited blank values, and were therefore under detection limit (30 nM) supports this assumption. Additionally, aerosol particles that serve as cloud condensation nuclei are primarily hydrophilic in character, which implies that most of the matrix will partition into the aqueous instead of the organic phase. Final concentrations were calculated from calibration curves performed following similar procedures at a series of pH values.

Trivalent chromium (Cr(III)) and hexavalent chromium (Cr(VI)) were determined by co-precipitation of Cr(III) with am-$Fe(OH)_3$ followed by filtration in the field. The filtrate was then measured for Cr ($Cr_{co\text{-}precipitation,filtrate}$), and this Cr concentration was attributed to Cr(IV). Cr(III) was calculated by calculating the difference between $Cr_{co\text{-}precipitation,filtrate}$ and Cr_{total}.

Formaldehyde (HCHO) was measured using the "Nash" method [*Nash*, 1953; *Smith and Erhardt*, 1975], which involves the reaction of HCHO with 2,4 pentane-dione and ammonia (the "Hantzsch" reaction), to form 3,5-diacetyl-1,4-dihydrolutidine which is quantified by its absorption at 415 nm. A 0.5 ml iodine solution (28 mM in acetone) was added to a 2.5 ml aliquot of the cloudwater sample to eliminate a S(IV) interference, followed by addition of the Nash reagent (15 g ammonium acetate + 0.2 ml 2,4-pentane-dione in 50 ml of H_2O). The absorbance was then measured at 415 nm.

Sulfite (S(IV)) was measured using the "Bunte" salt method [*Humphrey et al.*, 1970]. Sulfite ion reacts quantitatively at room temperature in aqueous buffers with and 5,5'-dithiobis(2-nitrobenzoic acid) (DTNB) to displace the thiol and form an organic thiosulfate. Sulfite is determined by measurement of the absorption of the thiol. A buffer was added (2.5 ml of 10% ammonium acetate buffer) to a 2.5 ml aliquot of cloudwater, followed by addition of 0.5 ml of disulfide reagent (40 mg of DTNB and 40 mg Na_2EDTA in 75 ml EtOH and 25 ml of 10% ammonium acetate). The absorbance was then measured at 412 nm.

Concentrations of Fe, Mn, Cu, Cr, Al, Na, Mg, Ca, and K were measured using inductively coupled plasma mass spectrometry (ICP-MS) with a Perkin Elmer-SCIEX Elan 5000 instrument. Dissolved and particulate fractions of Fe, Mn, Cu, Cr, Al, Na, Mg, Ca, and K were measured by filtering an aliquot of the cloudwater sample in the field, measuring the concentrations in the filtrate, and comparing these concentrations to the total concentrations in a non-filtered aliquot of the same cloudwater sample. An acid-cleaned Teflon filtering unit with a 0.05 μm Millipore filter was used to filter the sample. Filtering was always done within 10 minutes of sample collection. The filtrate was stored in an acid-cleaned PE bottle for analysis back in the laboratory.

Analytical Procedures Performed off Site

Hydrogen peroxide (H_2O_2) was measured by reacting H_2O_2 in the cloudwater sample with p-hydroxyphenylacetic acid (POPHA), which forms a fluorescent dimer of POPHA which is stable for several days [*Kok et al.*, 1986; *Lazrus et al.*, 1985]. The solution with the fluorescent dimer was then measured within 48 hours using a spectrofluorophotometer (Shimadzu RF-540) in the laboratory. This method is also sensitive to organic peroxides.

Organic anions (formate, acetate, glycolate, oxalate, etc.) and inorganic anions (sulfate, nitrate, chloride) were stabilized in the field by spiking an aliquot of the cloudwater sample with chloroform (to minimize the loss or organic acids due to microbiological mechanisms). The aliquot was stored (from one day to two weeks) in the dark under refrigerated conditions until analyzed by ion-chromatography in the laboratory. The chromatographic method used a Dionex BIO-LC gradient elution ion chromatograph with a PAX-500 anion column and NaOH eluent.

Metals were stabilized immediately after collection by adding a drop of concentrated ultra-pure HNO_3 (Seastar) to an aliquot of the cloudwater sample in the field. Total metal concentrations for Fe, Cu, Mn, Cr, Al, K, Ca, Na, Mg were measured using inductively

coupled plasma mass spectrometry (ICP-MS) using a Perkin Elmer-SCIEX Elan 5000 instrument. A similar method was used when analyzing for total metal concentrations in filtered samples. Samples were filtered in the field within 10 minutes after collection, through a acid-cleaned Millipore filter using an all Teflon filter holder.

Computational Determination of Chemical Speciation and Kinetics

Chemical speciation calculations were performed using the program MINEQL [*Westall et al.*, 1976] which uses the equilibrium constant approach (defined by a system of mass action equations) to solve a chemical equilibrium problem.

A computer program was also written to model the aqueous-phase kinetics of the transition metals. The program used an identical computational procedure as MINEQL [*Westall et al.*, 1976] to determine the speciation, followed by numerical integration using a second-order predictor, iterated-corrector scheme [*Young and Boris*, 1977].

Statistical Analysis

Multivariate statistical analysis was performed using SPSS software [*Kim*, 1975]. R-type principal component analysis with orthogonal varimax rotation was performed on the data set.

RESULTS AND DISCUSSION

Overview of Cloudwater Samples

Sixty five cloudwater samples were collected during several cloud events at Whiteface Mountain (NY), one cloud event at San Pedro Hill (CA) and one fog event at Bakersfield (CA). Table 1 shows the collection date, time, sampling duration, weight of sample, liquid water content (LWC) of the sampled cloud, pH, mass of filtered aliquot and sunlight conditions. The average sampling duration was 42 minutes. The sampling duration was chosen to collect the appropriate volume of sample for the specific analysis being performed. This procedure was used to minimize reactions occurring after sample collection.

Total Metal Concentrations

Total concentrations of Fe, Cu, Mn, Cr and Al were measured for 59 of the 64 cloudwater samples, and total concentrations of K, Ca, Na and Mg were measured for 51 of the 64 cloudwater samples (Table 2). A comparison of total metal concentrations and average concentrations for this study and previous studies in the literature are shown in Table 3. Liquid water content (LWC) was not included in this comparison, since LWC was not available for all the data sets.

Total Fe concentrations measured in this study were in reasonable agreement to previous studies, except for the extremely high Fe concentrations found in Zürich, Switzerland [*Behra and Sigg*, 1990] and Lennox, CA [*Munger et al.*, 1983]. Total Cu concentrations at WM were in good agreement with measurements by Khwaja *et al.* [*Khwaja et al.*, 1995], and overall were much lower than the measurements made in Switzerland [*Johnson et al.*, 1987; *Xue et al.*, 1991b]. Total Mn concentrations were in good agreement with other studies. Total Cr concentrations ranged from < 4 to 56 nM, and

could not be compared to previous studies since no other measurements of Cr in cloudwater were found in the literature. Total Al ranged from 50 to 12300 nM with an average concentration of 2400 nM. Aluminum and Fe have similar binding constants to many important ligands in natural waters (e.g., oxalate), and Al was investigated to quantify its potential role as a reservoir for these ligands.

Particulate Metal Concentrations

Table 4 shows the percentage of each element associated with the aqueous phase. All elements had a significant percentages associated with the aqueous phase. Overall, Fe had the lowest percentages associated with the aqueous phase, with the notable exception of the two Bakersfield, CA samples where more than half of the total Fe was associated with the aqueous phase. This was an unexpected result, because the pH measurements at Bakersfield, CA were much higher than the other sites (see Table 1), and at high pH most of the Fe would be expected to form Fe(III)-oxyhydroxide particles.

Fe, Cu, Mn and Cr Oxidation States

The oxidation states of Fe, Cu, Mn, and Cr were measured for a portion of the 64 cloudwater samples. Table 5 shows the results of these measurements along with the ratios of the oxidation state of each metal to the total concentration of the metal in the sample.

Fe(II) was measured for 43 of the 64 samples and ranged from < 60 nM (29 of the measurements were below the detection limit) to 1820 nM. The highest ratios of $Fe(II)/Fe_{total}$ were found in samples collected during the day. This is consistent with models which predict Fe to be in the reduced state (Fe(II)) during the day due to photochemical reactions which reduced Fe(III) to Fe(II). However, Fe(II) rarely accounted for more than 50% of the Fe_{total} even during the day, which indicates that a portion of the Fe is unavailable for photochemical reactions. This Fe fraction can either be in the aqueous phase as part of a complex with a ligand which does not undergo a charge transfer redox

reactions with Fe (e.g., F^-), or it is in the solid phase as either an un-reactive Fe-oxyhydroxide or it is bound in the matrix of an alumino-silicate mineral. WM 94-12 and WM 94-26 samples (both taken during the day) had data for both $Fe(II)/Fe_{total}$ ratios and $Fe_{particulate}/Fe_{total}$ ratios. For WM 94-12, Fe(II) accounted for 7% of the Fe_{total} and $Fe_{particulate}$ accounted for 93% of the Fe_{total}. Therefore, the soluble Fe was predominantly Fe(II). For WM 94-26, Fe(II) accounted for 9% of the total Fe, and $Fe_{particulate}$ accounted for 81% of the Fe_{total}. Therefore, half of the soluble Fe could be accounted for by Fe(II). BK 95-3 and BK 95-4 (both taken during the night) also had data for both $Fe(II)/Fe_{total}$ ratios and $Fe_{particulate}/Fe_{total}$ ratios. For BK 95-3, Fe(II) accounted for <13% of the Fe_{total}, and $Fe_{particulate}$ accounted for 43% of the Fe_{total}. Therefore, less than 23% of the soluble Fe could be accounted for by Fe(II). For BK 95-4, Fe(II) accounted for <9% of the Fe_{total}, and $Fe_{particulate}$ accounted for 47% of the Fe_{total}. Therefore, less than 17% of the soluble Fe could be accounted for by Fe(II). For the BK samples, there was a large percentage of soluble Fe(III).

Cu(I) concentrations were below the detection limit (< 30 nM) for 11 out of the 30 measurements. The average Cu(I) concentration was 63 nM for the 19 measurements within the detection limit, however this assumes that there was no interferences in the measurements (63 nM would be a maximum average Cu(I) concentration assuming all measurements had possible positive interferences). An interference was indicated by a discrepancy for some of the Cu(I) results, since Cu(I) measurements were found to be greater than total Cu measurements for 5 of the samples. Xue *et al.* [1991a] also measured Cu(I) and found much higher concentrations ($[Cu(I)]_{average}$ = 690 nM and $Cu_{total,average}$ = 1340 nM). Overall, the measurements for Cu(I) in this study were at least one order of magnitude lower in concentration compared to the measurements of Xue *et al.* [1991a]. Mn(IV) concentrations were below the detection limit (< 5 nM) for 10 of the 27 measurements. The average Mn(IV) concentrations was 25 nM for the 17 measurements within the detection limit. Again, discrepancies were found with the Mn(IV) measurements

since Mn(IV) measurements were found to be greater than Mn_{total} measurements for 4 of the samples. The discrepancies may be due to an oxidant (e.g., H_2O_2) which may also oxidize the LCV. Cr(III) concentrations were measured for only 3 samples (all at WM) with an average concentrations of 12 nM. The discrepancies in the Cu(I) and Mn(IV) measurements, underscores the need for more sensitive and selective analytical techniques for measuring cloudwater species at nM levels.

S(IV), Peroxides, HCHO and Anion Concentrations

Table 6 summarizes the measurements for S(IV), peroxides, HCHO and anions. These measurements were used in subsequent thermodynamic and kinetic models which are discussed later in this manuscript. S(IV) was usually below the detection limit for all of the samples except at BK. HCHO concentrations were almost always above the detection limit and also an order of magnitude higher than S(IV) except at BK. These results for S(IV) and HCHO are similar to a study by Rao and Collett [1995], who explained the results in terms of pH and hydroxymethanesulfonate (HMS) complexes of S(IV) and HCHO. Total organic carbon (TOC) was not analyzed for any of the samples. Pyruvate and malonate were detected in some of the WM samples, however their concentrations were not large enough to quantify (and therefore not tabulated). Pyruvate and malonate concentrations were always less than the oxalate concentrations. These observations were in agreement with similar measurements made by Khwaja *et al.* [1995] at WM. Overall the exclusion of pyruvate and malonate does not significantly change the speciation or chemistry of Fe(III) since pyruvate has a weak stability constant with Fe(III), and, although malonate does have a strong stability constant with Fe(III), Fe(III)-malonate complexes undergo similar photochemistry as Fe(III)-oxalate complexes [*Faust and Zepp*, 1993].

Enrichment Factors and Principal Component Analysis

Table 7 shows the enrichment factors (EFs) [*Duce et al.*, 1975; *Zoller et al.*, 1974] calculated for Fe, Cu, Mn and Cr in the cloudwater samples. Crustal averages from Taylor [*Taylor and McLennan*, 1985] were used as the reference source, and Al was used as the crustal tracer. In all samples, Fe had a strong crustal signature, since the average EF(Fe) for all samples was 0.95 and had a limited range. This strong correlation between Al and Fe also provides further validity to the assumption in the EF calculation that all Al is derived from crustal sources. EF(Cu) and EF(Cr) were consistently high in all samples, and therefore most the Cu and Cr was not derived from crustal sources (i.e., Cu and Cr were predominantly anthropogenic). Manganese, like Fe, also had an EF reasonably close to unity (Average EF(Mn) = 2.87) and therefore was predominantly crustal in origin, although a portion of some samples may be attributed to anthropogenic sources.

Principal component analysis was also performed using the total metal concentration data (Fe, Cu, Mn, Cr, Al, Ca and Mg) and several other measured species (pH, peroxides, chloride, nitrate and sulfate) from cloudwater samples collected at Whiteface, Mtn. A total of 46 samples collected during 8 separate cloud events were analyzed. Several species were not included in the analysis since they were below the detection limit for over 25% of the samples. The San Pedro Hill, CA and Bakersfield, CA cloudwater samples were not analyzed since there was only one cloud event for each of these sites. Three principal components were extracted from the data set (each with a minimum eigenvalue set at 1) which account for 84% of the variance in the data set. Table 8 shows the eigenvalue and percent variance described by each principal component. This analysis shows that at least three distinct sources of these species to the cloudwater samples. Table 9 lists the correlation coefficients for each of the principal components and associated species. PC1 has high correlation coefficients for sulfate and nitrate which would indicate an anthropogenic source. PC1 also has high correlation coefficients for several other species (Fe, Mn, Ca, Mg, peroxides and chloride). PC2 has high correlation

coefficients for Cu and Al and is probably a crustal source due to the high Al correlation coefficient. PC3 has high correlation coefficients for Fe, Cr, and Mg. Specifically, all of the species, except Fe, pH and peroxides, had a factorial complexity of 1. Fe, pH and peroxides loaded moderately on more than one factor which indicates that these species have a complicated source. This higher complexity factor of Fe is unexpected since the EF analysis indicated that the predominant source of Fe was crustal.

Thermodynamic Speciation Calculations

Thermodynamic speciation calculations using MINEQL [*Westall et al.*, 1976] were performed for 7 of the 65 samples. These 7 samples were chosen for the analysis because they had the most complete measurements. The 7 samples also represented cloud events from each site (including several events at the Whiteface Mtn. site). Several assumptions were made to perform the calculations: 1) no precipitation was allowed to occur, 2) the pH was kept constant, 3) the thermodynamic database in the MINEQL program was used except for oxalate species (see Table 10 for the thermodynamic values), 4) Fe(II) = 0.1 x $Fe_{soluble}$ if Fe(II) was below the detection limit or not measured, 5) Cu(I) = 0.5 x $Cu_{soluble}$ if Cu(I) was below the detection limit or not measured, 6) K^+, Ca^{2+}, Na^+ and Mg^{2+} were assumed to be equal to the concentration in the filtrate except for the San Pedro samples where K^+, Ca^{2+}, Na^+ and Mg^{2+} were assumed to be dominated by sea-salt and were calculated using the Cl^- measurements with the appropriate sea water ratios [*Millero and Sohn*, 1992], 7) Fe(III) = $Fe_{filtrate}$ - Fe(II) (this relationship has been observed for cloudwater in a previous study [*Pehkonen et al.*, 1992]), 8) Cu(II) = $Cu_{filtrate}$ - Cu(I), 9) Mn(II) = $Mn_{filtrate}$, 10) CrO_4^{2-} = $Cr_{filtrate}$, 11) Al(III) = $Al_{filtrate}$ and 12) no surface chemistry was included. Overall, 18 components were included in each calculation: Fe^{2+}, Fe^{3+}, Cu^+, Cu^{2+}, Mn^{2+}, CrO_4^{2-}, Al^{3+}, Na^+, K^+, Mg^{2+}, Ca^{2+}, Cl^-, CO_3^{2-}, NO_3^-, SO_4^{2-}, formate, acetate, oxalate, $^{\bullet}OH$, HO_2 and H_2O_2. Cl^- depletion, relative to Na^+, has been observed in Southern California aerosol samples [*Eldering et al.*, 1991], with Na^+/Cl^- ratios as high as 3.92

(Na^+/Cl^- is 0.858 for seawater). This results in underestimates for K^+, Ca^{2+}, Na^+ and Mg^{2+} for the San Pedro samples due to assumption 7. However, a sensitivity analysis using the highest Na^+/Cl^- ratio (i.e., greatest Cl^- depletion) was done, and the results did not significantly alter the trace metal speciation. Also, several components were omitted if their speciation was relatively simple and after it was determined that removal of the component did not effect the speciation of the other components. The omission of these components was necessary due to a limit on the maximum number of components accepted by MINEQL.

Figure 1a shows the calculated speciation of Fe(III) in the 7 samples. The predominant Fe(III) species were Fe(II)-oxalate and Fe(III)-hydroxy species. Fe(III)-oxalate complexes were calculated not to be significant in the BK samples because of the high pH and low oxalate concentrations in these samples. However, there was a high percentage of $Fe(III)_{aqueous}$ in these samples. The thermodynamic speciation calculations for Fe(III) show that the major species in these samples should be Fe(III)-hydroxy species. In the calculation no species were allowed to precipitate, since the data used for these calculations were measurements of soluble species. These results indicate other strong chelating ligand(s) for Fe(III) which stabilize it in solution.

Cu(I) was calculated to be predominantly Cu^+. $Cu(I)/NH_3(aq)/Cl^-$ complexes were investigated using estimates of $NH_3(aq)$ concentrations in cloudwater (e.g., maximum literature values) and thermodynamic stability constants from Solis *et al.* [*Solis et al.*, 1995]. These complexes were not found to be significant to Cu(I) speciation in the 7 cases. $Cu(I)\text{-}SO_3^{2-}$ complexes were also not found to be significant since SO_3^{2-} were very low (below the detection limit for many of the samples), and HCHO concentrations were high enough to assume that SO_3^{2-} would be predominantly complexed with HCHO as the hydroxymethanesulfonate (HMS) species. Rao and Collett [1995] also found SO_3^{2-} to be predominantly complexed with HCHO in fogwater and cloudwater samples. However,

Xue *et al.* [1991a] calculated from their measurements of Cu(I) and SO_3^{2-} in cloudwater samples collected in Switzerland, that Cu(I)-sulfite complexes were predominant.

Figure 1b shows the calculated speciation of Cu(II) in the 7 cloudwater samples. The predominant Cu(II) species was Cu^{2+}. Cu(II)-oxalate species never accounted for more than 30% of the Cu(II). In contrast, Xue *et al.* [1991a] calculated Cu(II)-oxalate species to be the predominant Cu(II) species.

Figure 1c shows the calculated speciation of oxalate in the 7 cloudwater samples. Most of the oxalate was calculated to be as free oxalate or oxalic acid. The next important species was Al-oxalate species which represented 10% of the total oxalate. These Al-oxalate species had a relatively small impact on the speciation of Fe(III) and Cu(II) in these calculations. However, it is possible that Al(III) could be an important reservoir of oxalate under certain conditions, which would change the photo-redox chemistry of the other trace metals.

The speciation calculations showed that Mn(II) was present as Mn^{2+} with a small amount of Mn(II)-SO_4^{2-} complexes (< 5%). Mn(IV) was in the form of particulate Mn-oxides, and Mn(III) was calculated to be $Mn(OH)^{2+}$. Cr(VI) was found to be either as $HCrO_4^-$ or CrO_4^{2-}, and Cr(III) calculated to be Cr^{3+}.

Kinetic Model

A model was used to investigate the aqueous-phase reactions of Fe, Mn, Cu and Cr. Table 10 shows the thermodynamic stability constants and Table 11 shows the reaction rate constants used in the model. Three model runs were performed using the data from BK 95-4, SP 94-4, and WM 94-12 as the initial concentrations (using the same assumptions as outlined in the thermodynamic speciation calculation section for missing data). These three samples were chosen because they represented the range of concentrations found in the fogwater and cloudwater samples in this study. An example of a model run is shown in Figure 2. The first part of the model run includes photochemical

reactions to simulate daylight conditions. After a pseudo-steady state had been reached, the photochemical reaction rate constants were set to zero to simulate nighttime conditions (or sample collection conditions).

Table 12 tabulates the results of the kinetic model runs. H_2O_2 and oxalate did not change significantly over the course of the runs and are not included in Table 12. For all runs, Fe(II) was greater than Fe(III) once a pseudo steady-state had been reached with the photochemical reactions, and Fe(III) was greater than Fe(II) during night conditions. This was in reasonable agreement with the measurements in Table 5, which shows that there was never any detectable Fe(II) for samples collected at night, and that Fe(II) was a significant percentage of the Fe_{total} during the day. However, it should be noted that the sampling time required for the collection of the samples was long enough for a portion of Fe(II) to be oxidized back to Fe(III).

Cu(II) was always greater than Cu(I) during day and night conditions. During the day conditions, Cu(I) did reach a pseudo steady-state concentration within a factor of 100 of the Cu(II) concentration. However, during night conditions, this Cu(I) concentration decreased dramatically (see Figure 1). The model also shows that the analysis of Cu(I) in the field should be extremely difficult to detect since the time between collecting a sample and analyzing it for Cu(I) is long enough for Cu(I) to be oxidized to Cu(II). However, Cu(I) was possibly detected in some of the samples in this study and other studies [*Xue et al.*, 1991a]. Xue *et al.* [1991a] concluded that Cu(I) was predominantly complexed with S(IV) in their samples, which would explain their concentrations of Cu(I). S(IV) concentrations in this study were usually below the detection limit and HCHO concentrations were high enough to assume that most S(IV) would be in the form of HMS. However, it is difficult to rule out Cu(I)-S(IV) complexes since the Cu(I) concentrations were less than the detection limit of S(IV) (i.e., 1 μM).

Mn(III) represented a small fraction (0.1 to 0.01) of the Mn_{total} concentration after a pseudo steady-state had been reached with the photochemical reactions. And Mn(III)

concentrations dropped quickly after the photochemical reaction rate constants were set to zero. Mn(III) is important to cloudwater chemistry because of its potential to oxidize Cr(III) to Cr(VI) [*Seigneur and Constantinou*, 1995]. Seigneur and Constantinou [*Seigneur and Constantinou*, 1995] developed a chemical kinetic mechanism of atmospheric Cr, and found Mn(III) to be an important oxidant of Cr(III) (their model did not include the dynamic redox chemistry of Fe, Cu or Mn, but assumed concentrations for the oxidation states of these trace metals). However, they also noted that the reduction of Cr(VI) by Fe(II), S(IV) and HCOOH was much greater than the oxidation of Cr(III) by Mn(III) except under extreme conditions. These reactions are:

Cr(VI) Reduction Reactions

$$Cr(VI) + 3Fe(II) \rightarrow Cr(III) + 3Fe(III)$$

$$d[Cr(III)]/dt = (4.4 \times 10^3 [H^+] + 3.0 \times 10^3 [H^+]^2) [Fe^{2+}] [CrO_4^-]$$

[*Espenson*, 1970]

$$2HCrO_4^- + 4HSO_3^- + 6H^+ \rightarrow 2Cr^{3+} + 2SO_4^{2-} + S_2O_6^{2-} + 6H_2O$$

$$d[Cr(III)]/dt = 3.9 \times 10^6 [Cr(VI)] [HSO_3^-] [H^+]$$

[*Beattie and Haight*, 1972]

$$2Cr(VI) + 3HCOOH \rightarrow 2Cr(III) + 3CO_2$$

$$d[Cr(III)]/dt = 1 \times 10^{-4} [HCOOH] [Cr(VI)]$$

[*Beattie and Haight*, 1972]

Cr(III) Oxidation Reactions

$$Cr(III) + 6Mn^{3+} \rightarrow Cr(VI) + 6Mn^{2+}$$

$$d[Cr(VI)]/dt = 0.086\ [Mn(III)]\ [Cr(III)]$$

[*Raphael*, 1982]

Using the results of the model for Mn(III) in Table 12 and the above rate laws for Cr oxidation and reduction, we also found similar results. Cr(VI) should be reduced to Cr(III) in each of the daytime model runs (with half-lifes from minutes to hours). Cr(III) accounted for about 50% of the total Cr for the three measurements in Table 5. The Cr(VI) in these samples may be explained by fact that the samples were collected soon after sunrise when Mn(III) concentrations would be expected to be lower than the predicted model concentration due to reduced photochemistry. Overall, Mn(III) concentrations in the model runs were never high enough to have a net production of Cr(VI).

CONCLUSIONS

The oxidation state of Fe, Mn, Cu and Cr, in cloudwater were measured during several cloud events at Whiteface Mountain (NY), San Pedro Hill (CA) and Bakersfield (CA). Fe(II) was measured for 43 of the 64 samples and ranged from < 60 nM (29 of the measurements were below the detection limit) to 1820 nM. Cu(I) concentrations were below the detection limit (< 30 nM) for 11 out of the 30 measurements. The average maximum Cu(I) concentration was 63 nM for the 19 measurements within the detection limit (a maximum value is given since there were possible positive interferences in these Cu(I) measurements). Mn(IV) concentrations were below the detection limit (< 5 nM) for 10 of the 27 measurements. The average Mn(IV) concentrations was 25 nM for the 17 measurements within the detection limit. Cr(III) concentrations were measured for only 3 samples (all at WM) with an average concentrations of 12 nM. Discrepancies were observed for a few of the Cu(I) and Mn(IV) measurements in this study, which underscores the need for better analytical techniques for investigating trace metal cloudwater chemistry. Enrichment factors (using Al_{total} as the crustal tracer) for Fe_{total} and Mn_{total} were close to unity, indicating these metals had a crustal origin, however, enrichment factors for Cu_{total} and Cr_{total} were much greater than unity (>10) indicating an anthropogenic source of these metals to the cloudwater. Thermodynamic speciation models revealed two different cases for $Fe(III)_{soluble}$ speciation. Fe(III) was either predominantly $Fe(OH)_2^+$ or $Fe(Oxalate)_2^-$. However, an un-identified strong chelating ligand with Fe(III) was also suggested by the data. Cu(I) and Cu(II) were calculated to be predominantly Cu^+ and Cu^{2+} (with less than 10% as Cu(II)-oxalate complexes). Results from a chemical kinetic model predicted Fe(II) would be the predominant chemical form of Fe during daylight conditions, which is in agreement with the field measurements, where the highest ratios of $Fe(II)/Fe_{total}$ were observed during the day. The model results also indicated

Fe(III) would be the predominant form of Fe during nighttime conditions, which is also in agreement with the field measurements. The kinetic model also predicted Cu(II) and Mn(II) to be the predominant oxidation states of Cu and Mn during daylight and nighttime conditions, with Cu(I) and Mn(III) increasing during daylight conditions. Predicted Mn(III) concentrations were never high enough to influence the redox chemistry of Cr. Overall, Cr(VI) in cloudwater is expected to be reduced to Cr(III) (with half-lifes from minutes to hours).

Acknowledgments: Special thanks are extended to Dr. K. L. Demerjian at the Atmospheric Sciences Research Center at Whiteface Mountain, Prof. Ted Murphy at California State University-Bakersfield and the FAA staff at San Pedro Hill. We also thank Prof. J. J. Morgan of Caltech for helpful discussions. Support for this research has been provided by a grant from the National Science Foundation, Division of Atmospheric Sciences, Atmospheric Chemistry Section (ATM 9015775; ATM 9303024). This research was also sponsored by the U.S. Department of Energy, Office of Energy Research, Environmental Sciences Division, Office of Health and Environmental Research, under appointment to the Graduate Fellowships for Global Change administered by Oak Ridge Institute for Science and Education.

REFERENCES

Balistrieri, L.S., J.W. Murray, and B. Paul, The biogeochemical cycling of trace-metals in the water column of lake Sammamish, Washington: Response to seasonally anoxic conditions, *Limnol. & Ocean.*, *37*, 1992.

Beattie, J.K., and G.P. Haight, Chromium(VI) oxidations of inorganic substrates, in *Inorganic Reaction Mechanisms*, edited by J.O. Edwards, pp. 93-145, John Wiley & Sons, New York, 1972.

Behra, P., and L. Sigg, Evidence for redox cycling of iron in atmospheric water droplets, *Nature*, *344* (6265), 419-421, 1990.

Berglund, J., and L.I. Elding, Manganese-catalyzed autooxidation of dissolved sulfur-dioxide in the atmospheric aqueous-phase, *Atmos. Environ.*, *29* (12), 1379-1391, 1995.

Berglund, J., S. Fronaeus, and L.I. Elding, Kinetics and mechanism for manganese-catalyzed oxidation of sulfur(IV) by oxygen in aqueous-solution, *Inorg. Chem.*, *32* (21), 4527-4538, 1993.

Bielski, B.H.J., D.E. Cabelli, R.L. Arudi, and A.B. Ross, Reactivity of HO_2/O_2^- radicals in aqueous solution, *J. Phys. Chem. Ref. Data*, *14*, 1041-1100, 1985.

Buxton, G.V., C.L. Greenstock, W.P. Helman, and A. Ross, Critical review of rate constants for reactions of hydrated electrons, hydrogen atoms and hydroxyl radicals ($^{\bullet}OH/^{\bullet}O^{-}$) in aqueous solution, *J. Phys. Chem. Ref. Data*, *17*, 513-886, 1988.

Cabelli, D.E., and B.H.J. Bielski, Pulse radiolysis study of the kinetics and mechanisms of the reactions between manganese(II) complexes and HO_2/O_2^- radicals, 2, The phosphate complex and an overview, *J. Phys. Chem.*, *88*, 6291-6294, 1984.

Carter, P., Spectrophotometric determination of serum iron at the submicrogram level with a new reagent (ferrozine), *Anal. Biochem.*, *40*, 450-458, 1971.

Christensen, H., and K. Sehested, Pulse radiolysis at high temperatures and pressures, *Radiat. Phys. Chem.*, *18*, 723-731, 1981.

Collett, J.L., Characterization of cloudwater and precipitation chemistry and deposition at elevated sites in central and southern California, Ph.D. thesis, California Inst. of Technol., 1989.

Conklin, M.H., and M.R. Hoffmann, Metal ion-sulfur(IV) chemistry. 2. Kinetic studies of the redox chemistry of copper(II)-sulfur(IV) complexes, *Environ. Sci. Technol.*, *22*, 891-898, 1988a.

Conklin, M.H., and M.R. Hoffmann, Metal ion-sulfur(IV) chemistry. 3. Thermodynamics and kinetics of transient iron(III)-sulfur(IV) complexes, *Environ. Sci. Technol.*, *22*, 899-907, 1988b.

Daube, B.C., R.C. Flagan, and M.R. Hoffmann, Active cloudwater collector, USA, 1987.

Davies, G., Some aspects of the chemistry of manganese(III) in aqueous solution, *Coord. Chem. Rev.*, *4*, 199-224, 1969.

Diehl, H., and F. Smith, *The copper reagents: cuproine, neocuproine, bathocuproine*, 48 pp., G. Frederick Smith Chemical Company, Colombus, OH, 1958.

Ditullio, G.R., D.A. Hutchins, and K.W. Bruland, Interaction of iron and major nutrients controls phytoplankton growth and species composition in the tropical North Pacific Ocean, *Limnol. & Ocean.*, *38* (3), 495-508, 1993.

Duce, R.A., G.L. Hoffman, and W.H. Zoller, Atmospheric trace metals at remote northern and southern hemisphere sites: Pollution or natural, *Science*, *187*, 59-61, 1975.

Eldering, A., P.A. Solomon, L.G. Salmon, T. Fall, and G.R. Cass, Hydrochloric acid: A regional perspective on concentrations and formation in the atmosphere of Southern California, *Atmos. Environ.*, *25* (10), 2091-2102, 1991.

EPA, Health assessment document for chromium, Environmental Protection Agency. Office of Criteria and Assessment: Research Triangle Park, NC, 1984.

EPA, IRIS. Integrated Risk Information System, Environmental Protection Agency, Environmental Criteria and Assessment Office: Cincinnati, OH, 1994.

Erel, Y., S.O. Pehkonen, and M.R. Hoffmann, Redox chemistry of iron in fog and stratus clouds, *J. Geophys. Res. A.*, *98* (D10), 18423-18434, 1993.

Espenson, J.H., Oxidation of transition metal complexes by chromium(VI), *Accounts Chem. Res.*, *3*, 347-353, 1970.

Faust, B.C., and J.M. Allen, Sunlight-initiated partial inhibition of the dissolved iron(III)-catalyzed oxidation of S(IV) species by molecular-oxygen in aqueous-solution, *Atmos. Environ.*, *28* (4), 745-748, 1994.

Faust, B.C., and M.R. Hoffmann, Photoinduced reductive dissolution of alpha-Fe2O3 by bisulfite, *Environ. Sci. Technol.*, *20*, 943-948, 1986.

Faust, B.C., and J. Hoigné, Photolysis of Fe(III)-hydroxy complexes as sources of OH radicals in clouds, fog and rain, *Atmos. Environ.*, *24A* (1), 79-89, 1990.

Faust, B.C., and R.G. Zepp, Photochemistry of aqueous iron(III)-polycarboxylate complexes: Roles in the chemistry of atmospheric and surface waters, *Environ. Sci. Technol.*, *27* (12), 2517-2522, 1993.

Galloway, J.N., J.D. Thornton, S.A. Norton, H.L. Volchok, and R.A.N. Mclean, Trace-metals in atmospheric deposition - A review and assessment, *Atmos. Environ.*, *16*, 1677-1700, 1982.

Graedel, T.E., M.L. Mandich, and C.J. Weschler, Kinetic model studies of atmospheric droplet chemistry, 2. Homogenous transition metal chemistry in raindrops, *J. Geophys. Res.*, *91*, 5205-5221, 1986.

Hartwick, T.J., The rate constant of the reaction between ferrous ions and hydrogen peroxide in acid solution, *Can. J. Chem.*, *35*, 428-436, 1957.

Hoffmann, M.R., and D.J. Jacob, Kinetics and mechanism of the catalytic oxidation of dissolved SO_2 in atmospheric droplets: Free radical, polar and photoassisted pathways, in *SO_2, NO, NO_2 Oxidation Mechanisms: Atmospheric Considerations*, edited by J.G. Calvert, pp. 101-172, Butterworth Publishers, Boston, 1984.

Hudson, R.J.M., and F.M.M. Morel, Iron transport in marine phytoplankton: Kinetics of cellular and medium coordination reactions, *Limnol. Ocean.*, *35* (5), 1002-1020, 1990.

Hudson, R.J.M., and F.M.M. Morel, Trace-metal transport by marine microorganisms: Implications of metal coordination kinetics, *Deep Sea Res.*, *40*, 129-150, 1993.

Humphrey, R.E., M.H. Ward, and W. Hinze, Spectrophotometric determination of sulfite with 4,4,'-dithiodipyridine and 5,5'-dithiobis-(2-nitrobenzoic acid), *Anal. Chem.*, *42* (7), 698-702, 1970.

Jacob, D.J., E.W. Gottlieb, and M.J. Prather, Chemistry of the polluted boundary layer, *J. Geophys. Res.*, *94*, 12975-13002, 1989.

Jacob, D.J., and M.R. Hoffmann, A dynamic model for the production of H^+, NO_3^-, and SO_4^{2-} in urban fog, *J. Geophys. Res.*, *88* (NC11), 6611-6621, 1983.

Johnson, C.A., L. Sigg, and U. Lindauer, The chromium cycle in a seasonally anoxic lake, *Limnol. & Ocean.*, *37*, 315-321, 1992.

Johnson, C.A., L. Sigg, and J. Zobrist, Case studies on the chemical composition of fogwater: The influence of local gaseous emissions, *Atmos. Environ.*, *21* (11), 2365-2374, 1987.

Kessick, M.A., J. Vuceta, and J.J. Morgan, Spectrophotometric determination of oxidized manganese with leuco crystal violet, *Environ. Sci. & Technol.*, *6*, 642-644, 1972.

Khwaja, H.A., S. Brudnoy, and H. Liaquat, Chemical characterization of three summer cloud episodes at Whiteface Mountain, *Chemosphere*, *31* (5), 3357-3381, 1995.

Kim, J., Factor Analysis, in *SPSS: Statistical Package for the Social Sciences*, edited by N.H. Nie, C.H. Hull, J.G. Jenkins, K. Steinbrenner, and D.H. Bent, pp. 468-514, McGraw-Hill, Inc., New York, 1975.

Kok, G.L., K. Thompson, and A.L. Lazrus, Derivatization technique for the determination of peroxides in precipitation, *Anal. Chem.*, *58*, 1192-1194, 1986.

Kolber, Z.S., R.T. Barber, K.H. Coale, S.E. Fitzwater, R.M. Greene, K.S. Johnson, S. Lindley, and P.G. Falkowski, Iron limitation of phytoplankton photosynthesis in the equatorial Pacific Ocean, *Nature*, *371* (6493), 145-149, 1994.

Kopcewicz, B., and M. Kopcewicz, Mossbauer study of iron-containing atmospheric aerosols, *Struct. Chem.*, *2* (3-4), 303-312, 1991.

Kopcewicz, B., and M. Kopcewicz, Seasonal variations of iron concentration in atmospheric aerosols, *Hyperfine Interactions*, *71* (1-4), 1457-1460, 1992.

Kotronarou, A., and L. Sigg, SO2 Oxidation in atmospheric water: role of Fe(II) and effect of ligands, *Environ. Sci. & Technol.*, *27* (13), 2725-2735, 1993.

Kraft, J., and R. Van Eldik, Kinetics and mechanism of the iron(III)-catalyzed autooxidation of sulfur(IV) oxides in aqueous-solution .1. Formation of transient iron(III) sulfur(IV) complexes, *Inorg. Chem.*, *28* (12), 2297-2305, 1989a.

Kraft, J., and R. Van Eldik, Kinetics and mechanism of the iron(III)-catalyzed autooxidation of sulfur(IV) oxides in aqueous-solution .2. Decomposition of transient iron(III) sulfur(IV) complexes, *Inorg. Chem.*, *28* (12), 2306-2312, 1989b.

Lantzy, R.J., and F.T. Mackenzie, Atmospheric trace metals: Global cycles and assessment of Man's impact, *Geochim. et Cosmochim. Acta*, *43*, 511-523, 1979.

Lazrus, A.L., G.L. Kok, S.N. Gitlin, J.A. Lind, and S.E. McLaren, Automated fluorometric method for hydrogen peroxide in atmospheric precipitation, *Anal. Chem.*, *57*, 917-922, 1985.

Logager, T., J. Holcman, K. Sehested, and T. Pedersen, Oxidation of ferrous-ions by ozone in acidic solutions, *Inorg. Chem.*, *31* (17), 3523-3529, 1992.

Martin, J.H., K.H. Coale, K.S. Johnson, S.E. Fitzwater, R.M. Gordon, S.J. Tanner, C.N. Hunter, V.A. Elrod, J.L. Nowicki, and e. al., Testing the iron hypothesis in ecosystems of the equatorial Pacific Ocean, *Nature*, *371* (6493), 123-129, 1994.

Martin, J.H., and R.M. Gordon, Northeast Pacific iron distributions in relation to phytoplankton productivity, *Deep Sea Res. A.*, *35* (2), 177-196, 1988.

Martin, L.R., and T.W. Good, Catalyzed oxidation of sulfur dioxide in solution: The iron-manganese synergism, *Atmos. Environ.*, *25* (10), 2395-2399, 1991.

Martin, L.R., and H.W. Hill, The iron catalyzed oxidation of sulfur: Reconciliation of the literature rates, *Atmos. Environ.*, *21*, 1487-1490, 1987.

Martin, L.R., M.W. Hill, A.F. Tai, and T.W. Good, The iron catalyzed oxidation of sulfur(IV) in aqueous-solution: Differing effects of organics at high and low pH, *J. Geophys. Res.*, *96* (ND2), 3085-3097, 1991.

Matthijsen, J., P.J.H. Builtjes, and D.L. Sedlak, Cloud model experiments of the effect of iron and copper on tropospheric ozone under marine and continental conditions, *Meteorol. Atmos. Phys.*, *57*, 43-60, 1995.

Millero, F.J., and M.L. Sohn, *Chemical Oceanography*, 531 pp., CRC Press, Boca Raton, FL, 1992.

Millero, F.J., and S. Sotolongo, The oxidation of Fe(II) with H_2O_2 in seawater, *Geochim. Cosmochim. Acta*, *53*, 1867-1873, 1989.

Moffett, J.W., and R.G. Zika, Reaction-kinetics of hydrogen-peroxide with copper and iron in seawater, *Environ. Sci. and Technol.*, *21* (8), 804-810, 1987.

Moffett, J.W., R.G. Zika, and R.G. Petasne, Evaluation of bathocuproine for the spectrophotometric determination of copper(I) in copper redox studies with applications in studies of natural-waters, *Anal. Chim. Acta*, *175*, 171-179, 1985.

Morel, F.M.M., R.J.M. Hudson, and N.M. Price, Limitation of productivity by trace-metals in the sea, *Limnol. Oceanogr.*, *36* (8), 1742-17455, 1991.

Munger, J.W., J.M. Waldman, D.J. Jacob, and M.R. Hoffmann, Fogwater chemistry in an urban atmosphere, *J. Geophys. Res.*, *88* (NC9), 5109-5121, 1983.

Murray, J.W., L.S. Balistrieri, and B. Paul, The oxidation state of manganese in marine sediments and ferromanganese modules, *Geochim. et Cosmochim. Acta*, *48*, 1237-1247, 1984.

Nash, T., The colorimetric estimation of formaldehyde by means of the Hantzsch reaction, *Biochem. J.*, *55*, 416-421, 1953.

Nriagu, J.O., A global assessment of natural sources of atmospheric trace metals, *Nature*, *338*, 47-49, 1989.

Nriagu, J.O., and C.I. Davidson, Toxic metals in the atmosphere, in *Advances in environmental science and technology*, Wiley, New York, 1986.

Patterson, C.C., and D.M. Settle, The reduction of orders of magnitude errors in lead analysis of biological materials and natural waters by evaluating and controlling the extent and sources of industrial lead contamination introduced during sampling, collecting,

handling and analysis, *National Bureau of Standards, Special Publication*, *422*, 321-351, 1976.

Pehkonen, S.O., Y. Erel, and M.R. Hoffmann, Simultaneous spectrophotometric measurement of Fe(II) and Fe(III) in atmospheric water, *Environ. Sci. & Technol.*, *26* (9), 1731-1736, 1992.

Pick-Kaplan, M., and J. Rabani, Pulse radiolysis studies of aqueous $Mn(ClO_4)_2$ solutions, *J. Phys. Chem.*, *80*, 1840-1843, 1976.

Price, N.M., B.A. Ahner, and F.M.M. Morel, The equatorial Pacific Ocean - grazer controlled phytoplankton populations in an iron limited ecosystem, *Limnol. & Ocean.*, *39* (3), 520-534, 1994.

Puxbaum, H., Metal compounds in the atmosphere, in *Metals and their compounds in the environment*, edited by E. Merian, pp. 257-286, VCH Publishers, 1991.

Rao, X., and J.L. Collett, Behavior of S(IV) and formaldehyde in a chemically heterogeneous cloud, *Environ. Sci. & Technol.*, *29* (4), 1023-1031, 1995.

Raphael, M.W., Kinetics of the oxidation of Chromium(III) by Manganese(III) in sulfuric-acid media, *Chem. Scr.*, *20* (4), 171-173, 1982.

Rush, J.D., and B.H.J. Bielski, Pulse radiolysis studies of the reactions of HO2/O2- with ferric ions and its implication on the occurrence of the Haber-Weiss reaction, *J. Phys. Chem.*, *89*, 5062-5066, 1985.

Sedlak, D.L., and J. Hoigné, The role of copper and oxalate in the redox cycling of iron in atmospheric waters, *Atmos. Environ.*, *27*, 2173-2185, 1993.

Sedlak, D.L., and J. Hoigné, Oxidation of S(IV) in atmospheric water by photooxidants and iron in the presence of copper, *Environ. Sci. & Technol.*, *28*, 1898-1906, 1994.

Seigneur, C., and E. Constantinou, Chemical kinetic mechanism for atmospheric chromium, *Environ. Sci. Technol.*, *29*, 222-231, 1995.

Sharma, V.K., and F.J. Millero, The oxidation of Copper(I) in seawater, *Environ. Sci. Technol.*, *22*, 768-771, 1988.

Siefert, R.L., S.O. Pehkonen, Y. Erel, and M.R. Hoffmann, Iron photochemistry of aqueous suspensions of ambient aerosol with added organic acids, *Geochim. et Cosmochim. Acta*, *58* (15), 3271-3279, 1994.

Smith, F., and D.H. Wilkins, New colorimetric reagent specific for copper, *Analyt. Chem.*, *25*, 510-511, 1953.

Smith, R.M., and A.E. Martell, *Critical Stability Constants*, Plenum Press, New York, 1974.

Smith, R.V., and P.W. Erhardt, Nash determination for formaldehyde in the presence of bisulfite, *Anal. Chem.*, *47* (14), 2462-2464, 1975.

Solis, J.S., G. Hefter, and P.M. May, Chemical speciation in the copper(I)-ammonia-chloride system, *Australian J. of Chem.*, *48* (7), 1283-1292, 1995.

Spokes, L.J., T.D. Jickells, and B. Lim, Solubilisation of aerosol trace metals by cloud processing: A laboratory study, *Geochim. et Cosmochim. Acta*, *58* (15), 3281-3287, 1994.

Spratt, H.G., E.C. Siekmann, and R.E. Hodson, Microbial manganese oxidation in saltmarsh surface sediments using a leuco crystal violet manganese oxide detection technique, *Estuarine, Coastal & Shelf Sci.*, *38*, 91-112, 1994.

Stookey, L.L., Ferrozine- a new spectrophotometric reagent for iron, *Anal. Chem.*, *42* (7), 119-781, 1970.

Taylor, S.R., and S.M. McLennan, *The continental crust: its composition and evolution*, 9-52 pp., Blackwell Scientific Publications, London, 1985.

von Piechowski, M., Der Einfluss von Kupferionen auf die Redoxchemie des Atmosphärischen Wassers, Ph.D. thesis, Swiss Federal Institute of Technology, Zürich, Switzerland, 1991.

Wells, M.L., N.M. Price, and K.W. Bruland, Iron limitation and the cyanobacterium synechococcus in equatorial pacific waters, *Limnol. Ocean.*, *39* (6), 1481-1486, 1994.

Wells, M.L., N.M. Price, and K.W. Bruland, Iron chemistry in seawater and its relationship to phytoplankton: a workshop report, *Marine Chem.*, *48*, 157-182, 1995.

Weschler, C.J., M.L. Mandich, and T.E. Graedel, Speciation, photosensitivity, and reactions of transition metal ions in atmospheric droplets, *J. Geophys. Res.*, *91*, 5189-5204, 1986.

Westall, J.C., J.L. Zachary, and F.M.M. Morel, MINEQL, a computer program for the calculation of chemical equilibrium composition of aqueous solutions, Dept. of Civil Engineering, Massachusetts Institute of Technology, 1976.

Wiersma, G.B., and C.I. Davidson, Trace metals in the atmosphere of remote areas, in *Toxic trace metals in the atmosphere*, edited by J.O. Nriagu, and C.I. Davidson, pp. 201-266, Wiley, New York, 1986.

Xue, H.B., M.D.S. Goncalves, M. Reutlinger, L. Sigg, and W. Stumm, Copper(I) in fogwater - determination and interactions with sulfite, *Environ. Sci. & Technol.*, *25* (10), 1716-1722, 1991a.

Xue, H.B., M.D.S. Goncalves, M. Reutlinger, L. Sigg, and W. Stumm, Copper(I) in fogwater: determination and interactions with sulfite, *Environ. Sci. & Technol.*, *25* (10), 1716-1722, 1991b.

Young, T.R., and J.P. Boris, A numerical technique for solving stiff ordinary differential equations associated with the chemical kinetics of reactive-flow problems, *J. Phys. Chem.*, *81*, 2424-2427, 1977.

Zhu, X.R., J.M. Prospero, D.L. Savoie, F.J. Millero, R.G. Zika, and E.S. Saltzman, Photoreduction of iron(III) in marine mineral aerosol solutions, *J. Geophys. Res. A.*, *98* (ND5), 9039-9046, 1993.

Zhuang, G., Z. Yi, R.A. Duce, and P.R. Brown, Link between iron and sulfur cycles suggested by detection of Fe(II) in remote marine aerosols, *Nature*, *355* (6360), 537-539, 1992.

Zoller, W.H., R.A. Gordon, and R.A. Duce, Atmospheric concentrations and sources of trace metals at the South Pole, *Science*, *183*, 198-200, 1974.

Zuo, Y., and J. Hoigné, Formation of hydrogen peroxide and depletion of oxalic acid in atmospheric water by photolysis of iron(III)-oxalato compounds, *Environ. Sci. Technol.*, *26* (5), 1014-1022, 1992.

Zuo, Y.G., and J. Hoigné, Photochemical decomposition of oxalic, glyoxalic and pyruvic-acid catalyzed by iron in atmospheric waters., *Atmos. Environ.*, *28* (7), 1231-1239, 1994.

FIGURE CAPTIONS

FIGURE 1 Speciation calculations for Fe(III), Cu(II) and Oxalate.

FIGURE 2 Example of kinetic model results for Fe, Cu and Mn.

TABLE 1. Fogwater and cloudwater sample collection information.

Sample Name[a]	Collection Date	Start Time (local)	Duration (min)	Weight (g)	LWC[b] (g/m^3)	pH	Filtered Aliquot (g)	Sunlight[c]
WM 93-1	16-Jun-93	16:50	10	NA[d]	0.23	3.62	0	day
WM 93-2	16-Jun-93	17:00	12	NA	0.23	3.90	0	day
WM 93-3	16-Jun-93	17:12	9	NA	NA	3.75	0	day
WM 93-4	16-Jun-93	17:22	8	NA	NA	3.76	0	day
WM 93-5	16-Jun-93	17:35	5	NA	NA	3.95	0	day
WM 93-6	16-Jun-93	17:50	15	NA	NA	4.55	0	day
WM 93-7	16-Jun-93	18:05	18	NA	NA	4.46	0	day
WM 93-8	16-Jun-93	18:30	20	NA	NA	4.45	0	day
WM 93-9	16-Jun-93	18:55	50	NA	NA	4.74	0	day
WM 93-10	16-Jun-93	20:00	18	NA	NA	4.56	0	day
WM 93-11	16-Jun-93	20:18	17	NA	NA	4.56	0	day
WM 93-12	16-Jun-93	20:35	20	NA	NA	4.62	0	day
WM 93-13	16-Jun-93	20:55	10	NA	NA	4.66	0	night
WM 93-14	16-Jun-93	21:10	20	NA	NA	NA	0	night
WM 93-15	18-Jun-93	06:45	30	NA	0.83	3.11	0	day
WM 93-16	18-Jun-93	07:35	17	NA	0.75	3.15	0	day
WM 93-17	18-Jun-93	08:07	33	NA	0.65	3.13	0	day
WM 93-18	18-Jun-93	08:52	20	NA	0.59	3.15	0	day
WM 93-19	18-Jun-93	09:25	45	NA	0.59	3.30	0	day
WM 93-20	18-Jun-93	10:55	40	NA	0.57	2.92	0	day
WM 93-21	18-Jun-93	12:10	15	NA	0.46	3.21	0	day
WM 93-22	18-Jun-93	18:47	5	NA	NA	4.01	0	day
WM 93-23	18-Jun-93	19:04	20	NA	NA	4.13	0	day
WM 93-24	18-Jun-93	19:58	27	NA	NA	NA	0	day
WM 93-25	18-Jun-93	22:14	37	NA	NA	4.19	0	night
SP 94-1	12-May-94	NA	NA	NA	NA	3.20	27	night
SP 94-2	15-May-94	NA	NA	NA	NA	4.30	13	night
SP 94-3	15-May-94	NA	NA	NA	NA	4.20	19	night
SP 94-4	15-May-94	NA	NA	NA	NA	4.20	21	night
SP 94-5	15-May-94	NA	NA	NA	NA	4.20	40	night
SP 94-6	15-May-94	NA	NA	NA	NA	4.10	0	night
WM 94-1	24-Jun-94	21:48	62	118	NA	3.80	19	night
WM 94-2	24-Jun-94	22:52	38	75.4	NA	3.75	0	night
WM 94-3	25-Jun-94	11:40	60	313	NA	3.70	0	day
WM 94-4	25-Jun-94	12:40	35	132	NA	3.64	17	day
WM 94-5	25-Jun-94	13:15	48	114	NA	3.55	0	day
WM 94-6	25-Jun-94	14:03	35	135	NA	3.73	29	day
WM 94-7	25-Jun-94	14:39	21	30	NA	NA	0	day
WM 94-8	25-Jun-94	17:00	80	165	NA	4.08	0	day
WM 94-9	25-Jun-94	19:16	130	340	NA	NA	0	day
WM 94-10	25-Jun-94	21:26	66	90	NA	3.71	0	night
WM 94-11	27-Jun-94	16:32	60	130	NA	3.35	0	day
WM 94-12	27-Jun-94	17:32	48	130	NA	3.55	31	day
WM 94-13	27-Jun-94	18:20	37	130	NA	3.58	0	day
WM 94-14	27-Jun-94	19:02	43	130	NA	NA	0	day

TABLE 1 (cont.). Fogwater and cloudwater sample collection information.

Sample Name[a]	Collection Date	Start Time (local)	Duration (min)	Weight (g)	LWC[b] (g/m^3)	pH	Filtered Aliquot (g)	Sunlight[c]
WM 94-15	28-Jun-94	04:13	28	130	NA	5.26	0	night
WM 94-16	28-Jun-94	04:41	44	130	NA	4.94	0	night
WM 94-17	28-Jun-94	05:25	31	130	NA	4.70	0	day
WM 94-18	28-Jun-94	05:56	48	130	NA	4.35	0	day
WM 94-19	28-Jun-94	06:44	27	130	NA	4.30	0	day
WM 94-20	28-Jun-94	07:11	28	130	NA	5.25	0	day
WM 94-21	28-Jun-94	07:46	101	500	NA	5.37	0	day
WM 94-22	28-Jun-94	09:27	28	130	NA	5.21	0	day
WM 94-23	28-Jun-94	09:55	26	130	NA	4:68	0	day
WM 94-24	28-Jun-94	12:34	37	130	NA	4.61	0	day
WM 94-25	28-Jun-94	13:11	35	130	NA	4.66	0	day
WM 94-26	29-Jun-94	14:00	120	130	NA	3.15	10	day
WM 94-27	1-Jul-94	09:43	26	130	NA	4.30	0	day
WM 94-28	1-Jul-94	10:12	32	130	NA	4.30	0	day
WM 94-29	1-Jul-94	12:25	189	116	NA	4.03	0	day
BK 95-1	1-Feb-95	00:00	65	114	0.09	6.87	0	night
BK 95-2	1-Feb-95	01:05	70	133	0.09	6.29	0	night
BK 95-3	1-Feb-95	02:15	85	133	0.08	6.34	15	night
BK 95-4	1-Feb-95	03:40	85	133	0.08	5.39	20	night
BK 95-5	1-Feb-95	05:05	110	130	0.06	4.93	0	night

[a] The first two letters in the sample ID are used to refer to the site location: "WM" refers to Whiteface Mountain, NY, "SP" refers to San Pedro, CA and "BK" refers to Bakersfield, CA.. [b] Liquid water content (LWC). [c] "day" refers to samples collected between sunrise and sunset. [d] Not available.

TABLE 2. Total elemental concentrations in the cloudwater and fogwater samples.

Sample*	Fe_{total} nM	Cu_{total} nM	Mn_{total} nM	Cr_{total} nM	Al_{total} nM	K_{total} μM	Ca_{total} μM	Na_{total} μM	Mg_{total} μM
WM 93-1	951	95	27	28	970	< 0.3	0.75	< 0.5	0.78
WM 93-2	2351	91	42	54	1011	< 0.3	< 0.3	< 0.5	1.64
WM 93-3	1001	54	51	48	551	< 0.3	0.44	< 0.5	1.59
WM 93-4	1696	51	64	49	549	< 0.3	< 0.3	< 0.5	1.89
WM 93-5	1611	40	55	47	439	< 0.3	< 0.3	< 0.5	1.86
WM 93-6	36	16	27	22	181	< 0.3	0.42	< 0.5	0.76
WM 93-7	1617	35	32	44	365	< 0.3	0.48	< 0.5	1.64
WM 93-8	1894	45	48	48	618	< 0.3	2.65	< 0.5	2.50
WM 93-9	2109	60	87	25	1002	1.8	7.85	< 0.5	4.20
WM 93-10	1877	53	125	47	1110	6.3	12.07	< 0.5	5.59
WM 93-11	1798	44	93	49	875	3.1	9.35	< 0.5	4.58
WM 93-12	6989	138	263	53	6866	13.8	20.23	< 0.5	19.34
WM 93-13	1792	30	88	42	831	3.2	9.06	< 0.5	4.61
WM 93-14	1532	24	79	23	534	2.5	10.38	< 0.5	3.96
WM 93-15	1640	84	232	22	2062	3.6	21.35	< 0.5	7.78
WM 93-16	1990	65	195	19	2756	2.6	16.38	< 0.5	6.51
WM 93-17	2221	96	261	21	3227	4.9	23.04	< 0.5	8.46
WM 93-18	2277	77	254	28	3909	6.0	23.81	< 0.5	8.66
WM 93-19	2950	56	171	21	4190	3.0	12.87	< 0.5	5.23
WM 93-20	3826	109	544	32	5388	12.1	86.35	< 0.5	27.19
WM 93-21	2374	48	236	21	3462	2.4	35.52	< 0.5	13.18
WM 93-22	< 20	10	9	13	99	< 0.3	< 0.3	< 0.5	0.10
WM 93-23	< 20	< 2	7	6	58	< 0.3	< 0.3	< 0.5	0.04
WM 93-24	< 20	< 2	3	5	50	< 0.3	< 0.3	< 0.5	0.02
WM 93-25	< 20	3	5	4	51	< 0.3	< 0.3	< 0.5	0.03
SP 94-1	4900	210	240	43	8200	NA	NA	NA	NA
SP 94-1f	1250	150	170	22	2630	NA	NA	NA	NA
SP 94-2	NA	NA	NA	NA	NA	NA	NA	NA	NA
SP 94-2f	210	47	42	14	1020	NA	NA	NA	NA
SP 94-3	2000	120	90	34	3800	NA	NA	NA	NA
SP 94-3f	230	60	44	23	1050	NA	NA	NA	NA
SP 94-4	720	74	57	20	1380	NA	NA	NA	NA
SP 94-4f	290	70	50	22	790	NA	NA	NA	NA
SP 94-5	580	51	54	15	1200	NA	NA	NA	NA
SP 94-5f	240	52	47	2	780	NA	NA	NA	NA
SP 94-6	1440	81	86	18	2300	NA	NA	NA	NA
WM 94-1	560	371	73	32	15567	2.3	0.92	< 0.5	0.88
WM 94-1f	45	48	13	10	537	2.3	0.75	< 0.5	0.37
WM 94-2	621	34	25	29	1386	2.3	1.57	< 0.5	0.98
WM 94-3	177	45	23	7	2643	3.0	1.58	0.9	0.66
WM 94-4	1826	127	82	47	12231	5.3	1.77	0.9	3.62
WM 94-4f	41	36	14	7	634	2.3	1.05	< 0.5	0.35
WM 94-5	1291	91	34	29	6079	4.9	2.07	1.9	1.34
WM 94-6	1277	72	52	7	4559	4.8	2.10	1.3	3.33

TABLE 2 (cont.). Total elemental concentrations in the cloudwater and fogwater samples.

Sample*	Fe_{total} nM	Cu_{total} nM	Mn_{total} nM	Cr_{total} nM	Al_{total} nM	K_{total} μM	Ca_{total} μM	Na_{total} μM	Mg_{total} μM
WM 94-6f	30	24	13	13	434	2.0	0.65	0.7	0.32
WM 94-7	NA	NA	NA	NA	NA	NA	NA	NA	NA
WM 94-8	86	20	17	< 4	649	2.6	0.66	0.8	0.43
WM 94-9	34	28	19	9	1001	3.2	1.30	0.9	0.44
WM 94-10	401	32	57	6	2624	5.3	2.97	0.6	1.05
WM 94-11	3527	93	186	< 4	7784	20.5	5.61	22.2	7.16
WM 94-12	6929	159	233	37	12305	20.7	9.91	22.8	9.42
WM 94-12f	510	66	136	31	1668	11.8	8.13	18.4	4.24
WM 94-13	2919	59	164	33	6079	12.5	9.13	23.4	7.12
WM 94-14	NA	NA	NA	NA	NA	NA	NA	NA	NA
WM 94-15	385	31	21	< 4	2198	1.4	1.00	0.7	0.54
WM 94-16	251	19	17	21	656	1.8	0.67	1.9	0.43
WM 94-17	NA	NA	NA	NA	NA	NA	NA	NA	NA
WM 94-18	NA	NA	NA	NA	NA	NA	NA	NA	NA
WM 94-19	85	9	5	13	254	< 0.3	< 0.3	< 0.5	0.12
WM 94-20	56	7	4	14	486	< 0.3	< 0.3	< 0.5	0.09
WM 94-21	NA	NA	NA	NA	NA	NA	NA	NA	NA
WM 94-22	NA	NA	NA	NA	NA	NA	NA	NA	NA
WM 94-23	NA	NA	NA	NA	NA	NA	NA	NA	NA
WM 94-24	NA	NA	NA	NA	NA	NA	NA	NA	NA
WM 94-25	NA	NA	NA	NA	NA	NA	NA	NA	NA
WM 94-26	3599	168	152	56	9192	34.8	9.43	> 40	4.20
WM 94-26f	686	200	116	38	2713	13.3	7.24	3.1	1.70
WM 94-27	705	107	20	24	1672	1.7	1.05	< 0.5	0.62
WM 94-28	392	73	18	28	1100	8.7	1.40	4.5	0.55
WM 94-29	958	72	39	27	2261	9.3	1.84	1.7	1.05
BK 95-1	624	22	1	23	326	2.7	2.37	1.4	0.49
BK 95-2	507	20	28	17	226	3.0	3.14	1.3	0.56
BK 95-3	476	11	21	16	101	2.7	1.85	< 0.5	0.31
BK 95-3f	271	8	18	7	72	2.5	1.95	0.6	0.29
BK 95-4	644	24	27	15	143	2.7	2.11	< 0.5	0.35
BK 95-4f	342	15	20	12	55	2.3	1.88	< 0.5	0.29
BK 95-5	533	69	34	22	239	4.0	2.73	1.2	0.49

* a letter f next to the sample name refers to the filtered aliquot of the sample.

TABLE 3. Concentration ranges of total metal concentrations and average concentrations for samples collected in this study and previous studies.

Location	$[Metal]_{total}$ nM	Average $[Metal]_{total}$ nM	Reference
	[Fe]	[Fe]	
Los Angeles, CA		26,000	Waldman *et al.* , 1982
Pasadena, CA	1,600 to 37,500		Munger *et al* ., 1983
Lennox, CA	6,360 to 420,000		Munger *et al* ., 1983
San Pedro Hill, CA	580 to 4900	1930	this study
San Pedro Hill, CA	900 to 20,600	5030	Erel *et al.* , 1993
Henninger Flats, CA	1,500 to 26,500	12,700	Erel *et al.* , 1993
Bakersfield, CA	480 to 640	560	this study
San Nicholas Island, CA		7700	Jacob *et al.* , 1985
Whiteface Mtn., NY	< 20 to 7000	1360	this study
Whiteface Mtn, NY	320 to 950	560	Khwaja *et al.* , 1995
Zürich, Switzerland	50,000 to 200,000		Behra & Sigg, 1990
	[Cu]	[Cu]	
San Pedro Hill, CA	51 to 210	110	this study
Bakersfield, CA	11 to 69	30	this study
Pasadena, CA	16 to 2,200		Munger *et al* ., 1983
Lennox, CA	140 to		Munger *et al* ., 1983
Whiteface Mtn., NY	< 30 to 121	71	Khwaja *et al.* , 1995
Whiteface Mtn., NY	< 2 to 371	65	this study
Duebendorf, Switzerland	300 to 10,600	1,900	Johnson *et al.* , 1987
Zürich, Switzerland	130 to 13,500	1,280	Xue *et al.* , 1991
	[Mn]	[Mn]	
San Pedro Hill, CA	54 to 240	105	this study
Bakersfield, CA	1 to 34	22	this study
Pasadena, CA	330 to 2910		Munger *et al* ., 1983
Lennox, CA	350 to 14,700		Munger *et al* ., 1983
Whiteface Mtn., NY	3 to 544	104	this study
Whiteface Mtn., NY	100 to 530	240	Khwaja *et al.* , 1995
	[Cr]	[Cr]	
San Pedro Hill, CA	15 to 43	30	this study
Bakersfield, CA	15 to 23	19	this study
Whiteface Mtn., NY	< 4 to 56	26	this study

TABLE 4. Percentage of each element associated with the aqueous phase.

Sample	Fe %	Cu %	Mn %	Cr %	Al %	K %	Ca %	Na %	Mg %
SP 94-1	26 ± 4	71 ± 10	71 ± 10	51 ± 7	32 ± 5	NA	NA	NA	NA
SP 94-3	11 ± 2	50 ± 7	49 ± 7	68 ± 10	28 ± 4	NA	NA	NA	NA
SP 94-4	40 ± 6	95 ± 13	88 ± 12	110 ± 16	57 ± 8	NA	NA	NA	NA
SP 94-5	41 ± 6	102 ± 14	87 ± 12	13 ± 2	65 ± 9	NA	NA	NA	NA
WM 94-1	8 ± 1	13 ± 2	18 ± 3	30 ± 4	3 ± 1	101 ± 14	81 ± 11	NA	42 ± 6
WM 94-4	2 ± 1	28 ± 4	18 ± 2	15 ± 2	5 ± 1	43 ± 6	59 ± 8	< 46	10 ± 1
WM 94-6	2 ± 1	33 ± 5	25 ± 3	100 ± 55	10 ± 1	41 ± 6	31 ± 4	50 ± 7	10 ± 1
WM 94-12	7 ± 1	41 ± 6	58 ± 8	84 ± 12	14 ± 2	57 ± 8	82 ± 12	81 ± 11	45 ± 6
WM 94-26	19 ± 3	119 ± 17	76 ± 11	67 ± 10	30 ± 4	38 ± 5	77 ± 11	< 8	40 ± 6
BK 95-3	57 ± 8	73 ± 10	86 ± 12	44 ± 6	71 ± 10	93 ± 13	105 ± 15	NA	93 ± 13
BK 95-4	53 ± 8	62 ± 10	74 ± 10	80 ± 11	38 ± 5	85 ± 12	89 ± 13	NA	81 ± 11

Table 5. Trace metal redox states in cloudwater and fogwater samples.

Sample	Light	Fe(II) nM	F(II)/Fe_{total} %	Cu(I) nM	Cu(I)/Cu_{total} %	Mn(IV) nM	Mn(IV)/Mn_{total} %	Cr(III) nM	Cr(III)/Cr_{total} %
WM 93-1	day	640	67%	NA	NA	NA	NA	NA	NA
WM 93-2	day	430	18%	40	44%	< 5.0	< 12%	NA	NA
WM 93-3	day	180	18%	NA	NA	NA	NA	NA	NA
WM 93-4	day	< 60	< 4%	NA	NA	< 5.0	< 8%	NA	NA
WM 93-8	day	< 60	< 3%	< 30	< 67%	NA	NA	NA	NA
WM 93-9	day	NA	NA	NA	NA	< 5.0	< 6%	NA	NA
WM 93-11	day	< 60	< 3%	< 30	< 68%	NA	NA	NA	NA
WM 93-12	day	NA	NA	< 30	< 22%	60	23%	NA	NA
WM 93-13	night	< 60	< 3%	NA	NA	< 5.0	< 6%	NA	NA
WM 93-15	day	1250	76%	NA	NA	< 5.0	< 2%	NA	NA
WM 93-16	day	40	2%	NA	NA	NA	NA	13	69%
WM 93-17	day	210	9%	< 30	< 31%	NA	NA	14	67%
WM 93-18	day	710	31%	NA	NA	NA	NA	NA	NA
WM 93-19	day	< 60	< 2%	< 30	< 54%	< 5.0	< 3%	9	44%
WM 93-20	day	1820	48%	92	84%	105	19%	NA	NA
WM 93-21	day	960	40%	NA	NA	NA	NA	NA	NA
WM 93-22	day	< 60	NA	< 30	< 100%	NA	NA	NA	NA
SP 94-2	night	< 60	NA	NA	NA	NA	NA	NA	NA
SP 94-3	night	< 60	< 3%	< 30	< 25%	NA	NA	NA	NA
SP 94-4	night	< 60	< 8%	< 30	< 41%	NA	NA	NA	NA
SP 94-5	night	< 60	< 10%	< 30	< 59%	NA	NA	NA	NA
SP 94-6	night	NA	NA	< 30	< 37%	NA	NA	NA	NA
WM 94-1	night	< 60	< 11%	91	25%	13	18%	NA	NA
WM 94-2	night	NA	NA	55	164%	NA	NA	NA	NA
WM 94-3	day	< 60	< 34%	18	40%	< 5.0	< 21%	NA	NA
WM 94-4	day	NA	NA	60	47%	NA	NA	NA	NA
WM 94-5	day	NA	NA	52	57%	< 5.0	< 14 %	NA	NA
WM 94-6	day	< 60	< 5%	62	86%	NA	NA	NA	NA
WM 94-8	day	< 60	< 70%	21	107%	6	35%	NA	NA
WM 94-10	night	NA	NA	109	338%	6	11%	NA	NA
WM 94-11	day	500	14%	161	172%	26	14%	NA	NA
WM 94-12	day	500	7%	184	116%	31	13%	NA	NA
WM 94-13	day	570	20%	49	83%	31	19%	NA	NA
WM 94-15	night	< 60	< 16%	< 10	< 32%	< 5.0	< 24%	NA	NA
WM 94-16	night	< 60	< 24%	10	< 54%	6	35%	NA	NA
WM 94-19	day	< 60	< 71%	< 10	< 100%	7	137%	NA	NA
WM 94-20	day	< 60	< 108%	10	< 100%	6	150%	NA	NA
WM 94-22	day	< 60	NA	NA	NA	NA	NA	NA	NA
WM 94-23	day	< 60	NA	NA	NA	NA	NA	NA	NA
WM 94-24	day	< 60	NA	NA	NA	NA	NA	NA	NA
WM 94-25	day	< 60	NA	NA	NA	7	NA	NA	NA
WM 94-26	day	320	9%	NA	NA	NA	NA	NA	NA
WM 94-27	day	< 60	< 9%	29	27%	< 5.0	< 24%	NA	NA
WM 94-28	day	110	28%	49	67%	NA	NA	NA	NA
WM 94-29	day	< 60	< 6%	101	140%	NA	NA	NA	NA

Table 5 (cont.). Trace metal redox states in cloudwater and fogwater samples.

Sample	Light	Fe(II) nM	F(II)/Fe_{total} %	Cu(I) nM	Cu(I)/Cu_{total} %	Mn(IV) nM	Mn(IV)/Mn_{total} %	Cr(III) nM	Cr(III)/Cr_{total} %
BK 95-1	night	< 60	< 10%	NA	NA	18	1800%	NA	NA
BK 95-2	night	< 60	< 12%	NA	NA	25	89%	NA	NA
BK 95-3	night	< 60	< 13%	NA	NA	5	24%	NA	NA
BK 95-4	night	< 60	< 9%	NA	NA	40	148%	NA	NA
BK 95-5	night	< 60	< 11%	NA	NA	30	88%	NA	NA

* assuming all the oxidizing equivalents are due to Mn(IV).

TABLE 6. S(IV), peroxides, HCHO and anions concentrations in the cloudwater and fogwater samples.

Sample ID	S(IV)	Peroxides μM	HCHO μM	Acetate μM	Glycolate μM	Formate μM	Oxalate μM	Chloride μM	Nitrate μM	Sulfate μM
WM 93-1	NA*	NA	NA	NA	NA	NA	NA	NA	NA	NA
WM 93-2	NA	NA	NA	NA	NA	NA	NA	NA	NA	NA
WM 93-3	NA	NA	NA	< 1	NA	< 1	< 0.5	< 1	66.0	14.0
WM 93-4	NA	NA	NA	< 1	NA	4.0	< 0.5	< 1	58.0	11.0
WM 93-5	NA	18.4	NA	< 1	NA	< 1	< 0.5	6.5	61.0	10.0
WM 93-6	NA	19.1	NA	< 1	NA	< 1	< 0.5	< 1	17.0	23.0
WM 93-7	< 1	25.8	NA	< 1	NA	2.1	< 0.5	< 1	40.0	65.0
WM 93-8	< 1	35.1	12.0	< 1	NA	3.7	< 0.5	4.3	48.0	15.0
WM 93-9	< 1	37.9	11.0	< 1	NA	< 1	< 0.5	4.7	56.0	16.0
WM 93-10	< 1	40.2	9.5	2.2	NA	< 1	< 0.5	9.4	59.0	23.0
WM 93-11	< 1	32.9	8.3	< 1	NA	< 1	< 0.5	7.7	57.0	14.0
WM 93-12	< 1	30.6	8.1	< 1	NA	< 1	< 0.5	6.3	40.0	14.0
WM 93-13	< 1	25.2	9.1	< 1	NA	< 1	< 0.5	9.5	43.0	10.0
WM 93-14	NA	NA	NA	< 1	NA	< 1	< 0.5	4.7	48.0	12.0
WM 93-15	< 1	52.5	10.3	< 1	NA	5.3	< 0.5	40.0	432.0	637.0
WM 93-16	< 1	52.9	18.8	41.0	NA	6.0	< 0.5	37.0	524.0	773.0
WM 93-17	< 1	48.1	12.4	9.9	NA	7.0	< 0.5	33.0	506.0	646.0
WM 93-18	< 1	50.9	15.2	< 1	NA	5.6	< 0.5	35.0	374.0	492.0
WM 93-19	NA	54.5	16.9	< 1	NA	4.5	< 0.5	24.0	200.0	239.0
WM 93-20	< 1	46.1	17.4	13.0	NA	10.0	< 0.5	49.0	996.0	971.0
WM 93-21	NA	51.5	23.4	12.0	NA	7.2	< 0.5	32.0	401.0	431.0
WM 93-22	NA	0.2	22.1	< 1	NA	< 1	< 0.5	8.0	61.0	58.0
WM 93-23	NA	0.1	16.3	NA	NA	NA	NA	NA	NA	NA
WM 93-24	NA	NA	NA	NA	NA	NA	NA	NA	NA	NA
WM 93-25	NA	NA	NA	NA	NA	NA	NA	NA	NA	NA
SP 94-1	NA	NA	6.5	12.6	12.3	30.0	9.6	133.0	607.0	305.0
SP 94-2	NA	15.7	2.3	18.0	8.4	70.0	12.0	49.0	267.0	86.0
SP 94-3	NA	21.1	1.2	25.0	11.0	81.0	11.0	80.0	227.0	86.0
SP 94-4	NA	24.9	< 1	42.5	12.6	69.0	11.5	106.0	346.0	93.0
SP 94-5	NA	28.8	< 1	63.0	8.7	63.0	7.5	231.0	578.0	86.0
SP 94-6	NA	39.7	NA	26.0	17.0	58.0	9.6	373.0	276.0	118.0
WM 94-1	NA	23.2	NA	16.3	2.1	2.7	3.1	5.8	36.7	65.9
WM 94-2	NA	NA	NA	NA	NA	NA	NA	NA	NA	NA
WM 94-3	NA	36.1	11.1	18.6	5.8	21.1	7.0	9.6	69.3	97.4
WM 94-4	NA	43.4	11.9	22.3	6.8	25.1	6.1	10.0	84.6	109.9
WM 94-5	NA	47.4	13.1	24.0	8.2	28.0	7.2	11.7	99.2	132.7
WM 94-6	NA	45.6	11.5	18.5	5.0	22.3	4.9	9.6	52.4	72.7
WM 94-7	NA	46.1	11.1	12.7	2.9	18.2	4.0	6.4	41.6	49.1
WM 94-8	NA	48.4	12.4	12.2	2.7	16.2	2.2	5.3	29.2	41.9
WM 94-9	NA	NA	< 1	NA	NA	NA	NA	NA	NA	NA
WM 94-10	< 1	18.0	< 1	8.5	3.1	9.9	2.5	7.4	50.3	107.5
WM 94-11	2.2	43.6	3.7	34.4	18.8	37.5	19.7	30.8	269.7	395.7
WM 94-12	NA	43.3	3.8	33.0	13.9	30.8	14.4	35.5	222.3	260.5
WM 94-13	NA	43.3	3.7	27.2	10.9	29.6	7.2	31.4	175.2	177.8

TABLE 6 (cont.). S(IV), peroxides, HCHO and anions concentrations in the cloudwater and fogwater samples.

Sample ID	S(IV)	Peroxides	HCHO	Acetate	Glycolate	Formate	Oxalate	Chloride	Nitrate	Sulfate
		μM	μM	μM	μM	μM	μM	μM	μM	μM
WM 94-14	NA	NA	< 1	NA	NA	NA	NA	NA	NA	NA
WM 94-15	< 1	1.3	< 1	11.0	1.1	3.6	< 0.5	12.3	8.1	12.7
WM 94-16	NA	1.6	< 1	4.0	< 1	3.2	< 0.5	9.7	8.8	13.9
WM 94-17	NA	NA	NA	NA	NA	NA	NA	NA	NA	NA
WM 94-18	NA	NA	NA	NA	NA	NA	NA	NA	NA	NA
WM 94-19	NA	1.3	< 1	3.6	< 1	2.9	< 0.5	5.6	7.4	14.7
WM 94-20	NA	0.3	NA	3.9	< 1	2.0	< 0.5	3.2	6.6	6.6
WM 94-21	NA	NA	NA	NA	NA	NA	NA	NA	NA	NA
WM 94-22	NA	NA	NA	NA	NA	NA	NA	NA	NA	NA
WM 94-23	NA	NA	NA	NA	NA	NA	NA	NA	NA	NA
WM 94-24	NA	NA	NA	NA	NA	NA	NA	NA	NA	NA
WM 94-25	< 1	18.8	< 1	7.1	< 1	5.4	< 0.5	3.0	5.8	7.7
WM 94-26	NA	37.2	5.1	32.4	19.8	37.7	10.6	23.0	245.8	491.4
WM 94-27	NA	18.5	< 1	11.9	< 1	7.1	1.1	22.5	18.3	28.0
WM 94-28	NA	20.2	< 1	13.9	< 1	9.7	1.1	9.0	14.6	28.2
WM 94-29	NA	43.3	NA	10.7	4.1	13.5	2.9	6.8	33.6	59.8
BK 95-1	4.4	1.5	21.0	124.0	21.2	54.7	2.2	10.3	123.0	64.0
BK 95-2	11.1	5.0	17.8	71.7	17.5	50.7	3.0	11.4	60.1	80.0
BK 95-3	12.3	7.7	15.8	28.5	7.0	19.5	2.8	10.0	17.0	61.0
BK 95-4	27.6	7.6	16.6	24.0	6.8	24.0	3.0	7.4	9.4	76.0
BK 95-5	49.2	7.3	22.6	30.0	10.0	36.0	4.6	9.4	7.5	120.0

* not available.

TABLE 7. Enrichment factors (EF) for Fe, Cu, Mn and Cr.

	EF(Fe)		EF(Cu)		EF(Mn)		EF(Cr)	
Samples	Range	Avg	Range	Avg	Range	Avg	Range	Avg
All	0.03 to 3.77	0.95	1.43 to 269	46.6	0.14 to 9.71	2.87	1.29 to 87.3	25.8
WM	0.03 to 3.55	0.82	9.05 to 97.3	38.8	0.22 to 6.91	2.63	1.97 to 62.2	23.7
SP	0.39 to 0.50	0.44	1.43 to 50.0	29.5	1.11 to 2.10	1.65	9.94 to 18.9	14.8
BK	1.53 to 3.77	2.50	62.9 to 269	134	0.14 to 9.71	6.22	1.29 to 87.3	55.9

TABLE 8. Factor analysis statistics for Whiteface Mountain cloudwater samples.

PC	Eigenvalue	% Of Variance	Cumulative %
1	6.70	55.9	55.9
2	2.06	17.2	73.0
3	1.30	10.9	83.9

TABLE 9. Principal components (PCs) after factor analysis of Whiteface Mountain cloudwater samples.

	PC 1	PC 2	PC 3
pH	-0.722	-0.504	0.231
Fe_{total}	0.409	0.299	0.719
Cu_{total}	0.059	0.873	0.225
Mn_{total}	0.882	0.163	0.429
Cr_{total}	-0.144	0.231	0.796
Al_{total}	0.146	0.887	0.250
Ca_{total}	0.879	-0.149	0.310
Mg_{total}	0.774	0.043	0.575
Peroxides	0.586	0.410	0.111
Chloride	0.895	0.193	-0.016
Nitrate	0.979	0.075	0.033
Sulfate	0.944	0.188	-0.085

Table 10. Thermodynamic tableau for speciation calculation.

	Components											$\log_{10}ß$	Ref[a]
Species	H^+	$OH^\bullet$	$O2^{\bullet-}$	H_2O_2	Fe^{2+}	Fe^{3+}	Ox^{2-}	Cu^+	Cu^{2+}	Mn^{2+}	Mn^{3+}		
H^+	1											0.0	
OH^-	-1											-14.0	
$OH^\bullet$		1										0.0	
$HO_2^\bullet$	1		1									4.8	1
$O2^{\bullet-}$			1									0.0	
H_2O_2				1								0.0	
Fe^{2+}					1							0.0	
$Fe(OH)^+$	-1				1							-9.5	2
Fe^{3+}						1						0.0	
$Fe(OH)^{2+}$	-1					1						-2.2	2
$Fe(Ox)^+$						1	1					9.4	2
$Fe(Ox)_2^-$						1	2					16.2	2
$Fe(Ox)_3^{3+}$						1	3					20.4	2
Ox^{2-}							1					0.0	
HOx^-	1						1					5.5	2
H_2Ox	2						1					1.2	2
Cu^+								1				0.0	
Cu^{2+}									1			0.0	
Cu(Ox)							1		1			5.1	2
Mn^{2+}										1		0.0	
Mn^{3+}											1	0.0	
$Mn(OH)^{2+}$	-1										1	0.4	2

[a] References: (1) Bielski *et al.* (1985); (2) Smith and Martell (1974)

Table 11. Reactions and rate constants.

Number	Reactions	k	Reference[a]
R01)	$Fe(OH)^{2+} \rightarrow Fe^{2+} + OH^{\bullet}$	$6.3 \times 10^{-4}\ s^{-1}$	1
R02)	$Fe^{2+} + H_2O_2 \rightarrow Fe^{3+} + OH^- + OH^{\bullet}$	$6.3 \times 10^{+1}\ M\ s^{-1}$	2
R03)	$Fe(OH)^{+} + H_2O_2 \rightarrow Fe(OH)^{2+} + OH^- + OH^{\bullet}$	$5.9 \times 10^{+6}\ M\ s^{-1}$	3
R04)	$Fe(Ox)^{+} \rightarrow Fe^{2+} + O_2^{\bullet-}$	$5.8 \times 10^{-2}\ s^{-1}$	4
R05)	$Fe(Ox)_2^{-} \rightarrow Fe^{2+} + Ox^{2-} + O_2^{\bullet-}$	$5.8 \times 10^{-2}\ s^{-1}$	4
R06)	$Fe(Ox)_3^{-} \rightarrow Fe^{2+} + 2Ox^{2-} + O_2^{\bullet-}$	$5.8 \times 10^{-2}\ s^{-1}$	4
R07)	$Fe^{2+} + O_2^{\bullet-} \rightarrow Fe^{3+} + H_2O_2 + 2OH^-$	$1.0 \times 10^{+7}\ M\ s^{-1}$	5
R08)	$Fe^{2+} + HO_2^{\bullet} \rightarrow Fe^{3+} + H_2O_2 + OH^-$	$1.2 \times 10^{+6}\ M\ s^{-1}$	5
R09)	$Fe(OH)^{2+} + O_2^{\bullet-} \rightarrow Fe^{2+} + OH^-$	$1.5 \times 10^{+8}\ M\ s^{-1}$	5
R10)	$HO_2^{\bullet} + O_2^{\bullet-} \rightarrow H_2O_2 + OH^-$	$9.7 \times 10^{+7}\ M\ s^{-1}$	6
R11)	$2HO_2^{\bullet} \rightarrow H_2O_2$	$8.3 \times 10^{+5}\ M\ s^{-1}$	6
R12)	$Ox^{2-} + OH^{\bullet} \rightarrow HO_2^{\bullet} + 2OH^-$	$7.7 \times 10^{+6}\ M\ s^{-1}$	7
R13)	$HOx^{-} + OH^{\bullet} \rightarrow HO_2^{\bullet} + OH^-$	$4.7 \times 10^{+7}\ M\ s^{-1}$	7
R14)	$H_2Ox + OH^{\bullet} \rightarrow HO_2^{\bullet}$	$1.4 \times 10^{+6}\ M\ s^{-1}$	7
R15)	$Fe^{2+} + OH^{\bullet} \rightarrow Fe^{3+} + OH^-$	$4.3 \times 10^{+8}\ M\ s^{-1}$	8
R16)	$Fe(OH)^{+} + OH^{\bullet} \rightarrow Fe(OH)^{2+} + OH^-$	$4.3 \times 10^{+8}\ M\ s^{-1}$	8
R17)	$Fe^{2+} + O_3 \rightarrow Fe^{3+} + OH^{\bullet}$	$6.2 \times 10^{-4}\ s^{-1}$	9[b]
R18)	$Cu^{+} + O_2^{\bullet-} \rightarrow Cu^{2+} + H_2O_2 + 2OH^-$	$9.0 \times 10^{+9}\ M\ s^{-1}$	10
R19)	$Cu^{+} + HO_2^{\bullet} \rightarrow Cu^{2+} + H_2O_2 + OH^-$	$1.0 \times 10^{+9}\ M\ s^{-1}$	6
R20)	$Cu^{+} + H_2O_2 \rightarrow Cu^{2+} + OH^{\bullet} + OH^-$	$4.0 \times 10^{+5}\ M\ s^{-1}$	11
R21)	$Cu^{+} + O_2 \rightarrow Cu^{2+} + O_2^{\bullet-}$	$1.2 \times 10^{+1}\ s^{-1}$	12[c]
R22)	$Cu^{+} + Fe(OH)^{2+} \rightarrow Cu^{2+} + Fe^{2+} + OH^-$	$3.0 \times 10^{+7}\ M\ s^{-1}$	13
R23)	$Cu^{2+} + O_2^{\bullet-} \rightarrow Cu^{+} + O_2$	$8.0 \times 10^{+9}\ M\ s^{-1}$	10
R24)	$Cu^{2+} + HO_2^{\bullet} \rightarrow Cu^{+} + O_2 + H^+$	$5.0 \times 10^{+7}\ M\ s^{-1}$	6
R25)	$Mn^{2+} + OH^{\bullet} \rightarrow Mn^{3+} + OH^-$	$3.4 \times 10^{+7}\ M\ s^{-1}$	14
R26)	$Mn^{2+} + HO_2^{\bullet} \rightarrow Mn^{3+} + H_2O_2 + OH^-$	$6.0 \times 10^{+6}\ M\ s^{-1}$	15
R27)	$Mn^{2+} + O_2^{\bullet-} \rightarrow Mn^{3+} + H_2O_2 + 2OH^-$	$1.1 \times 10^{+8}\ M\ s^{-1}$	14
R28)	$Mn^{3+} + H_2O_2 \rightarrow Mn^{2+} + HO_2^{\bullet} + H^+$	$3.2 \times 10^{+4}\ M\ s^{-1}$	16
R29)	$Mn^{3+} + Fe^{2+} \rightarrow Mn^{2+} + Fe^{3+}$	$2.1 \times 10^{+4}\ M\ s^{-1}$	16

[a] References: (1) Faust and Hoigné (1990); (2) Hartwick (1957); (3) Millero and Sotolongo (1989); (4) Zuo and Hoigné (1992); (5) Rush and Bielski (1985); (6) Bielski *et al.* (1985); (7) Buxton *et al.* (1988); (8) Christensen and Sehested (1981); (9) Logager *et al.* (1992); (10) von Piechowski *et al.* (1992); (11) Moffett and Zika (1987); (12) Sharma and Millero (1988); (13) Sedlak and Hoigné (1993); (14) Pick-Kaplan and Rabani (1976); (15) Cabelli and Bielski (1984); (16) Davies (1969).1

[b] Pseudo-first order rate constant assuming $[O_3] = 7.5 \times 10^{-10}$ M.

[c] Pseudo-first order rate constant assuming $[O_2] = 2.6 \times 10^{-4}$ M.

Table 12. Results of kinetic model (all concentrations are Molar).

Run	Conditions[a]	Fe(II)	Fe(III)	Cu(I)	Cu(II)	Mn(II)	Mn(III)	$^{\bullet}OH$	HO_2 & $O_2^{\bullet-}$
BK 95-4	initial	3.4E-08	3.1E-07	7.5E-09	7.5E-09	1.0E-08	1.0E-08		
	day	2.7E-07	8.4E-08	9.4E-10	1.4E-08	1.9E-08	1.4E-09	2.4E-11	1.9E-10
	night	D[b]	3.4E-07	D	1.5E-08	2.0E-08	D	D	D
SP 94-4	initial	2.9E-08	2.6E-07	3.5E-08	3.5E-08	2.5E-08	2.5E-08		
	day	2.2E-07	6.8E-08	1.4E-09	6.9E-08	5.0E-08	5.1E-10	3.1E-11	2.6E-10
	night	D	2.9E-07	D	7.0E-08	5.0E-08	D	D	D
WM 94-12	initial	5.0E-07	5.0E-08	1.8E-07	1.8E-08	6.8E-08	6.8E-08		
	day	4.2E-07	1.3E-07	1.7E-09	2.0E-07	1.4E-07	7.0E-10	3.6E-11	5.1E-10
	night	D	5.5E-07	D	2.0E-07	1.4E-07	D	D	D

[a] conditions: 1) "initial" = initial conditions, 2) "day" = concentrations after a psuedo-equilibrium was reached with photochemical reactions, and 3) "night" = concentrations with the photochemical reaction rate constants set to zero to simulate night conditions.

[b] D = decreasing.

Figure 1

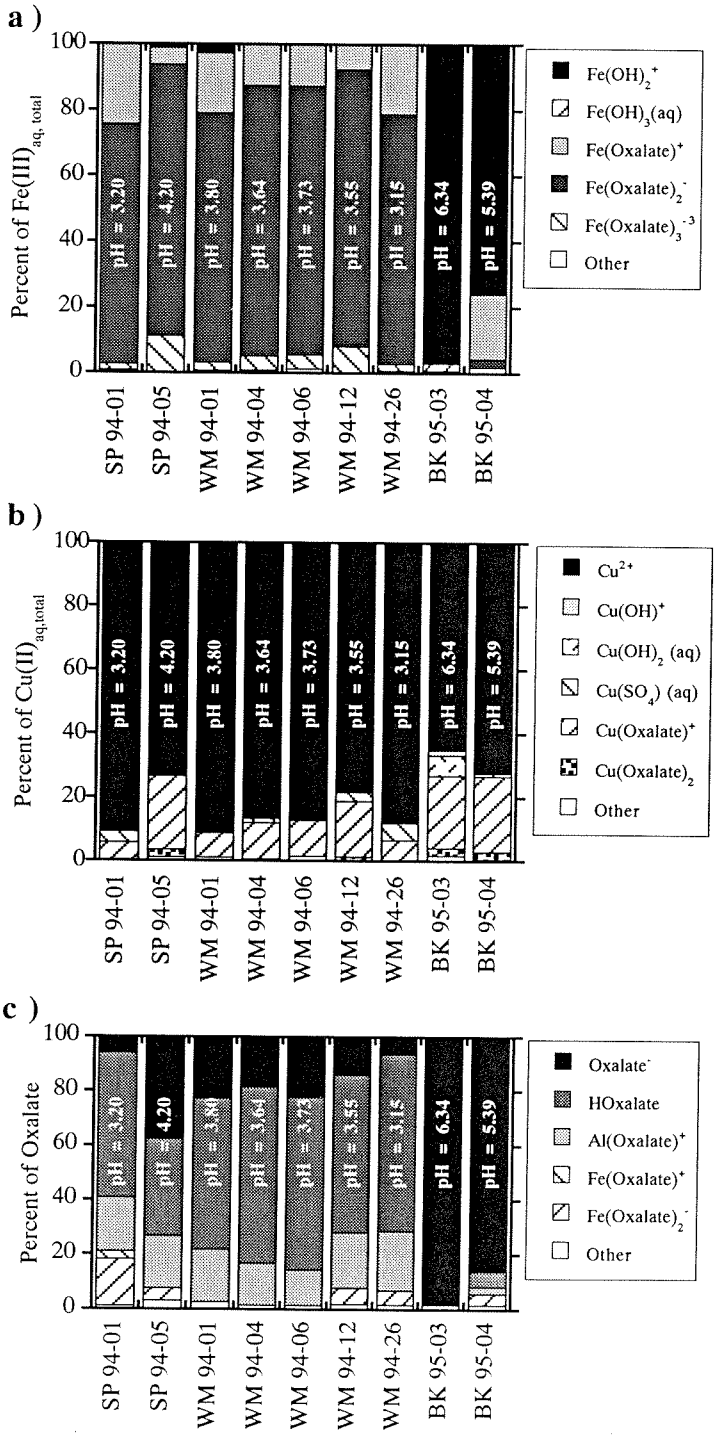
a)
Percent of Fe(III)aq, total
100
80
60
40
20
0
pH = 3.20
pH = 4.20
pH = 3.80
pH = 3.64
pH = 3.73
pH = 3.55
pH = 3.15
pH = 6.34
pH = 5.39
Fe(OH)2+
Fe(OH)3(aq)
Fe(Oxalate)+
Fe(Oxalate)2-
Fe(Oxalate)3-3
Other
SP 94-01
SP 94-05
WM 94-01
WM 94-04
WM 94-06
WM 94-12
WM 94-26
BK 95-03
BK 95-04
b)
Percent of Cu(II)aq,total
Cu2+
Cu(OH)+
Cu(OH)2 (aq)
Cu(SO4) (aq)
Cu(Oxalate)+
Cu(Oxalate)2
Other
c)
Percent of Oxalate
Oxalate-
HOxalate
Al(Oxalate)+
Fe(Oxalate)+
Fe(Oxalate)2-
Other

Figure 2

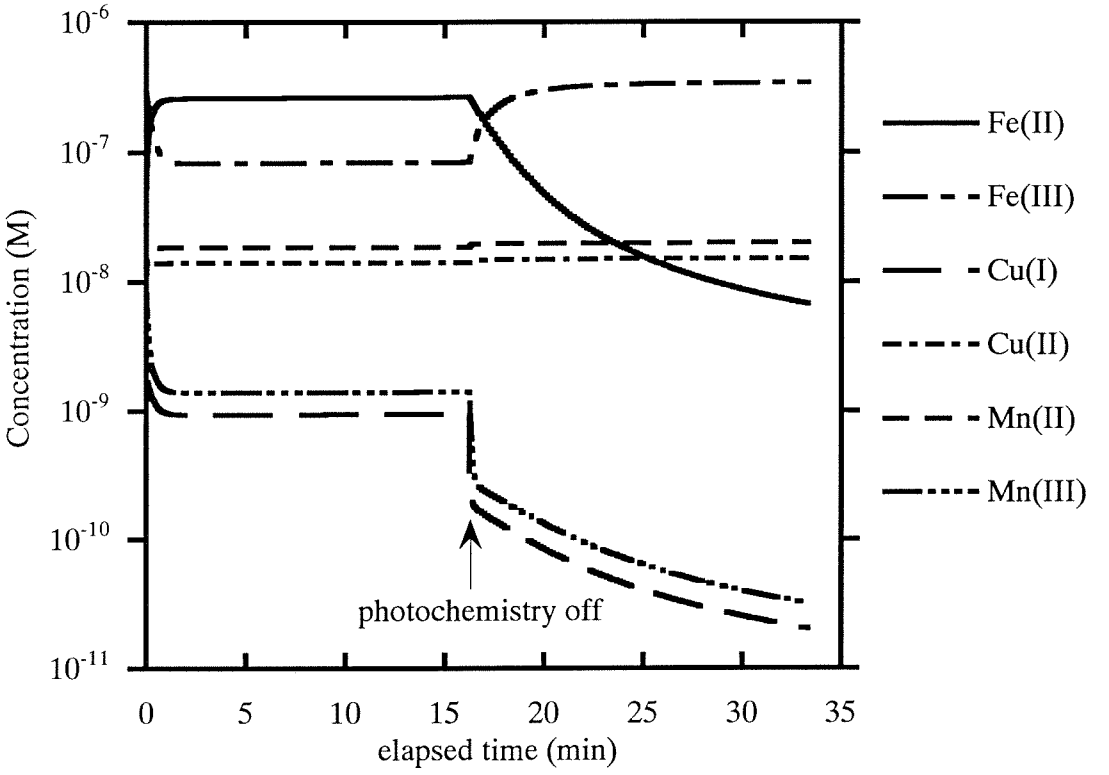
Concentration (M)
10-6
10-7
10-8
10-9
10-10
10-11
0
5
10
15
20
25
30
35
elapsed time (min)
photochemistry off
Fe(II)
Fe(III)
Cu(I)
Cu(II)
Mn(II)
Mn(III)

Chapter 5:

Chemical Characterization of Ambient Aerosol Collected During the Southwest-Monsoon and Inter-Monsoon Periods over the Arabian Sea: Labile Fe(II) and Other Trace Metals

[Ronald L. Siefert, Anne M. Johansen and Michael R. Hoffmann, submitted to *The Journal of Geophysical Research-Atmospheres*]

ABSTRACT

Ambient aerosol samples were collected during the inter-monsoon and southwest-monsoon periods on the Arabian Sea aboard the German research vessel Meteor (Meteor Cruise 32). Aerosol collection took place during the third (M32/3) and fifth (M32/5) legs of Meteor cruise 32. The third leg occurred during the "inter-monsoon" period of May and early June (i.e., before the southwest-monsoon and after the northeast-monsoon). The fifth leg occurred during the "Southwest-monsoon" period of mid-July to mid-August. A high-volume dichotomous virtual impactor (HVDVI) with an aerodynamic cutoff size of 3 μm was used to collect the fine and coarse aerosol fractions for metal analysis. A low volume collector (LVC) was used to collect aerosol samples for anion and cation analysis. The primary purpose of this study was to characterize the chemical composition of the ambient aerosol during the southwest-monsoon and inter-monsoon periods, including the measurement of labile ferrous iron (Fe(II)) in the fine and coarse fractions of ambient aerosol samples. Atmospheric deposition of Fe to certain regions of the oceans is an important nutrient source of Fe to the biota, and the ability of the biota to uptake Fe is dependent on the speciation of the Fe. Therefore, understanding the speciation of Fe in the atmosphere is critical to understanding the role of Fe as a nutrient source in surface ocean waters. The analysis for labile-Fe(II) was done immediately after sample collection to minimize any possible Fe redox reactions which might occur during sample storage. The analytical procedure involved filter extraction in a formate/formic acid buffered solution at pH 4.2 followed by analysis for soluble Fe(II). Metals, anions and cations measurements were done after the cruise. Total atmospheric aqueous labile-Fe(II) concentrations during M32/3 (inter-monsoon) were between 7.48 ng m^{-3} to < 0.089 ng m^{-3}. The aqueous-labile Fe(II) was predominantly in the "fine" fraction (< 3.0 μm), with the "fine" fraction of aqueous-labile-Fe(II) accounting for an average of 90% of the total aqueous-labile-Fe(II).

In contrast, during M32/5 (southwest-monsoon), the atmospheric aqueous-labile-Fe(II) concentrations were consistently below the detection limit (< 0.34 ng m^{-3} to < 0.089 ng m^{-3} depending on the volume of air sampled). Factor analysis revealed a significant source of Fe and Mn which was not associated with the main aeolian dust component or any typical anthropogenic metals (e.g. V, Pb). This component did not include any loadings of labile-Fe(II). Overall, Fe sources to the Arabian Sea were found to have a complicated behavior which was not explained by the aeolian dust loadings. The air mass back trajectories (5 day, three-dimensional) showed that air masses sampled during the southwest-monsoon had origins over the open Indian Ocean, and air masses sampled during the inter-monsoon had origins from southeast Africa, Saudi Arabian peninsula, and southern Asia.

INTRODUCTION

A knowledge of the detailed chemical speciation of metals in atmospheric aerosols is important to understanding their role in atmospheric chemistry (cloud chemistry), and also understanding their fate in surface ocean waters after deposition. Once deposited in the ocean, the metal speciation is critical to assessing the ability of marine biota to utilize atmospherically-derived trace elements as micronutrients [*Hudson and Morel*, 1990; *Hudson and Morel*, 1993; *Morel et al.*, 1991; *Wells et al.*, 1994; *Wells et al.*, 1995]. Recent studies have found Fe to be a rate-limiting nutrient to primary phytoplankton growth in certain regions of the open ocean [*Ditullio et al.*, 1993; *Kolber et al.*, 1994; *Martin et al.*, 1994; *Martin and Gordon*, 1988; *Price et al.*, 1994]; and the speciation of Fe is critical to the rate of Fe uptake by phytoplankton. Overall, a knowledge of the speciation of trace-metals in atmospheric deposition and the subsequent speciation changes upon introduction to marine waters is important to the assessment of the ability of marine biota to utilize atmospherically-derived elements for nutritional needs .

A knowledge of the detailed chemical speciation of metals in atmospheric aerosol is also important to understanding the speciation of these metals in cloudwater. "Dry" aerosol is the source of metals to cloudwater through processes such as condensation nucleation of cloud drops, or through differential impaction of an interstitial "dry" aerosol particles with cloud droplets. And the speciation of these metals in cloudwater has a direct effect on the reactivity of these metals in cloudwater. Several first-row transition metals are thought to play a major role in the redox cycle of sulfur and organic compounds in the troposphere, as well as controlling free radical production in clouds [*Conklin and Hoffmann*, 1988a; *Conklin and Hoffmann*, 1988b; *Faust and Hoffmann*, 1986; *Graedel et al.*, 1986; *Hoffmann and Jacob*, 1984; *Jacob et al.*, 1989; *Jacob and Hoffmann*, 1983; *Kotronarou and Sigg*, 1993; *Martin and Hill*, 1987; *Siefert et al.*, 1994; *Weschler et al.*, 1986; *Xue et al.*, 1991; *Zhuang et al.*, 1992b; *Zuo and Hoigné*, 1992]. Both Mn and Fe can catalyze the

oxidation of S(IV) by oxygen and together they have a synergistic effect [*Berglund and Elding*, 1995; *Berglund et al.*, 1993; *Conklin and Hoffmann*, 1988b; *Faust and Allen*, 1994; *Kraft and Van Eldik*, 1989a; *Kraft and Van Eldik*, 1989b; *Martin and Good*, 1991; *Martin et al.*, 1991]. Sedlak and Hoigné [*Sedlak and Hoigné*, 1993; *Sedlak and Hoigné*, 1994] have investigated the redox cycling of Fe and Cu in the presence of oxalate, and its implications on sulfur oxidation. The photoredox chemistry of Fe(III)-hydroxy and Fe(III)-oxalato complexes with the production of Fe(II) and oxidants ($OH^{\bullet}$, $HO_2^{\bullet}/O_2^{\bullet-}$) has also been studied [*Faust and Hoigné*, 1990; *Zuo and Hoigné*, 1992]. Zuo *et al.* [*Zuo and Hoigné*, 1994] have also looked at the photochemical decomposition of oxalic, glyoxalic and pyruvic-acid catalyzed by iron in atmospheric waters.

Modeling studies have also looked at transition metal redox chemistry in cloudwater [*Jacob et al.*, 1989; *Matthijsen et al.*, 1995; *Seigneur and Constantinou*, 1995]. Jacob *et al.* [*Jacob et al.*, 1989] modeled the accumulation of pollutants observed over Bakersfield, CA, and found iron to be important for the catalytic oxidation of S(IV), while Matthijsen *et al.* [*Matthijsen et al.*, 1995] used a cloud model to investigate the effect of iron and copper on tropospheric ozone. In addition, Fe(III) has been shown to be an important reductant of Cr(VI) to Cr(III) in cloudwater [*Seigneur and Constantinou*, 1995].

Many investigators have determined the occurrence, particle-size distribution and sources of transition metals in the atmosphere [*Galloway et al.*, 1982; *Lantzy and Mackenzie*, 1979; *Nriagu*, 1989; 1986; *Puxbaum*, 1991]. But only a few studies have investigated the speciation or reactivity of trace metals in cloudwater [*Behra and Sigg*, 1990; *Erel et al.*, 1993; *Kotronarou and Sigg*, 1993; *Xue et al.*, 1991] or in ambient aerosol [*Kopcewicz and Kopcewicz*, 1991; *Kopcewicz and Kopcewicz*, 1992; *Siefert et al.*, 1994; *Spokes et al.*, 1994; *Zhu et al.*, 1993; *Zhuang et al.*, 1992b]. Some of these studies have investigated the speciation of Fe in ambient aerosols by determining: 1) the concentration of Fe(II) [*Zhu et al.*, 1993; *Zhuang et al.*, 1992a], 2) the concentration of soluble Fe [*Spokes et al.*, 1994; *Zhu et al.*, 1993], and 3) the mineral form of the Fe through

Mossbauer spectroscopy [*Kopcewicz and Kopcewicz*, 1991; *Kopcewicz and Kopcewicz*, 1992].

Iron (Fe), which is one of the most abundant elements in the earth's crust, is present primarily as various Fe(II) and Fe(III) species [*Taylor and McLennan*, 1985]. Particulate Fe is transferred to the atmosphere by wind, volcanic activity, and through anthropogenic sources [*Cass and McRae*, 1983; *Gomes and Gillette*, 1993; *Seinfeld*, 1986]. Total Fe concentrations in tropospheric aerosols range from: 0.6 to 4160 ng/m^3 in remote areas, 55 to 14500 ng/m^3 in rural areas and 21 to 32820 ng/m^3 in urban areas [*Schroeder et al.*, 1987], and cloudwater concentrations range from 0.4 μM to 424 μM [*Behra and Sigg*, 1990; *Fuzzi et al.*, 1988; *Jacob et al.*, 1985; *Munger et al.*, 1983; *Waldman et al.*, 1982].

Previous studies have investigated the aerosol over the Indian Ocean. Chester *et al.* [*Chester et al.*, 1991] investigated the distributions of aerosol trace metals over the Indian Ocean. Samples were collected during the northeast monsoon period off the coast of Oman, and also in the Tropical Southern Indian Ocean where there were no large-scale up-wind continental sources. They found strong latitudinal variations in the chemical signatures of aerosols over the Indian Ocean. Savoie *et al.* [*Savoie et al.*, 1987] collected aerosol samples in the northwestern Indian Ocean and found significant variations in nitrate and NSS-sulfate concentrations which were a consequence of the variation in the impact of continentally derived aerosol.

The purpose of this study was to determine the chemical characterization of ambient aerosol in both the "fine" and "coarse" aerosol fractions during the "inter-monsoon" and "southwest monsoon" periods over the Arabian Sea. Specific attention was given to the speciation of Fe in the ambient aerosol by conducting labile-Fe(II) measurements immediately after sample collection during the cruise. Overall, the chemical characterization of the aerosol was used to investigate the sources and other factors which control both total-Fe and labile-Fe concentrations.

METHODS

Aerosol Collection

Ambient aerosol samples were collected using two collector types: 1) a high volume dichotomous virtual impactor (HVDVI) [*Solomon et al.*, 1983] and 2) a low volume collector (LVC). The HVDVI was used to collect fine and coarse ambient aerosol sample fractions ($D_{p,50}$ = 3.0 μm), which were used to analyze for total elemental composition and Fe(II). The HVDVI was constructed out of polycarbonate with nylon screws in order to minimize trace metal contamination, and had a total flow rate of 335 ± 15 l min^{-1}. The fine and coarse sample fractions were collected on two 90 millimeter diameter Teflon filters (Gelman Zefluor, 1 μm pore size). Two LVCs were used to collect aerosol samples for cation and anion analysis (each LVC had a flow rate of 27 l min^{-1}). Gelman Zefluor filters (47 mm in diameter) were also used with two LVCs which had a flow rate of 27 l min^{-1} through each collector. The LVC used a Nucleopore filter holder (constructed out of polycarbonate) placed in an inverted high density polyethylene 2 liter bottle. The aerosol collectors and were acid-cleaned before use by following similar procedures as outlined by *Patterson and Settle* [*Patterson and Settle*, 1976]. The collectors were also cleaned periodically in the field by wiping the surfaces clean with KimWipes wetted with Milli-Q UV water. Acid-cleaned polystyrene petri dishes were used to store the filters. The petri dishes were placed inside 2 plastic bags and stored in a refrigerator during the cruise. After the cruise the filters were sent back to Caltech (via air-freight) and stored in a freezer until analysis. Ultra-pure acids from Seastar Chemicals (Sidney, B.C., Canada), and 18.2 MΩ-cm Milli-Q UV water were used in the cleaning protocols.

A sector sampling system was used to simultaneously control both collectors. The system was configured to allow collection of ambient aerosol samples only when the relative wind direction was plus or minus ninety degrees off the bow. Usually, 24 hour

averaged aerosol samples were collected (the actual sampling duration varied depending on the ship's cruise track during the collection period).

Labile Fe(II) Measurements Performed Immediately After Sample Collection

A sequential aqueous extraction procedure measured several labile fractions of ferrous iron (Fe(II)) collected on the coarse and fine HVDVI filters. These measurements were performed immediately (within 1 hour) after sample collection in order to minimize any changes in Fe oxidation state due to possible redox reactions occurring during sample storage. Table 1 outlines the sequential extraction procedure. Three labile fractions of Fe were quantified using the procedure: 1) aqueous-labile-Fe(II) ($Fe_{aq,labile}$), 2) 5-minute Ferrozine-labile-Fe(II) ($Fe_{FZ,5min}$), and 3) 22 hour Ferrozine-labile-Fe(II) ($Fe_{total,labile}$). During the extraction procedure, aqueous Fe(II) concentrations were measured colorimetrically by complexation with ferrozine [*Carter*, 1971; *Stookey*, 1970] and absorption measurement using a portable spectrophotometer (Shimadzu UV-1201).

Analysis Performed After the Cruise

Total concentrations for 17 elements (Na, Mg, Al, K, Ca, Ti, V, Cr, Mn, Fe, Ni, Cu, Zn, Cd, Sb, Ba and Pb) were measured in both the coarse and fine fractions of the atmospheric aerosol (using the filters from the HVDVI). The method included a strong acid digestion of the aerosol samples, and subsequent analysis using inductively coupled plasma mass spectrometry (ICP-MS) with a Perkin Elmer-SCIEX Elan 5000 instrument. Table 2 outlines the strong acid digestion technique. Gallium was used as an internal standard for all samples. Analysis of multiple isotopes was done for Ca (isotopes 43 and 44), Ti (isotopes 47 and 48), Cr (isotopes 52 and 53) and Fe (isotopes 54, 57 and 58). These redundant measurements were made to check for possible interference problems, and

only the isotope with the best detection limit is shown in Table A-1 (supplemental material) for these elements.

Total atmospheric aerosol concentrations of organic anions (formate, acetate, glycolate, oxalate, succinate, malonate, maleate, fumarate, citrate), inorganic anions (sulfate, nitrate, nitrite, phosphate, chloride, bromide) and cations (sodium, calcium, magnesium, ammonium) were measured using the filters from the LVCs. The procedure included an ion extraction method, similar to Derrick and Moyers [*Derrick and Moyers*, 1981], followed by ion-chromatography. The anion chromatographic method used a PAX-500 anion column (Dionex) and NaOH eluent (in the gradient mode). The cation chromatographic method used an IonPac CS10 cation column (Dionex) and HCl eluent (isocratic). Both methods used a Dionex BIO-LC gradient elution ion chromatograph.

Total suspended particulate concentrations were determined by measuring the mass of atmospheric aerosols collected on the LVC filters and knowing the volume of air sampled. The weighing procedure involved equilibrating the filters to air at 21°C and a relative humidity of 50% overnight and then weighing (these were the same conditions used to pre-weigh the filters). This weighing technique is similar to the one followed by *Ligocki et al.* [*Ligocki et al.*, 1993].

Error Analysis

All errors in this manuscript are estimated errors based on the precision of the analytical instrument (ICP-MS or Ion-Chromatography), errors introduced in the filter extraction procedure and errors introduced in the calculation of the volume of air sampled. A propagation of error treatment was used to determine the overall estimated error. The detection limit of the ICP-MS and Ion-Chromatograph was determined by measuring the blank intensity and the standard deviation of the blank intensity. The detection limit was defined as 3 times the standard deviation of the blank (95% confidence level) divided by the slope of the calibration curve.

Statistical Analysis

Multivariate statistical analysis was performed using SPSS software [*Kim*, 1975]. R-type principal component analysis with orthogonal varimax rotation was performed on the data set.

RESULTS AND DISCUSSION

Cruise Tracks and Air-Mass Back Trajectories

Figure 1 shows four examples (at four different locations) of 5 day air-mass back-trajectories (AMBTs) for both the M32/3 and M32/5 cruise legs. AMBTs were obtained for all days for both cruise legs, and the four AMBT examples in Figure 1 were chosen since there were representative of the meteorological conditions encountered during both cruise legs. The cruise track for the appropriate leg is also shown in Figure 1 as a solid line. Figure 1 (a) and (b) are AMBTs for M32/3 (inter-monsoon) which began in Oman and ended in the Seychelles, and Figure 1 (c) and (d) are AMBTs for M32/5 (south-west monsoon) which began in the Seychelles and ended in Oman. There are four different AMBTs which correspond to different initial elevations (based on pressure) at the initial position. The vertical motion of each AMBT is shown in the graph at the bottom of each diagram in Figure 1. Each symbol in the diagrams represents a period of 6 hours.

On cruise leg M32/3 (inter-monsoon), the AMBTs (e.g., Figure 1(a)) showed that the air-masses generally came from continental sources including Africa, Middle East and Asia during most of the cruise. However, during the southern portion of the cruise track (e.g. Figure 1(b)) the 5 day AMBTs did not reach any continental land masses, and wind velocities were also reduced.

On cruise leg M32/5 (southwest-monsoon), the AMBTs (e.g., Figure 1(c)) showed that the air-masses generally came from the "open" Indian Ocean during most of the cruise. However, during the northern portion of the cruise track (e.g. Figure 1(d)), some the higher elevation 5 day AMBTs (e.g., Figure 1(c)) were advected over continental land masses.

Overall, wind velocities were generally lower during the inter-monsoon period (M32/5) compared to the south-west monsoon period (M32/5). Air-masses also had

usually advected over continental air masses during M32/3, whereas during M32/5 the air-masses had predominantly been from the "open" ocean.

Total Elemental Concentrations

Concentrations of Na, Mg, Al, K, Ca, Ti, V, Cr, Mn, Fe, Ni, Cu, Zn, Cd, Sb, Ba and Pb were measured in both the fine and coarse fractions of the ambient aerosol (a detailed table of this data is included in the supplemental material). Table 3 describes the collection times and locations for each aerosol sample.

Figure 2 shows the variations in Fe_{total}, Mn_{total}, Cu_{total} and Cr_{total} vs. Latitude, where the total concentrations represent the sum of the concentrations of the elements in the fine and coarse fractions of aerosol. Overall, the above metals exhibited higher concentrations during M32/3 (inter-monsoon) than during M32/5 (south-west monsoon). In addition, during M32/3 there were higher observed concentrations of these metals at higher latitudes, when the AMBTs showed shorter travel times and distances from continental sources. Fe_{total} spanned a concentration range of 3 orders of magnitude during M32/3. Figure 3 shows plots of Mg_{total}, Al_{total}, Ti_{total}, Ni_{total}, Zn_{total} and Ba_{total}. Mg_{total} was very similar for M32/3 and M32/5 due to the strong sea-salt sources of Mg_{total} (see the factor analysis). Al_{total}, Ti_{total}, Zn_{total}, Ba_{total} were all higher in concentrations during M32/3 compared to M32/5. Ni_{total} was generally higher in concentrations during M32/5

Enrichment Factors

Table 4 lists crustal enrichment factors (EFs) [*Duce et al.*, 1975; *Zoller et al.*, 1974] calculated using the total (i.e., fine and coarse) concentrations of Ti, V, Cr, Mn, Fe, Ni, Cu, Zn, Ba and Pb. Crustal averages from Taylor [*Taylor and McLennan*, 1985] were used as a reference source, and Al was used as the crustal tracer.

For aerosol samples collected during M32/5 and towards the second half of M32/3, the EF(Fe) was close to 1 and had a limited range, indicating Fe had a predominantly

crustal source. However, EF(Fe) and EF(Mn) were slightly higher during the first half of M32/3 indicating another possible source of Fe and Mn (hereafter referred to as $S_{Fe,Mn}$). This source could either be anthropogenic, or possibly a natural source with higher Fe and Mn content compared to Al. One possible natural source of enriched Fe and Mn are mafic and ultra-mafic rocks associated with the Samail ophiolite formation on the Oman coast [*Hess*, 1989]. These rocks also have relatively higher Mn content, and the EF(Mn) also follows the same trend as EF(Fe). However, the EF for both Fe and Mn are too high to be explained by mafic rocks. The EF(Ti) should also increase as EF(Fe) and EF(Mn) do, but it remains relatively constant. Another possible source which would explain the high EF(Fe) and EF(Mn) would be "desert varnish", a coating commonly found on desert rocks which is a combination of Fe-oxides and Mn-oxides. Chester *et al.* [*Chester et al.*, 1991] did not see this behavior for Fe during a field study off near the coast of Oman during the northwest monsoon. However the air mass sources observed by Chester *et al.* [*Chester et al.*, 1991] during the northeast monsoon are more consistent in direction and source than were the AMBTs for M32/3. This may indicate that the $S_{Fe,Mn}$ may have originated from a location other than Pakistan or northern India (e.g., northern Africa, southern India, Middle East, etc.).

The EF(Pb) was consistently high in all the M32/3 samples (Pb was below detection limit in the M32/5 samples and therefore the EF was not quantifiable). The high EF(Pb) is probably due to the use of leaded fuels in the countries surrounding the Arabian Sea. The EF(Ni) varied from 5 to 51000 during M32/3, and from 930 to 21000 during M32/5, but no explanation for this behavior is known.

Fe(II) Concentrations

Several labile fractions of Fe(II) were measured immediately after aerosol collection. Table 1 describes the sequential extraction procedure and Table 5 lists the atmospheric concentrations for $Fe(II)_{aq,labile}$ and $Fe(II)_{total,labile}$ for both the coarse and fine

aerosol fractions. Only measurements for M32/3 are shown in Table 5 since all the measurements for M32/5 are below the detection limit. Table 5 also shows the ratio of $Fe(II)_{labile}$ to Fe_{total}. Overall, $Fe(II)_{labile}$ represented only a small fraction (< 2%) of the total iron in all samples. Figure 4 shows a plot of the distribution of the $Fe(II)_{labile}$ between the fine and coarse fractions. Except for a few measurements, most of the $Fe(II)_{aq,labile}$ (> 80%) was found in the fine fraction. $Fe(II)_{total,labile}$ was also predominantly in the fine fraction but not as high as $Fe(II)_{aq,labile}$. These observations may be due to different sources of iron to both fractions with different chemical forms, or it could also be due to different "weathering" processes effecting both fractions as the aerosol is advected in the atmosphere.

Zhu *et al.* [*Zhu et al.*, 1992] observed $Fe(II)_{labile}/Fe_{total}$ fractions in four Barbados aerosol samples of 0.87, 0.92, 0.47 and 0.53% which were similar to our observations. Zhuang *et al.* [*Zhuang et al.*, 1992b] observed much higher $Fe(II)_{labile}/Fe_{total}$ fractions: 2.2% to 49% in marine aerosol samples collected over the central North Pacific and Barbados (see [*Zhu et al.*, 1992] for a correction of [*Zhuang et al.*, 1992b] results). These higher fractions, compared to our observations on the Arabian Sea, may be the result of increased cloud processing of the aerosol in the central North Pacific and Barbados. However, both Zhu *et al.* [*Zhu et al.*, 1992] and Zhuang *et al.* [*Zhuang et al.*, 1992b] had a significant delay between collection and analysis of the aerosol samples; whereas, in this study, analysis was performed immediately (within 1 hour) after sample collection (which took $\approx$ 24 hours).

Our observation that $Fe(II)_{labile}$ is predominantly in the fine fraction, has important implications for the deposition of atmospheric Fe to the ocean surface. Overall, particle size is important to the deposition rate [*Arimoto and Duce*, 1986; *Rojas et al.*, 1993]. Particle size is also an important factor to the particles probability of being a nucleus for a cloud drop [*Seinfeld*, 1986], and therefore its probability of being involved in cloud

chemistry. The size distribution is also important to the residence time of the aerosol in the atmosphere.

Anions and Cations

Figures 5 and 6 show plots of anion and cation concentrations versus latitude. These measurements were included and discussed in the factor analysis below, however, a more detailed discussion of this data will be included in a future paper.

Factor Analysis

Factor analysis with principal component extraction and varimax rotation was performed using the elemental concentration data (for both fine and coarse fractions), total anion concentrations, total cation concentrations and labile-Fe(II) concentrations. Certain measurements were not included in the analysis if there were excessive values below the detection limit. This analysis was performed to identify elements/species with similar sources and also factors which may influence labile-Fe(II).

Table 6 shows the statistical results for a factor which combined the M32/3 and M32/5 data sets. Seven principal components which explained 88.6% of the variance were extracted using a lower limit for the eigenvalue of 1. Table 7 lists the principal components and Figure 7 shows the factor scores for the first 4 principal components (the factor scores for PC 5, PC 6 and PC 7 showed little variation, similar to PC 4).

The concentration profile of PC 1 is strongly suggestive of a crustal source. Most of the elements analyzed in the coarse fraction have high correlation coefficients for PC 1, which is consistent with a crustal source since aeolian dust is normally associated with the coarse particle size fraction. There are also relatively high correlation coefficients for these same elements in the fine fraction, which is probably due to the 3.0 μm cutoff size of the HVDVI. Coarse Al had the highest correlation coefficient (0.929) of all the elements, and also indicates that PC 1 is from a crustal source since Al is commonly used as a crustal

tracer. The factor scores for PC 1 also are higher during the inter-monsoon period compared to the southwest-monsoon period, which also suggests PC 1 is a crustal component since crustal sources are expected to increase during the inter-monsoon period.

The concentration profile of PC 2 suggests aerosol derived from the ocean (sea-spray). Total Mg^{2+} has the highest correlation coefficient (0.965), and the other common ions found in sea-water also have high correlation coefficients (K^+, Na^+, SO_4^{2-}, and Cl^-). The factor scores for PC 2 also show a general trend of being greater at higher latitudes (i.e., the decreasing slope during the inter-monsoon period and the increasing slope during the southwest monsoon). This behavior is probably due to the fact that sea-salt aerosols increase as wind speeds increase, and wind speeds were greater at higher latitudes during both cruises.

PC 3 shows high correlation coefficients for both Fe and Mn in the coarse and fine fractions. This source of Fe and Mn was first believed to be contamination from the ship, however, the observations do not seem to support this hypothesis. First, the concentrations of Fe and Mn were greatest during most of M32/3 and fell almost three orders of magnitude during the end of M32/3 and during all of the M32/5 cruise. We believe that if the source of Fe and Mn was from the ship, then it should observed in most of the aerosol samples since both cruises followed identical sampling and analytical procedures. The enrichment factor analysis also indicated another strong source of Fe and Mn (i.e., $S_{Fe,Mn}$), which was present only during the first two weeks of the inter-monsoon when the AMBTs indicated the aerosol had advected from nearby continental regions. This relationship between $S_{Fe,Mn}$ and the AMBTs, which indicated the aerosol was from nearby continental regions, also suggests that $S_{Fe,Mn}$ has a continental origin. The factor scores for PC 3 also show more variablity during the inter-monsoon period than during the south-west monsoon. Overall, the atmospheric concentrations of Fe and Mn, enrichment factors, AMBTs, and factor analysis suggest a distinct source of Fe and Mn to the ambient aerosol over the Arabian Sea which is not associated with the main continental source (PC 1).

However, contamination from the ship cannot be completely dismissed. If this source of Fe and Mn is from the surrounding continents, then understanding this source would be important to both the cloudwater chemistry occurring over the Arabian Sea, and also to understanding the fluxes of these metals to the surface ocean waters.

PC 4 had high correlation coefficients for several elements in the fine fraction (Ti, Cr, Ni, and Zn). The factor scores for PC 4 were relatively constant compared to PC 1, PC 2 and PC 3. The constant nature of the factor scores indicates a relatively constant concentration of these elements in the background marine aerosol over the Arabian Sea, or a possible contamination of these elements in the samples. The contamination may be from the ship, since Ti is a common element found in paints (TiO_2 is used as a pigment), and Cr is a common element found in primers for metal surfaces (chromates are used to prevent corrosion) [*U.S. Dept. of the Interior*, 1976]. However, the high correlation coefficients were for elements in the fine fraction, and we would expect high correlation coefficients for these elements in the coarse fraction if the source was from the ships surfaces.

Another factor analysis was done using only data from M32/3 and including measurements for labile-Fe(II), V and Pb (these measurements were not included in the first factor analysis due to most values being below the detection limit for M32/5). This factor analysis was done to investigate if labile-Fe(II) or V/Pb (common indicators of anthropogenic sources) were associated with the PC 3 in Table 7 which had high correlation coefficients of both Fe and Mn. Table A-2 (supplemental material) shows the results of this factor analysis. PC 3 in Table A-2 also had similar high correlation coefficients for Fe and Mn as PC 3 from the first factor analysis (Table 7). The results of this second factor analysis showed that PC 3 did not have high correlation coefficients for labile-Fe(II), V, or Pb (all were less than 0.1). This result indicates that the source for PC 3 (Table 7) is not likely associated with an anthropogenic source, but is probably due to another aeolian dust source with high concentrations of Fe and Mn. The result of this factor analysis also resulted in an addition principal component (compared to Table 7) with

high correlation coefficients for labile-Fe(II) in the coarse and fine fractions. This principal component also had a relatively high (0.73) correlation coefficient with NH_4^+. The reason for this correlation between labile-Fe(II) and NH_4^+ is not known. It is also interesting that the organic anions (formate, acetate and oxalate) did not have high correlation coefficients with this principal component, since previous studies have shown the potential of these anions as electron donors for the photochemical reduction of Fe(III) to Fe(II) [*Erel et al.*, 1993; *Pehkonen et al.*, 1993; *Zuo and Hoigné*, 1992].

CONCLUSIONS

Ambient aerosol samples were collected and analyzed for trace metals, anions cations and labile-Fe(II) during the inter-monsoon and southwest-monsoon periods on the Arabian Sea aboard the German research vessel Meteor (Meteor Cruise 32). Total atmospheric aqueous-labile-Fe(II) concentrations during M32/3 (inter-monsoon) were between 7.48 ng m^{-3} to < 0.089 ng m^{-3}. The aqueous-labile Fe(II) was predominantly in the "fine" fraction (< 3.0 μm), with the "fine" fraction of aqueous labile-Fe(II) accounting for an average of 90% of the total aqueous labile-Fe(II). In contrast, during M32/5 (southwest-monsoon), the atmospheric aqueous labile-Fe(II) concentrations were consistently below the detection limit (< 0.34 ng m^{-3} to < 0.089 ng m^{-3} depending on the volume of air sampled). Overall, labile-Fe(II) represented only a small fraction (< 2%) of the total Fe measured in both aerosol fractions. This distribution of labile-Fe(II) has important implications to the deposition of labile-Fe(II) since the deposition rates are a strong function of the particle size. The results also indicate that the Fe in the fine aerosol fraction undergo different chemical transformations then Fe in the coarse aerosol fraction.

The atmospheric concentrations of Fe and Mn, enrichment factors, AMBTs, and factor analysis suggest a distinct source of Fe and Mn to the ambient aerosol over the Arabian Sea during the inter-monsoon period which is not associated with the main continental source (PC 1). However, contamination from the ship cannot be completely dismissed. The factor analysis also showed that labile-Fe(II) measurements did not correlate with any other measured species in the data set including organic anions (formate, acetate or oxalate). This also suggests that the concentrations of labile-Fe(II) is due to meteorological conditions (e.g. atmospheric weathering of the particles) and not directly related to crustal or anthropogenic sources.

Acknowledgments Special thanks are extended to the crew of the FS Meteor for their help. We also thank Prof. J. J. Morgan (Caltech) and Prof. M. O. Andreae (Max Planck Institute for Chemistry, Mainz, Germany) for helpful discussions. Support for this research has been provided by a grant from the National Science Foundation, Division of Atmospheric Sciences, Atmospheric Chemistry Section (ATM 9015775; ATM 9303024). This research was also sponsored by the U.S. Department of Energy, Office of Energy Research, Environmental Sciences Division, Office of Health and Environmental Research, under appointment to the Graduate Fellowships for Global Change administered by Oak Ridge Institute for Science and Education.

REFERENCES

Arimoto, R., and R.A. Duce, Dry deposition models and the air/sea exchange of trace elements, *J. Geophys. Res.*, *91* (D2), 2787-2792, 1986.

Behra, P., and L. Sigg, Evidence for redox cycling of iron in atmospheric water droplets, *Nature*, *344* (6265), 419-421, 1990.

Berglund, J., and L.I. Elding, Manganese-catalyzed autooxidation of dissolved sulfur-dioxide in the atmospheric aqueous-phase, *Atmos. Environ.*, *29* (12), 1379-1391, 1995.

Berglund, J., S. Fronaeus, and L.I. Elding, Kinetics and mechanism for manganese-catalyzed oxidation of sulfur(IV) by oxygen in aqueous-solution, *Inorg. Chem.*, *32* (21), 4527-4538, 1993.

Carter, P., Spectrophotometric determination of serum iron at the submicrogram level with a new reagent (ferrozine), *Anal. Biochem.*, *40*, 450-458, 1971.

Cass, G.R., and G.J. McRae, Source-receptor reconciliation of routine air monitoring data for trace metals: An emission inventory assisted approach, *Environ. Sci. Technol.*, *17* (3), 129-139, 1983.

Chester, R., A.S. Berry, and K.J.T. Murphy, The distributions of particulate atmospheric trace metals and mineral aerosols over the Indian Ocean, *Marine. Chem.*, *34*, 261-290, 1991.

Conklin, M.H., and M.R. Hoffmann, Metal ion-sulfur(IV) chemistry. 2. Kinetic studies of the redox chemistry of copper(II)-sulfur(IV) complexes, *Environ. Sci. Technol.*, *22*, 891-898, 1988a.

Conklin, M.H., and M.R. Hoffmann, Metal ion-sulfur(IV) chemistry. 3. Thermodynamics and kinetics of transient iron(III)-sulfur(IV) complexes, *Environ. Sci. Technol.*, *22*, 899-907, 1988b.

Derrick, M., and J. Moyers, Precise and sensitive water soluble ion extraction method for aerosol samples collected on polytetrafluoroethylene filters, *Anal. Lett.*, *14* (A19), 1637-1652, 1981.

Ditullio, G.R., D.A. Hutchins, and K.W. Bruland, Interaction of iron and major nutrients controls phytoplankton growth and species composition in the tropical North Pacific Ocean, *Limnol. & Ocean.*, *38* (3), 495-508, 1993.

Duce, R.A., G.L. Hoffman, and W.H. Zoller, Atmospheric trace metals at remote northern and southern hemisphere sites: Pollution or natural, *Science*, *187*, 59-61, 1975.

Erel, Y., S.O. Pehkonen, and M.R. Hoffmann, Redox chemistry of iron in fog and stratus clouds, *J. Geophys. Res. A.*, *98* (D10), 18423-18434, 1993.

Faust, B.C., and J.M. Allen, Sunlight-initiated partial inhibition of the dissolved iron(III)-catalyzed oxidation of S(IV) species by molecular-oxygen in aqueous-solution, *Atmos. Environ.*, *28* (4), 745-748, 1994.

Faust, B.C., and M.R. Hoffmann, Photoinduced reductive dissolution of alpha-Fe2O3 by bisulfite, *Environ. Sci. Technol.*, *20*, 943-948, 1986.

Faust, B.C., and J. Hoigné, Photolysis of Fe(III)-hydroxy complexes as sources of OH radicals in clouds, fog and rain, *Atmos. Environ.*, *24A* (1), 79-89, 1990.

Fuzzi, S., G. Orsi, G. Nardini, M.C. Facchini, E. McLaren, and M. Mariotti, Heterogeneous processes in the Po Valley radiation fog, *J. Geophys. Res. A.*, *93* (ND9), 11141-11151, 1988.

Galloway, J.N., J.D. Thornton, S.A. Norton, H.L. Volchok, and R.A.N. Mclean, Trace-metals in atmospheric deposition - A review and assessment, *Atmos. Environ.*, *16*, 1677-1700, 1982.

Gomes, L., and D.A. Gillette, A comparison of characteristics of aerosol from dust storms in central Asia with soil derived dust from other regions, *Atmos. Environ.*, *27* (16), 2539-2544, 1993.

Graedel, T.E., M.L. Mandich, and C.J. Weschler, Kinetic model studies of atmospheric droplet chemistry, 2. Homogenous transition metal chemistry in raindrops, *J. Geophys. Res.*, *91*, 5205-5221, 1986.

Hess, P.C., *Origins of igneous rocks*, Harvard Univ. Press, Cambridge, MA, 1989.

Hoffmann, M.R., and D.J. Jacob, Kinetics and mechanism of the catalytic oxidation of dissolved SO_2 in atmospheric droplets: Free radical, polar and photoassisted pathways, in

SO_2, NO, NO_2 Oxidation Mechanisms: Atmospheric Considerations, edited by J.G. Calvert, pp. 101-172, Butterworth Publishers, Boston, 1984.

Hudson, R.J.M., and F.M.M. Morel, Iron transport in marine phytoplankton: Kinetics of cellular and medium coordination reactions, *Limnol. Ocean., 35* (5), 1002-1020, 1990.

Hudson, R.J.M., and F.M.M. Morel, Trace-metal transport by marine microorganisms: Implications of metal coordination kinetics, *Deep Sea Res., 40*, 129-150, 1993.

Jacob, D.J., E.W. Gottlieb, and M.J. Prather, Chemistry of the polluted boundary layer, *J. Geophys. Res., 94*, 12975-13002, 1989.

Jacob, D.J., and M.R. Hoffmann, A dynamic model for the production of H^+, NO_3^-, and SO_4^{2-} in urban fog, *J. Geophys. Res., 88* (NC11), 6611-6621, 1983.

Jacob, D.J., J.M. Waldman, J.W. Munger, and M.R. Hoffmann, Chemical composition of fogwater collected along the California coast, *Environ. Sci. Technol., 19* (8), 730-736, 1985.

Kim, J., Factor Analysis, in *SPSS: Statistical Package for the Social Sciences*, edited by N.H. Nie, C.H. Hull, J.G. Jenkins, K. Steinbrenner, and D.H. Bent, pp. 468-514, McGraw-Hill, Inc., New York, 1975.

Kolber, Z.S., R.T. Barber, K.H. Coale, S.E. Fitzwater, R.M. Greene, K.S. Johnson, S. Lindley, and P.G. Falkowski, Iron limitation of phytoplankton photosynthesis in the equatorial Pacific Ocean, *Nature, 371* (6493), 145-149, 1994.

Kopcewicz, B., and M. Kopcewicz, Mossbauer study of iron-containing atmospheric aerosols, *Struct. Chem.*, *2* (3-4), 303-312, 1991.

Kopcewicz, B., and M. Kopcewicz, Seasonal variations of iron concentration in atmospheric aerosols, *Hyperfine Interactions*, *71* (1-4), 1457-1460, 1992.

Kotronarou, A., and L. Sigg, SO2 Oxidation in atmospheric water: role of Fe(II) and effect of ligands, *Environ. Sci. & Technol.*, *27* (13), 2725-2735, 1993.

Kraft, J., and R. Van Eldik, Kinetics and mechanism of the iron(III)-catalyzed autooxidation of sulfur(IV) oxides in aqueous-solution .1. Formation of transient iron(III) sulfur(IV) complexes, *Inorg. Chem.*, *28* (12), 2297-2305, 1989a.

Kraft, J., and R. Van Eldik, Kinetics and mechanism of the iron(III)-catalyzed autooxidation of sulfur(IV) oxides in aqueous-solution .2. Decomposition of transient iron(III) sulfur(IV) complexes, *Inorg. Chem.*, *28* (12), 2306-2312, 1989b.

Lantzy, R.J., and F.T. Mackenzie, Atmospheric trace metals: Global cycles and assessment of Man's impact, *Geochim. et Cosmochim. Acta*, *43*, 511-523, 1979.

Ligocki, M.P., L.G. Salmon, T. Fall, M.C. Jone, W.W. Nazaroff, and G.R. Cass, Characteristics of airborne particles inside southern California museums, *Atmos. Environ.*, *27(5)*, 697-711, 1993.

Martin, J.H., K.H. Coale, K.S. Johnson, S.E. Fitzwater, R.M. Gordon, S.J. Tanner, C.N. Hunter, V.A. Elrod, J.L. Nowicki, and e. al., Testing the iron hypothesis in ecosystems of the equatorial Pacific Ocean, *Nature, 371* (6493), 123-129, 1994.

Martin, J.H., and R.M. Gordon, Northeast Pacific iron distributions in relation to phytoplankton productivity, *Deep Sea Res. A., 35* (2), 177-196, 1988.

Martin, L.R., and T.W. Good, Catalyzed oxidation of sulfur dioxide in solution: The iron-manganese synergism, *Atmos. Environ., 25* (10), 2395-2399, 1991.

Martin, L.R., and H.W. Hill, The iron catalyzed oxidation of sulfur: Reconciliation of the literature rates, *Atmos. Environ., 21*, 1487-1490, 1987.

Martin, L.R., M.W. Hill, A.F. Tai, and T.W. Good, The iron catalyzed oxidation of sulfur(IV) in aqueous-solution: Differing effects of organics at high and low pH, *J. Geophys. Res., 96* (ND2), 3085-3097, 1991.

Matthijsen, J., P.J.H. Builtjes, and D.L. Sedlak, Cloud model experiments of the effect of iron and copper on tropospheric ozone under marine and continental conditions, *Meteorol. Atmos. Phys., 57*, 43-60, 1995.

Morel, F.M.M., R.J.M. Hudson, and N.M. Price, Limitation of productivity by trace-metals in the sea, *Limnol. Oceanogr., 36* (8), 1742-17455, 1991.

Munger, J.W., J.M. Waldman, D.J. Jacob, and M.R. Hoffmann, Fogwater chemistry in an urban atmosphere, *J. Geophys. Res., 88* (NC9), 5109-5121, 1983.

Nriagu, J.O., A global assessment of natural sources of atmospheric trace metals, *Nature*, *338*, 47-49, 1989.

Nriagu, J.O., and C.I. Davidson, Toxic metals in the atmosphere, in *Advances in environmental science and technology*, Wiley, New York, 1986.

Patterson, C.C., and D.M. Settle, The reduction of orders of magnitude errors in lead analysis of biological materials and natural waters by evaluating and controlling the extent and sources of industrial lead contamination introduced during sampling, collecting, handling and analysis, *National Bureau of Standards, Special Publication*, *422*, 321-351, 1976.

Pehkonen, S.O., R.L. Siefert, Y. Erel, S. Webb, and M.R. Hoffmann, Photoreduction of iron oxyhydroxides in the presence of important atmospheric organic compounds, *Environ. Sci. Technol.*, *27* (10), 2056-2062, 1993.

Price, N.M., B.A. Ahner, and F.M.M. Morel, The equatorial Pacific Ocean - grazer controlled phytoplankton populations in an iron limited ecosystem, *Limnol. & Ocean.*, *39* (3), 520-534, 1994.

Puxbaum, H., Metal compounds in the atmosphere, in *Metals and their compounds in the environment*, edited by E. Merian, pp. 257-286, VCH Publishers, 1991.

Rojas, C.R., R.E. Van Grieken, and R. Laane, Comparison of three dry deposition models applied to field measurements in the southern bight of the North Sea, *Atmos. Environ.*, *27A* (3), 363-370, 1993.

Savoie, D.L., J.M. Prospero, and R.T. Nees, Nitrate, non-sea-salt sulfate, and mineral aerosol over the Northwestern Indian Ocean, *J. Geophys. Res.*, *92* (D1), 933-942, 1987.

Schroeder, W.H., M. Dobson, D.M. Kane, and N.D. Johnson, Toxic trace elements associated with airborne particulate matter: A review, *J. Air Pollut. Control Assoc.*, *37* (11), 1267-1285, 1987.

Sedlak, D.L., and J. Hoigné, The role of copper and oxalate in the redox cycling of iron in atmospheric waters, *Atmos. Environ.*, *27*, 2173-2185, 1993.

Sedlak, D.L., and J. Hoigné, Oxidation of S(IV) in atmospheric water by photooxidants and iron in the presence of copper, *Environ. Sci. & Technol.*, *28*, 1898-1906, 1994.

Seigneur, C., and E. Constantinou, Chemical kinetic mechanism for atmospheric chromium, *Environ. Sci. Technol.*, *29*, 222-231, 1995.

Seinfeld, J.H., *Atmospheric Chemistry and Physics of Air Pollution*, 738 pp., Wiley, New York, 1986.

Siefert, R.L., S.O. Pehkonen, Y. Erel, and M.R. Hoffmann, Iron photochemistry of aqueous suspensions of ambient aerosol with added organic acids, *Geochim. et Cosmochim. Acta*, *58* (15), 3271-3279, 1994.

Solomon, P.A., J.L. Moyers, and R.A. Fletcher, High-volume dichotomous virtual impactor for the fractionation and collection of particles according to aerodynamic size, *Aerosol Sci. & Technol.*, *2*, 455-464, 1983.

Spokes, L.J., T.D. Jickells, and B. Lim, Solubilisation of aerosol trace metals by cloud processing: A laboratory study, *Geochim. et Cosmochim. Acta*, *58* (15), 3281-3287, 1994.

Stookey, L.L., Ferrozine- a new spectrophotometric reagent for iron, *Anal. Chem.*, *42* (7), 119-781, 1970.

Taylor, S.R., and S.M. McLennan, *The continental crust: its composition and evolution*, 9-52 pp., Blackwell Scientific Publications, London, 1985.

U.S. Dept. of the Interior, B.o.R., *Paint manual: A manual for the control of protective coatings and their application*, The Bureau, Denver, CO, 1976.

Waldman, J.M., J.W. Munger, D.J. Jacob, R.C. Flagan, J.J. Morgan, and M.R. Hoffmann, The chemical composition of acid fog, *Science*, *218* (4573), 677-680, 1982.

Wells, M.L., N.M. Price, and K.W. Bruland, Iron limitation and the cyanobacterium synechococcus in equatorial pacific waters, *Limnol. Ocean.*, *39* (6), 1481-1486, 1994.

Wells, M.L., N.M. Price, and K.W. Bruland, Iron chemistry in seawater and its relationship to phytoplankton: a workshop report, *Marine Chem.*, *48*, 157-182, 1995.

Weschler, C.J., M.L. Mandich, and T.E. Graedel, Speciation, photosensitivity, and reactions of transition metal ions in atmospheric droplets, *J. Geophys. Res.*, *91*, 5189-5204, 1986.

Xue, H.B., M.D.S. Goncalves, M. Reutlinger, L. Sigg, and W. Stumm, Copper(I) in fogwater: determination and interactions with sulfite, *Environ. Sci. & Technol.*, *25* (10), 1716-1722, 1991.

Zhu, X.R., J.M. Prospero, F.J. Millero, D.L. Savoie, and G.W. Brass, The solubility of ferric iron in marine mineral aerosol solutions at ambient relative humidities, *Marine Chem.*, *38*, 91-107, 1992.

Zhu, X.R., J.M. Prospero, D.L. Savoie, F.J. Millero, R.G. Zika, and E.S. Saltzman, Photoreduction of iron(III) in marine mineral aerosol solutions, *J. Geophys. Res. A.*, *98* (ND5), 9039-9046, 1993.

Zhuang, G., Z. Yi, R.A. Duce, and P.R. Brown, The chemistry of iron in marine aerosols, *Global Biogeochem. Cycles*, *7* (3), 711, 1992a.

Zhuang, G., Z. Yi, R.A. Duce, and P.R. Brown, Link between iron and sulfur cycles suggested by detection of Fe(II) in remote marine aerosols, *Nature*, *355* (6360), 537-539, 1992b.

Zoller, W.H., R.A. Gordon, and R.A. Duce, Atmospheric concentrations and sources of trace metals at the South Pole, *Science*, *183*, 198-200, 1974.

Zuo, Y., and J. Hoigné, Formation of hydrogen peroxide and depletion of oxalic acid in atmospheric water by photolysis of iron(III)-oxalato compounds, *Environ. Sci. Technol.*, *26* (5), 1014-1022, 1992.

Zuo, Y.G., and J. Hoigné, Photochemical decomposition of oxalic, glyoxalic and pyruvic-acid catalyzed by iron in atmospheric waters., *Atmos. Environ.*, *28* (7), 1231-1239, 1994.

FIGURE CAPTIONS

FIGURE 1 Five day air-mass back trajectories for four different elevations (based on pressure) above sea level for: a) May 13, 1996 18:00 UTC, b) May 31, 1996 18:00 UTC, c) July 23, 1996 18:00 UTC and d) August 5, 1996 18:00 UTC.

FIGURE 2 Log plots of first-row transition metals versus Latitude. ❍ symbols represent data collected during M32/3 (inter-monsoon) and □ symbols represent data collected during M32/5 (south-west monsoon).

FIGURE 3 Log plots of Mg_{total}, Al_{total}, Ti_{total}, Ni_{total}, Zn_{total} and Ba_{total} versus Latitude. ❍ symbols represent data collected during M32/3 (inter-monsoon) and □ symbols represent data collected during M32/5 (south-west monsoon).

FIGURE 4 Plots of the ratios of $Fe(II)_{labile}$ in the "fine" fraction to total $Fe(II)_{labile}$ versus Latitude for two labile fractions of Fe(II) (i.e. $Fe(II)_{aqueous,\ labile}$ and $Fe(II)_{total,\ labile}$).

FIGURE 5 Log plots of Na^{+}_{total}, K^{+}_{total}, Mg^{2+}_{total}, Ca^{2+}_{total}, and $NH_4^{+}{}_{total}$ versus Latitude. ❍ symbols represent data collected during M32/3 (inter-monsoon) and □ symbols represent data collected during M32/5 (south-west monsoon).

FIGURE 6 Log plots of Cl^{-}_{total}, Fl^{-}_{total}, $SO_4^{2-}{}_{total}$, $NO_3^{-}{}_{total}$, MSA_{total} and $C_2O_4^{2-}{}_{total}$ versus Latitude. ❍ symbols represent data collected during M32/3 (inter-monsoon) and □ symbols represent data collected during M32/5 (south-west monsoon).

FIGURE 7 Factor score plots for the first 4 principal components shown in Table 7.

TABLE 1. Sequential extraction procedure for measuring labile fractions of ferrous iron (Fe(II)) collected on the coarse and fine HVDVI filters.

Step	Description
1	cut a 47 mm diameter piece of the 90 mm filter using a ceramic knife and a polycarbonate die
2	place filter cut in a Teflon jar
3	"wet" the filter cut by adding approximately 0.1 ml (in 0.01 ml increments) of ethanol
4	add 20 ml of formate buffer solution (pH = 4.2, $[formate]_{total}$ = 500 μM) to the jar
5	place Teflon grid on top of filter to keep it submersed, and gently swirl solution periodically
6	after 30 minutes remove 5 ml aliquot and filter (using a 0.2 μm cellulose acetate syringe filter)
7	place filtered aliquot in spectrophotometric cell (5 cm path length, semi-low volume)
8	measure absorbance, ABS(background)
9	add 0.1 ml of ferrozine solution ([ferrozine] = 6.1 mM) to spectrophotometeric cell and mix
10	measure absorbance, ABS(extraction #1): $Fe(II)_{aq.labile}$
11	rinse spectrophotometer cell
12	add 0.3 ml of ferrozine soloution to remaining 15 ml of solution in jar and gently swirl solution
13	after 5 minutes remove 5 ml aliquot and filter (using a 0.2 μm cellulose acetate syringe filter)
14	place filtered aliquot in spectrophotometric cell
15	measure absorbance, ABS(extraction #2): $Fe(II)_{FZ.5min.labile}$
16	rinse spectrophotometer cell
17	let extraction solution stand overnight (periodically swirling solution)
18	measure absorbance, ABS(extraction #3): $Fe(II)_{total.labile}$

TABLE 2. Strong acid digestion method for HVDVI filters.

Step	Description
1	cut a piece from the 90 mm filter using a ceramic knife and a polycarbonate die
2	place filter cut in 10 ml Teflon vial
3	add 1 g concentrated HNO_3 and 1 g concentrated HF to the vial
4	place Teflon grid on top of filter to keep it submerged, and cap vial
5	place vial on shaker table, and set temperature to 50 °C
6	shake vial at 50 °C overnight (> 12 hours)
7	remove filter cut and Teflon grid from vial
8	rinse filter cut and grid with ≈ 1 g H_20, with rinse solution falling into vial
9	evaporate solution in vial to dryness (purging vial with N_2 gas)
10	add 0.5 g HNO_3 to vial and shake for 1/2 hour
11	add 9.5 g H_2O to vial
12	analyze solution using ICP-MS

TABLE 3. Aerosol sample collection times and positions.

Label	Start Date/Time UTC	Stop Date/Time UTC	Latitude ° North	Longitude ° East
M32/3_01	05/09/95 09:16	05/09/95 17:26	16.3	65.0
M32/3_02	05/09/95 17:50	05/10/95 04:15	16.7	65.0
M32/3_03	05/10/95 06:40	05/10/95 12:00	18.0	65.0
M32/3_04	05/10/95 13:00	05/11/95 02:21	18.0	65.0
M32/3_05	05/11/95 02:40	05/11/95 07:15	18.0	65.0
M32/3_06	05/11/95 14:10	05/11/95 23:30	18.1	65.0
M32/3_07	05/12/95 04:15	05/12/95 22:30	18.1	65.0
M32/3_08	05/13/95 04:30	05/13/95 22:00	18.1	65.0
M32/3_09	05/14/95 03:10	05/14/95 22:15	18.1	65.0
M32/3_10	05/15/95 03:20	05/15/95 22:30	18.1	65.0
M32/3_11	05/16/95 03:15	05/16/95 16:55	18.1	65.0
M32/3_12	05/17/95 03:21	05/18/95 03:10	18.1	65.0
M32/3_13	05/18/95 03:35	05/19/95 03:05	16.9	65.0
M32/3_14	05/19/95 03:20	05/20/95 03:15	14.3	65.0
M32/3_15	05/20/95 03:35	05/21/95 03:10	11.5	65.0
M32/3_16	05/21/95 03:35	05/22/95 03:10	10.0	65.0
M32/3_17	05/22/95 03:20	05/23/95 03:15	10.0	65.0
M32/3_18	05/23/95 03:30	05/24/95 03:15	10.0	65.0
M32/3_19	05/24/95 03:25	05/25/95 03:15	10.0	65.0
M32/3_20	05/25/95 03:30	05/26/95 03:25	10.0	65.0
M32/3_21	05/26/95 03:35	05/27/95 03:15	9.9	65.0
M32/3_22	05/27/95 03:35	05/28/95 03:20	9.5	65.0
M32/3_23	05/28/95 03:35	05/29/95 03:15	7.5	65.0
M32/3_24	05/29/95 03:30	05/30/95 03:20	4.5	65.0
M32/3_25	05/30/95 04:00	05/30/95 21:00	3.0	65.0
M32/3_26	05/31/95 03:40	06/01/95 03:00	2.9	65.0
M32/3_27	06/01/95 07:25	06/01/95 21:55	1.4	65.0
M32/3_28	06/02/95 04:55	06/02/95 11:55	0.0	65.0
M32/5_01	07/16/95 09:10	07/17/95 10:19	0.0	65.0
M32/5_02	07/18/95 04:46	07/20/95 10:25	1.5	65.0
M32/5_03	07/20/95 10:43	07/21/95 04:02	3.1	65.0
M32/5_04	07/21/95 11:37	07/22/95 14:15	6.0	65.0
M32/5_05	07/24/95 01:02	07/25/95 02:40	10.0	65.0
M32/5_06	07/26/95 04:09	07/26/95 13:15	13.0	65.0
M32/5_07	07/26/95 23:57	07/28/95 11:15	14.5	64.7
M32/5_08	07/28/95 11:47	07/30/95 00:21	15.2	63.5
M32/5_09	07/30/95 00:33	07/31/95 04:05	16.1	62.0
M32/5_10	07/31/95 04:23	08/01/95 04:12	16.7	60.7
M32/5_11	08/01/95 04:30	08/02/95 03:14	17.1	59.8
M32/5_12	08/02/95 03:30	08/03/95 04:02	17.6	58.7
M32/5_13	08/03/95 04:27	08/04/95 05:15	18.4	57.5
M32/5_14	08/04/95 05:31	08/05/95 03:09	18.6	57.2
M32/5_15	08/05/95 03:22	08/06/95 13:57	18.4	57.3
M32/5_16	08/06/95 14:11	08/07/95 13:00	18.0	58.5
M32/5_17	08/07/95 13:52	08/08/95 10:09	17.4	59.6
M32/5_18	08/08/95 10:20	08/09/95 14:07	16.4	61.0
M32/5_19	08/09/95 23:29	08/11/95 03:41	16.2	61.5
M32/5_20	08/11/95 03:54	08/11/95 23:56	16.0	62.0

TABLE 4. Enrichment factors using the total concentration of each element (i.e. fine + coarse).

Label	EF(Ti)	EF(V)	EF(Cr)	EF(Mn)	EF(Fe)	EF(Ni)	EF(Cu)	EF(Zn)	EF(Ba)	EF(Pb)
M32/3_01_T	1.39	3.02	9.61	1.21	0.98	245	9.8	24.9	1.14	71.3
M32/3_02_T	1.03	2.95	9.60	1.38	1.01	278	10.8	26.7	1.24	88.0
M32/3_03_T	3.76	5.58	142.32	1.73	2.15	1451	16.3	100.2	1.03	66.8
M32/3_04_T	0.79	1.67	3.42	5.04	9.07	67	14.7	11.3	1.14	40.6
M32/3_05_T	0.78	1.67	5.01	4.16	7.27	209	53.3	9.1	1.18	NM
M32/3_06_T	0.88	1.62	6.54	13.19	25.16	484	85.3	6.8	1.24	21.8
M32/3_07_T	0.88	1.63	3.00	3.69	5.62	434	90.1	6.2	1.18	20.4
M32/3_08_T	0.86	1.55	2.37	2.33	3.04	44	14.3	5.7	1.19	25.4
M32/3_09_T	0.90	1.43	2.73	3.28	5.08	149	57.6	6.2	1.07	20.6
M32/3_10_T	0.96	1.68	3.81	2.38	2.97	77	11.2	5.2	1.20	20.5
M32/3_11_T	0.96	1.70	3.34	4.30	6.86	174	41.3	5.2	1.25	19.0
M32/3_12_T	1.02	1.59	2.44	2.81	3.72	224	150.4	8.7	1.18	24.3
M32/3_13_T	0.99	1.65	2.31	1.95	2.79	90	7.3	5.3	1.22	22.4
M32/3_14_T	1.12	1.67	2.69	2.04	2.29	178	64.2	4.2	1.24	14.6
M32/3_15_T	1.08	1.66	2.54	1.71	1.83	49	6.6	4.1	1.23	15.8
M32/3_16_T	1.39	2.72	3.23	1.47	1.22	5	4.2	4.8	1.49	19.7
M32/3_17_T	1.05	2.20	2.35	1.25	1.10	15	8.7	3.9	1.20	16.0
M32/3_18_T	1.06	1.94	3.00	1.19	1.00	5	4.2	4.6	1.21	25.9
M32/3_19_T	1.24	2.43	3.87	1.26	1.32	88	24.6	8.8	1.28	26.3
M32/3_20_T	1.27	3.00	1.87	1.20	1.01	7	4.4	5.5	1.27	30.2
M32/3_21_T	1.04	2.60	1.92	1.21	0.99	5	5.0	4.8	1.37	17.3
M32/3_22_T	1.17	1.95	1.85	1.50	1.20	10	5.0	3.9	1.65	12.5
M32/3_23_T	1.07	1.81	1.75	1.38	1.13	21	2.8	4.1	1.47	13.7
M32/3_24_T	1.28	2.06	15.62	0.86	0.96	2228	10.2	NM	0.91	29.0
M32/3_25_T	4.42	NM	66.68	NM	1.37	11230	51.2	NM	NM	NM
M32/3_26_T	4.57	NM	145.35	NM	3.10	28325	112.8	94.6	NM	NM
M32/3_27_T	4.71	NM	163.86	NM	2.15	18784	201.8	NM	NM	NM
M32/3_28_T	6.86	NM	268.93	NM	2.83	50794	235.6	NM	NM	NM
M32/5_01_T	NM[a]	NM	NM	NM	0.00	NM	NM	NM	NM	NM
M32/5_02_T	1.02	NM	NM	1.17	1.08	5107	11.6	22.7	1.17	NM
M32/5_03_T	1.29	NM	NM	1.20	1.33	6177	32.8	18.6	NM	NM
M32/5_04_T	1.65	NM	NM	1.18	1.55	6915	35.5	42.9	NM	NM
M32/5_05_T	1.12	NM	NM	1.24	1.07	5287	20.7	NM	NM	NM
M32/5_06_T	1.38	NM	NM	NM	NM	14824	39.2	23.6	NM	NM
M32/5_07_T	1.13	NM	NM	1.23	1.16	3233	17.5	22.5	1.03	NM
M32/5_08_T	1.17	NM	NM	1.23	1.15	3197	17.6	9.1	1.05	NM
M32/5_09_T	1.21	NM	18.34	1.05	1.06	5673	11.2	8.0	0.72	NM
M32/5_10_T	0.92	NM	32.94	1.16	1.10	3882	8.8	9.4	0.73	NM
M32/5_11_T	0.97	NM	NM	1.04	0.93	1427	NM	5.9	NM	NM
M32/5_12_T	0.88	NM	3.75	0.98	0.95	1982	6.9	6.0	0.63	NM
M32/5_13_T	0.93	NM	3.55	1.10	0.96	927	12.4	5.2	0.68	NM
M32/5_14_T	1.14	NM	11.92	1.52	0.99	2999	29.9	11.8	NM	NM
M32/5_15_T	0.98	NM	NM	1.06	1.01	1476	NM	5.1	0.72	NM
M32/5_16_T	1.39	NM	14.68	2.13	1.04	8132	43.6	16.2	NM	NM
M32/5_17_T	1.39	NM	14.78	1.91	0.99	20875	69.0	24.3	NM	NM
M32/5_18_T	1.15	NM	16.44	1.32	1.11	8687	30.7	10.6	0.80	NM
M32/5_19_T	1.09	NM	2.82	1.15	1.07	1150	11.5	4.7	0.74	NM
M32/5_20_T	1.02	NM	8.03	1.10	0.97	2266	8.5	6.3	0.84	NM

[a] not measureable

TABLE 5. Labile Fe(II) concentrations in the Fine and Coarse aerosol fractions for M32/3 (inter-

Label	Fine $Fe(II)_{aq.labile}$		Fine $Fe(II)_{total.labile}$		Coarse $Fe(II)_{aq.labile}$		Coarse $Fe(II)_{total.labile}$	
	Conc. ng m-3	% of Fe_{total} %	Conc. ng m-3	% of Fe_{total} %	Conc. ng m-3	% of Fe_{total} %	Conc. ng m-3	% of Fe_{total} %
M32/3_01	2.73	2.83%	2.73	2.83%	4.75	6.198%	4.75	6.198%
M32/3_02	0.60	1.04%	9.77	17.02%	4.02	6.709%	4.02	6.709%
M32/3_03	1.02	0.31%	1.64	0.50%	0.25	0.301%	1.54	1.824%
M32/3_04	1.35	0.12%	2.12	0.19%	< 0.07	< 0.008%	1.63	0.207%
M32/3_05	0.41	0.06%	0.41	0.06%	< 0.10	< 0.012%	< 0.10	< 0.012%
M32/3_06	0.66	0.03%	0.66	0.03%	< 0.10	< 0.002%	0.49	0.008%
M32/3_07	0.66	0.05%	1.86	0.15%	< 0.05	< 0.015%	0.10	0.033%
M32/3_08	1.58	0.22%	4.09	0.58%	< 0.05	< 0.006%	2.08	0.233%
M32/3_09	1.37	0.17%	2.57	0.31%	< 0.05	< 0.002%	0.15	0.008%
M32/3_10	0.59	0.06%	5.06	0.49%	0.05	0.005%	0.05	0.005%
M32/3_11	0.72	0.06%	2.79	0.23%	0.15	0.004%	0.15	0.004%
M32/3_12	0.96	0.11%	2.62	0.31%	< 0.05	< 0.004%	0.15	0.012%
M32/3_13	0.72	0.36%	3.99	2.02%	0.09	0.010%	1.46	0.177%
M32/3_14	0.59	0.12%	2.37	0.47%	0.01	0.002%	0.93	0.145%
M32/3_15	1.08	0.35%	3.66	1.17%	0.02	0.002%	1.38	0.167%
M32/3_16	1.01	0.47%	4.01	1.87%	0.00	0.000%	1.57	0.316%
M32/3_17	1.21	0.69%	5.07	2.89%	0.01	0.002%	2.18	0.349%
M32/3_18	0.44	0.35%	2.30	1.82%	< 0.04	< 0.025%	0.72	0.440%
M32/3_19	0.35	0.44%	0.88	1.10%	< 0.04	< 0.068%	0.73	1.276%
M32/3_20	0.45	0.77%	1.24	2.12%	0.07	0.097%	0.31	0.424%
M32/3_21	0.45	0.53%	1.60	1.87%	0.02	0.017%	0.85	0.653%
M32/3_22	0.34	0.10%	1.86	0.55%	< 0.04	< 0.008%	1.99	0.365%
M32/3_23	0.66	0.24%	1.98	0.73%	0.07	0.020%	1.42	0.417%
M32/3_24	< 0.04	< 0.35%	0.06	0.47%	< 0.04	< 0.290%	0.07	0.469%
M32/3_25	< 0.05	< 0.96%	0.16	2.77%	< 0.05	< 1.268%	< 0.05	< 1.268%
M32/3_26	< 0.07	< 1.45%	0.38	7.63%	< 0.07	< 0.713%	0.32	3.138%
M32/3_27	< 0.06	< 1.02%	< 1.02%	< 1.02%	< 0.06	NA	< 0.06	NA
M32/3_28	< 0.17	< 0.88%	< 0.88%	< 0.88%	< 0.17	NA	< 0.17	NA

TABLE 6. Factor analysis statistics for inter-monsoon and southwest-monsoon data.

PC	Eigenvalue	% Of Variance	Cumulative %
1	18.64	45.5	45.5
2	6.89	16.8	62.3
3	3.82	9.3	71.6
4	2.86	7.0	78.6
5	1.71	4.2	82.7
6	1.33	3.2	86.0
7	1.09	2.7	88.6

TABLE 7. Principal components (PCs) after factor analysis of inter-monsoon and southwest-monsoon aerosol samples.

	PC 1	PC 2	PC 3	PC 4	PC 5	PC 6	PC 7
COARSE Mg	0.659	0.439	0.437	0.136	0.156	0.134	0.143
COARSE Al	0.929	-0.082	0.201	0.072	0.203	0.143	0.055
COARSE K	0.812	0.213	0.224	0.134	0.262	0.162	0.102
COARSE Ca_{43}[a]	0.882	0.063	0.366	0.018	0.108	0.044	0.155
COARSE Ca_{44}	0.872	0.081	0.362	0.014	0.126	0.074	0.171
COARSE Ti_{47}	0.932	-0.141	0.091	0.072	0.191	0.116	0.033
COARSE Ti_{48}	0.948	-0.139	0.104	0.052	0.165	0.096	0.067
COARSE Cr	0.695	-0.248	0.491	0.337	0.063	-0.181	-0.028
COARSE Mn	0.443	-0.106	0.850	0.000	0.158	-0.069	0.050
COARSE Fe	0.277	-0.044	0.914	-0.007	0.115	-0.105	0.042
COARSE Ni	-0.225	0.158	0.105	-0.062	-0.009	-0.691	-0.142
COARSE Cu	0.426	0.019	0.325	0.004	0.457	-0.078	0.106
COARSE Zn	0.842	-0.162	0.224	0.327	0.183	0.078	-0.001
COARSE Ba	0.907	-0.257	0.134	0.059	0.206	0.117	0.019
FINE Mg	0.246	0.657	0.164	-0.040	0.636	-0.112	0.024
FINE Al	0.724	-0.159	0.229	0.229	0.535	0.190	-0.030
FINE K	0.448	0.392	0.183	0.200	0.673	-0.021	-0.045
FINE Ca_{43}	0.567	0.130	0.292	-0.010	0.717	0.003	0.024
FINE Ca_{44}	0.580	0.201	0.287	0.022	0.696	0.021	0.038
FINE Ti_{47}	0.469	-0.077	0.086	0.779	0.365	0.041	0.009
FINE Ti_{48}	0.490	-0.064	0.103	0.754	0.389	0.044	0.009
FINE Cr	-0.095	0.101	-0.057	0.942	0.004	-0.161	0.056
FINE Mn	0.415	-0.078	0.807	0.124	0.235	0.147	0.206
FINE Fe	0.304	0.028	0.865	0.110	0.091	0.157	0.210
FINE Ni	-0.329	0.229	-0.051	0.331	-0.010	-0.514	0.426
FINE Cu	0.209	0.071	0.346	0.030	0.013	0.093	0.812
FINE Zn	0.050	0.038	0.054	0.971	0.040	-0.019	0.097
FINE Ba	0.695	-0.264	0.142	0.151	0.591	0.157	-0.046
TOTAL Fl^-	0.430	0.035	0.088	0.613	-0.260	0.187	-0.040
TOTAL $H_3CCO_2^-$	0.742	0.025	0.095	0.039	-0.116	-0.298	-0.267
TOTAL HCO_2^-	-0.020	0.459	0.680	0.148	0.272	-0.190	-0.166
TOTAL MSA	-0.143	0.808	-0.023	0.085	-0.080	-0.203	-0.144
TOTAL Cl^-	-0.213	0.923	-0.106	-0.144	0.047	-0.204	0.044
TOTAL NO_3^-	0.712	-0.176	0.122	0.269	0.214	0.224	-0.045
TOTAL SO_4^{2-}	0.475	0.695	-0.005	0.274	0.267	0.168	0.022
TOTAL $C_2O_4^{2-}$	0.487	0.574	0.309	0.260	0.282	0.252	0.136
TOTAL Na^+	-0.224	0.933	-0.099	-0.125	-0.015	-0.128	0.043
TOTAL NH_4^+	0.069	-0.048	0.357	0.664	-0.158	0.485	-0.205
TOTAL K^+	-0.017	0.877	0.105	0.100	0.088	0.120	0.093
TOTAL Mg^{2+}	-0.107	0.965	-0.020	-0.056	0.011	-0.024	0.061
TOTAL Ca^{2+}	0.768	0.185	0.215	0.043	0.378	0.223	0.047

[a] the isotope mass is included when multiple isotopes are used for a single element.

Figure 1

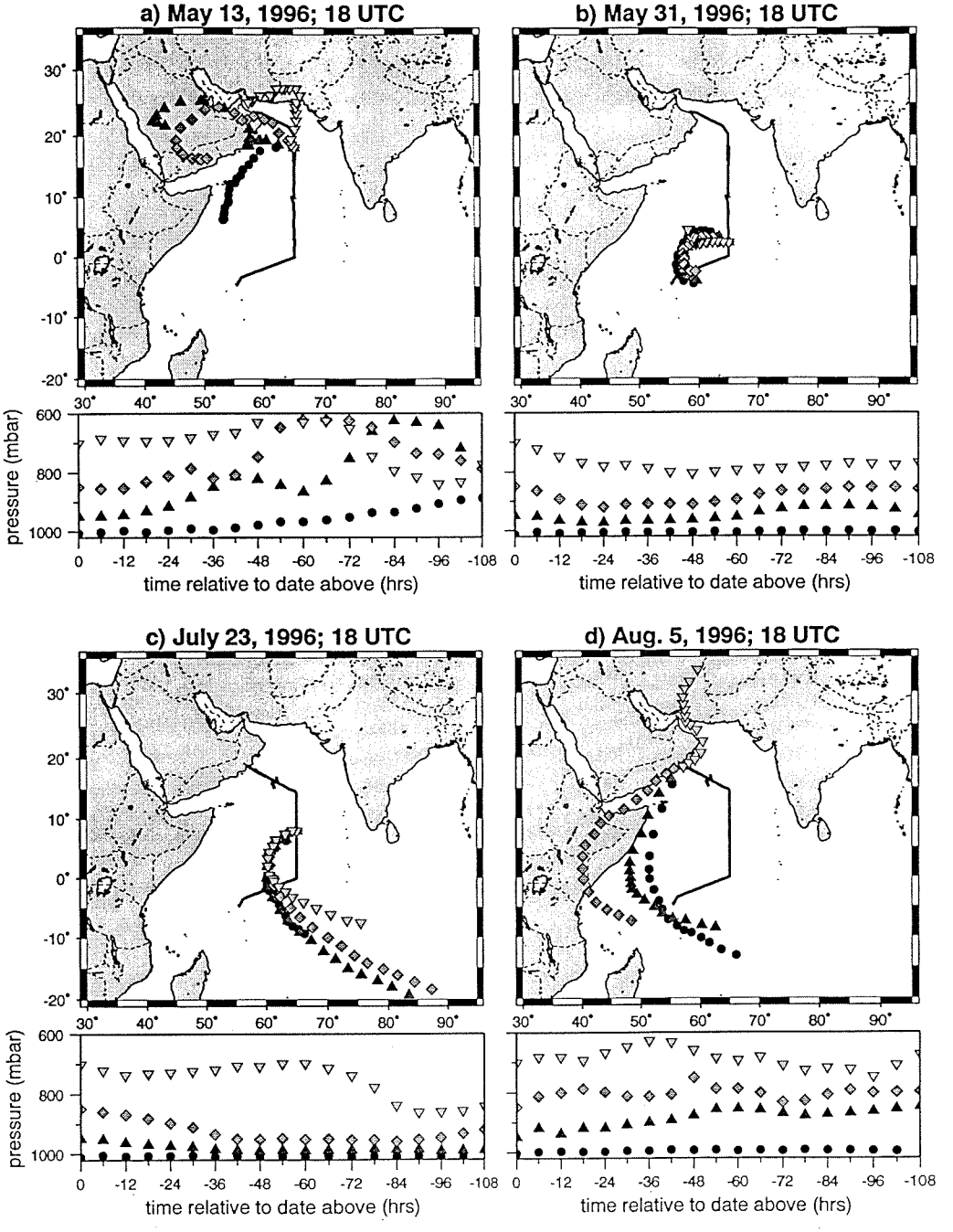
a) May 13, 1996; 18 UTC
b) May 31, 1996; 18 UTC
c) July 23, 1996; 18 UTC
d) Aug. 5, 1996; 18 UTC
30°
20°
10°
0°
-10°
-20°
30° 40° 50° 60° 70° 80° 90°
pressure (mbar)
600
800
1000
0 -12 -24 -36 -48 -60 -72 -84 -96 -108
time relative to date above (hrs)

Figure 2

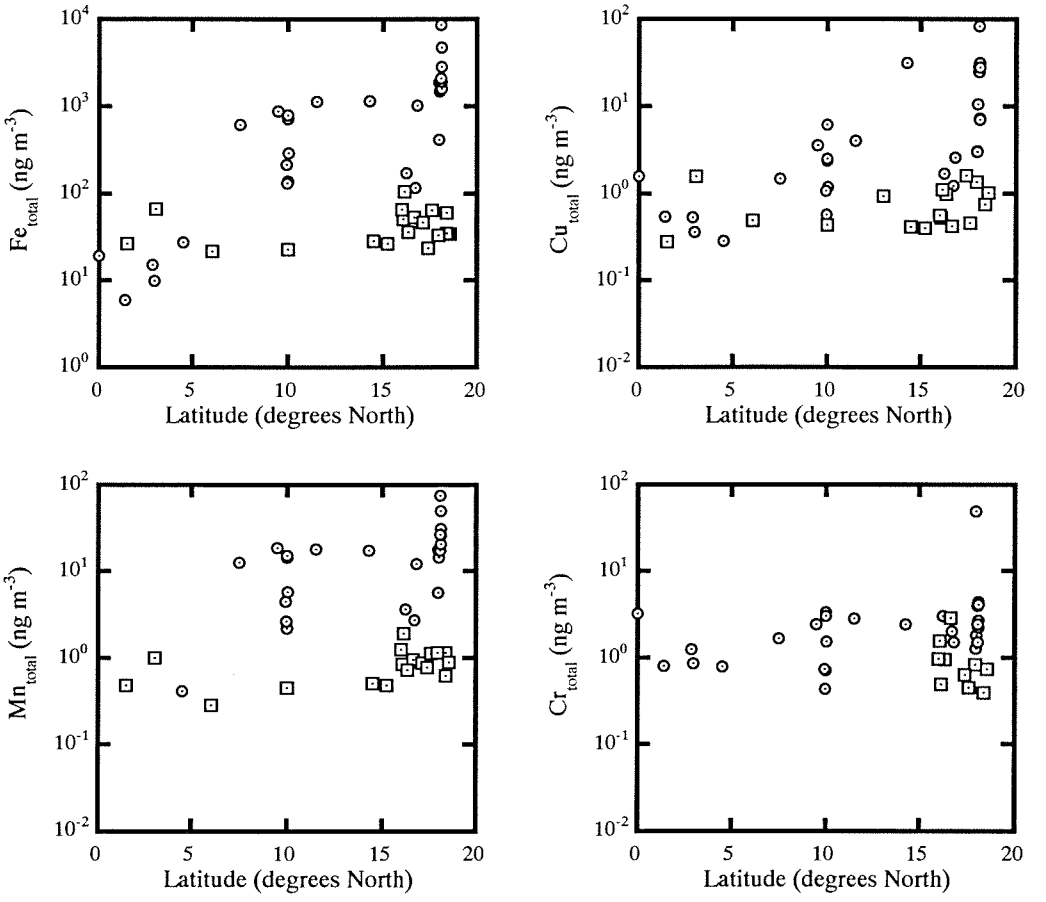
Fe_{total} (ng m^{-3})
Cu_{total} (ng m^{-3})
Mn_{total} (ng m^{-3})
Cr_{total} (ng m^{-3})
Latitude (degrees North)
Latitude (degrees North)
Latitude (degrees North)
Latitude (degrees North)

Figure 3

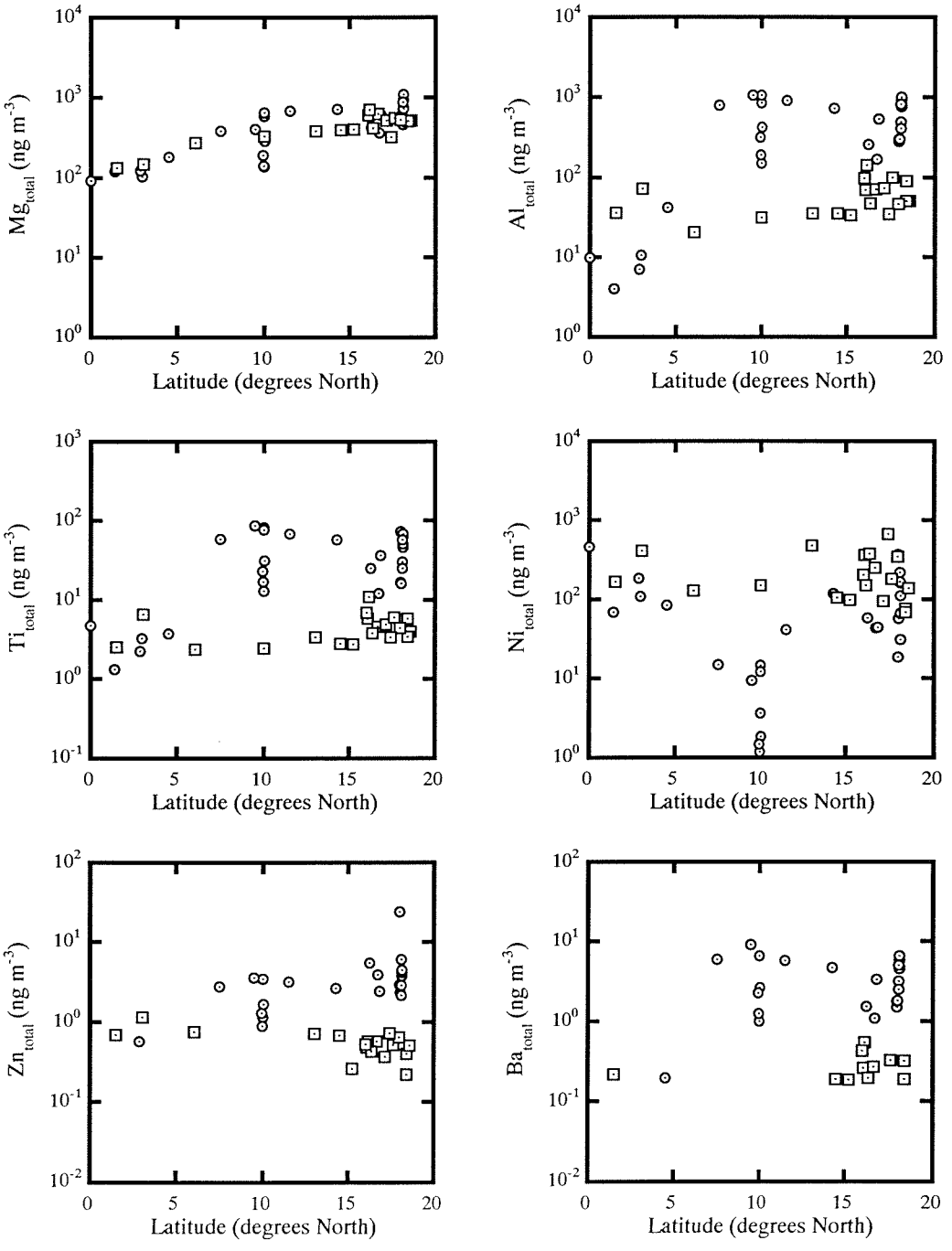
Mg_{total} (ng m^{-3})
Al_{total} (ng m^{-3})
Ti_{total} (ng m^{-3})
Ni_{total} (ng m^{-3})
Zn_{total} (ng m^{-3})
Ba_{total} (ng m^{-3})
Latitude (degrees North)

Figure 4

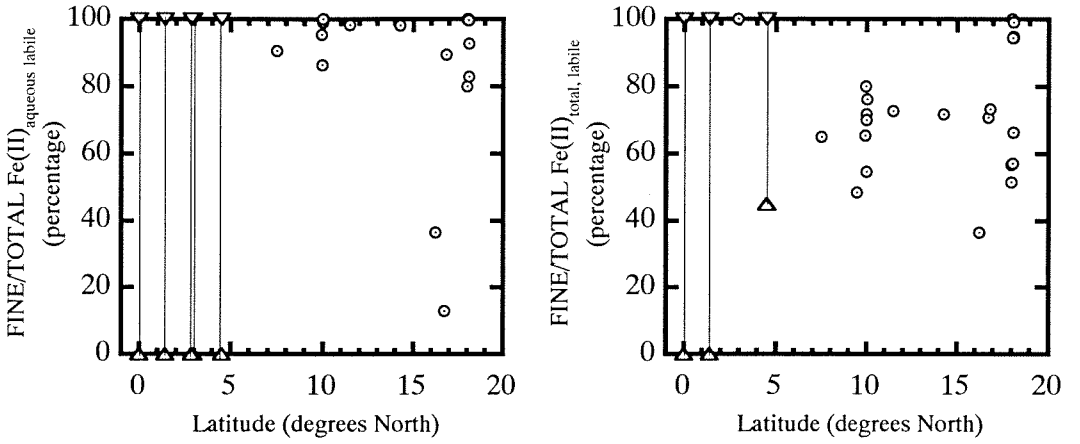
FINE/TOTAL Fe(II)aqueous labile (percentage)
100
80
60
40
20
0
0
5
10
15
20
Latitude (degrees North)
FINE/TOTAL Fe(II)total, labile (percentage)
100
80
60
40
20
0
0
5
10
15
20
Latitude (degrees North)

Figure 5

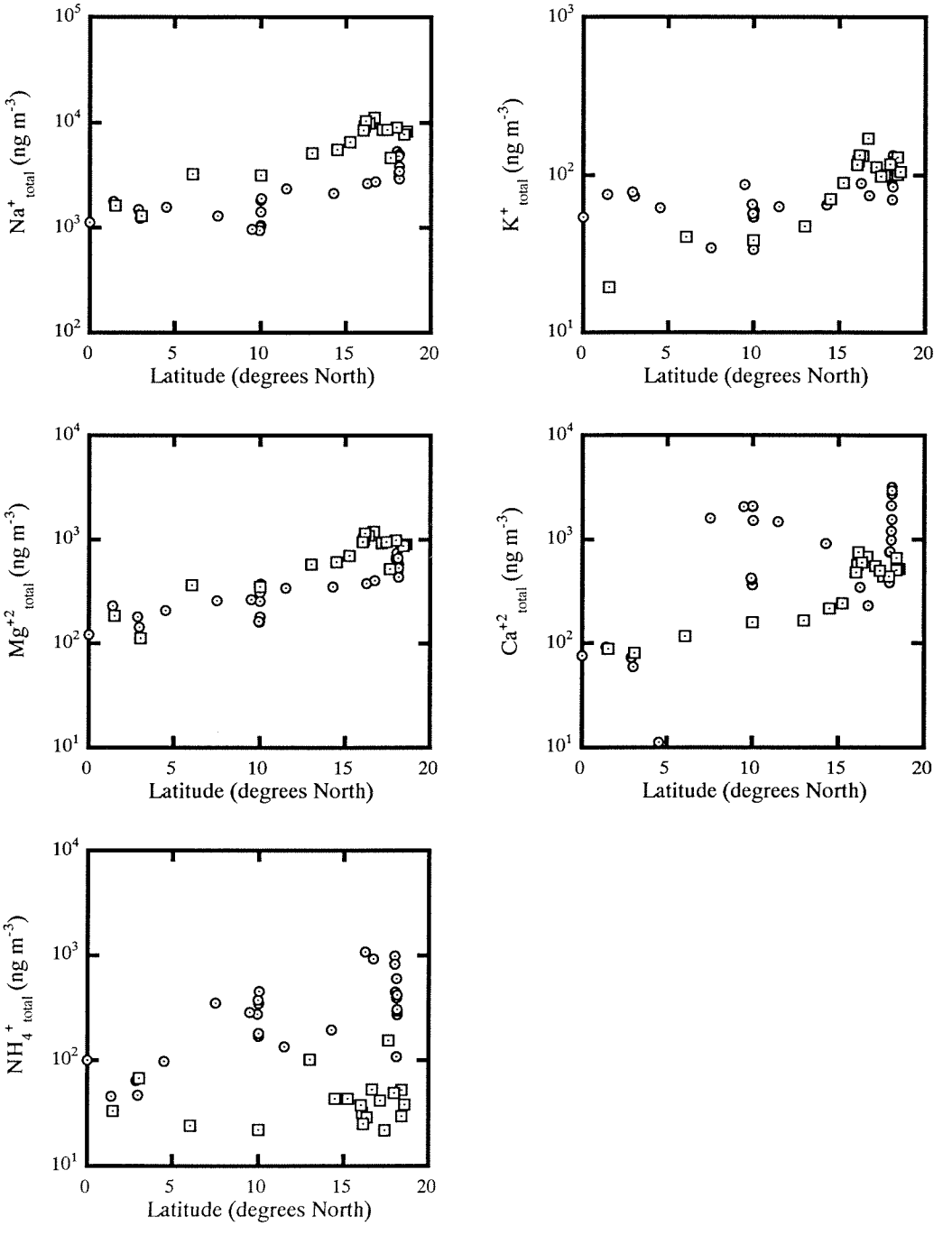
Na^{+}_{total} (ng m^{-3})
K^{+}_{total} (ng m^{-3})
Mg^{+2}_{total} (ng m^{-3})
Ca^{+2}_{total} (ng m^{-3})
$NH_4^{+}_{total}$ (ng m^{-3})
Latitude (degrees North)
Latitude (degrees North)
Latitude (degrees North)
Latitude (degrees North)
Latitude (degrees North)

Figure 6

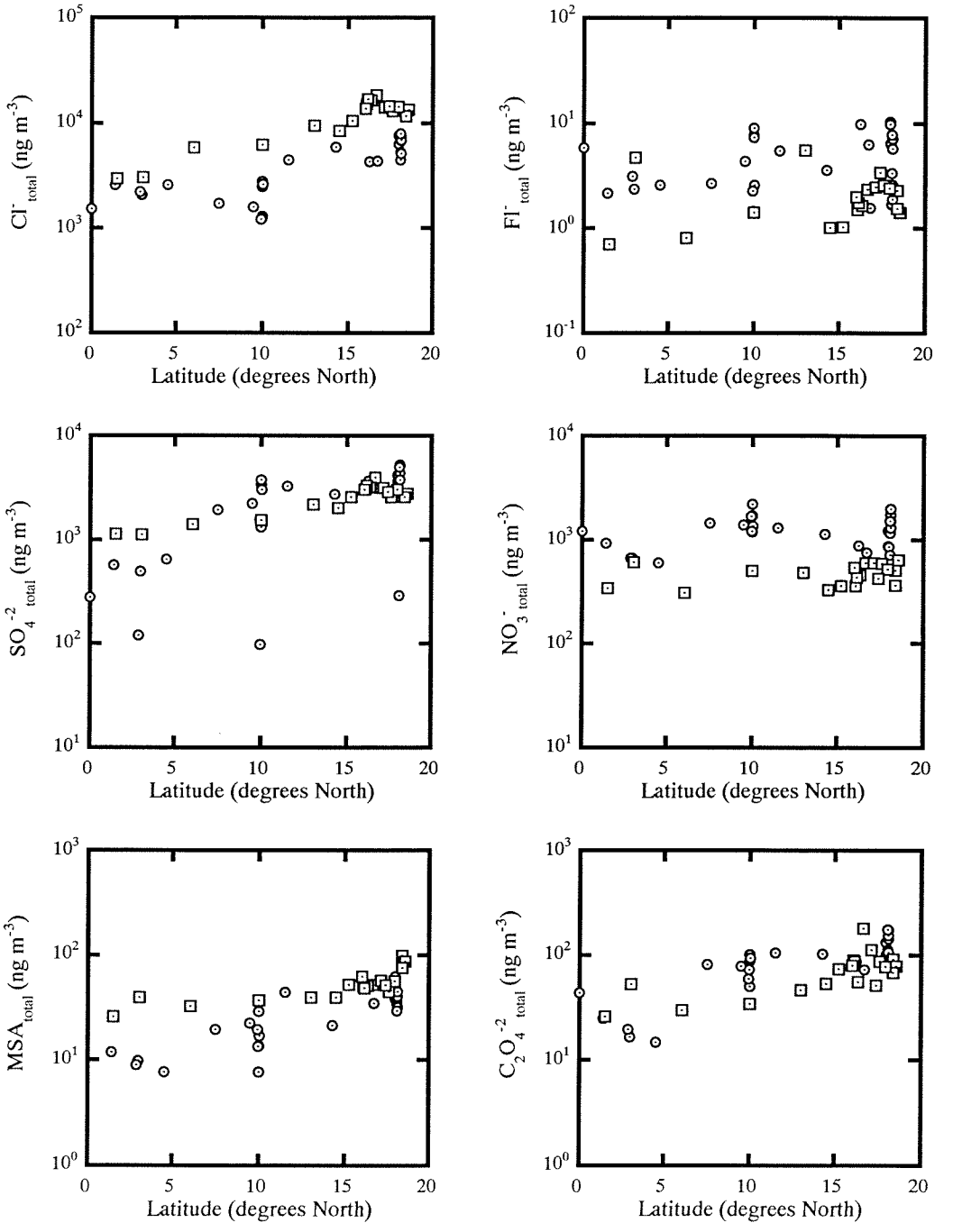
Cl^-_{total} (ng m^{-3})
Fl^-_{total} (ng m^{-3})
$SO_4^{-2}{}_{total}$ (ng m^{-3})
$NO_3^-{}_{total}$ (ng m^{-3})
MSA_{total} (ng m^{-3})
$C_2O_4^{-2}{}_{total}$ (ng m^{-3})
Latitude (degrees North)
0
5
10
15
20

Figure 7

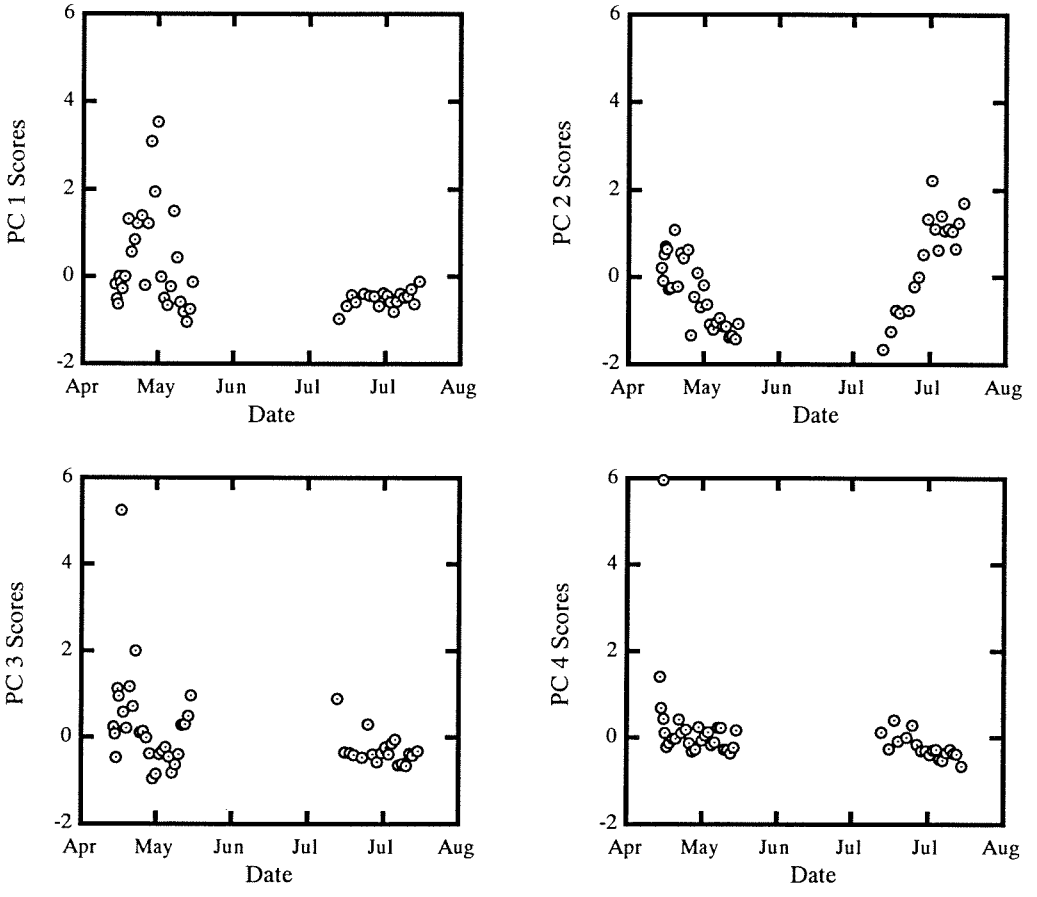
PC 1 Scores
PC 2 Scores
PC 3 Scores
PC 4 Scores
6
4
2
0
-2
Apr
May
Jun
Jul
Jul
Aug
Date

SUPPLEMENTAL MATERIAL

Tables A-1, A-2 and A-3

TABLE A-1. Coarse (labels with a "C") and Fine (labels with a "F") elemental concentrations.

Label	Na 23 pmoles m^{-3}	Mg 24 pmoles m^{-3}	Al 27 pmoles m^{-3}	K 39 pmoles m^{-3}
M32/3_01_C	1.08E+5 ± 9.1E+3	1.27E+4 ± 8.3E+2	4.22E+3 ± 3.1E+2	3.15E+3 ± 3.2E+2
M32/3_01_F	2.92E+4 ± 3.1E+3	4.79E+3 ± 3.2E+2	5.36E+3 ± 3.8E+2	2.56E+3 ± 2.7E+2
M32/3_02_C	8.52E+4 ± 7.6E+3	1.10E+4 ± 7.5E+2	3.04E+3 ± 2.3E+2	2.50E+3 ± 2.7E+2
M32/3_02_F	2.76E+4 ± 2.8E+3	4.01E+3 ± 3.0E+2	3.27E+3 ± 2.4E+2	2.20E+3 ± 2.3E+2
M32/3_03_C	1.26E+5 ± 1.0E+4	1.56E+4 ± 9.7E+2	4.26E+3 ± 3.0E+2	3.55E+3 ± 3.8E+2
M32/3_03_F	3.87E+4 ± 3.9E+3	6.52E+3 ± 4.0E+2	6.18E+3 ± 3.8E+2	2.72E+3 ± 2.8E+2
M32/3_04_C	SD[a]	1.71E+4 ± 8.5E+2	7.75E+3 ± 3.9E+2	3.49E+3 ± 1.9E+2
M32/3_04_F	2.65E+4 ± 1.5E+3	4.12E+3 ± 2.3E+2	3.53E+3 ± 2.0E+2	1.71E+3 ± 1.3E+2
M32/3_05_C	9.45E+4 ± 4.1E+3	1.53E+4 ± 7.0E+2	7.48E+3 ± 3.5E+2	3.30E+3 ± 1.7E+2
M32/3_05_F	3.28E+4 ± 1.9E+3	4.73E+3 ± 2.7E+2	3.60E+3 ± 2.1E+2	1.72E+3 ± 1.6E+2
M32/3_06_C	1.07E+5 ± 5.0E+3	2.26E+4 ± 1.1E+3	1.29E+4 ± 7.1E+2	4.78E+3 ± 2.9E+2
M32/3_06_F	3.61E+4 ± 2.2E+3	6.38E+3 ± 3.8E+2	5.49E+3 ± 3.1E+2	1.86E+3 ± 1.8E+2
M32/3_07_C	SD	1.42E+4 ± 7.4E+2	1.04E+4 ± 6.0E+2	3.22E+3 ± 2.0E+2
M32/3_07_F	2.45E+4 ± 1.1E+3	4.80E+3 ± 2.2E+2	4.87E+3 ± 2.3E+2	1.53E+3 ± 8.2E+1
M32/3_08_C	SD	2.31E+4 ± 1.1E+3	1.99E+4 ± 9.0E+2	5.62E+3 ± 2.7E+2
M32/3_08_F	3.25E+4 ± 1.6E+3	8.00E+3 ± 4.0E+2	8.69E+3 ± 4.8E+2	2.76E+3 ± 1.6E+2
M32/3_09_C	SD	1.82E+4 ± 8.2E+2	1.79E+4 ± 8.3E+2	4.72E+3 ± 2.4E+2
M32/3_09_F	4.16E+4 ± 2.0E+3	1.16E+4 ± 6.1E+2	1.23E+4 ± 6.5E+2	3.55E+3 ± 1.9E+2
M32/3_10_C	SD	2.30E+4 ± 1.1E+3	1.98E+4 ± 9.5E+2	6.12E+3 ± 3.1E+2
M32/3_10_F	4.28E+4 ± 2.2E+3	1.60E+4 ± 8.2E+2	1.53E+4 ± 8.3E+2	4.16E+3 ± 2.4E+2
M32/3_11_C	7.26E+4 ± 3.4E+3	2.54E+4 ± 1.3E+3	1.97E+4 ± 1.1E+3	5.56E+3 ± 3.0E+2
M32/3_11_F	4.77E+4 ± 2.3E+3	1.94E+4 ± 9.9E+2	1.78E+4 ± 9.3E+2	4.96E+3 ± 2.7E+2
M32/3_12_C	SD	2.40E+4 ± 1.1E+3	1.97E+4 ± 9.0E+2	6.64E+3 ± 3.2E+2
M32/3_12_F	5.45E+4 ± 2.6E+3	1.23E+4 ± 6.8E+2	1.07E+4 ± 6.3E+2	3.76E+3 ± 2.2E+2
M32/3_13_C	SD	1.54E+4 ± 7.2E+2	1.19E+4 ± 5.7E+2	4.16E+3 ± 2.1E+2
M32/3_13_F	4.72E+4 ± 2.3E+3	9.65E+3 ± 5.2E+2	7.95E+3 ± 4.7E+2	2.83E+3 ± 1.7E+2
M32/3_14_C	SD	2.15E+4 ± 1.4E+3	1.93E+4 ± 1.2E+3	5.53E+3 ± 3.5E+2
M32/3_14_F	3.78E+4 ± 2.2E+3	7.76E+3 ± 4.8E+2	8.06E+3 ± 4.8E+2	2.40E+3 ± 1.4E+2
M32/3_15_C	SD	2.18E+4 ± 1.4E+3	2.52E+4 ± 1.5E+3	5.86E+3 ± 3.6E+2
M32/3_15_F	2.17E+4 ± 1.3E+3	6.09E+3 ± 3.9E+2	8.54E+3 ± 5.1E+2	2.09E+3 ± 1.3E+2
M32/3_16_C	5.58E+4 ± 3.3E+3	1.69E+4 ± 1.1E+3	2.02E+4 ± 1.2E+3	6.01E+3 ± 3.7E+2
M32/3_16_F	2.15E+4 ± 1.5E+3	7.02E+3 ± 5.1E+2	1.13E+4 ± 7.7E+2	2.60E+3 ± 2.0E+2
M32/3_17_C	4.33E+4 ± 2.7E+3	2.11E+4 ± 1.4E+3	2.98E+4 ± 1.8E+3	5.86E+3 ± 3.8E+2
M32/3_17_F	1.31E+4 ± 8.8E+2	5.34E+3 ± 3.8E+2	9.37E+3 ± 6.1E+2	2.01E+3 ± 1.4E+2
M32/3_18_C	2.67E+4 ± 1.6E+3	7.60E+3 ± 4.8E+2	8.79E+3 ± 5.3E+2	2.09E+3 ± 1.3E+2
M32/3_18_F	1.31E+4 ± 8.1E+2	4.19E+3 ± 2.7E+2	6.90E+3 ± 4.2E+2	1.52E+3 ± 9.9E+1
M32/3_19_C	2.16E+4 ± 1.9E+3	3.56E+3 ± 3.4E+2	3.06E+3 ± 2.8E+2	1.07E+3 ± 1.3E+2
M32/3_19_F	8.69E+3 ± 5.8E+2	2.05E+3 ± 1.4E+2	2.55E+3 ± 1.6E+2	7.66E+2 ± 5.8E+1
M32/3_20_C	1.60E+4 ± 9.7E+2	3.71E+3 ± 2.3E+2	3.98E+3 ± 2.4E+2	1.02E+3 ± 6.5E+1
M32/3_20_F	8.44E+3 ± 5.6E+2	2.10E+3 ± 1.4E+2	3.09E+3 ± 2.0E+2	7.71E+2 ± 5.9E+1
M32/3_21_C	2.13E+4 ± 1.3E+3	5.31E+3 ± 3.4E+2	7.16E+3 ± 4.5E+2	1.95E+3 ± 1.3E+2
M32/3_21_F	8.49E+3 ± 5.2E+2	2.61E+3 ± 1.7E+2	4.60E+3 ± 2.8E+2	1.18E+3 ± 7.4E+1
M32/3_22_C	2.47E+4 ± 1.5E+3	9.27E+3 ± 5.9E+2	2.34E+4 ± 1.4E+3	7.54E+3 ± 4.7E+2
M32/3_22_F	7.37E+3 ± 4.5E+2	7.30E+3 ± 4.6E+2	1.65E+4 ± 9.6E+2	3.96E+3 ± 2.4E+2
M32/3_23_C	2.35E+4 ± 1.5E+3	9.73E+3 ± 6.6E+2	1.57E+4 ± 9.7E+2	4.69E+3 ± 3.0E+2
M32/3_23_F	9.85E+3 ± 6.2E+2	6.06E+3 ± 3.9E+2	1.35E+4 ± 8.1E+2	3.44E+3 ± 2.1E+2
M32/3_24_C	5.06E+4 ± 4.3E+3	5.94E+3 ± 3.9E+2	8.17E+2 ± 5.7E+1	1.33E+3 ± 1.4E+2
M32/3_24_F	1.11E+4 ± 1.2E+3	1.48E+3 ± 9.5E+1	7.28E+2 ± 4.8E+1	3.42E+2 ± 6.7E+1

[a] saturated detector

TABLE A-1 (cont). Coarse (labels with a "C") and Fine (labels with a "F") elemental concentrations.

Label	Na 23 pmoles m-3	Mg 24 pmoles m-3	Al 27 pmoles m-3	K 39 pmoles m-3
M32/3_25_C	3.20E+4 ± 3.0E+3	3.38E+3 ± 2.2E+2	1.52E+2 ± 1.1E+1	7.09E+2 ± 1.0E+2
M32/3_25_F	8.57E+3 ± 1.0E+3	8.95E+2 ± 5.3E+1	2.41E+2 ± 1.8E+1	2.36E+2 ± 6.3E+1
M32/3_26_C	3.95E+4 ± 3.8E+3	4.17E+3 ± 2.7E+2	1.06E+2 ± 1.0E+1	9.15E+2 ± 1.4E+2
M32/3_26_F	8.23E+3 ± 9.2E+2	8.71E+2 ± 5.4E+1	1.57E+2 ± 1.3E+1	< 279.21E+0
M32/3_27_C	4.12E+4 ± 3.3E+3	3.96E+3 ± 2.5E+2	5.56E+1 ± 4.9E+0	9.47E+2 ± 1.0E+2
M32/3_27_F	9.85E+3 ± 1.2E+3	1.01E+3 ± 7.1E+1	9.43E+1 ± 6.9E+0	2.53E+2 ± 7.6E+1
M32/3_28_C	2.21E+4 ± 2.9E+3	2.74E+3 ± 1.8E+2	1.48E+2 ± 1.6E+1	< 658.31E+0
M32/3_28_F	1.10E+4 ± 2.4E+3	1.07E+3 ± 8.6E+1	2.20E+2 ± 1.9E+1	< 658.31E+0
M32/5_01_C	SD	2.84E+3 ± 1.5E+2	1.36E+2 ± 1.4E+1	6.67E+2 ± 5.3E+1
M32/5_01_F	SD	9.81E+2 ± 4.8E+1	< 50.13E+0	< 267.43E+0
M32/5_02_C	SD	4.03E+3 ± 1.9E+2	7.42E+2 ± 3.8E+1	9.12E+2 ± 5.2E+1
M32/5_02_F	SD	1.47E+3 ± 7.9E+1	5.88E+2 ± 3.3E+1	3.84E+2 ± 3.6E+1
M32/5_03_C	SD	4.02E+3 ± 2.0E+2	1.46E+3 ± 7.6E+1	1.15E+3 ± 1.3E+2
M32/5_03_F	2.39E+4 ± 1.4E+3	2.02E+3 ± 1.1E+2	1.23E+3 ± 6.8E+1	< 1.12E+3
M32/5_04_C	SD	8.12E+3 ± 3.7E+2	4.47E+2 ± 2.3E+1	1.60E+3 ± 8.6E+1
M32/5_04_F	SD	3.04E+3 ± 1.6E+2	3.19E+2 ± 1.8E+1	6.58E+2 ± 5.2E+1
M32/5_05_C	SD	8.16E+3 ± 3.8E+2	8.64E+2 ± 4.4E+1	1.55E+3 ± 8.4E+1
M32/5_05_F	SD	5.24E+3 ± 2.5E+2	2.97E+2 ± 1.8E+1	1.02E+3 ± 6.0E+1
M32/5_06_C	SD	5.58E+3 ± 2.6E+2	1.95E+2 ± 1.2E+1	7.78E+2 ± 7.1E+1
M32/5_06_F	SD	1.01E+4 ± 4.8E+2	1.12E+3 ± 6.0E+1	1.73E+3 ± 1.0E+2
M32/5_07_C	SD	9.20E+3 ± 4.1E+2	8.22E+2 ± 3.9E+1	1.97E+3 ± 9.4E+1
M32/5_07_F	SD	7.08E+3 ± 3.3E+2	4.94E+2 ± 2.6E+1	1.53E+3 ± 8.1E+1
M32/5_08_C	SD	7.70E+3 ± 3.7E+2	6.91E+2 ± 3.5E+1	2.06E+3 ± 1.1E+2
M32/5_08_F	SD	8.99E+3 ± 4.7E+2	5.65E+2 ± 3.2E+1	1.81E+3 ± 1.1E+2
M32/5_09_C	SD	1.61E+4 ± 7.3E+2	1.96E+3 ± 9.6E+1	3.50E+3 ± 1.7E+2
M32/5_09_F	SD	9.05E+3 ± 4.0E+2	6.31E+2 ± 3.0E+1	1.83E+3 ± 8.4E+1
M32/5_10_C	SD	1.43E+4 ± 8.4E+2	1.71E+3 ± 1.0E+2	3.12E+3 ± 2.5E+2
M32/5_10_F	SD	1.16E+4 ± 6.0E+2	9.37E+2 ± 5.2E+1	3.22E+3 ± 2.1E+2
M32/5_11_C	SD	1.12E+4 ± 6.0E+2	1.81E+3 ± 1.0E+2	2.35E+3 ± 1.8E+2
M32/5_11_F	SD	1.02E+4 ± 4.7E+2	8.99E+2 ± 4.4E+1	2.36E+3 ± 1.4E+2
M32/5_12_C	SD	1.12E+4 ± 5.5E+2	2.15E+3 ± 1.1E+2	2.45E+3 ± 1.6E+2
M32/5_12_F	SD	1.17E+4 ± 5.9E+2	1.54E+3 ± 8.4E+1	2.82E+3 ± 1.9E+2
M32/5_13_C	SD	1.07E+4 ± 5.1E+2	2.08E+3 ± 1.0E+2	2.31E+3 ± 1.4E+2
M32/5_13_F	SD	1.07E+4 ± 7.5E+2	1.28E+3 ± 9.2E+1	2.60E+3 ± 2.5E+2
M32/5_14_C	SD	1.23E+4 ± 6.2E+2	1.34E+3 ± 7.1E+1	2.58E+3 ± 1.8E+2
M32/5_14_F	SD	9.06E+3 ± 4.7E+2	5.42E+2 ± 3.0E+1	1.94E+3 ± 1.5E+2
M32/5_15_C	SD	1.24E+4 ± 7.2E+2	1.32E+3 ± 7.8E+1	2.94E+3 ± 2.8E+2
M32/5_15_F	SD	8.52E+3 ± 5.0E+2	5.58E+2 ± 3.5E+1	2.12E+3 ± 2.1E+2
M32/5_16_C	SD	1.16E+4 ± 6.7E+2	1.16E+3 ± 6.8E+1	2.52E+3 ± 2.6E+2
M32/5_16_F	SD	1.03E+4 ± 6.4E+2	5.59E+2 ± 3.4E+1	2.47E+3 ± 2.6E+2
M32/5_17_C	SD	4.30E+3 ± 2.8E+2	5.71E+2 ± 3.8E+1	1.03E+3 ± 1.5E+2
M32/5_17_F	SD	8.94E+3 ± 5.1E+2	7.32E+2 ± 4.8E+1	2.03E+3 ± 2.2E+2
M32/5_18_C	SD	7.00E+3 ± 4.4E+2	8.70E+2 ± 5.5E+1	1.67E+3 ± 1.8E+2
M32/5_18_F	SD	1.02E+4 ± 6.2E+2	8.89E+2 ± 5.6E+1	2.45E+3 ± 2.5E+2
M32/5_19_C	SD	1.86E+4 ± 9.9E+2	4.15E+3 ± 2.3E+2	5.02E+3 ± 4.6E+2
M32/5_19_F	SD	1.04E+4 ± 8.5E+2	1.16E+3 ± 9.9E+1	2.46E+3 ± 3.4E+2
M32/5_20_C	SD	SD ±	2.93E+3 ± 1.4E+2	3.81E+3 ± 1.9E+2
M32/5_20_F	SD	8.79E+3 ± 4.0E+2	7.10E+2 ± 3.5E+1	1.78E+3 ± 9.0E+1

TABLE A-1 (cont). Coarse (labels with a "C") and Fine (labels with a "F") elemental concentrations.

Label	Ca 44 pmoles m^{-3}	Ti 47 pmoles m^{-3}	V 51 pmoles m^{-3}	Cr 52 pmoles m^{-3}
M32/3_01_C	4.90E+3 ± 3.9E+2	2.01E+2 ± 1.8E+1	7.71E+0 ± 9.1E-1	2.82E+1 ± 2.6E+0
M32/3_01_F	2.39E+3 ± 2.5E+2	3.20E+2 ± 2.2E+1	1.74E+1 ± 1.3E+0	2.98E+1 ± 3.1E+0
M32/3_02_C	3.81E+3 ± 3.0E+2	1.26E+2 ± 1.2E+1	4.60E+0 ± 4.7E-1	1.63E+1 ± 1.7E+0
M32/3_02_F	1.81E+3 ± 1.7E+2	1.27E+2 ± 1.2E+1	1.16E+1 ± 8.1E-1	2.20E+1 ± 2.4E+0
M32/3_03_C	5.67E+3 ± 4.7E+2	1.70E+2 ± 1.4E+1	7.08E+0 ± 9.5E-1	3.25E+1 ± 3.4E+0
M32/3_03_F	2.26E+3 ± 2.6E+2	1.36E+3 ± 8.8E+1	4.35E+1 ± 2.7E+0	9.04E+2 ± 5.2E+1
M32/3_04_C	1.51E+4 ± 7.2E+2	2.35E+2 ± 1.3E+1	8.12E+0 ± 5.7E-1	1.42E+1 ± 9.8E-1
M32/3_04_F	1.95E+3 ± 1.3E+2	1.11E+2 ± 5.9E+0	8.30E+0 ± 6.8E-1	1.01E+1 ± 1.2E+0
M32/3_05_C	1.20E+4 ± 6.0E+2	2.23E+2 ± 1.3E+1	7.15E+0 ± 6.7E-1	1.62E+1 ± 9.7E-1
M32/3_05_F	1.63E+3 ± 1.2E+2	1.15E+2 ± 7.9E+0	8.97E+0 ± 7.3E-1	1.88E+1 ± 1.4E+0
M32/3_06_C	2.83E+4 ± 1.4E+3	4.62E+2 ± 2.7E+1	1.48E+1 ± 1.1E+0	5.02E+1 ± 3.6E+0
M32/3_06_F	3.99E+3 ± 2.5E+2	1.70E+2 ± 1.2E+1	1.10E+1 ± 8.7E-1	2.54E+1 ± 2.1E+0
M32/3_07_C	1.96E+4 ± 1.0E+3	3.79E+2 ± 2.1E+1	1.09E+1 ± 7.7E-1	1.38E+1 ± 9.2E-1
M32/3_07_F	3.60E+3 ± 1.8E+2	1.43E+2 ± 7.2E+0	1.07E+1 ± 5.4E-1	1.50E+1 ± 4.5E+0
M32/3_08_C	3.06E+4 ± 1.4E+3	6.68E+2 ± 3.1E+1	2.15E+1 ± 1.2E+0	2.66E+1 ± 1.4E+0
M32/3_08_F	6.73E+3 ± 3.5E+2	2.89E+2 ± 1.6E+1	1.71E+1 ± 1.1E+0	1.62E+1 ± 1.1E+0
M32/3_09_C	2.52E+4 ± 1.2E+3	5.92E+2 ± 3.3E+1	1.61E+1 ± 8.9E-1	2.77E+1 ± 1.6E+0
M32/3_09_F	1.08E+4 ± 5.3E+2	4.67E+2 ± 2.6E+1	2.12E+1 ± 1.3E+0	2.41E+1 ± 1.7E+0
M32/3_10_C	3.16E+4 ± 1.6E+3	7.68E+2 ± 3.8E+1	2.47E+1 ± 1.2E+0	3.46E+1 ± 1.8E+0
M32/3_10_F	1.62E+4 ± 7.9E+2	5.42E+2 ± 2.9E+1	2.65E+1 ± 1.7E+0	4.98E+1 ± 3.1E+0
M32/3_11_C	3.61E+4 ± 1.7E+3	7.26E+2 ± 4.3E+1	2.35E+1 ± 1.4E+0	4.21E+1 ± 2.5E+0
M32/3_11_F	2.13E+4 ± 1.0E+3	6.86E+2 ± 3.8E+1	3.21E+1 ± 1.8E+0	3.69E+1 ± 2.1E+0
M32/3_12_C	3.91E+4 ± 1.9E+3	7.77E+2 ± 3.9E+1	2.26E+1 ± 1.2E+0	2.83E+1 ± 1.6E+0
M32/3_12_F	1.23E+4 ± 6.2E+2	4.28E+2 ± 3.0E+1	1.92E+1 ± 1.2E+0	1.84E+1 ± 1.3E+0
M32/3_13_C	1.73E+4 ± 8.1E+2	4.51E+2 ± 2.2E+1	1.37E+1 ± 7.9E-1	1.77E+1 ± 9.8E-1
M32/3_13_F	7.56E+3 ± 4.0E+2	3.14E+2 ± 1.6E+1	1.48E+1 ± 9.0E-1	1.13E+1 ± 8.2E-1
M32/3_14_C	3.08E+4 ± 2.0E+3	8.60E+2 ± 5.5E+1	2.45E+1 ± 3.1E+0	2.94E+1 ± 2.1E+0
M32/3_14_F	6.86E+3 ± 4.3E+2	3.36E+2 ± 2.1E+1	1.52E+1 ± 2.0E+0	1.70E+1 ± 1.3E+0
M32/3_15_C	3.99E+4 ± 2.4E+3	1.07E+3 ± 6.7E+1	3.12E+1 ± 3.9E+0	3.91E+1 ± 2.5E+0
M32/3_15_F	6.54E+3 ± 4.3E+2	3.47E+2 ± 2.3E+1	1.75E+1 ± 2.2E+0	1.50E+1 ± 1.2E+0
M32/3_16_C	1.61E+4 ± 1.0E+3	1.21E+3 ± 7.9E+1	3.77E+1 ± 4.8E+0	3.74E+1 ± 2.4E+0
M32/3_16_F	7.81E+3 ± 5.5E+2	4.96E+2 ± 3.6E+1	3.67E+1 ± 4.8E+0	2.67E+1 ± 2.5E+0
M32/3_17_C	4.72E+4 ± 3.1E+3	1.24E+3 ± 8.3E+1	3.98E+1 ± 5.0E+0	4.03E+1 ± 2.9E+0
M32/3_17_F	5.67E+3 ± 4.4E+2	3.71E+2 ± 2.6E+1	3.51E+1 ± 4.6E+0	1.78E+1 ± 1.6E+0
M32/3_18_C	1.22E+4 ± 7.5E+2	3.69E+2 ± 2.5E+1	1.10E+1 ± 1.4E+0	1.59E+1 ± 2.0E+0
M32/3_18_F	4.24E+3 ± 2.8E+2	2.81E+2 ± 1.9E+1	1.54E+1 ± 1.9E+0	1.38E+1 ± 1.3E+0
M32/3_19_C	4.17E+3 ± 3.9E+2	1.30E+2 ± 1.3E+1	4.34E+0 ± 7.4E-1	5.44E+0 ± 1.2E+0
M32/3_19_F	1.45E+3 ± 1.0E+2	1.42E+2 ± 1.1E+1	7.50E+0 ± 1.0E+0	8.25E+0 ± 8.1E-1
M32/3_20_C	5.09E+3 ± 3.1E+2	1.77E+2 ± 1.2E+1	6.33E+0 ± 8.8E-1	6.23E+0 ± 7.0E-1
M32/3_20_F	1.83E+3 ± 1.3E+2	1.75E+2 ± 1.3E+1	1.21E+1 ± 1.6E+0	2.09E+0 ± 7.9E-1
M32/3_21_C	6.68E+3 ± 4.4E+2	2.84E+2 ± 1.8E+1	9.83E+0 ± 1.3E+0	8.14E+0 ± 4.4E+0
M32/3_21_F	1.86E+3 ± 1.2E+2	1.94E+2 ± 1.4E+1	1.67E+1 ± 2.1E+0	6.11E+0 ± 6.5E-1
M32/3_22_C	1.84E+4 ± 1.2E+3	1.23E+3 ± 7.7E+1	3.89E+1 ± 4.9E+0	3.05E+1 ± 2.2E+0
M32/3_22_F	7.58E+3 ± 4.7E+2	5.92E+2 ± 3.8E+1	2.87E+1 ± 3.6E+0	1.59E+1 ± 1.2E+0
M32/3_23_C	1.11E+4 ± 7.2E+2	7.15E+2 ± 4.6E+1	2.21E+1 ± 2.9E+0	1.85E+1 ± 1.6E+0
M32/3_23_F	5.64E+3 ± 3.8E+2	5.01E+2 ± 3.3E+1	2.38E+1 ± 3.0E+0	1.37E+1 ± 1.1E+0
M32/3_24_C	1.88E+3 ± 1.4E+2	2.74E+1 ± 4.0E+0	1.02E+0 ± 1.2E-1	6.22E+0 ± 6.9E-1
M32/3_24_F	5.85E+2 ± 7.1E+1	5.00E+1 ± 5.1E+0	1.75E+0 ± 2.2E-1	9.00E+0 ± 7.9E-1

TABLE A-1 (cont). Coarse (labels with a "C") and Fine (labels with a "F") elemental concentrations.

Label	Ca 44 pmoles m-3	Ti 47 pmoles m-3	V 51 pmoles m-3	Cr 52 pmoles m-3
M32/3_25_C	8.01E+2 ± 9.9E+1	4.98E+1 ± 4.2E+0	< 486.90E-3	1.02E+1 ± 1.1E+0
M32/3_25_F	3.52E+2 ± 6.6E+1	1.79E+1 ± 3.1E+0	5.95E-1 ± 1.4E-1	6.32E+0 ± 7.5E-1
M32/3_26_C	9.75E+2 ± 1.3E+2	3.08E+1 ± 4.9E+0	< 642.26E-3	1.30E+1 ± 1.4E+0
M32/3_26_F	3.51E+2 ± 8.5E+1	1.62E+1 ± 4.2E+0	< 642.26E-3	1.12E+1 ± 1.4E+0
M32/3_27_C	8.88E+2 ± 1.0E+2	1.13E+1 ± 3.0E+0	< 539.41E-3	6.41E+0 ± 9.9E-1
M32/3_27_F	3.10E+2 ± 7.4E+1	1.63E+1 ± 2.7E+0	< 539.41E-3	9.07E+0 ± 9.0E-1
M32/3_28_C	7.47E+2 ± 2.2E+2	5.34E+1 ± 9.9E+0	< 1.51E+0	3.60E+1 ± 3.3E+0
M32/3_28_F	6.86E+2 ± 2.6E+2	4.54E+1 ± 7.3E+0	< 1.51E+0	2.65E+1 ± 3.6E+0
M32/5_01_C	6.54E+2 ± 5.6E+1	6.43E+1 ± 5.6E+0	< 3.30E+0	1.89E+1 ± 1.6E+0
M32/5_01_F	1.60E+2 ± 2.1E+1	2.67E+1 ± 2.7E+0	< 3.30E+0	< 5.53E+0
M32/5_02_C	1.31E+3 ± 7.3E+1	2.58E+1 ± 2.3E+0	< 2.33E+0	< 3.91E+0
M32/5_02_F	5.08E+2 ± 4.5E+1	2.71E+1 ± 2.4E+0	< 2.33E+0	6.54E+0 ± 6.2E-1
M32/5_03_C	1.42E+3 ± 1.4E+2	6.86E+1 ± 7.8E+0	< 13.84E+0	< 23.15E+0
M32/5_03_F	7.95E+2 ± 1.2E+2	6.67E+1 ± 6.0E+0	< 13.84E+0	2.52E+1 ± 3.5E+0
M32/5_04_C	1.92E+3 ± 1.0E+2	3.08E+1 ± 2.6E+0	< 3.42E+0	< 5.73E+0
M32/5_04_F	6.48E+2 ± 6.1E+1	1.86E+1 ± 2.3E+0	< 3.42E+0	< 5.73E+0
M32/5_05_C	2.37E+3 ± 1.3E+2	3.58E+1 ± 3.4E+0	< 3.28E+0	< 5.49E+0
M32/5_05_F	9.82E+2 ± 6.0E+1	1.50E+1 ± 1.7E+0	< 3.28E+0	< 5.49E+0
M32/5_06_C	9.98E+2 ± 9.2E+1	1.63E+1 ± 2.6E+0	< 8.54E+0	< 14.30E+0
M32/5_06_F	2.95E+3 ± 1.7E+2	5.45E+1 ± 5.6E+0	< 8.54E+0	< 14.30E+0
M32/5_07_C	2.70E+3 ± 1.3E+2	3.90E+1 ± 2.4E+0	< 2.47E+0	< 4.14E+0
M32/5_07_F	1.57E+3 ± 8.7E+1	1.90E+1 ± 1.4E+0	< 2.47E+0	< 4.14E+0
M32/5_08_C	2.69E+3 ± 1.4E+2	3.61E+1 ± 3.1E+0	< 2.23E+0	4.16E+0 ± 4.0E-1
M32/5_08_F	2.06E+3 ± 1.2E+2	2.13E+1 ± 1.9E+0	2.98E+0 ± 2.5E-1	< 3.73E+0
M32/5_09_C	6.69E+3 ± 3.3E+2	7.92E+1 ± 5.1E+0	< 2.98E+0	7.93E+0 ± 7.3E-1
M32/5_09_F	2.90E+3 ± 1.3E+2	4.29E+1 ± 3.3E+0	< 2.98E+0	2.20E+1 ± 1.2E+0
M32/5_10_C	6.07E+3 ± 4.1E+2	6.54E+1 ± 5.2E+0	< 2.15E+0	3.09E+0 ± 9.6E-1
M32/5_10_F	4.25E+3 ± 2.5E+2	3.00E+1 ± 2.8E+0	< 2.15E+0	5.18E+1 ± 2.8E+0
M32/5_11_C	5.03E+3 ± 3.2E+2	7.39E+1 ± 4.9E+0	< 2.28E+0	3.74E+0 ± 1.1E+0
M32/5_11_F	3.63E+3 ± 2.0E+2	2.88E+1 ± 2.5E+0	< 2.28E+0	< 2.46E+0
M32/5_12_C	6.12E+3 ± 3.4E+2	7.55E+1 ± 5.0E+0	< 2.08E+0	3.08E+0 ± 7.9E-1
M32/5_12_F	5.71E+3 ± 3.4E+2	5.09E+1 ± 4.2E+0	< 2.08E+0	5.64E+0 ± 8.8E-1
M32/5_13_C	5.87E+3 ± 3.2E+2	7.34E+1 ± 5.0E+0	< 2.00E+0	4.60E+0 ± 7.7E-1
M32/5_13_F	5.32E+3 ± 4.2E+2	4.84E+1 ± 4.6E+0	6.61E+0 ± 9.7E-1	2.92E+0 ± 1.2E+0
M32/5_14_C	5.06E+3 ± 2.9E+2	5.43E+1 ± 5.2E+0	< 2.43E+0	4.27E+0 ± 9.0E-1
M32/5_14_F	3.32E+3 ± 2.2E+2	2.92E+1 ± 2.6E+0	2.87E+0 ± 6.4E-1	9.89E+0 ± 1.3E+0
M32/5_15_C	4.89E+3 ± 3.6E+2	5.43E+1 ± 5.5E+0	< 1.50E+0	1.77E+0 ± 5.9E-1
M32/5_15_F	2.91E+3 ± 2.1E+2	1.76E+1 ± 2.3E+0	7.23E+0 ± 6.0E-1	< 1.62E+0
M32/5_16_C	4.02E+3 ± 3.2E+2	6.53E+1 ± 6.0E+0	< 2.34E+0	6.84E+0 ± 1.0E+0
M32/5_16_F	3.00E+3 ± 2.5E+2	2.75E+1 ± 4.3E+0	3.19E+0 ± 6.6E-1	9.04E+0 ± 1.2E+0
M32/5_17_C	1.49E+3 ± 1.5E+2	2.65E+1 ± 3.4E+0	< 2.43E+0	7.27E+0 ± 1.3E+0
M32/5_17_F	2.97E+3 ± 2.4E+2	4.40E+1 ± 4.9E+0	< 2.43E+0	4.86E+0 ± 1.1E+0
M32/5_18_C	2.46E+3 ± 1.9E+2	4.28E+1 ± 4.1E+0	< 1.86E+0	9.17E+0 ± 1.2E+0
M32/5_18_F	3.99E+3 ± 3.0E+2	3.61E+1 ± 3.5E+0	< 1.86E+0	9.06E+0 ± 1.1E+0
M32/5_19_C	1.08E+4 ± 7.7E+2	1.78E+2 ± 1.1E+1	< 2.00E+0	6.93E+0 ± 9.4E-1
M32/5_19_F	4.31E+3 ± 4.3E+2	4.72E+1 ± 5.7E+0	< 2.00E+0	2.50E+0 ± 1.1E+0
M32/5_20_C	6.52E+3 ± 3.3E+2	1.18E+2 ± 7.4E+0	< 4.03E+0	8.14E+0 ± 7.8E-1
M32/5_20_F	2.15E+3 ± 1.1E+2	2.68E+1 ± 2.8E+0	< 4.03E+0	1.03E+1 ± 1.3E+0

TABLE A-1 (cont). Coarse (labels with a "C") and Fine (labels with a "F") elemental concentrations.

Label	Mn 55 pmoles m^{-3}	Fe 57 pmoles m^{-3}	Ni 60 pmoles m^{-3}	Cu 63 pmoles m^{-3}
M32/3_01_C	2.85E+1 ± 2.3E+0	1.37E+3 ± 1.6E+2	5.12E+2 ± 3.4E+1	1.12E+1 ± 1.3E+0
M32/3_01_F	3.72E+1 ± 3.0E+0	1.73E+3 ± 1.9E+2	4.72E+2 ± 3.4E+1	1.54E+1 ± 1.5E+0
M32/3_02_C	2.10E+1 ± 2.2E+0	1.07E+3 ± 1.3E+2	3.93E+2 ± 2.8E+1	8.98E+0 ± 8.8E-1
M32/3_02_F	2.83E+1 ± 2.1E+0	1.03E+3 ± 1.1E+2	3.43E+2 ± 2.4E+1	1.04E+1 ± 1.1E+0
M32/3_03_C	3.10E+1 ± 2.7E+0	1.52E+3 ± 1.5E+2	1.33E+3 ± 8.2E+1	1.80E+1 ± 1.3E+0
M32/3_03_F	7.16E+1 ± 5.8E+0	5.89E+3 ± 5.5E+2	5.02E+3 ± 3.0E+2	3.04E+1 ± 3.0E+0
M32/3_04_C	1.58E+2 ± 7.8E+0	1.41E+4 ± 7.2E+2	1.43E+2 ± 7.6E+0	2.71E+1 ± 1.6E+0
M32/3_04_F	1.64E+2 ± 9.1E+0	1.97E+4 ± 1.1E+3	1.74E+2 ± 9.5E+0	2.00E+1 ± 1.5E+0
M32/3_05_C	1.49E+2 ± 7.1E+0	1.48E+4 ± 7.1E+2	6.42E+2 ± 3.2E+1	8.52E+1 ± 4.2E+0
M32/3_05_F	1.13E+2 ± 7.0E+0	1.19E+4 ± 7.4E+2	3.27E+2 ± 2.0E+1	8.22E+1 ± 4.9E+0
M32/3_06_C	9.83E+2 ± 5.2E+1	1.11E+5 ± 5.5E+3	2.14E+3 ± 1.1E+2	4.73E+1 ± 2.6E+0
M32/3_06_F	3.91E+2 ± 2.3E+1	4.18E+4 ± 2.6E+3	1.58E+3 ± 8.5E+1	3.97E+2 ± 2.1E+1
M32/3_07_C	8.54E+1 ± 4.7E+0	5.35E+3 ± 3.5E+2	1.12E+2 ± 7.7E+0	1.47E+1 ± 1.1E+0
M32/3_07_F	2.33E+2 ± 1.1E+1	2.30E+4 ± 1.0E+3	2.66E+3 ± 1.2E+2	3.75E+2 ± 1.7E+1
M32/3_08_C	2.36E+2 ± 1.1E+1	1.60E+4 ± 7.7E+2	3.78E+2 ± 1.9E+1	7.81E+1 ± 3.7E+0
M32/3_08_F	1.42E+2 ± 7.8E+0	1.27E+4 ± 7.3E+2	1.46E+2 ± 8.0E+0	3.77E+1 ± 2.1E+0
M32/3_09_C	3.81E+2 ± 1.9E+1	3.59E+4 ± 2.7E+3	1.62E+3 ± 7.7E+1	4.69E+2 ± 2.2E+1
M32/3_09_F	1.79E+2 ± 1.1E+1	1.47E+4 ± 8.7E+2	2.55E+2 ± 1.3E+1	2.28E+1 ± 1.3E+0
M32/3_10_C	2.35E+2 ± 1.2E+1	1.59E+4 ± 7.9E+2	3.69E+2 ± 1.9E+1	8.61E+1 ± 4.4E+0
M32/3_10_F	2.38E+2 ± 1.3E+1	1.86E+4 ± 9.8E+2	7.63E+2 ± 4.1E+1	2.57E+1 ± 1.4E+0
M32/3_11_C	6.19E+2 ± 3.3E+1	6.29E+4 ± 3.2E+3	1.55E+3 ± 8.0E+1	3.63E+2 ± 1.8E+1
M32/3_11_F	2.95E+2 ± 1.6E+1	2.21E+4 ± 1.2E+3	1.18E+3 ± 6.0E+1	7.68E+1 ± 3.7E+0
M32/3_12_C	2.79E+2 ± 1.3E+1	2.22E+4 ± 1.0E+3	6.06E+2 ± 2.9E+1	2.38E+2 ± 1.1E+1
M32/3_12_F	2.05E+2 ± 1.2E+1	1.51E+4 ± 9.0E+2	2.24E+3 ± 1.2E+2	1.06E+3 ± 5.4E+1
M32/3_13_C	1.55E+2 ± 7.7E+0	1.48E+4 ± 7.3E+2	6.90E+2 ± 3.3E+1	2.83E+1 ± 2.1E+0
M32/3_13_F	6.48E+1 ± 3.7E+0	3.55E+3 ± 2.3E+2	5.76E+1 ± 3.5E+0	1.27E+1 ± 7.9E-1
M32/3_14_C	1.94E+2 ± 1.2E+1	1.15E+4 ± 1.0E+3	1.55E+3 ± 9.5E+1	4.60E+2 ± 2.9E+1
M32/3_14_F	1.22E+2 ± 7.2E+0	9.12E+3 ± 8.0E+2	4.81E+2 ± 2.9E+1	3.80E+1 ± 2.8E+0
M32/3_15_C	2.46E+2 ± 1.5E+1	1.48E+4 ± 1.3E+3	5.60E+2 ± 3.4E+1	4.36E+1 ± 2.7E+0
M32/3_15_F	8.14E+1 ± 5.0E+0	5.61E+3 ± 4.9E+2	1.38E+2 ± 8.8E+0	1.99E+1 ± 1.3E+0
M32/3_16_C	1.84E+2 ± 1.1E+1	8.91E+3 ± 7.9E+2	4.24E+1 ± 3.1E+0	2.32E+1 ± 1.7E+0
M32/3_16_F	7.83E+1 ± 5.6E+0	3.85E+3 ± 3.7E+2	1.92E+1 ± 1.7E+0	1.45E+1 ± 1.1E+0
M32/3_17_C	2.14E+2 ± 1.4E+1	1.12E+4 ± 1.0E+3	2.13E+2 ± 1.4E+1	7.58E+1 ± 4.8E+0
M32/3_17_F	6.30E+1 ± 4.2E+0	3.14E+3 ± 2.8E+2	3.63E+1 ± 2.7E+0	2.15E+1 ± 1.6E+0
M32/3_18_C	5.99E+1 ± 3.7E+0	2.95E+3 ± 2.6E+2	1.90E+1 ± 1.6E+0	1.45E+1 ± 1.1E+0
M32/3_18_F	4.57E+1 ± 2.9E+0	2.26E+3 ± 2.0E+2	1.25E+1 ± 1.2E+0	4.19E+0 ± 4.1E-1
M32/3_19_C	2.05E+1 ± 1.9E+0	1.02E+3 ± 1.3E+2	7.72E+0 ± 1.0E+0	5.72E+0 ± 6.4E-1
M32/3_19_F	1.95E+1 ± 1.3E+0	1.43E+3 ± 1.4E+2	1.98E+2 ± 1.3E+1	3.34E+1 ± 2.2E+0
M32/3_20_C	2.70E+1 ± 1.8E+0	1.31E+3 ± 1.2E+2	8.19E+0 ± 1.1E+0	6.23E+0 ± 4.1E-1
M32/3_20_F	2.12E+1 ± 1.5E+0	1.05E+3 ± 1.0E+2	1.19E+1 ± 1.4E+0	2.66E+0 ± 2.6E-1
M32/3_21_C	5.17E+1 ± 3.2E+0	2.33E+3 ± 2.1E+2	1.35E+1 ± 1.1E+0	5.24E+0 ± 4.3E-1
M32/3_21_F	2.88E+1 ± 1.8E+0	1.53E+3 ± 1.4E+2	1.16E+1 ± 1.0E+0	1.16E+1 ± 8.4E-1
M32/3_22_C	2.22E+2 ± 1.3E+1	9.74E+3 ± 8.6E+2	1.29E+2 ± 8.2E+0	3.88E+1 ± 2.6E+0
M32/3_22_F	1.18E+2 ± 7.0E+0	6.02E+3 ± 5.2E+2	3.14E+1 ± 2.0E+0	1.77E+1 ± 1.3E+0
M32/3_23_C	1.35E+2 ± 8.6E+0	6.10E+3 ± 5.4E+2	2.28E+2 ± 1.4E+1	1.50E+1 ± 1.1E+0
M32/3_23_F	9.29E+1 ± 5.8E+0	4.85E+3 ± 4.3E+2	2.56E+1 ± 2.3E+0	8.36E+0 ± 6.0E-1
M32/3_24_C	3.86E+0 ± 7.7E-1	2.69E+2 ± 3.5E+1	4.77E+2 ± 3.3E+1	2.00E+0 ± 3.1E-1
M32/3_24_F	3.65E+0 ± 6.5E-1	2.22E+2 ± 3.0E+1	9.65E+2 ± 6.4E+1	2.46E+0 ± 4.9E-1

TABLE A-1 (cont). Coarse (labels with a "C") and Fine (labels with a "F") elemental concentrations.

Label	Mn 55 pmoles m-3	Fe 57 pmoles m-3	Ni 60 pmoles m-3	Cu 63 pmoles m-3
M32/3_25_C	< 1.53E+0	7.65E+1 ± 1.9E+1	1.47E+3 ± 9.7E+1	3.45E+0 ± 3.5E-1
M32/3_25_F	< 1.53E+0	1.01E+2 ± 1.8E+1	3.80E+2 ± 2.2E+1	2.26E+0 ± 4.3E-1
M32/3_26_C	< 2.02E+0	1.81E+2 ± 3.0E+1	1.63E+3 ± 1.1E+2	3.09E+0 ± 5.9E-1
M32/3_26_F	< 2.02E+0	8.92E+1 ± 2.6E+1	1.50E+3 ± 9.1E+1	5.33E+0 ± 8.8E-1
M32/3_27_C	< 1.69E+0		4.67E+2 ± 3.0E+1	5.06E+0 ± 5.7E-1
M32/3_27_F	< 1.69E+0	1.06E+2 ± 2.9E+1	7.12E+2 ± 4.5E+1	3.52E+0 ± 4.7E-1
M32/3_28_C	< 4.76E+0	< 186.52E+0	7.26E+3 ± 4.3E+2	1.28E+1 ± 1.7E+0
M32/3_28_F	< 4.76E+0	3.44E+2 ± 6.2E+1	5.87E+2 ± 3.9E+1	1.19E+1 ± 1.4E+0
M32/5_01_C	< 1.65E+0	< 89.71E+0	3.96E+3 ± 2.1E+2	3.82E+0 ± 4.4E-1
M32/5_01_F	< 1.65E+0	< 89.71E+0	6.47E+2 ± 3.1E+1	3.22E+0 ± 3.5E-1
M32/5_02_C	4.64E+0 ± 3.1E-1	2.48E+2 ± 2.4E+1	2.01E+2 ± 1.0E+1	1.81E+0 ± 1.3E-1
M32/5_02_F	4.18E+0 ± 3.0E-1	2.25E+2 ± 2.2E+1	2.64E+3 ± 1.4E+2	2.57E+0 ± 3.0E-1
M32/5_03_C	8.99E+0 ± 1.0E+0	5.81E+2 ± 6.6E+1	1.31E+3 ± 6.6E+1	1.22E+1 ± 1.5E+0
M32/5_03_F	9.29E+0 ± 9.2E-1	6.05E+2 ± 7.5E+1	5.65E+3 ± 2.8E+2	1.29E+1 ± 1.2E+0
M32/5_04_C	2.52E+0 ± 2.7E-1	1.65E+2 ± 2.0E+1	7.45E+2 ± 3.6E+1	3.27E+0 ± 4.1E-1
M32/5_04_F	2.61E+0 ± 2.4E-1	2.26E+2 ± 2.4E+1	1.47E+3 ± 7.7E+1	4.43E+0 ± 4.2E-1
M32/5_05_C	6.02E+0 ± 4.1E-1	3.01E+2 ± 2.9E+1	8.04E+2 ± 3.8E+1	4.22E+0 ± 3.1E-1
M32/5_05_F	2.18E+0 ± 2.7E-1	1.08E+2 ± 1.3E+1	1.77E+3 ± 8.5E+1	2.59E+0 ± 3.7E-1
M32/5_06_C	< 4.27E+0	< 231.94E+0	3.76E+3 ± 1.8E+2	6.50E+0 ± 7.5E-1
M32/5_06_F	5.81E+0 ± 5.2E-1	4.57E+2 ± 5.2E+1	4.40E+3 ± 2.0E+2	8.11E+0 ± 9.8E-1
M32/5_07_C	5.65E+0 ± 3.1E-1	3.23E+2 ± 2.8E+1	9.37E+2 ± 4.2E+1	3.30E+0 ± 2.7E-1
M32/5_07_F	3.53E+0 ± 3.5E-1	1.82E+2 ± 1.9E+1	8.46E+2 ± 4.0E+1	3.23E+0 ± 2.9E-1
M32/5_08_C	5.01E+0 ± 3.3E-1	2.67E+2 ± 2.4E+1	1.13E+3 ± 5.6E+1	2.54E+0 ± 2.2E-1
M32/5_08_F	3.75E+0 ± 2.6E-1	2.10E+2 ± 2.1E+1	5.54E+2 ± 3.0E+1	3.74E+0 ± 3.0E-1
M32/5_09_C	1.17E+1 ± 6.2E-1	6.53E+2 ± 5.3E+1	1.99E+3 ± 9.3E+1	4.47E+0 ± 3.3E-1
M32/5_09_F	3.74E+0 ± 2.5E-1	2.57E+2 ± 2.3E+1	4.16E+3 ± 1.8E+2	3.77E+0 ± 2.7E-1
M32/5_10_C	1.03E+1 ± 7.2E-1	5.28E+2 ± 4.9E+1	3.24E+3 ± 1.9E+2	3.81E+0 ± 4.7E-1
M32/5_10_F	7.10E+0 ± 5.1E-1	4.30E+2 ± 3.9E+1	1.06E+3 ± 5.2E+1	2.82E+0 ± 3.4E-1
M32/5_11_C	1.09E+1 ± 6.7E-1	5.68E+2 ± 5.2E+1	1.26E+3 ± 6.9E+1	< 1.32E+0
M32/5_11_F	5.05E+0 ± 3.8E-1	2.69E+2 ± 2.7E+1	3.59E+2 ± 1.8E+1	2.47E+0 ± 3.6E-1
M32/5_12_C	1.20E+1 ± 6.5E-1	6.57E+2 ± 5.4E+1	3.35E+2 ± 1.7E+1	3.73E+0 ± 3.3E-1
M32/5_12_F	8.63E+0 ± 5.3E-1	5.00E+2 ± 4.2E+1	2.73E+3 ± 1.4E+2	3.48E+0 ± 3.9E-1
M32/5_13_C	1.35E+1 ± 7.9E-1	6.59E+2 ± 5.2E+1	8.06E+2 ± 4.0E+1	8.72E+0 ± 6.5E-1
M32/5_13_F	7.47E+0 ± 6.6E-1	4.08E+2 ± 4.5E+1	4.99E+2 ± 3.4E+1	3.11E+0 ± 4.5E-1
M32/5_14_C	9.74E+0 ± 6.4E-1	4.35E+2 ± 3.9E+1	1.06E+3 ± 5.4E+1	5.21E+0 ± 5.7E-1
M32/5_14_F	6.45E+0 ± 4.4E-1	1.81E+2 ± 2.1E+1	1.31E+3 ± 7.0E+1	1.08E+1 ± 8.9E-1
M32/5_15_C	8.36E+0 ± 7.3E-1	4.43E+2 ± 5.6E+1	5.60E+2 ± 3.3E+1	3.28E+0 ± 5.4E-1
M32/5_15_F	2.92E+0 ± 4.7E-1	1.84E+2 ± 2.9E+1	6.04E+2 ± 3.5E+1	
M32/5_16_C	1.23E+1 ± 1.2E+0	3.92E+2 ± 5.4E+1	1.87E+3 ± 1.1E+2	9.77E+0 ± 1.0E+0
M32/5_16_F	8.42E+0 ± 1.0E+0	1.97E+2 ± 3.3E+1	3.98E+3 ± 2.3E+2	1.15E+1 ± 1.2E+0
M32/5_17_C	6.61E+0 ± 1.0E+0	1.80E+2 ± 3.1E+1	9.50E+3 ± 5.9E+2	1.51E+1 ± 1.3E+0
M32/5_17_F	7.53E+0 ± 1.1E+0	2.45E+2 ± 3.8E+1	1.90E+3 ± 1.1E+2	1.04E+1 ± 1.2E+0
M32/5_18_C	6.34E+0 ± 6.5E-1	3.20E+2 ± 4.4E+1	3.30E+3 ± 2.0E+2	7.00E+0 ± 7.5E-1
M32/5_18_F	6.82E+0 ± 7.6E-1	3.27E+2 ± 4.5E+1	3.10E+3 ± 1.9E+2	8.34E+0 ± 8.4E-1
M32/5_19_C	2.80E+1 ± 1.9E+0	1.50E+3 ± 1.7E+2	1.25E+3 ± 7.2E+1	1.06E+1 ± 1.7E+0
M32/5_19_F	6.51E+0 ± 1.1E+0	3.78E+2 ± 5.7E+1	1.31E+3 ± 1.0E+2	6.66E+0 ± 1.1E+0
M32/5_20_C	1.84E+1 ± 9.4E-1	9.04E+2 ± 7.2E+1	2.14E+3 ± 9.9E+1	4.44E+0 ± 5.0E-1
M32/5_20_F	4.33E+0 ± 3.1E-1	2.69E+2 ± 2.7E+1	1.32E+3 ± 6.4E+1	4.37E+0 ± 4.4E-1

TABLE A-1 (cont). Coarse (labels with a "C") and Fine (labels with a "F") elemental concentrations.

Label	Zn 66 pmoles m^{-3}	Cd 111 pmoles m^{-3}	Sb 121 pmoles m^{-3}	Ba 137 pmoles m^{-3}
M32/3_01_C	1.83E+1 ± 2.4E+0	< 1.58E+0	< 1.11E+0	5.55E+0 ± 7.7E-1
M32/3_01_F	6.53E+1 ± 6.6E+0	< 1.58E+0	1.85E+0 ± 7.0E-1	5.53E+0 ± 5.1E-1
M32/3_02_C	1.10E+1 ± 2.0E+0	< 1.20E+0	< 840.41E-3	3.92E+0 ± 4.8E-1
M32/3_02_F	4.83E+1 ± 4.8E+0	< 1.20E+0	< 840.41E-3	4.05E+0 ± 5.7E-1
M32/3_03_C	2.12E+1 ± 3.1E+0	< 2.39E+0	< 1.68E+0	4.77E+0 ± 8.2E-1
M32/3_03_F	3.46E+2 ± 2.1E+1	< 2.39E+0	< 1.68E+0	6.12E+0 ± 1.1E+0
M32/3_04_C	1.30E+1 ± 1.6E+0	< 637.16E-3	< 762.87E-3	8.94E+0 ± 6.5E-1
M32/3_04_F	3.18E+1 ± 2.4E+0	< 637.16E-3	< 762.87E-3	4.12E+0 ± 4.2E-1
M32/3_05_C	1.08E+1 ± 1.2E+0	< 944.06E-3	< 1.13E+0	9.13E+0 ± 7.1E-1
M32/3_05_F	2.47E+1 ± 2.7E+0	< 944.06E-3	< 1.13E+0	4.09E+0 ± 5.3E-1
M32/3_06_C	1.78E+1 ± 1.6E+0	< 1.00E+0	< 1.20E+0	1.73E+1 ± 1.5E+0
M32/3_06_F	2.61E+1 ± 2.3E+0	< 1.00E+0	< 1.20E+0	5.82E+0 ± 5.9E-1
M32/3_07_C	1.19E+1 ± 9.8E-1	< 449.67E-3	< 538.38E-3	1.28E+1 ± 1.0E+0
M32/3_07_F	2.12E+1 ± 1.5E+0	< 449.67E-3	< 538.38E-3	5.39E+0 ± 3.6E-1
M32/3_08_C	2.31E+1 ± 1.6E+0	< 536.65E-3	< 642.54E-3	2.41E+1 ± 1.3E+0
M32/3_08_F	3.44E+1 ± 2.9E+0	< 536.65E-3	< 642.54E-3	1.05E+1 ± 6.8E-1
M32/3_09_C	3.02E+1 ± 2.6E+0	< 1.89E+0	< 1.65E+0	1.83E+1 ± 1.0E+0
M32/3_09_F	3.49E+1 ± 2.7E+0	< 467.14E-3	< 559.31E-3	1.45E+1 ± 1.1E+0
M32/3_10_C	2.33E+1 ± 1.9E+0	< 456.50E-3	< 546.56E-3	2.43E+1 ± 1.3E+0
M32/3_10_F	4.08E+1 ± 2.4E+0	#VALUE!	< 546.56E-3	1.85E+1 ± 1.3E+0
M32/3_11_C	2.43E+1 ± 1.9E+0	< 693.52E-3	< 830.35E-3	2.49E+1 ± 1.4E+0
M32/3_11_F	4.41E+1 ± 3.3E+0	< 693.52E-3	< 830.35E-3	2.27E+1 ± 1.5E+0
M32/3_12_C	2.28E+1 ± 1.9E+0	< 450.79E-3	< 539.73E-3	2.35E+1 ± 1.4E+0
M32/3_12_F	7.00E+1 ± 3.9E+0	5.37E-1 ± 1.4E-1	< 539.73E-3	1.30E+1 ± 8.7E-1
M32/3_13_C	1.30E+1 ± 1.3E+0	< 412.62E-3	< 494.03E-3	1.47E+1 ± 7.7E-1
M32/3_13_F	2.40E+1 ± 1.6E+0	< 412.62E-3	< 494.03E-3	9.85E+0 ± 6.4E-1
M32/3_14_C	2.27E+1 ± 2.1E+0	< 246.51E-3	2.16E-1 ± 8.9E-2	2.46E+1 ± 1.5E+0
M32/3_14_F	1.74E+1 ± 1.4E+0	< 246.51E-3	2.79E-1 ± 7.5E-2	9.71E+0 ± 6.4E-1
M32/3_15_C	2.81E+1 ± 2.4E+0	< 280.18E-3	3.32E-1 ± 7.6E-2	3.16E+1 ± 2.1E+0
M32/3_15_F	2.04E+1 ± 1.5E+0	< 280.18E-3	2.66E-1 ± 7.9E-2	1.03E+1 ± 7.2E-1
M32/3_16_C	2.67E+1 ± 2.2E+0	< 301.50E-3	2.96E-1 ± 2.2E-1	3.39E+1 ± 2.2E+0
M32/3_16_F	2.59E+1 ± 2.1E+0	< 301.50E-3	3.99E-1 ± 2.3E-1	1.38E+1 ± 1.1E+0
M32/3_17_C	3.22E+1 ± 2.8E+0	< 369.37E-3	4.29E-1 ± 4.7E-1	3.64E+1 ± 2.4E+0
M32/3_17_F	2.08E+1 ± 2.1E+0	< 369.37E-3	4.70E-1 ± 3.0E-1	1.13E+1 ± 9.2E-1
M32/3_18_C	1.09E+1 ± 1.3E+0	< 258.14E-3	5.33E-1 ± 7.8E-1	1.08E+1 ± 8.9E-1
M32/3_18_F	1.44E+1 ± 1.3E+0	< 258.14E-3	4.51E-1 ± 4.3E-1	8.43E+0 ± 6.4E-1
M32/3_19_C	4.68E+0 ± 8.0E-1	< 244.41E-3	< 90.27E-3	3.99E+0 ± 4.7E-1
M32/3_19_F	1.27E+1 ± 1.2E+0	< 244.41E-3	1.32E-1 ± 2.6E-2	3.30E+0 ± 3.3E-1
M32/3_20_C	5.95E+0 ± 7.1E-1	< 289.35E-3	< 106.86E-3	4.73E+0 ± 4.0E-1
M32/3_20_F	7.70E+0 ± 7.5E-1	< 289.35E-3	< 106.86E-3	4.35E+0 ± 3.6E-1
M32/3_21_C	9.47E+0 ± 1.0E+0	< 231.60E-3	9.41E-2 ± 3.5E-2	1.02E+1 ± 6.5E-1
M32/3_21_F	1.02E+1 ± 1.1E+0	< 231.60E-3	1.63E-1 ± 4.6E-2	6.12E+0 ± 4.3E-1
M32/3_22_C	2.76E+1 ± 2.4E+0	< 269.02E-3	4.07E-1 ± 2.1E-1	4.37E+1 ± 2.7E+0
M32/3_22_F	2.67E+1 ± 2.3E+0	< 269.02E-3	4.33E-1 ± 1.3E-1	2.29E+1 ± 1.5E+0
M32/3_23_C	1.88E+1 ± 1.8E+0	< 236.36E-3	4.89E-1 ± 3.6E-1	2.44E+1 ± 1.7E+0
M32/3_23_F	2.34E+1 ± 1.8E+0	< 236.36E-3	5.10E-1 ± 1.8E-1	1.90E+1 ± 1.3E+0
M32/3_24_C		< 603.90E-3	< 424.17E-3	7.33E-1 ± 1.6E-1
M32/3_24_F	3.84E+0 ± 8.0E-1	< 603.90E-3	< 424.17E-3	6.91E-1 ± 1.9E-1

TABLE A-1 (cont). Coarse (labels with a "C") and Fine (labels with a "F") elemental concentrations.

Label	Zn 66 pmoles m-3	Cd 111 pmoles m-3	Sb 121 pmoles m-3	Ba 137 pmoles m-3
M32/3_25_C	2.67E+0 ± 1.0E+0	< 755.32E-3	< 530.52E-3	< 251.01E-3
M32/3_25_F	< 1.74E+0	< 755.32E-3	< 530.52E-3	2.92E-1 ± 1.2E-1
M32/3_26_C	5.60E+0 ± 1.1E+0	< 996.31E-3	< 699.80E-3	1.01E+0 ± 2.9E-1
M32/3_26_F	3.14E+0 ± 1.0E+0	< 996.31E-3	< 699.80E-3	< 331.09E-3
M32/3_27_C	< 1.93E+0	< 836.77E-3	< 587.74E-3	< 278.08E-3
M32/3_27_F	< 1.93E+0	< 836.77E-3	< 587.74E-3	< 278.08E-3
M32/3_28_C	6.74E+0 ± 2.1E+0	< 2.35E+0	< 1.65E+0	< 780.65E-3
M32/3_28_F	< 5.41E+0	< 2.35E+0	< 1.65E+0	< 780.65E-3
M32/5_01_C	4.10E+0 ± 7.5E-1	< 1.46E+0	< 1.27E+0	< 420.23E-3
M32/5_01_F	< 1.24E+0	< 1.46E+0	< 1.27E+0	< 420.23E-3
M32/5_02_C	1.35E+0 ± 3.2E-1	< 1.03E+0	< 898.52E-3	8.46E-1 ± 8.2E-2
M32/5_02_F	9.22E+0 ± 6.1E-1	< 1.03E+0	< 898.52E-3	7.30E-1 ± 9.2E-2
M32/5_03_C	9.66E+0 ± 2.2E+0	< 6.10E+0	< 5.33E+0	
M32/5_03_F	7.94E+0 ± 1.5E+0	< 6.10E+0	< 5.33E+0	
M32/5_04_C	5.06E+0 ± 5.3E-1	< 1.51E+0	< 1.32E+0	5.59E-1 ± 1.3E-1
M32/5_04_F	6.48E+0 ± 6.9E-1	< 1.51E+0	< 1.32E+0	
M32/5_05_C	< 1.23E+0	< 1.45E+0	< 1.26E+0	9.69E-1 ± 1.4E-1
M32/5_05_F	2.23E+0 ± 4.5E-1	4.53E+0 ± 5.7E-1	< 1.26E+0	< 416.98E-3
M32/5_06_C	5.47E+0 ± 1.1E+0	< 3.77E+0	< 3.29E+0	< 1.09E+0
M32/5_06_F	5.41E+0 ± 1.2E+0	< 3.77E+0	< 3.29E+0	1.19E+0 ± 2.2E-1
M32/5_07_C	8.67E+0 ± 9.3E-1	< 1.09E+0	< 952.68E-3	8.05E-1 ± 1.0E-1
M32/5_07_F	1.71E+0 ± 2.5E-1	< 1.09E+0	< 952.68E-3	5.74E-1 ± 8.8E-2
M32/5_08_C	2.06E+0 ± 3.9E-1	< 982.76E-3	< 858.45E-3	7.43E-1 ± 1.2E-1
M32/5_08_F	1.94E+0 ± 3.4E-1	< 982.76E-3	< 858.45E-3	5.98E-1 ± 9.1E-2
M32/5_09_C	3.16E+0 ± 4.5E-1	< 1.31E+0	< 1.15E+0	1.36E+0 ± 1.5E-1
M32/5_09_F	4.14E+0 ± 5.7E-1	< 1.31E+0	< 1.15E+0	5.35E-1 ± 7.5E-2
M32/5_10_C	3.92E+0 ± 5.5E-1	< 1.07E+0	< 1.19E+0	1.24E+0 ± 1.7E-1
M32/5_10_F	4.76E+0 ± 7.9E-1	< 1.07E+0	< 1.19E+0	7.22E-1 ± 1.3E-1
M32/5_11_C	2.60E+0 ± 5.8E-1	< 1.14E+0	< 1.27E+0	1.34E+0 ± 2.0E-1
M32/5_11_F	2.98E+0 ± 7.4E-1	< 1.14E+0	< 1.27E+0	< 651.30E-3
M32/5_12_C	2.54E+0 ± 5.1E-1	< 1.03E+0	< 1.15E+0	1.37E+0 ± 1.8E-1
M32/5_12_F	5.28E+0 ± 8.7E-1	< 1.03E+0	< 1.15E+0	9.95E-1 ± 1.8E-1
M32/5_13_C	3.32E+0 ± 6.5E-1	< 995.26E-3	< 1.11E+0	1.42E+0 ± 1.8E-1
M32/5_13_F	2.81E+0 ± 6.1E-1	< 995.26E-3	< 1.11E+0	9.00E-1 ± 1.5E-1
M32/5_14_C	2.08E+0 ± 5.7E-1	< 1.21E+0	< 1.35E+0	1.02E+0 ± 2.6E-1
M32/5_14_F	5.72E+0 ± 8.1E-1	< 1.21E+0	< 1.35E+0	< 693.53E-3
M32/5_15_C	1.68E+0 ± 5.2E-1	< 747.69E-3	< 832.46E-3	9.21E-1 ± 2.8E-1
M32/5_15_F	1.68E+0 ± 4.4E-1	< 747.69E-3	< 832.46E-3	4.61E-1 ± 1.7E-1
M32/5_16_C	6.31E+0 ± 8.5E-1	< 1.17E+0	< 1.30E+0	9.53E-1 ± 3.5E-1
M32/5_16_F	3.46E+0 ± 8.3E-1	< 1.17E+0	< 1.30E+0	< 668.16E-3
M32/5_17_C	8.00E+0 ± 9.3E-1	< 1.21E+0	< 1.35E+0	< 692.33E-3
M32/5_17_F	3.13E+0 ± 7.7E-1	< 1.21E+0	< 1.35E+0	< 692.33E-3
M32/5_18_C	3.38E+0 ± 8.2E-1	< 927.11E-3	< 1.03E+0	7.55E-1 ± 2.1E-1
M32/5_18_F	3.16E+0 ± 7.1E-1	< 927.11E-3	< 1.03E+0	6.72E-1 ± 2.0E-1
M32/5_19_C	5.55E+0 ± 7.5E-1	< 996.47E-3	< 1.11E+0	3.09E+0 ± 4.1E-1
M32/5_19_F	3.19E+0 ± 6.5E-1	< 996.47E-3	< 1.11E+0	8.75E-1 ± 2.4E-1
M32/5_20_C	4.47E+0 ± 7.4E-1	< 1.78E+0	< 1.55E+0	2.35E+0 ± 2.3E-1
M32/5_20_F	3.56E+0 ± 5.2E-1	< 1.78E+0	< 1.55E+0	7.39E-1 ± 1.3E-1

TABLE A-1 (cont). Coarse (labels with a "C") and Fine (labels with a "F") elemental concentrations.

Label	Pb 208 pmoles m^{-3}
M32/3_01_C	1.58E+0 ± 2.6E-1
M32/3_01_F	1.19E+1 ± 8.8E-1
M32/3_02_C	1.65E+0 ± 2.2E-1
M32/3_02_F	9.34E+0 ± 6.8E-1
M32/3_03_C	2.22E+0 ± 2.6E-1
M32/3_03_F	1.16E+1 ± 7.7E-1
M32/3_04_C	1.41E+0 ± 2.3E-1
M32/3_04_F	7.66E+0 ± 5.4E-1
M32/3_05_C	< 630.51E-3
M32/3_05_F	6.31E+0 ± 6.6E-1
M32/3_06_C	1.99E+0 ± 4.8E-1
M32/3_06_F	5.94E+0 ± 6.7E-1
M32/3_07_C	1.18E+0 ± 1.6E-1
M32/3_07_F	4.99E+0 ± 3.3E-1
M32/3_08_C	3.52E+0 ± 3.5E-1
M32/3_08_F	1.08E+1 ± 6.6E-1
M32/3_09_C	2.88E+0 ± 2.0E-1
M32/3_09_F	9.38E+0 ± 6.6E-1
M32/3_10_C	2.52E+0 ± 1.8E-1
M32/3_10_F	1.17E+1 ± 7.5E-1
M32/3_11_C	2.14E+0 ± 3.2E-1
M32/3_11_F	1.20E+1 ± 7.0E-1
M32/3_12_C	2.88E+0 ± 1.9E-1
M32/3_12_F	1.17E+1 ± 9.0E-1
M32/3_13_C	1.46E+0 ± 1.5E-1
M32/3_13_F	7.36E+0 ± 5.3E-1
M32/3_14_C	2.32E+0 ± 1.9E-1
M32/3_14_F	5.57E+0 ± 3.8E-1
M32/3_15_C	3.40E+0 ± 2.5E-1
M32/3_15_F	7.17E+0 ± 5.7E-1
M32/3_16_C	3.47E+0 ± 3.1E-1
M32/3_16_F	8.80E+0 ± 6.9E-1
M32/3_17_C	4.07E+0 ± 3.7E-1
M32/3_17_F	8.34E+0 ± 6.2E-1
M32/3_18_C	1.57E+0 ± 2.5E-1
M32/3_18_F	6.47E+0 ± 4.8E-1
M32/3_19_C	7.95E-1 ± 1.5E-1
M32/3_19_F	2.12E+0 ± 2.3E-1
M32/3_20_C	1.56E+0 ± 1.7E-1
M32/3_20_F	2.66E+0 ± 2.0E-1
M32/3_21_C	1.09E+0 ± 1.4E-1
M32/3_21_F	2.94E+0 ± 2.5E-1
M32/3_22_C	3.18E+0 ± 2.6E-1
M32/3_22_F	6.67E+0 ± 4.5E-1
M32/3_23_C	1.84E+0 ± 1.8E-1
M32/3_23_F	6.09E+0 ± 4.3E-1
M32/3_24_C	2.41E-1 ± 4.7E-2
M32/3_24_F	6.47E-1 ± 9.5E-2

TABLE A-1 (cont). Coarse (labels with a "C") and Fine (labels with a "F") elemental concentrations.

Label	Pb 208 pmoles m-3
M32/3_25_C	< 211.61E-3
M32/3_25_F	3.78E-1 ± 7.6E-2
M32/3_26_C	5.10E-1 ± 1.1E-1
M32/3_26_F	< 279.13E-3
M32/3_27_C	5.49E-1 ± 9.0E-2
M32/3_27_F	< 234.43E-3
M32/3_28_C	< 658.13E-3
M32/3_28_F	< 658.13E-3
M32/5_01_C	< 413.46E-3
M32/5_01_F	< 413.46E-3
M32/5_02_C	< 292.04E-3
M32/5_02_F	5.87E-1 ± 8.4E-2
M32/5_03_C	< 1.73E+0
M32/5_03_F	< 1.73E+0
M32/5_04_C	< 428.43E-3
M32/5_04_F	< 428.43E-3
M32/5_05_C	< 410.26E-3
M32/5_05_F	< 410.26E-3
M32/5_06_C	< 1.07E+0
M32/5_06_F	< 1.07E+0
M32/5_07_C	< 309.64E-3
M32/5_07_F	4.16E-1 ± 6.6E-2
M32/5_08_C	< 279.02E-3
M32/5_08_F	4.07E-1 ± 6.0E-2
M32/5_09_C	< 372.68E-3
M32/5_09_F	< 372.68E-3
M32/5_10_C	< 539.93E-3
M32/5_10_F	< 539.93E-3
M32/5_11_C	< 572.93E-3
M32/5_11_F	< 572.93E-3
M32/5_12_C	< 521.05E-3
M32/5_12_F	< 521.05E-3
M32/5_13_C	< 501.11E-3
M32/5_13_F	< 501.11E-3
M32/5_14_C	< 610.08E-3
M32/5_14_F	< 610.08E-3
M32/5_15_C	< 376.46E-3
M32/5_15_F	< 376.46E-3
M32/5_16_C	< 587.76E-3
M32/5_16_F	< 587.76E-3
M32/5_17_C	< 609.03E-3
M32/5_17_F	< 609.03E-3
M32/5_18_C	< 466.80E-3
M32/5_18_F	< 466.80E-3
M32/5_19_C	< 501.72E-3
M32/5_19_F	< 501.72E-3
M32/5_20_C	< 504.78E-3
M32/5_20_F	< 504.78E-3

TABLE A-2. Factor analysis statistics for inter-monsoon data with Pb and V measurements.

PC	Eigenvalue	% Of Variance	Cumulative %
1	21.11	43.1	43.1
2	7.70	15.7	58.8
3	5.63	11.5	70.3
4	3.46	7.1	77.4
5	2.49	5.1	82.4
6	2.19	4.5	86.9
7	1.26	2.6	89.5
8	1.19	2.4	91.9
9	1.03	2.1	94

TABLE A-3. Principal components (PCs) after factor analysis of inter-monsoon aerosol samples with V and Pb measurements.

	PC 1	PC 2	PC 3	PC 4	PC 5	PC 6	PC 7	PC 8	PC 9
COARSE Mg	0.563	0.457	0.422	0.280	0.093	0.204	-0.126	0.246	0.240
COARSE Al	0.935	0.114	0.144	0.226	-0.031	0.046	-0.153	0.066	0.130
COARSE K	0.864	0.198	0.241	0.262	0.112	0.154	0.062	0.147	-0.085
COARSE Ca43[a]	0.750	0.248	0.297	0.223	-0.080	-0.010	0.071	0.246	0.367
COARSE Ca44	0.748	0.269	0.293	0.236	-0.075	0.006	-0.121	0.250	0.346
COARSE Ti47	0.973	-0.014	0.047	0.156	0.004	0.048	-0.119	0.033	0.048
COARSE Ti48	0.971	-0.016	0.073	0.164	-0.010	0.054	-0.122	0.079	0.091
COARSE Cr	0.652	0.131	0.520	0.097	0.265	0.209	0.292	-0.002	0.140
COARSE Mn	0.300	0.074	0.907	0.146	-0.071	-0.129	0.242	0.074	0.066
COARSE Fe	0.157	0.092	0.942	0.121	-0.035	-0.056	0.123	0.062	0.079
COARSE Ni	-0.145	-0.141	0.476	0.030	0.088	-0.109	0.919	-0.011	0.016
COARSE Cu	0.209	0.174	0.219	0.590	-0.017	-0.106	-0.006	0.132	0.403
COARSE Zn	0.836	0.170	0.124	0.222	0.221	0.165	-0.058	-0.006	0.172
COARSE Ba	0.978	-0.059	0.086	0.131	-0.051	-0.080	0.027	-0.009	-0.048
FINE Mg	0.424	0.258	0.322	0.766	0.159	0.070	-0.119	0.084	0.057
FINE Al	0.725	0.079	0.169	0.604	0.162	0.080	-0.177	-0.105	-0.141
FINE K	0.521	0.183	0.217	0.690	0.246	0.231	0.140	0.019	-0.171
FINE Ca43	0.460	0.108	0.219	0.836	-0.002	-0.171	0.208	0.046	0.070
FINE Ca44	0.505	0.173	0.243	0.779	0.050	-0.029	-0.086	0.042	0.089
FINE Ti47	0.370	0.147	0.012	0.304	0.847	0.100	-0.113	-0.089	-0.012
FINE Ti48	0.395	0.152	0.032	0.340	0.822	0.102	-0.118	-0.085	-0.008
FINE Cr	-0.112	0.190	-0.041	-0.108	0.949	0.018	0.012	-0.030	0.033
FINE Mn	0.191	0.355	0.799	0.275	-0.038	-0.213	0.173	0.212	-0.088
FINE Fe	0.147	0.422	0.822	0.103	-0.020	-0.074	-0.238	0.191	-0.044
FINE Ni	-0.220	0.276	0.152	-0.021	0.760	-0.144	0.048	0.378	0.008
FINE Cu	0.107	0.302	0.191	0.078	0.003	-0.121	-0.002	0.820	-0.078
FINE Zn	-0.114	0.280	-0.038	-0.036	0.940	0.135	0.164	0.035	-0.001
FINE Ba	0.697	-0.048	0.111	0.626	0.107	-0.060	0.035	-0.156	-0.225
TOTAL Fl^-	0.221	0.505	-0.213	-0.254	0.299	0.449	0.238	0.026	0.015
TOTAL $H_3CCO_2^-$	0.524	0.010	0.105	0.037	0.040	0.075	0.037	-0.200	0.704
TOTAL HCO_2^-	-0.026	0.381	0.769	0.283	0.182	0.006	0.028	-0.181	0.103
TOTAL MSA	0.071	0.660	0.283	-0.006	0.397	0.403	0.105	-0.112	0.241
TOTAL Cl^-	0.081	0.856	0.253	0.194	0.206	0.082	-0.034	0.176	0.168
TOTAL NO_3^-	0.623	0.250	-0.161	0.284	0.111	-0.173	0.058	-0.246	0.179
TOTAL SO_4^{2-}	0.428	0.689	-0.106	0.408	0.194	0.263	-0.061	-0.001	0.153
TOTAL $C_2O_4^{2-}$	0.474	0.639	0.243	0.375	0.208	0.171	-0.101	0.180	0.030
TOTAL Na^+	-0.006	0.927	0.215	0.045	0.181	0.096	-0.059	0.139	0.017
TOTAL NH_4^+	-0.302	0.336	0.161	-0.129	0.346	0.731	-0.237	-0.124	-0.111
TOTAL K^+	0.020	0.882	0.169	0.125	0.149	0.003	0.066	0.010	-0.097
TOTAL Mg^{2+}	0.127	0.922	0.209	0.063	0.137	0.099	-0.128	0.078	-0.054
TOTAL Ca^{2+}	0.745	0.420	0.112	0.399	-0.066	-0.057	-0.113	-0.079	-0.076
COARSE $Fe(II)_{aq,ex}$	-0.282	0.029	-0.087	0.037	-0.049	0.878	0.102	-0.027	-0.013

TABLE A-3 (cont.). Principal components (PCs) after factor analysis of inter-monsoon aerosol samples with V and Pb measurements.

	PC 1	PC 2	PC 3	PC 4	PC 5	PC 6	PC 7	PC 8	PC 9
COARSE $Fe(II)_{tot,ex}$	0.131	-0.007	-0.179	-0.175	0.050	0.927	-0.022	-0.100	-0.078
FINE $Fe(II)_{aq,ex}$	0.259	0.364	0.039	0.011	0.100	0.693	-0.077	-0.007	0.169
FINE $Fe(II)_{tot,ex}$	0.327	0.062	-0.159	0.284	-0.066	0.667	-0.110	0.071	0.085
COARSE V	0.995	-0.117	-0.009	0.099	-0.024	-0.089	0.137	-0.001	0.003
COARSE Pb	0.895	0.250	0.030	0.038	0.105	0.156	0.117	-0.006	0.126
FINE V	0.620	0.037	-0.068	0.256	0.653	0.094	0.117	-0.191	-0.021
FINE Pb	0.347	0.476	0.094	0.449	0.319	0.483	0.233	0.066	-0.020

Chapter 6:

Conclusions and Future Work

CONCLUSIONS

Experiments, using ambient aerosol samples suspended in aqueous solutions to simulate cloudwater chemistry, along with the measurement of different chemical species of Fe in aerosol and cloudwater samples, were used to assess the role of Fe in cloudwater chemistry. These measurements included several labile fractions of Fe(II) and photochemically-available Fe. Many other species, relevant to the chemistry of Fe, were also measured. The aerosol and cloudwater samples were collected from a variety of locations to understand spatial variability. The sampling sites included: Pasadena (CA), San Nicholas Island (CA), Sequoia National Park (CA), Yosemite National Park (CA), Whiteface Mountain (NY), and the Arabian Sea. Thermodynamic and kinetic models, along with statistical methods were used to interpret the field observations.

Experiments to simulate cloudwater conditions were carried out by suspending ambient aerosol samples in an aqueous solution and then irradiating the solution with ultraviolet light. A total of four different ambient aerosol samples were used in the simulated cloudwater experiments; they were collected from Whiteface Mountain, NY (1), Pasadena, CA (2) and Sequoia National Park, CA (1). In all cases, the production rates for $Fe(II)_{aq}$ and H_2O_2 in the light were greater than production rates in non-irradiated control experiments. The simulated cloudwater experiments (with 4 different aerosol samples) showed similar behavior to previous experiments carried out with synthetic Fe-oxyhydroxy polymorphs in the presence of oxalate, formate or acetate. The Fe present in the ambient aerosol appears to be a critical component for the production of H_2O_2 in the simulated cloudwater experiments.

A novel photochemical extraction procedure was developed and used to determine the concentration of photochemically-available Fe in ambient aerosol samples. Ambient aerosol samples, collected at Whiteface Mountain (NY), Pasadena (CA) and San Nicholas

Island (CA), were suspended in an aqueous solution within a photochemical reactor and irradiated. Under these conditions, which were favorable to the photo-chemical weathering of aerosol particles, the relative amount of $Fe(II)_{aq}$ to Fe_{total} was shown to increase and used to characterize the Fe in the aerosol samples. Photochemically-available Fe concentrations found ranged from < 4 ng/m^3 to 308 ng/m^3 and the percentage of photochemically-available Fe to Fe_{total} ranged from 2.8% to 100%. Aerosol samples were also collected during biomass burning events in Southern California; these samples showed insignificant changes in the photochemically-available Fe (compared to non-biomass burning samples) in conjunction with large increases of Fe_{total}. Calculations based on these experiments also provides further evidence that redox reactions of Fe in cloudwater could be an important *in situ* source of oxidants ($^{\bullet}OH$, $HO_2^{\bullet}/O_2^{-}$).

Other transition metals also may play an important role in the atmospheric chemistry of Fe. Therefore, the oxidation state of Fe and three other transition metals (Mn, Cu & Cr) in cloudwater were investigated during several cloud events at Whiteface Mountain (NY), one cloud event at San Pedro Hill (CA) and one fog event at Bakersfield (CA). Other measurements performed, relevant to the redox chemistry of these metals, included pH, total elemental concentrations (Fe, Cu, Mn, Cr, Al, K, Ca, Na and Mg), organic anions (formate, acetate, glycolate, oxalate), inorganic anions (chloride, sulfate, nitrate, sulfite), cations (sodium, calcium, magnesium, potassium), peroxides, and formaldehyde. These measurements were then used in thermodynamic speciation models to understand the speciation of ambient fog and cloudwater. From this analysis, two different cases were found for $Fe(III)_{soluble}$ speciation. Fe(III) was found to exist either as $Fe(OH)_2^+$ or $Fe(Oxalate)_2^-$. However, an un-identified strong chelating ligand with Fe(III) was also suggested by the data. Cu(I) and Cu(II) were calculated to be predominantly Cu^+ and Cu^{2+} (with less than 10% as Cu(II)-oxalate complexes). A chemical kinetic model was also used to investigate the transition metal chemistry. The model results indicate Fe(II) should be the predominant chemical form of Fe during daylight conditions. This prediction is in

agreement with the field measurements in which the highest ratios of $Fe(II)/Fe_{total}$ were found in samples collected during the day. The model results also indicated Fe(III) should be the predominant form of Fe during nighttime conditions, this is also in agreement with the field measurements. In the model, Cu(II) and Mn(II) were the predominant oxidation states during daylight and nighttime conditions, with Cu(I) and Mn(III) increasing during daylight conditions. Mn(III) concentrations were never high enough to influence the redox chemistry of Cr. Overall, Cr(VI) in cloudwater is predicted to be reduced to Cr(III).

Ambient aerosol samples were also collected during the inter-monsoon and southwest-monsoon periods on the Arabian Sea. A high-volume dichotomous virtual impactor (HVDVI) with an aerodynamic cutoff size of 3 μm was used to collect the fine and coarse aerosol fractions for metal analysis. A low volume collector (LVC) was used to collect aerosol samples for anion and cation analysis. The primary purpose of this study was to characterize the chemical composition of the ambient aerosol during the southwest-monsoon and inter-monsoon periods, including the measurement of labile ferrous iron (Fe(II)) in the fine and coarse fractions of ambient aerosol samples. The analysis for labile-Fe(II) was done immediately after sample collection to minimize any possible Fe redox reactions which might occur during sample storage. Total atmospheric aqueous labile-Fe(II) concentrations during the inter-monsoon period were between 7.48 ng m^{-3} to < 0.089 ng m^{-3}. The aqueous-labile Fe(II) was predominantly in the "fine" fraction (< 3.0 μm), with the "fine" fraction of aqueous labile Fe(II) accounting for an average of 90% of the total aqueous labile Fe(II). In contrast, during the southwest-monsoon period, the atmospheric aqueous labile Fe(II) concentrations were consistently below the detection limit (< 0.34 ng m^{-3} to < 0.089 ng m^{-3} depending on the volume of air sampled). Factor analysis revealed a significant source of Fe and Mn which was not associated with the main aeolian dust component or any typical anthropogenic metals (e.g. V, Pb). This component did not include any loadings of labile-Fe(II). The air mass back trajectories (5 day, three-dimensional) showed that air masses sampled during the southwest-monsoon had origins

over the open Indian Ocean, and air masses sampled during the inter-monsoon had origins from southeast Africa, Saudi Arabian peninsula, and southern Asia.

FUTURE WORK

This thesis has provided insight into the role of Fe chemistry in the atmosphere. However, much is still unknown about Fe and other transition metal chemistry in aerosol and cloudwater. The major challenge in this thesis was the difficulty associated with analyzing trace species in aerosol and cloudwater. Current spectrophotometric techniques used in this thesis for the quantification of Fe(II) and other trace metal oxidation states have serious limitations. These limitations include interferences with other aerosol and cloudwater chemical species, and sensitivity. Great care must be taken to eliminate the interferences or account for them. As for sensitivity, relatively large sample sizes must be collected for both aerosol and cloudwater in order to be in the range of the analytical technique. These large sample sizes ultimately require long sampling times, which are usually longer than the characteristic times associated with the reactions occurring in the aerosol or cloudwater system being sampled. Improved analytical and collection techniques which provide for the near real-time analysis of trace metal speciation in ambient aerosol and cloudwater systems would provide invaluable knowledge. Techniques, such as electro-spray mass spectrometry (ES-MS) show a great deal of promise, however their application to field studies is currently limited by the size and complexity of the instrumentation. And the problems associated with coupling an ES-MS instrument to a cloudwater collector are numerous.